NOVEL TECHNOLOGY FOR CRYSTAL ENGINEERING OF PHARMACEUTICAL SOLIDS

N.B.JADAV

PHD

2018

Novel Technology for Crystal Engineering of Pharmaceutical Solids

NITEN BAGAWAN JADAV

Submitted for the degree of Doctor of Philosophy

School of Life Sciences

University of Bradford

2018

Abstract

Niten Bagawan Jadav

Novel Technology for Crystal Engineering of Pharmaceutical Solids

Keywords: Microwave-assisted sub-critical water, cocrystals, polymorphism, hydroxyapatite, paracetamol, ibuprofen, inverse gas chromatography, RotoSYNTH.

The research work described in this thesis, the environmentally friendly novel “Microwave Assisted Sub-Critical water (MASCW)” technology for particle engineering of active pharmaceutical ingredients and excipients was developed. The present novel technology MASCW process is described as green technology as water is used as the solvent medium and microwave energy as external source of heat energy for generation of a particle with different morphological and chemical properties.

In MASCW process supersaturated solution of APIs is prepared by dissolving solute in water at high temperature and pressure conditions. Upon rapid and controlled cooling, based on the aqueous solubility of solute, solute/solvent concentration and dielectric constant of water rapid precipitation of API with narrow particle size distribution occurs.

Using paracetamol (pca) as API moiety understanding of the mechanism of MASCW crystallisation process was investigated. The effect of different process and experimental parameters on crystallisation pathway and end product attributes were analysed. Correlation between the degree of supersaturation concentration of pca solution against temperature and pressure parameters was explained by generating binary phase diagram. Determination of polymorphic transformation pathway of pca from form I (stable) to form II metastable polymorphs in solution was analysed using

Raman spectroscopy. The difference between conventional heating and subcritical treatment was explored by determining the change in the solvent dielectric constant and solubility of hydrophobic API molecule.

Based on the process understanding results, this technology was further implemented to explore its application in generating phase pure stable and metastable cocrystal phase. Based on the solubility of API and cocrystal former congruent (CBZ/SAC, SMT/SAC, SMZ/SAC) and incongruent (CAF/4HBA) cocrystal pairs were selected. For the first time generation of anhydrous phase of CAF: 4HBA cocrystal in 1:1 stoichiometric ration was reported and generation of metastable cocrystal phase of CA CBZ: SAC form II was reported.

The application of this technology was explored in generating phase pure metastable polymorph of paracetamol which retain higher compressibility and dissolution rate. The potential of MASCW micronisation process, theophylline is used as the model component to produce micro-sized particles for pulmonary drug delivery system via dry powder inhaler (Foradil inhaler). The results demonstrate that the THF particles generated using MASCW process displayed greater aerodynamic performance compared to conventional spray-dried THF sample.

In the final chapter, synthesis of inorganic biomaterial (nano-crystalline hydroxyapatite) was reported for the first time and the prospects of combining API like ibuprofen (IBU) with a biologically active component like nano-crystalline hydroxyapatite (HA) through hydrogen bonding was mechanistically explained using X-ray diffractometer and spectroscopic techniques.

Dedicated To My Beloved

Family and Friends

"Guru Brahma, Guru Vishnu, Guru devo

Maheshwara, Guru sakshat, param

Brahma, tasmai shri guravay namah"

Acknowledgement

I would like to express my deepest appreciation to my supervisor, Professor Anant Paradkar, who has the attitude and the substance of a genius: he continually and convincingly conveyed the spirit of adventure in regards to my research. Without his guidelines and persistent help, this dissertation would not have been possible. He had always provided me the positive attitude to see beyond the boundaries of my research, his determined pursuit in the field of pharmaceutical engineering research and innovative thinking aspect has provided a strong background for this research work.

I also express my deep sense of gratitude to my co-supervisor Dr. Venu Vangala who has supported me throughout my studies, his expertise in crystal engineering made a significant contribution to the success of this project. Dr. Venu is also an important mentor for helping me in the field of co-crystallisation, chemistry and providing me with feedback whenever required.

I am also very grateful to all (postdoctoral research associates, University of Bradford) for their continuous support, guidance and helpful discussions. I especially acknowledge the support of my friends Aniket Sabnis, Sudhir Pagire, Sachin Korde, Ratnadeep Bansode, Amit Sonawane, and Yousef Al Ayuob for providing me with motivation, moral support, and happiness during my practical experiments. My special acknowledgment for the support provided by Analytical Centre, the University of Bradford offering me with analytical characterisation support, I am also thankful to MeDe for providing me with the opportunity to do collaborative research with Prof Peter Twigg's group at IRC, University of Bradford.

Special thanks to my family who have always supported me with their efforts and prayers to attain success in my life. I don’t have any words to express my feelings towards them for their guidance, support and the sacrifices they made on my behalf. I would like to thank my wife Dr. Priya Jadav for supporting and believing in me, her love and kindness have supported me to face all the challenges during my studies with complete confidence. Finally, my family and friends have always been their there to support me and I am grateful for their continuous love and support.

Table of Contents

Abstract ..... **i**
Acknowledgement ..... **iv**
Table of Contents ..... **vi**
Abbreviations and symbols ..... **xi**
List of Figures ..... **xiii**
List of Tables ..... **xx**
Chapter 1: Introduction **1**
1.1 Introduction 1
1.2 Research objectives 7
1.3 Thesis outline 8
Chapter 2: Literature review **13**
2.1 Introduction 13
2.1.1 Supramolecular chemistry 15
2.1.2 Solid State chemistry 16
2.1.3 Classification of Solid forms 17
2.2 Cocrystal 20
2.2.1 Introduction 20
2.2.2 Design of cocrystal 22
2.2.3 Challenges in cocrystallisation process 24
2.2.3.1 Incongruent co-crystal pair 25
2.2.3.2 Spring-parachute effect 26
2.2.4 Mechanism of cocrystal formations 27
2.2.4.1 Solution state crystallisation mechanism; 28
2.2.4.2 Heat fusion mechanism; 30
2.2.4.3 Eutectic or vapor phase mechanism; 32
2.2.4.4 Deliquescence mediated cocrystallisation; 33
2.2.5 Applications of cocrystals 34
2.2.6 Synthesis of cocrystals 36
2.3 Polymorphism 38
2.3.1 Thermodynamics and rules to predict polymorphism 40
2.3.2 Rules for predicting polymorphs 43
2.3.2 Properties of polymorphs 47

2.4 Summary 47
Chapter 3: Sub-Critical Water 49
3.1 Introduction 49
3.2 Water structural properties at subcritical state 51
3.2.1 Process taking place at SCW level 54
3.3 Factors effecting Sub-critical water process 56
3.3.1 Effect of solvent conditions 56
3.3.2 Effect of nature of solute 57
3.4 Computational model to study solubility parameter of solute in SCW 57
3.5 Applications of SCW process 60
3.6 Microwave Assisted Sub-Critical Water process 61
3.6.1 Microwave heating mechanism 63
3.6.1.1 Key attributes of microwave heating over conventional heating 64
3.6.2 Advantages of subcritcal water process 67
3.7 Mechanism of MASCW process 68
Chapter 4: Materials and Methods 71
4.1 Materials 71
4.1.1 Active pharmaceutical ingredients (APIs) and excipients 71
4.1.2 Chemicals and solvents 74
4.1.3 Characterisation analytical instruments 74
4.1.4 Software 75
4.2 Experimental methods 76
4.2.1 Process understanding and validation method 77
4.2.1. A) Investigation of effect of supersaturated concentration of paracetamol and process temperature/pressure parameters 77
4.2.1. B) Crystallisation time 78
4.2.1. C) Crystallisation kinetic studies 78
4.2.1. D) Effect of solvent mixture on dielectric constant of solution and solubility of paracetamol 79
4.2.2 Application of MASCW process in cocrystallisation process 80
4.2.2.1 Cocrystallisation of CBZ: SAC cocrystals 80
4.2.2.2 Cocrystallisation of SMT: SAC and SMZ: SAC cocrystal pairs 93
4.2.2.3 Application of MASCW process for generation of incongruent pair cocrystal pair (CAF: 4HBA 1:1) 96

4.2.2.4 Application of MASCW process in particle engineering of paracetamol. 99
4.2.2.5 Application of MASCW process for inhalation drug delivery system 106
4.2.2.6 Application of MASCW process in hydrogen bonding between nanocrystalline hydroxyapatite and Ibuprofen 116
4.2.3 Characterisation of MASCW processed samples 118
4.2.3.1 Powder X-ray diffraction (PXRD) 118
4.2.3.2 Differential Scanning Calorimetry (DSC) 119
4.2.3.3 Thermogravimetric analysis (TGA) 119
4.2.3.4 Scanning electron microscopy 119
4.2.3.5 Particle size analysis 120
4.2.3.6 Fourier Transform Infrared (FTIR) spectra 120
4.2.3.7 Raman spectroscopy 120
4.2.3.8 Inverse Gas Chromatography (iGC) 121
4.2.3.9 ^{1}H- Nuclear magnetic resonance: 123
Chapter 5: MASCW process understanding and validation 124
5.1 Introduction 124
5.2 Results 126
5.2.1 Development of temperature and solubility curve using MASCW technology. 126
5.2.1.1 PXRD data 131
5.2.1.2 Raman data 132
5.2.2 Monitoring crystallisation time and pca supersaturated solution concentration using MASCW process 133
5.2.2.1 SEM images 137
5.2.3 Crystallisation kinetic data 139
5.2.4 Effect of the solvent mixture on the dielectric constant of solution and crystallisation of paracetamol 140
5.2.4.1 PXRD data 148
5.2.4.2 DSC data 150
5.2.4.3 Raman data 150
5.2.5 Conclusion 153
Chapter 6: Application of MASCW technology in cocrystallisation process 154
6.1 Introduction 154

6.2 Results and Discussion 156
6.2.1 Preliminary experiments of cocrystallisation 156
6.2.1. a) PXRD data 157
6.2.1. b) DSC thermogram 164
6.2.1. c) HPLC analysis 169
6.2.1. d) Scanning electron microscopy 171
6.2.1. e) Surface Energy Analysis (SEA) 173
6.2.1. f) Solubility data 175
6.2.2 Screening experiment: cocrystallisation of SMT: SAC and SMZ: SAC cocrystal pairs 176
6.2.2. a) PXRD data 177
6.2.2.b) DSC data 178
6.2.3 Cocrystallisation of CAF – 4-HBA acid using MASCW process 180
6.2.3.1 Introduction 180
6.3.2.2 Results and discussion 182
6.3.2.2. a Summary of experimental data 182
6.3.2.2. b PXRD data 183
6.3.2.2. c ^{1}H-NMR- spectra 187
6.2.4 Conclusion 189
Chapter 7: Application of MASCW process in polymorphism 190
7.1 Generation of metastable paracetamol form II polymorph using MASCW process 190
7.1.1 Introduction 190
7.1.2 Results and discussion 193
7.1.2.1 MASCW crystallisation of commercial paracetamol 193
7.1.2.2 PXRD data 195
7.1.2.3 Raman spectroscopic data 196
7.1.2.4 Differential Scanning Calorimetry 198
7.1.2.5 Degradation study of MASCW processed pca samples 199
7.1.2.6 Scanning Electron Microscopy 201
7.1.2.7 Surface Energy Analysis 202
7.1.2.8 Solubility analysis of MASCW processed pca samples 207
7.1.2.9 Drug dissolution data 208
7.1.3 Conclusion 211

7.2 Pharmaceutical analysis and in-vitro aerodynamic characterisation of inhaled theophylline formulations generated by Microwave Assisted Sub-Critical water process 212
7.2.1 Introduction 212
7.2.2 Results and discussion 214
7.2.2.1 Re-crystallisation process and particle size distribution 214
7.2.2.2 Scanning Electron Microscopy 215
7.2.2.3 Powder X-ray diffraction data 216
7.2.2.4 Thermal analysis of THF 217
7.2.2.5 FTIR spectroscopy data 220
7.2.2.6 Inverse gas chromatography 221
7.2.2.7 In-vitro evaluation of the aerodynamic performance of MASCW processed theophylline using NGI 225
7.2.3 Conclusion 232
Chapter 8: A Green route for the synthesis of API-loaded nano-crystalline hydroxyapatite 233
8.1 Introduction 233
8.2 Results 235
8.2.1 Characterisation of synthesised hydroxyapatite 235
8.2.1 (a) PXRD results 235
8.2.1 (b) FTIR spectral results 238
8.2.2 Characterisation of Ibuprofen/ HA complex formation 241
8.2.2.a PXRD data 241
8.2.2.b Scanning electron microscopy images 242
8.2.2. c ATR-FTIR spectral data 244
8.2.3 Analysis of ibuprofen monomer, dimer and attached species using ATR-FTIR spectroscopy 246
8.2.4 Dissolution studies 249
8.3 Conclusions 252
Chapter 9: Global Conclusions 253
Chapter 10: Suggestions for future work 259
Chapter 11: Bibliography 260
Appendix 1 277

Abbreviations and symbols

Abbreviations

4-HBA	:	4-hydroxybenzoic acid
API	:	Active pharmaceutical ingredient
CAF	:	Caffeine
CBZ	:	Carbamazepine
CCF	:	Cocrystal former
CSD	:	Crystal Structure Database
DMSO	:	Dimethyl sulfoxide
DPI	:	Dry powder inhaler
DSC	:	Differential scanning calorimetry
ECD	:	Effective cut-off diameter
FDA	:	Food and Drug Administration
FPF	:	Fine Particle fraction
FT-IR	:	Fourier Transform Infrared spectroscopy
GSD	:	Geometrical standard deviation
HA	:	Hydroxyapatite
HPLC	:	High Performance Liquid Chromatography
HSM	:	Hot stage microscopy
HTS	:	High throughput screening
IBU	:	Ibuprofen
iGC	:	Inverse gas chromatography
LAC-IG	:	Lactose inhalation grade
MASCW	:	Microwave-Assisted Sub-Critical Water
MMAD	:	Mass median aerodynamic diameter
NGI	:	Next Generation Impactor
NMR	:	Nuclear Magnetic Resonance
PAR	:	Paracetamol
PXRD	:	Powder X-ray diffraction
SAC	:	Saccharin
SCW	:	Sub-Critical water
SD	:	Spray Dryer
SEA	:	Surface Energy Analyser
SEM	:	Scanning electron microscopy

SFCC	:	Solvent free continuous co-crystallisation
SMT	:	Sulfamethazine
SMZ	:	Sulfamerazine
TGA	:	Thermogravimetric analysis
THF	:	Theophylline

Symbols

2θ(°)	:	2-Theta degrees
∆pKa	:	acid dissociation constant
γDS	:	Dispersive surface energy
ΔH	:	enthalpy
ΔH_f	:	Enthalpy of fusion
ΔH_t	:	Enthalpy of transition
ΔS	:	entropy
ΔGc	:	Gibbs free energy
µg/ml	:	microgram/millilitres
µ	:	micron
mmol	:	mille-moles
mg	:	milligrams
nm	:	nano-meters
ppm	:	parts per million
%	:	percent
rpm	:	rotation per minute
S	:	Solubility
sccm	:	standard cubic centimetres per minute
K_{sp}	:	Solubility product
T_p	:	Transition point
v/v	:	volume / volume
w	:	watts
w/w	:	weight /weight

List of Figures

Fig. no	Description	Pg. no
1.1	Phase diagram of water at elevated temperature and pressure conditions	7
1.2	Schematic representation of research structure	10
2.1	Pictographic representation of comparison between molecular chemistry and supramolecular chemistry	15
2.2	Classification of solid forms based on structure and composition	18
2.3	Possible multicomponent systems: cocrystals, salt cocrystals, and derived multicomponent systems	19
2.4	Schematic representation of steps involved in design of cocrystal	22
2.5	Types of hydrogen bonding between two synthons (a) acid-acid, (b) acid-amine, (c) acid-amide, (d) acid-imide, I amide-amide and (f) alcohol-ether	23
2.6	Graphical representation of spring-parachute effect	27
2.7	Solubility phase diagram of three components A, B, and cocrystal AB in single solvent system	29
2.8	Zone of mixing in fusion mechanism for cocrystal formation	31
2.9	Pictogram of mechanism of moisture in cocrystallisation, Ds deliquescent material, dissolution of cocrystal component and generation of cocrystal of two components A and B	34
2.10	Different thermodynamic and kinetic properties governing solid states	41
2.11	Correlation of energy and temperature of polymorphs to determine enantiotropy and monotropy	44
3.1	Representation of phase diagram of water as the function of temperature and pressure	50
3.2	Properties of water at various conditions	51
3.3	Chemical structure of water molecule	51
3.4	Schematic representations of dipole moments of water molecule	52
3.5	Comparison between the dielectric constant of water and organic solvents at elevated temperatures	53
3.6	Trendline of solubility data of anthracene (diamond shape), p-terphenyl (square shaped) and 1, 8-cineole (triangle shape) in SCW. The effect of dielectric constant of water with increase in temperature	55
3.7	Electromagnetic spectra and distribution of frequency range	61

3.8	RotoSYNTH microwave reactor with pressure vessel for sub-critical water processing	66
3.9	Summary of mechanism of molecular association of particles in SCW process	68
4.1	Calculated PXRD pattern of CBZ Form III	81
4.2	Crystal structure of CBZ III	82
4.3	Calculated PXRD pattern of carbamazepine dihydrate	82
4.4	Crystal structure of CBZD	83
4.5	Calculated PXRD pattern of saccharin	83
4.6	Crystal structure of saccharin	84
4.7	Calculated PXRD pattern of CBZ/SAC 1:1 cocrystal FI	85
4.8	Crystal structure of CBZ/SAC 1:1 cocrystal	85
4.9	Schematic representation of CBZ/SAC 1:1 cocrystal motif	85
4.10	Calculated PXRD pattern of CBZ/SAC 1:1 cocrystal FII	86
4.11	Crystal structure of CBZ/SAC 1:1 cocrystal	86
4.12	Difference between homosynthon (FI) and heterosynthon (FII) of CBZ/SAC cocrystals	87
4.13	Crystal structure of sulfamerazine	94
4.14	Calculated PXRD pattern of sulfamerazine form I polymorph	94
4.15	Crystal structure of SMT: SAC 1:1 cocrystal	95
4.16	Calculated PXRD pattern of SMT: SAC 1:1 cocrystal	95
4.17	Crystal structure of caffeine anhydrous	97
4.18	Calculated PXRD pattern of caffeine anhydrous	97
4.19	Crystal structure of 4-hydroxybenzoic acid	98
4.20	Calculated PXRD pattern of 4-hydroxybenzoic acid	98
4.21	Crystal structure of paracetamol	100
4.22	Calculated PXRD pattern of paracetamol Form I	101
4.23	Calculated PXRD pattern of paracetamol Form II	101
4.24	Crystal structure of anhydrous theophylline	107
4.25	Calculated PXRD pattern of anhydrous THF	107
4.26	Description of the Next Generation impaction	112
4.27	Graphical representation of calibration curve of THF	114
5.1	Solubility curve and MSZW	125
5.2	Binary phase diagram of concentration of solution and corresponding temperature and pressure	131
5.3	PXRD pattern of : a-raw form I paracetamol, b- form II paracetamol c-5% paracetamol, d-10%paracetamol, e-15%paracetamol, f-20%paracetamol, g-25%paracetamol, h-30%paracetamol	132
5.4	Overlay of Raman spectra of Paracetamol form I raw and MASCW processed paracetamol samples of different solution concentrations	133

5.5	SEM images of paracetamol crystallised from the MASCW process and conventional heating.	138
5.6	Overlay of Raman spectra spotting the characteristic peak of paracetamol form II (1623cm-1) and form I (1565 cm-1) polymorph	139
5.7	Graphical presentation of dielectric constant of solvent mixtures from 10 to 100%v/v concentrations	142
5.8	Dielectric constant values for: water-MeOH blank and water- MeOH-paracetamol solution at 10, 20 and 30% v/v concentration of MeOH –water.	144
5.9	Dielectric constant values for water-ACN blank and water-ACN-paracetamol solution at 10, 20 and 30% v/v concentration of ACN-water	144
5.10	Dielectric constant values for water-EtOH blank and water- EtOH –paracetamol solution at 10, 20 and 30% v/v concentration of EtOH –water	145
5.11	Dielectric constant values for water-ACE blank and water- ACE –paracetamol solution at 10, 20 and 30% v/v concentration of ACE –water	145
5.12	Equilibrium solubility (mg/ml) of paracetamol in untreated and MASCW treated solvent mixtures	147
5.13	PXRD pattern of A- Para raw form I, B- Para form II, C-10% ACE-water, D-20% ACE-water, E- 30% ACE-water	148
5.14	PXRD pattern of A- Para raw form I, B- Para form II, C-10% ACN-water, D-20% ACN-water, E- 30% ACN-water	148
5.15	PXRD pattern of A- Para raw form I, B- Para form II, C-10% EtOH-water, D-20% EtOH-water, E- 30% EtOH-water	149
5.16	PXRD pattern of A- Para raw form I, B- Para form II, C-10% MeOH-water, D-20% MeOH-water, E- 30% MeOH-water	149
5.17	DSC thermogram overlays of all paracetamol crystals obtained from all solvent mixtures	150
5.18	Raman spectra overlay for raw paracetamol form I, solid materials obtained from 10%, 20% and 30% MeOH-water solvent mixtures	151
5.19	Raman spectra overlay for raw paracetamol form I, solid materials obtained from 10%, 20% and 30% ACN-water solvent mixtures	151
5.20	Raman spectra overlay for raw paracetamol form I, solid materials obtained from 10%, 20% and 30% EtOH-water solvent mixtures	152

5.21	Raman spectra overlay for raw paracetamol form I, solid materials obtained from 10%, 20% and 30% ACE-water solvent mixtures	152
6.1	PXRD patterns of batches carried out at A-115°C and B-120°C	157
6.2	PXRD data of experiments carried with A- 10mL, B-12.5mL and C- 15mL water as solvent system	159
6.3	PXRD patterns of batches carried out at A-300W and B-400W	160
6.4	PXRD patterns for the batches carried out using different heating rates A) 26 °C/minute and B) 46 °C/minute	161
6.5	PXRD pattern of: A) CBZ: SAC 1:1.5_12.5ml water, B) CBZ: SAC 1:1.5_15ml, C) CBZ: SAC 1:2_12.5ml water and D) CBZ: SAC 1:2_15ml water	162
6.6	PXRD pattern of A- CBZ/SAC FII CSD data, B-CBZ/SAC FII MASCW processed, C- CBZ/SAC FI CSD data and D-CBZ/SAC FI MASCW processed	163
6.7	DSC thermograms of batches carried at different process temperatures	165
6.8	DSC thermograms of experiments performed at different amount of water	166
6.9	DSC endotherms of batches carried out at 300W and 400W	167
6.10	DSC thermograms of two cocrystal batches at different heating rates	167
6.11	DSC thermograms of A) CBZ: SAC 1:1.5_12.5ml water, B) CBZ: SAC 1:1.5_15ml water, C) CBZ: SAC 1:2_12.5ml water and D) CBZ: SAC 1:2_15ml water	168
6.12	DSC thermograms of CBZ/SAC Form I and FII processed by MASCW	168
6.13	Calibration curve for iminostilbene	169
6.14	Chromatogram representing the separation of CBZ and iminostilbene	170
6.15	SEM images of CBZ/SAC cocrystal form I process from MASCW	171
6.16	SEM images of CBZ / SAC co-crystal Form I obtained from solution crystallisation	172
6.17	SEM images of CBZ/SAC cocrystal form II process from MASCW	172
6.18	Dispersive surface energy plot for CBZ/SAC cocrystal FI and FII obtained from MASCW process and CBZ/SAC FI obtained from solution crystallisation	174
6.19	Solubility vs temperature profile for CBZ: SAC form I	176

	and form II cocrystal phase	
6.20	PXRD patters of : A) SMT_SAC 1:1 CSD-(XOBCOH), B) SMT raw, C) SAC raw and D) SMT: SAC 1:1 cocrystal	177
6.21	PXRD patterns of A) SMZ raw, B) SAC raw and C) SMZ: SAC 1:1 cocrystal	178
6.22	DSC endotherms of: A) SMT raw, B) SAC raw, C) SMT/SAC 1:1 physical mixture and D) SMT/SAC 1:1 cocrystal	179
6.23	DSC endotherms of A) SMZ raw, B) SAC raw, C) SMZ/SAC 1:1 physical mixture and D) SMZ/SAC 1:1 cocrystal	180
6.24	PXRD patterns of solution crystallisation pattern of CAF/4HBA cocrystals A-CAF-4HBA (1:1) CSD, B-CAF-4HBA (1:2) CSD, C-CAF-4HBA (2:1) CSD, D- CAF-4HBA (2:1) Solcryst, E-CAF-4HBA (1:2) Solcryst and F-CAF-4HBA (1:1) Solcryst	183
6.25	PXRD patterns of MASCW process batches of CAF/4HBA cocrystals **A**-CAF-4HBA (1:1) CSD, **B**-CAF-4HBA (1:2) CSD, **C**- CAF-4HBA (2:1)CSD,**D**-CAF-4HBA(1:1)-SCWP,**E**-CAF-4HBA(1:2)-SCWP,**F**-CAF-4HBA (2:1) – SCWP	184
6.26	PXRD patterns of CAF/4HBA 1:1 cocrystals produced from a MASCW process using a solvent mixture (50%-50% MeOH-water) as a solvent system. **A**-CAF/4HBA 1:1 cocrystals produced from MASCW, **B**- CAF-4HBA (1:1) CSD, **C**- CAF-4HBA (1:2) CSD, **D**- CAF-4HBA (2:1) CSD	185
6.27	Overlay of DSC and TGA thermogram of CAF/4HBA 1:1 processed using MASCW process	187
6.28	NMR spectral comparison of CAF: 4HBA 1:1 cocrystal in d6-DMSO	188
7.1	PXRD patterns of MASCW processed samples-**A**-PAR FI CSD, **B**- PAR FII CSD, **C**-PAR starting material, **D**- PAR FII MASCW processed, **E** – PAR FI MASCW processed	195
7.2	A) Full range spectra of pcal raw form I, MASCW processed a form I and MASCW processed form II. B) Zoomed spectral region to identify the characteristic distinct peak marking of form II polymorph of pca generated by MASCW process	196
7.3	Practical DSC thermogram of paracetamol FII processed	198
7.4	Practical DSC thermogram of paracetamol FI processed	198

7.5	HPLC chromatogram of distinctive peaks of paracetamol and 4-aminophenol raw	200
7.6	Calibration curve plot for 4-aminophenol	200
7.7	SEM images of paracetamol raw, PAR FII MASCW processed, PAR FI MASCW processed	202
7.8 A	Comparative profile of dispersive surface energies of pca raw form I, MASCW processed form I and form II	205
7.8 B	Comparative profile of specific surface energies of pca raw form I, MASCW processed form I and form II	205
7.8 C	Comparative profile of total surface energies of pca raw form I, MASCW processed form I and form II	206
7.9	Solubility profile of raw and MASCW process pca in water at ambient conditions	208
7.10	Drug release profile of paracetamol raw and MASCW treated	210
7.11	Raman spectral data for pca form II suspension a) full range spectra and B) magnified view of Raman shift between (1150-1300cm-1) highlighting presence of pca form II characteristic peak at 1220 and 1245cm-1	211
7.12	SEM images of THF S1 raw theophylline, THF S2 antisolvent treated THF, THF S3 ultrasound treated THF, THF S4 manually treated THF and THF S5 spray dried THF	215
7.13	PXRD pattern for all processed and raw THF samples	217
7.14	DSC thermogram of raw and processed THF powder samples	218
7.15	TGA thermograms of raw and processed THF samples	219
7.16	FTIR spectra for theophylline raw and processed samples	220
7.17	Total surface energy of THF raw, THF MASCW and THF SD	222
7.18	Thermodynamic work of cohesion (mJ/m2) of THF raw, THF MASCW and THF SD processed	223
7.19	Thermodynamic work of adhesion (mJ/m^2) between THF and Lac IG blend	224
7.20	Graphical representation of amount deposition of theophylline dose in different stages of NGI	227
7.21	Graphical representation of amount deposition of theophylline-lactose IG blend formulations in different stages of NGI	230
8.1	Structures of: (a) ibuprofen monomer, 2-(4-isobutylphenyl) propanoic acid, and (b) dimer of ibuprofen highlighting the hydrogen bond between carboxyl groups	234

8.2	PXRD pattern of A) HA synthesised using conventional mixing method and B) HA synthesised using MASCW process	236
8.3	PXRD patterns of a) raw, or as-prepared, hydroxyapatite, b) hydroxyapatite calcined at 1000 °C	237
8.4	ATR-FTIR spectrum of raw hydroxyapatite	239
8.5	XRPD patterns of a) raw hydroxyapatite, b) commercial, or as received, ibuprofen from the supplier, c)commercial ibuprofen recrystallised in ethanol, d) ibuprofen/hydroxyapatite (ibuprofen/HA) complex.	241
8.6	SEM micrographs of a) raw hydroxyapatite, b) commercial, or as received, ibuprofen from the supplier, c) commercial ibuprofen recrystallised in ethanol, d) ibuprofen/hydroxyapatite (ibuprofen/HA) complex	242
8.7	SEM micrographs of a) as received ibuprofen, b) same as a but after 4 min exposure to electron beam radiation; c) ibuprofen/HA complex, d) same as c but after 4 min exposure to electron beam radiation	244
8.8	ATR-FTIR spectra of a) ibuprofen/HA complex and b) ibuprofen recrystallised in ethanol	245
8.9	ATR-FTIR spectra of a) Ibuprofen in ethanol on the ATR crystal, b) same as a) but dried on the ATR crystal for 4 hours	246
8.10	Area of the FTIR spectra characteristic of H-bonding attachment: (---) pure Ibuprofen, (---) physical mixture of Ibuprofen and HA and (---) microwave assisted synthesis of Ibuprofen/HA complex.	247
8.11	Kinetics of the ibuprofen/HA complex formation, *ex situ* ATR-FTIR measurements of the carbonyl region of ibuprofen between 6 and 180 min.	249
8.12	Drug release profile of: as received ibuprofen (■), physical mixture of ibuprofen and hydroxyapatite (●) and hydrogen bonded ibuprofen-hydroxyapatite complex (ibuprofen/HA) (▲)	250

List of Tables

Table no	Description	Pg. no
2.1	Definitions incorporating terms used in polymorphism	40
2.2	Different rules reported understanding the relationship between polymorphs and single component system	46
4.1	Summary of materials used and their chemical structure	71
4.2	Equipment specification	74
4.3	List of software used for data processing	75
4.4	Exp design for cocrystallisation using MASCW process	88
4.5	Exp design used to analyse the specific surface area	92
4.6	Experimental design to analyse surface heterogeneity	92
4.7	Experimental conditions for SMT: SAC and SMZ: SAC cocrystals	96
4.8	Summary of experimental design of CAF-4HBA cocrystallisation using MASCW process	99
4.9	Summary of experimental conditions used to process paracetamol using MASCW process	103
4.10	Summary of HPLC method (gradient)	104
4.11	Experimental description of various batched of theophylline	109
4.12	Experimental parameters used to crystallise THF using SD	110
5.1	Summary of solubility vs temperature data	128
5.2	Pictographic representation of the correlation between solubility of different concentrations of paracetamol and corresponding temperature conditions.	130
5.3	Summary of crystallisation time vs solution concentration for MASCW process and conventional heating experiments	136
5.4	Summary percent purity of paracetamol solutions using SCWT and conventional heating	137
5.5	Dielectric constant values of different solvent mixtures at RT	141
5.6	Summary of dielectric constant of pure solvent system, solvent mixtures and with paracetamol solute after MASCW treatment	143
5.7	Equilibrium solubility of paracetamol in solvent mixtures when treated using MASCW process and conventional temperatures and percent purity of MASCW process samples	146
6.1	Result summary of cocrystal phase obtained by altering different process parameters.	158
6.2	Summary of CBZ: SAC cocrystal phase obtained during	164

	crystallisation and the technique used	
6.3	Percent degradation of MASCW processed CBZ: SAC cocrystal samples using different parameters	170
6.4	Experimental data of CAF/4HBA cocrystals process using MASCW technique	182
7.1	Summary of experimental results of MASCW treated pca	194
7.2	Measured peak positions of all three polymorphs of pca	197
7.3	Percent assay of paracetamol treated at high temperatures	201
7.4	BET surface area of raw and processed paracetamol	203
7.5	Surface heterogeneity of pca raw sample	203
7.6	Surface heterogeneity of pca form I MASCW processed	204
7.7	Surface heterogeneity of pca form I MASCW processed	204
7.8	Summary of aqueous solubility of paracetamol MASCW treated versus commercial sample	207
7.9	PSD of pca raw form I, MASCW processed form I and form II	208
7.10	IDR dissolution data for pca raw, processed form I and form II	209
7.11	Mean particle size distribution data for raw and processed theophylline samples using different crystallisation techniques	214
7.12	Description of melting point and enthalpy values for all THF	218
7.13	Transition temperatures of THF samples	219
7.14	IR-band range index and structural properties of anhy THF	220
7.15	Description of emitted dose of theophylline samples	226
7.16	Total emitted dose of THF and lactose (IG) blend	229
7.17	Summary of NGI results of all THF formulations	231
8.1	Unit cell parameters from Rietveld refinement and crystallinity evaluations of nano-HA as-synthesised and calcined at 1000 °C.	238
8.2	FTIR active sites and structural regions of raw HA	240

Chapter 1: Introduction

1.1 Introduction

Active pharmaceutical ingredients (APIs) are frequently delivered to the patients in the solid state form (e.g., tablets, capsules, pellets) as part of an approved dosage forms as during storage of API or drug formulations solid state provides the most compact, convenient and generally stable state. In drug development and processing industry, understanding and controlling the solid-state chemistry of API, both as pure drug and in the formulation is the important challenge to be considered (Morissette et al., 2004). Recently, due to increased interest in the field of crystal engineering high throughput screening (HTS) is implemented to elucidate different physical and chemical properties of APIs. Based on recent finding of HTS about 30-40% of all identified APIs are hydrophobic in nature. The bioavailability of these insoluble drugs is highly based on its aqueous solubility and therefore to enhance the solubility and dissolution property is an important challenge for pharmaceutical processing and development industry (Maniruzzaman et al., 2013). As it is not feasible to substitute poorly soluble drugs with highly soluble drugs so large proportions of academic researchers and pharmaceutical industries are focused in developing new crystallisation or processing technologies to enhance their physicochemical properties like solubility, stability, rate of dissolution, bioavailability and compressibility by altering chemical and morphological properties of chemical components. There are various process technologies reported targeting the followings requirements in crystal engineering of APIs: 1) product purity to retain quality standards, 2) isolation of chosen crystal form, 3) generate targeted uniform

particle size and shape which will significantly affect bioavailability and processability, 4) high yield and 5) reasonable cycle time (Variankaval et al., 2008). Most traditionally used crystallisation technique is solution state crystallisation method in which based on the solubility of the solute in the organic solvent; a saturated solution is prepared and left for the solvent to evaporate when concentration between solute and solvent increases than the crystal starts inducing out. The main disadvantage of this method is use of an organic solvent which may cause toxicity side effects, formation of phase impurities (formation of solvates, hydrates) and time required for the crystallisation varies from days to weeks (Bruni et al., 2012). Sonic energy or Ultrasound assisted crystallisation is implemented in crystal engineering this is also referred as sonochemical crystallisation which includes sonic energy to induce crystal from supersaturated solution or slurry. Limitations of this technology includes the use of organic solvents, no phase pure crystals are formed, this technology is lacking in scalability (Aher et al., 2010) (Dejan-Kresimir Bucar et al., 2015). Another technique which includes use of organic solvents or aqueous solvent mixtures in particle crystallisation is Spray drying technique; this involves production of dry powder by rapid evaporation of solvents due to presence of hot air stream. Limitations of this technique are generation of impure crystal phases, less yield percentage, high static charges and use of organic solvents (Alhalaweh and Velaga., 2010). Freeze drying technique is used for generation of co-crystals, it is the technology where crystallisation occurs from amorphous state due to sublimation of solvent, the limiting factors are use of organic solvents, stability issues due to presence of residual solvent molecules, drying step is

long lasting and cost of processing is not economical (Eddleston et al., 2013). Solvent free technologies like Hot-melt extrusion (Choy 2003; Yang et al., 2007) are developed to eradicate the use of organic solvents, HME is the process where external shear and temperature is used to dissolve the ingredients by forming melts and generate co-crystals or amorphous solid dispersions of API and excipients (polymers, co-formers), the limiting factor in this technology is due to use of high temperature and shear conditions thermal degradation of drugs and polymers takes place (Dhumal et al., 2010) and due to use of polymer the stable drug load for formulation is less between 20-25%w/w between API and polymer. Recently supercritical fluid technology is developed to process non-polar bioactive and thermally labile components; this technology includes the use of supercritical carbon dioxide at high stress conditions as solvent system for the generation of particles. Due to its high capital cost, difficulty in controlling crystallisation pathway and use of solvent modifiers hindered its application in pharmaceutical processing industry (Revelli et al., 2014). Chemical vapour deposition (CVD) is the recent technology developed in crystal engineering; this technology involves dissociation of gaseous reactants in the activated heat, light, plasma environment which is followed by generation of powdered samples of solid products. The limiting factor is use of large volume of toxic, corrosive precursor gases, high temperature and pressure conditions, difficulty to work with multi-component materials, impurities in the final product and use of very sophisticated reactors which are not economically feasible (Choy 2003). Based on the above mentioned limitations of exiting technologies a novel green technology as Microwave assisted sub-critical water processing

(MASCW) technology for particle engineering was developed. Sub-critical water-process technology is a widely applied technology in biomass processing industry and extraction of biological active components from natural sources (Gbashi et al., 2016). As the longevity and lifestyle of humans has been profoundly impacted by modern pharmaceutics, since last few years this sub-critical water technology has been implemented in the field of pharmaceuticals to enhance the pharmacokinetic properties of pharmaceutical ingredients particularly hydrophobic drugs (Carr et al., 2011) but the experiments are performed in milligrams scale lacking commercial importance. In the present thesis upon considering all the limiting factors and challenges in the crystallisation and pharmaceutical processing technologies, scalable MASCW crystallisation technology has been reported for the first time, where water is acting as the green solvent system used for crystallisation and complex formation, microwave energy is used as external energy source to speed up the reaction by retaining chemical integrity of the components. This technology in my thesis is further explored for the generation of cocrystals (congruent and incongruent pairs), metastable polymorphs, API micronisation process for pulmonary drug delivery system and synthesis of biomaterials like hydroxyapatite and API loaded biomaterial complexes.

The present thesis work is categorised based on two major objectives: First objective, is process understanding and validation of different experimental and process parameters, secondly includes investigation the application of this technology for generation of cocrystals, polymorph, micro, and nano-sized particles for inhalation drug delivery system and complex formation

between API with inorganic biomaterials (hydroxyapatite). A brief description of individual chapters is explained below (Refer Section 1.2).

This technology is based on micronisation process where pharmaceutical ingredients are crystallised into micron or nano sized particles with altered smooth crystal habit. By micronising API particularly poorly soluble drugs, the rate of dissolution can be enhanced prominently which will aid in the drug distribution to the site of reaction (Clarke et al., 2011). Reduction in the particle size of the drugs the effectiveness of the drug can be increased, which could reduce the required drug dose, reducing cost and risk of side effects caused due to excessive use of drugs.

Various process parameters of the crystallisation process determine different chemical and physical attributes of crystal products such as size, shape, purity and polymorphic form, these properties affect the different physicochemical properties of individual drugs or drug formulations (Yu et al., 2007). The positive aspects of this technology are:

- Pathway of crystallisation and specifications of the end products can be monitored easily by controlling different process parameters.
- It is a single continuous process where reaction kinetics is continuous and quick.
- Based on the dielectric constant of water and level of supersaturation metastable phases of co-crystal pairs and polymorphs can be generated with enhanced physical and chemical properties.
- It includes water as the only green solvent system for the formation of a non-covalent interaction between APIs and excipients; therefore the risk of residual organic solvent is eliminated.

- Heating and cooling steps are well controlled retaining bioactivity of APIs. There is no degradation of the API taking place as it is not subjected to large shear conditions.
- Due to the use of microwave energy uniform heat transfer occurs between solute and solvent molecules which prevent product impurities and reduce the processing duration add reference.
- Most importantly, this technology is scalable from small scale to industrial processing scale; these experiments were performed by our industrial partner.

Microwave energy is used as the heating source for the water to enable faster and effective heating of water molecules to achieve the desired processing conditions and to retain solute chemical stability. The main principle on which the water at sub-critical level works is the change in dielectric constant of water at elevated temperature and pressure conditions, as it is well known fact that at high temperatures the dielectric constant of water decreases and the polarity increases, hence solubilisation property of water increases. The temperature range between 100°C – 374°C is referred as sub-critical temperature and the water in this range is referred as subcritical water. The water molecule in this temperature conditions has the properties to retain its elastic property (liquid state) upon cooling step (Adachi 2009) and when treated above this temperature than it is referred as supercritical water where the elastic property of water is lost in this region. The clear mechanism of this sub-critical water is pictographically represented in (Figure 1.1).

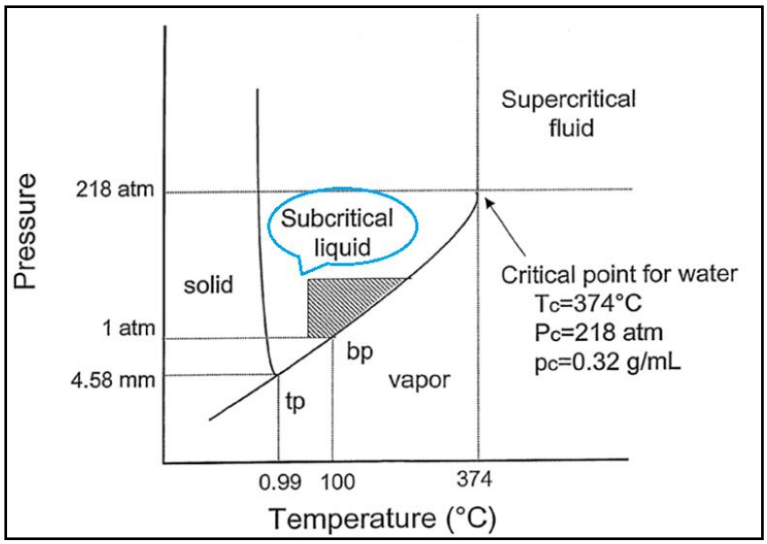

Figure 1.1 Phase diagram of water at elevated temperature and pressure conditions (Asl and Khajenoori 2013)

In MASCW technology volumetric and homogenous heating of water is involved which aid for the homogeneous nucleation process to take place during cooling step. Different properties of MASCW processed pharmaceutical ingredients are studied like surface properties, kinetic property, aerodynamic performance, solubility, dissolution rate and stability. While exploring this technology for cocrystallisation and polymorphism the challenges associated with thermal degradation, hydrate formation and effect of different process parameters on the end product was considered.

1.2 Research objectives

The main focus of this thesis is to investigate the potential applications of MASCW process technology in the field of crystal engineering for generation of micro and nano-sized API particles with enhanced physicochemical properties.

1. Understanding the physical and chemical properties of water at the subcritical level and proposing the mechanism of crystallisation.

2. Explore understanding regarding crystallisation kinetic of API using MASCW process.
3. Explore this novel technology in the field of crystal engineering for the generation of stable and metastable phases of both congruent and incongruent cocrystal pairs.
4. To understand the correlation between process and experimental parameters for the synthesis of stable and metastable polymorphs of API.
5. To develop commercially potential technology for transformation from small scale to large scale.
6. To investigate the use of this process for development of drugs with high compressibility for tableting process and aerodynamic performance for inhalation drug delivery system.
7. To investigate the use of the MASCW process for complex formation between API and biomaterials.

1.3 Thesis outline

Chapter 2 – includes literature review and background, literature review includes three sections 1) brief description regarding supramolecular chemistry, different solid form, 2) include description regarding cocrystal complex, mechanism of cocrystallisation, its applications, challenges and different technologies used for cocrystallisation, 3) this section includes description regarding polymorphism, rules for predicting pathway of polymorphism and applications.

Chapter 3 – includes background description of subcritical water process, its applications, the structure of water and effect of different process parameters

on subcritical water process. A brief discussion of the chemical structure of water, the effect of microwave energies and application of microwave reactor is described. The description regarding present work and proposed mechanism of microwave assisted subcritical water (MASCW) is schematically described.

Chapter 4 - includes the materials and methods section, this section is further categories into three sections. Section one includes the structural and chemical description of all the drugs, excipients and solvents used in this research work. Section two includes the summary of different experimental designs and conditions implemented to study and understand the technology and the final section includes the brief description regarding the general working principles of different analytical tools and software versions used to analyse the data.

Chapter 5 - includes process understanding and validation of MASCW process, for this, different process and experimental conditions were considered to understand and validate MASCW process technology. Based on the solubility, physical and chemical properties paracetamol was selected as a model compound to investigate the correlation between supersaturation solution concentration and crystallisation time using MASCW process and further comparing the results with conventional heating process. Correlation between the paracetamol solubility and temperature-pressure parameters is explored. Effect of process temperature and pressure conditions on the chemical stability of paracetamol is analysed using high-performance liquid chromatography.

Crystallisation kinetics of MASCW treated a supersaturated solution of paracetamol is monitored using Raman spectroscopy over 22hrs. Different solvent mixtures of methanol-water, ethanol-water, acetonitrile-water and acetone-water at 10, 20 and 30% v/v concentration were selected to understand the effect of the solvent mixture on the dielectric constant of the solution, equilibrium solubility of paracetamol in solvent mixtures, physical state and chemical stability of paracetamol.

Below Figure 1.2 represents the schematic diagram to summarise different experiments performed to explore the application of the MASCW process in crystal engineering and complex formation.

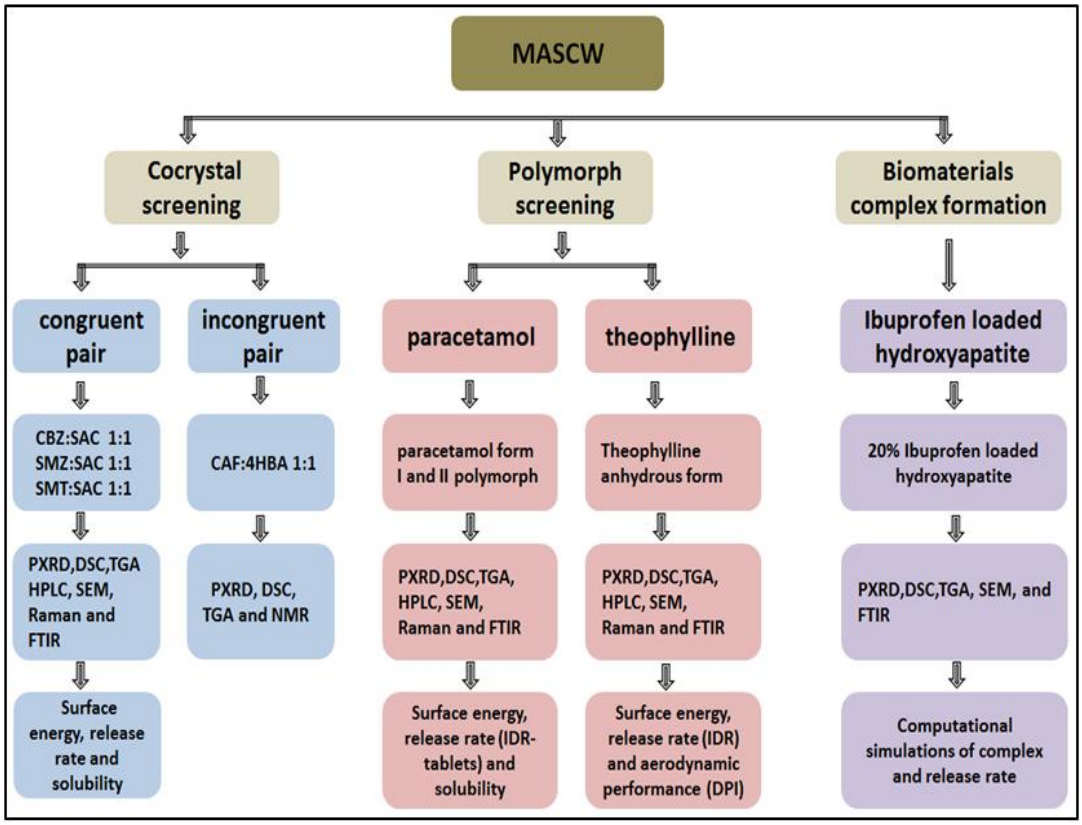

Figure 1.2 Schematic representation of research work

Chapter 6: After process validation in this section the application of MASCW technology for generation of stable and metastable cocrystal pairs was explored. Carbamazepine (CBZ) and saccharine (SAC) cocrystal pair were

considered for the production of stable form I and metastable form II cocrystals of CBZ-SAC cocrystal in 1:1 stoichiometric ratio, along with this pair sulfamerazine and sulfamethazine cocrystals were produced using SAC as co-former. Effect of process parameters like temperature, energy, solvent concentration, and solute (API)-solute (coformer) concentration on phase purity of end product is investigated. All the above pairs for cocrystallisation are congruent pairs based on their solubility in water. For the first time, the effect of solvent mixture for the product of incongruent pair cocrystal of CAF: 4HBA in 1:1 stoichiometric ratio was explored (Aher et al.,2010).

Chapter 7: This section is further divided into two section, the first section includes generation of stable and metastable polymorphs is investigated using paracetamol as the lead API for production of paracetamol form I stable and paracetamol form II metastable polymorph. Equilibrium solubility, intrinsic dissolution rate and surface properties of this MASCW treated paracetamol form I and form II is investigated keeping raw paracetamol form I as a reference. In this section, the scalability of this technology is explored by performing the experiment on the large-scale manufacturing unit by our industrial partner.

In the second section, MASCW technology is used to explore its application for the generation of micron-sized stable particles for inhalation drug delivery route using dry-powder inhaler device. Anhydrous theophylline (THF) is selected as a model component for inhalation drug delivery route and aerodynamic performance of MASCW treated THF is investigated against conventional spray-dried THF.

Chapter 8: In this final chapter this technology is implemented in the synthesis of phase-pure hydroxyapatite (nano-crystalline) and further complex material is formed between the synthesised nano-crystalline HA and ibuprofen as API. Mechanism of the hydrogen-bonded complex formation between IBU and microcrystalline HA is studied using infra-red spectroscopy and computational simulations were performed to understand the mechanism of complex formation.

Chapter 2: Literature review

2.1 Introduction

The drug discovery and processing industries are facing considerable challenges as they progress through development stages due to increase in processing cost, a decrease in productivity, side effects caused due to use of chemicals during processing pharmaceutical products. Most of the biopharmaceutical industries are facing challenges due to decrease in output in comparison with the enormous increase in pharma R&D spending. Most of the big pharma companies had prodigiously invested a huge amount in novel technologies such as combinatorial chemistry, structural based design of the drug, high-throughput screening (Rodríguez-Spong, 2004) and genomics but all failed in generating productivity. US companies have invested $100 million dollars in HTS technology with the promise of enhancing drug productivity but so far it has been successful with very few products. This challenge of cost, productivity issues, challenges from generics and ever-increasing regulatory issues has forced many drug developers to become more creative in finding new applications of present drugs, to develop new novel green technologies for processing pharmaceutical drugs and to develop new versions of existing drugs with enhanced physicochemical properties (Ashburn and Thor, 2004).

Due to present trend of mixed models of drug discovery and development, it has driven great opportunity for the different collaboration partners of different expertise to contribute unitedly in the field of pharmaceutical drug discovery and processing industry. Academic research has traditionally proved to be the powerhouses for the discovery of innovative drug

processing technologies and understanding the science and applications of the technology (Tralau-Stewart et al., 2009). The main objective of the pharma industries is to develop and discover medicines which are acceptable by regulatory authorities, patient healthcare bodies and healthcare providers. They expect to reduce the cost of the drug processing, maintain process drugs safely and improve patients quality of life, thus based on the current challenges cost of processing drugs, quality of drugs and speed of processing has become the potential requirement for all the drug discovery and development activities (Elebring et al., 2012).

Pharmaceutical product development is proprietarily driven by rigorous and continuous innovation in the fields of drug discovery, process engineering, drug polymorph design and dosage form design fulfilling regulatory standards. About 90% of the new APIs are having low aqueous solubility so micromeritic properties and solubility of APIs has become very prevalent in the research and development of new drugs. Thus primary aim of the pharmaceutical industry is to generate new pharmaceutical material engineering technologies to design pharmaceutical particles and dosage forms which results in an increase in efficiency of the manufacturing process, resulting the high degree of functionality to the drugs and pharmaceutical excipients (El-Zhry El-Yafi and El-Zein 2015).

In the present thesis, the proposed new technology is implemented to manipulate the physical properties and chemical form of pharmaceutical ingredients and excipients to enhance their chemical stability, thermodynamic and kinetic performance. Earlier drug discovery is based on serendipitous discoveries or through traditional ways but since last two

decades due to increasing in the number of unknown diseases and development of drug resistance by the microbes, the development of new rational remedies for the design and processing of drugs is highly in demand (Thakuria et al., 2013b). Various drug processing technologies like high-throughput screening and combinatorial chemistry were developed to enhance the solubility and dissolution rate of lipophilic drugs. Various studies have been proposed to understand the molecular association and molecular chemistry of chemical ingredients.

2.1.1 Supramolecular chemistry

Supramolecular Chemistry is firstly proposed by Jean-Marie Lehn (Chiou, 1969) which deals with the study of molecular association and intramolecular bonding involved between the reactant molecules. This involves the study of the non-covalent interaction between two chemical entities where one is referred as a host molecule and the other is referred as a guest molecule. Currently, supramolecular chemistry has further extended its understanding of molecular assembly, molecular recognition and self-assembly. Supramolecular chemistry has become interdisciplinary study as it includes nano-chemistry and certain complex materials (Ismael Rafols., 2010).

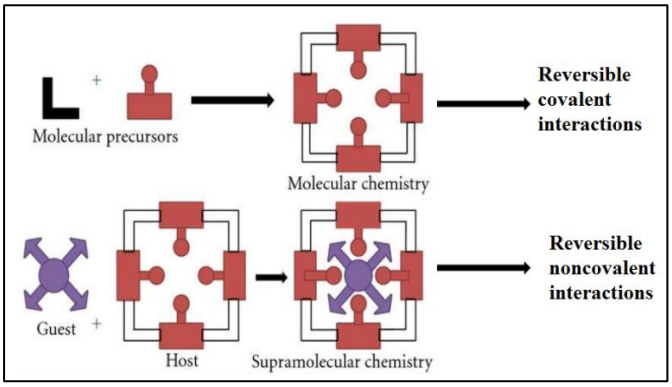

Figure 2.1 Pictographic representation of a comparison between molecular chemistry and supramolecular chemistry (Kumar 2014)

2.1.2 Solid State chemistry

Due to vast variations in the chemical properties of the solid materials, it is not understood completely. To understand the solid-state chemistry it is very important to have the knowledge regarding the physical, chemical properties of the solid materials and the interactions which are responsible for holding the solid materials together. The study of the solid state generally deals with the synthesis of organic and inorganic materials, its characterisation, crystal structure properties and applications in various medical devices. Recently a new branch of chemistry has taken birth from solid state chemistry which is termed as *"Materials Chemistry"* which deals with the non-molecular and molecular materials. These materials are increasing the interest of the researchers as it has improved the understanding of structure-property relationships. Generally, X-ray diffraction technique is used to study the molecular motions in the lattice, lattice arrangement of the molecules, and the extent of crystallinity. Crystal Engineering is the newly evolved section of solid state chemistry which deals with the design and modeling of new crystal structures with similar or different molecules which act as building blocks. This study demands the detailed understanding of the molecular structure and interactions between the molecules which act as a building glue for the crystal. This study gained importance when Bragg's discovered X-ray crystallographic study of naphthalene and anthracene.

Most of the pharmaceutical industries are concerned with the optimisation of API to attain required therapeutic activity. During formulation, certain physical properties like dissolution rate, solubility, physical and chemical stability and hygroscopicity are considered (Jones.W, 2006). Most of the API dosage

forms are solid dosage forms which exist in the crystalline or amorphous forms, but due to instability under storage and processing conditions they get converted into different forms which are responsible to induce adverse effects or desired effect is not attained. This diversity is due to non-covalent interactions between the components and the interplay between the enthalpy and entropy (Duarte, 2006). To surmount this hurdle various substituted forms like API hydrate, solvate, salts, polymorphs were generated and analysed using single crystal data and advanced analytical tools but recently pharmaceutical co-crystal has brought into focus which has given positive results in optimising physical and chemical properties of various API's (Jones. W, 2006). Various studies and process technologies were developed to produce API with improved physicochemical properties out of which cocrystal generation displayed improved physicochemical properties of API displaying good stability.

2.1.3 Classification of Solid forms

Solids are defined as the form of matter with definite shape and volume due to their rigid molecular arrangements. Intermolecular forces in the solids are strong interactions so they don't possess translatory motion, they can only vibrate from their positions until an external force or stress is applied. Based on the above properties of the solids there are mainly classified into two categories amorphous and crystalline solid forms (Sekhon, 2009). Figure 2.2 illustrates the classification of different solid forms of API into its substituent's based on its chemical structure composition and molecular arrangements. Co-crystals come under the category of multicomponent crystalline forms which consist of two or more chemical components fused together in a single

crystal lattice. Polymorphs are categorised under the single component system as they occur within the same molecule.

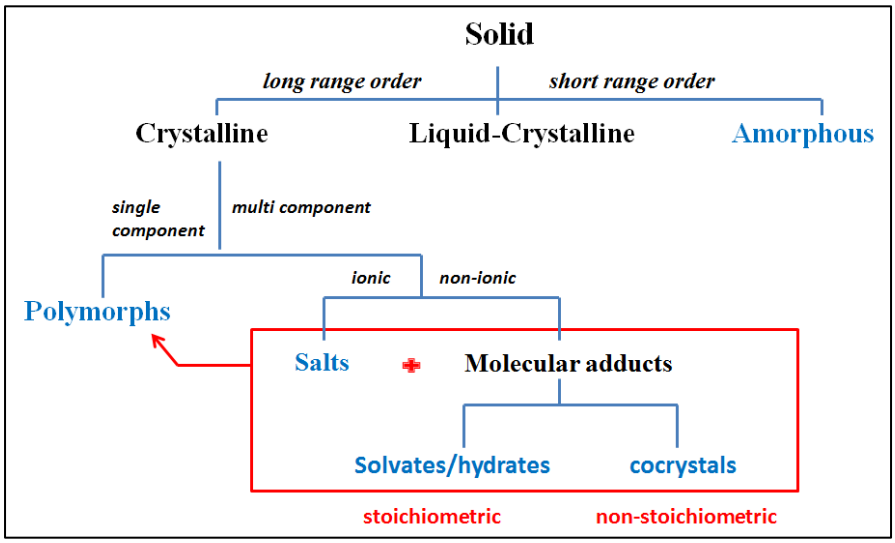

Figure 2.2 Classification of solid forms based on structure and composition

Amorphous solid forms are also referred as non-crystalline solid forms as they lack arrangement in long-range order which is characteristic of a crystal. The molecules in the amorphous solid are not arranged in the particular order so they lack crystallinity. Other materials which come under amorphous solid forms are gels, polymers. Crystalline solid forms based on the number of components are further classified as a single component when only one chemical component is involved in representing the crystalline structure and multicomponent system when two or more chemical components are involved in the formation of single components through different covalent and noncovalent interactions. Polymorphs are categorised under the single component system as this polymorphs keep the ability to retain similar molecular structure but vary in molecular conformations. In multicomponent system is referred as hydrates when the crystal lattice consists of a bonded water molecule. In a multicomponent system if there are molecules with

ionisable acid and base functional groups than these are referred as salts. APIs which undergo ionisation are included in this class of solids, there are very few salts like sildenafil sodium salt, piroxicam salt exists in zwitterion form (Mahajan and Sharma 2011). Salts, hydrates, and solvates are multicomponent systems which are similar to cocrystals but different in intermolecular bonding, stability, crystal structure and molecular arrangement (Newman 2009). Cocrystals are the multicomponent solid form which consists of two solid molecules which form a single complex through intermolecular bonding, which is attained in the presence or in absence of solvent system (Sekon 2009).

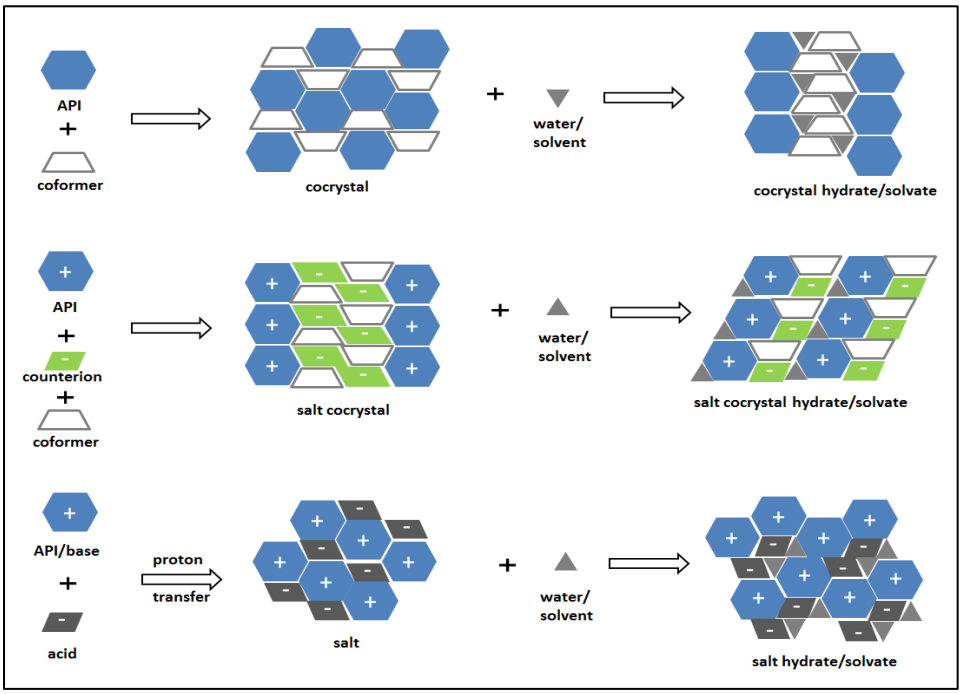

Figure 2.1 Possible multicomponent systems: cocrystals, salt cocrystals and derived multicomponent systems (Newman 2009)

Multicomponent system is referred as solvates when the solvent molecules retain the capacity to interact with the API and form the complex (Figure 2.3) (Aitipamula et al., 2012). It is analysed that about one third of the

pharmaceutical materials and formulations are sensitive to humidity conditions as they undergo hydrate formation during storage or when exposed to atmospheric moisture (Andrew V. Trask, 2005). Cocrystals gain advantage over amorphous material due to its low Gibbs free energy and stability to maintain its crystalline structure and they retain the phase purity whereas amorphous materials undergo phase transformation to crystal state during storage due to its molecular rearrangement.

2.2 Cocrystal

2.2.1 Introduction

The term “cocrystal” originates from “a composite crystal” (Rahul Banerjee, 2005), over the last decade, the co-crystallisation has become prominent and gained importance in the pharmaceutical processing sector. This increase in importance is due to the ability of the co-crystals to enhance the physicochemical properties like solubility, chemical stability, physical stability, dissolution rate, and bioavailability without altering the therapeutic properties of active APIs (Clarke, 2011) or without modifying the bioactivity of APIs (Newman, 2009). In the process of co-crystallisation involves molecular rearrangement and interaction between two or more chemical components which are responsible to sustain the fundamental physical properties (Newman, 2009). This new technique of cocrystallisation has gained the support of FDA on intellectual property right for developing and patenting new forms from “old drugs” (Duarte, 2006). According to FDA guidelines of 2013, the cocrystals are defined as “Molecular association of two or more ingredients in the same chemical crystal lattice” . Pharmaceutical cocrystal is defined as the crystalline complex of two or more chemical molecules

arranged in a three dimensional crystal lattice which are held together by non-covalent interactions generally hydrogen bond, halogen bond or π-π interactions (Jones. W, 2006). As discussed before that cocrystal molecular lattice consists of two components, one of the components is referred as Active Pharmaceutical Ingredient and other as cocrystal former (CCF, pharmaceutical excipient) (Clarke et al., 2011). This excipient (CCF) is responsible for the formation of weak non-covalent interactions with the API (Jones .W, 2006). As most of the API's exists in the crystalline form, a small modifications in its crystal structure may alter its physical and chemical properties, based on the similar hypothesis co-crystals are designed where the weak non-covalent bonds would exist between the API and CCF, which can alter chemical and physical properties without altering the therapeutic properties of the API (Sekon, 2009). To design cocrystal complex between two chemical components is not an easy task as various factors such as individual component solubility, lattice-free energy, Pka values are considered before forming cocrystal complex. Due to reported enhancement of physical and chemical performance of APIs through cocrystallisation process gained interest of various researchers, they have developed various methods for preparation of cocrystals, which include liquid assisted grinding (Trask et al., 2006), solution crystallisation, spray drying (Mehta, 2013), hot-melt extrusion (Kelly et al., 2012), ultrasound assisted crystallisation (Aher et al., 2010), supercritical crystallisation (Bala Subramaniam, 1997). In all these technologies, there are certain challenges which proved to be negative such as the use of large amount of solvents, process temperature is very high so degradation percentage is more, time consuming processes, non-uniform

ratios of API and co-formers are processed and very limited control over the process parameters (Daurio et al., 2011).The new technique introduced by research group from University of Bradford (UoB), omitted the use of solvent and the cocrystals were prepared from the solid-melt using hot-melt extrusion technology. UoB have introduced new solvent-free technology which is twin screw extrusion technology and titled it as SFCC (Dhumal et al., 2010).

2.2.2 Design of cocrystal

Cocrystallisation process is induces due to result of competing molecular association between two similar (homomers) or two different molecules (heteromers) through intermolecular non-covalent interactions such as hydrogen bond, Van-der-Waals forces and π-π interactions (Jampilek and Dohnal 2012). The two components in a cocrystal may exist in different stoichiometric ratios like 1:1, 2:1, 1:2. Crystal structure of cocrystal complex is different from original starting materials and as such they often exhibit different physical and chemical properties than the starting materials. Design and preparation of cocrystals of pharmaceutical ingredients is a multistage process as described schematically in Figure 2.4 (Qiao et al., 2011).

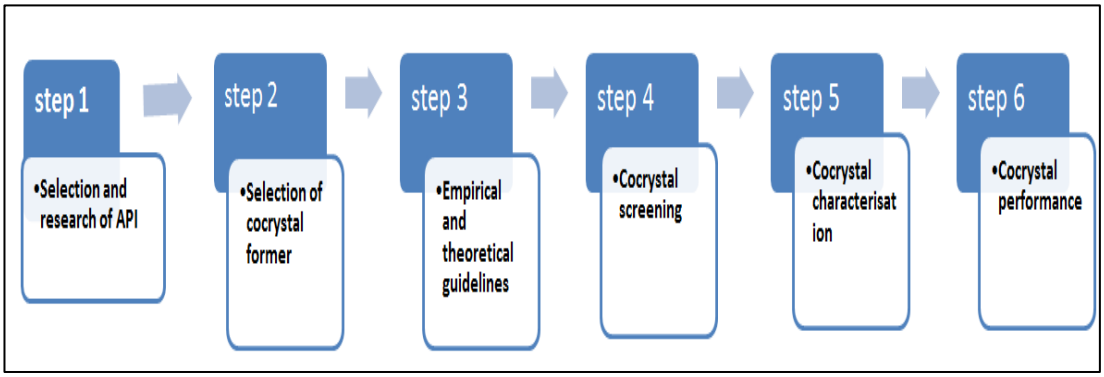

Figure 2.4 Schematic representation of steps involved in design of cocrystal

For the process of cocrystallisation to take place knowledge regarding the chemical nature of the coformer is very important because the chemical nature of the co-former decides the type of bonding between the API and coformer. Desiraju and co-workers have postulated that the selection of coformer is based on the “synthon” approach which is responsible for the interaction of specific fragments of API for the formation of “supramolecular synthon”. The functional group present on the drug and the coformer should be complementary to each other to form co-crystals. This association is based on the type and bonding properties of the functional groups present on the API and coformer. Some typical supramolecular synthons are carboxylic acid-acid synthon, amide-amide synthon, the acid-pyridine heterosynthon and acid-amide synthon are shown in below Figure 2.5 (Thakuria et al., 2013a).

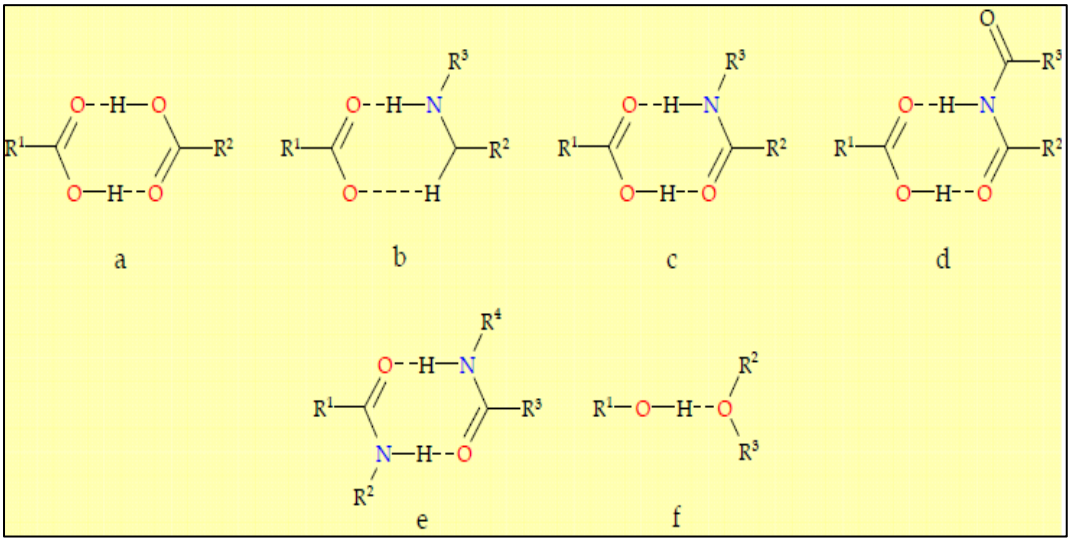

Figure 2.5 Types of hydrogen bonding between two synthons (a) acid-acid, (b) acid-amine, (c) acid-amide, (d) acid-imide, (e) amide-amide and (f) alcohol-ether.(Thakuria et al., 2013a)

The limitations of the synthon approach are that the steric hindrance, molecular arrangement, steric density around the functional groups and

competition between them are not considered. Later, Fabian and Fayos considered the polar density and crystal shape which are the important factors for the generation of co-crystal (Khuwijitjaru, 2014). The computational prediction is done by Hunter, Sally Price and coworkers for predicting cocrystal formation, this method is accepted and brought into practice by various researchers (Thakuria et al., 2013a). According to US-FDA guidelines, the selection of API and cocrystal former for cocrystallisation are based on its pKa value between the acidic and basic conjugates. This enables us to study the interaction between API and coformer is either ionic or non-ionic interactions.

If ∆pKa value is less than zero, where very less proton transfer take place than the reaction is driven to form cocrystals

$$\mathbf{A-H+B \leftrightarrow A-H\ldots.B} \quad \text{(Properties)}$$

If the ∆pKa value is greater than three, proton transfer is expected then the reaction results in salt formations.

$$\mathbf{A-H+B \leftrightarrow A-B^{+}\ H^{-}} \quad \text{(salts)}$$

If ∆pKa is > 0 < 3 then it becomes difficult to predict the degree of ionisation.

2.2.3 Challenges in cocrystallisation process

There are various obstacles in the co-crystallisation process such as scalability, reproducibility, stability, purity and other physical and chemical properties. Apart from various advantages for the co-crystallisation, there are certain factors need to be considered as process parameters, selection of co-crystal pair, incongruent soluble pair, spring-parachute effect and various physicochemical properties.

2.2.3.1 Incongruent co-crystal pair

Technologies like solution crystallisation spray drying, slurry crystallisation, solvent evaporation, cooling crystallisation and anti-solvent crystallisation include the use of the solvent system for the generation of co-crystal. So it is very important to consider the solubility of two components in the solvent, if they are miscible then they are referred as a congruent pair and if the two co-crystallisation components are having a large variation in the solubility parameter in the given solvent then this type of pairs are referred as an incongruent pair. In incongruent pair as the solubility of the two components vary largely, the level of supersaturation in the selected solvent system will not be achieved and as a result crystals of API or co-former or their solvates or hydrates induce as an impurity (Rager and Hilfiker 2010). Example for the incongruent pair is caffeine and maleic acid, recently Mehta and group (Alhalaweh et al., 2013) proposed the diversities obtained in stoichiometric ratio when caffeine and maleic acid in aqueous solutions were spray dried.

Different approaches are been adopted by various researchers to for stable cocrystal complexes of incongruent pairs: (1) preparation of a supersaturated solution of two components using a solvent mixture, the solvent mixture will further reduce the dielectric constant of the solution compared with the individual solvent system. This promoted the increase in solubility of the two components in the solvent mixture (Childs et al., 2008; Rager and Hilfiker 2010),Sander and group selection of two components in different stoichiometric ratios to prevent stoichiometric diversity (Sander et al., 2010) (Porter et al.,2008), (Aher et al., 2010) used surfactants to enhance the solubility of sparingly soluble pharmaceutical compounds.

2.2.3.2 Spring-parachute effect

The spring-parachute effect is implemented to increase the bioavailability of poorly soluble APIs by enhancing their solubility. This effect is used in formulations like amorphous formulation (solid dispersion), salts, self-emulsifying formulations and co-crystals (Childs et al., 2008). It has been derived based on the solubility curve generated by the API formulations. Spring represents the sudden increase in the solubility of the API in the media and parachute indicates the time interval where the desired therapeutic concentration has been attained. These two effects occurring simultaneously are important to attain desired therapeutic effect. If parachute effect is missing, the drug release is very fast and quick that the desired therapeutic effect is not attained. In the field of co-crystals, this effect is seen when the crystalline API gets transformed into an amorphous form which is spring effect and this amorphous form over a period of time gets converted into insoluble crystalline API which is parachute effect. Nangia and group have proposed the importance of selection of coformers to obtain this effect (Babu and Nangia, 2011)

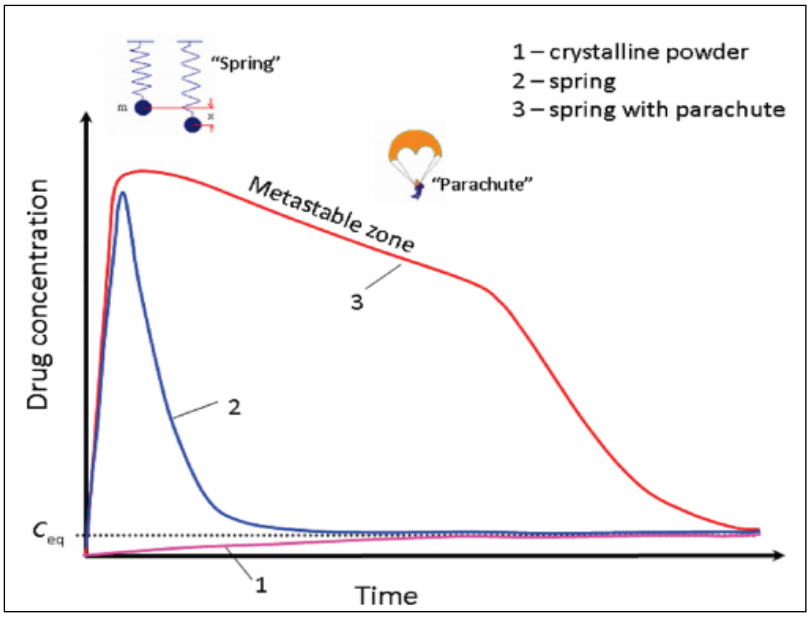

Figure 2.6 Graphical representation of spring-parachute effect. (Babu and Nangia 2011)

Velaga group has demonstrated the spring without parachute effect in case of indomethacin/saccharin co-crystals with less in vivo bioavailability. Recently to enhance the bioavailability of API in the dissolution media, certain biocompatible polymers are used which enhances the solubility and bioavailability (Childs et al., 2013).

2.2.4 Mechanism of cocrystal formations

Understanding the molecular interactions responsible for the formation of molecular complexes is very important not only in understanding the ability to control pharmaceutical properties by monitoring covalent bonds but also it is used to design new pharmaceutical materials. In the recent years, advances in the field of crystal engineering and supramolecular chemistry have gained the interest of many scientists to perform advanced research on pharmaceutical materials to form cocrystals (Jones.S., 2006).

Different technology and methods were developed to produce and understand the mechanisms of cocrystallisation. The proposed mechanisms are solution state reaction crystallisation, thermal fusion method, the eutectic and vapor phase method and deliquescence methods.

2.2.4.1 Solution state crystallisation mechanism; is an ancient method of crystallisation where the solute based on the solubility it is dissolved in the solvent and kept in the ambient conditions for the solvent to evaporate and based on solute/solvent supersaturation level crystals starts inducing out. This reaction crystallisation mechanism is based on the chemical association between the solute and the solvent molecules, this molecular association acts as the driving force for the crystallisation to take place. The theory states that difference between the individual solubility of the chemicals at the equilibrium and at the supersaturated state is an important factor to be considered to predict the rate of crystallisation.

If a binary phase cocrystal pair of 1:1 molar stoichiometric ratio is dissolved in the pure solvent system into its individual components with no further complexation to form a saturated solution, the molar mass balance of individual components in the solution system can be explained in terms of molar solubility of cocrystals (*S*).

$$(\mathbf{A}) = \mathbf{S}\ \mathbf{and}\ (\mathbf{B}) = \mathbf{S}\ (\mathbf{equation.1})$$

The solubility product of the cocrystal components

$$\mathbf{K_{sp}} = \mathbf{S^2}\ \mathbf{and}\ \mathbf{S} = (\mathbf{K_{sp}})^{\mathbf{1/2}}\ (\boldsymbol{equation.2})$$

The above solubility product is derived for the solutions where the two cocrystal components are added in the equimolar ratios to form saturated solution but if non-stoichiometric solution component is selected with excess

amount of cocrystal component or ligand is added (*C*), then the molar solubility becomes

$$(\mathbf{A}) = \mathbf{S}\ \mathbf{and}\ (\mathbf{B}) = \mathbf{S} + \mathbf{C}\ (\mathbf{equation.3})$$

$$\text{therefore}\ \mathbf{K_{sp}} = \mathbf{S}(\mathbf{S} + \mathbf{C})\ (\boldsymbol{equation.4})$$

If excess amount of cocrystal former or ligand is present ***C>>S***, then

$$\mathbf{S} = \mathbf{K_{sp}}/\mathbf{C}\ (\boldsymbol{equation.5})$$

The derived quadratic equation is:

$$\mathbf{S} = \frac{-\mathbf{C} + \sqrt{\mathbf{C^2} + \mathbf{4K_{sp}}}}{\mathbf{2}} \qquad (\mathbf{equation.6})$$

The above-proposed equation predicts that excess addition of cocrystal component or ligand reduces the solubility of the cocrystal in the solvent system under ambient conditions. The equilibrium constant for this reaction is proportional to the thermodynamic activity product of the API and co-former. The co-crystal solubility can, therefore, be predicted by the solubility product if the activity of the solid is constant or equal to 1.

This relation is explained with the help of solubility phase diagram in Figure 2.7 (J. Sarah., 2006).

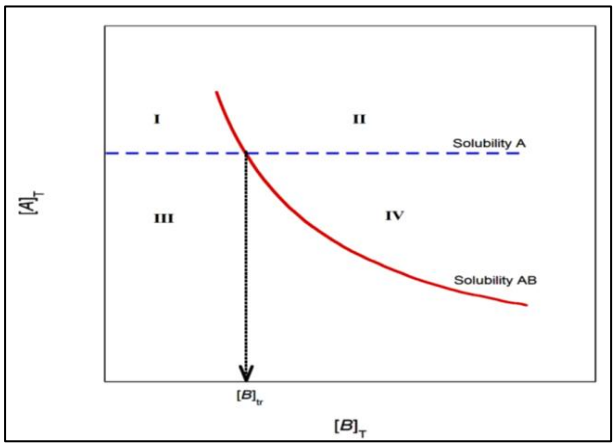

Figure 2.7 Solubility phase diagram of three components A, B, and cocrystal AB in the single solvent system.

The subscript ‘T’ is a total concentration of components and $[B]_{tr}$ is the transition concentration. The four different zones in the phase diagram is referred as I-IV. The above phase diagram is based on the following assumptions: 1) Component A is less soluble than component B, 2) A is less soluble than component cocrystal AB in the stoichiometric solution, 3) there is no complexation or ionisation of the cocrystals in the solution, and 4) solubility of component A is independent on solubility of B in the solution system. $[B]_{tr}$ is the transition temperature where the solubility of the cocrystal AB is equal to the solubility of component A.

Zone I in the phase diagram is the region where the component A is supersaturated and undersaturated with respect to cocrystal AB. In Zone II both AB and A is supersaturated and undersaturated in zone III. Zone IV is supersaturated with respect to AB and undersaturated with respect to A. The intersection point between the solubility of component A and AB cocrystal refers to the eutectic point and the solubility of the cocrystal can be calculated by using concentration of drug and coformer used. Group of (J. Sarah., 2006) proposed the above phase diagram to explains phase transformation occurring between the crystal and cocrystal in the solution. They have explained the effect of nonstoichiometric concentration of the two cocrystal components causing a reduction in the solubility of the cocrystal due to increase in the concentration of coformer and thus promote cocrystal crystallisation.

2.2.4.2 Heat fusion mechanism; is a thermal method where the external thermal energy is used to fuse two cocrystal components for the formation of

cocrystals. Recent years mixed Kofler method is used as the screening tool to visualise the cocrystal formation of different pharmaceutical components (Berry 2008). David and group have implemented this thermal fusion technique as the screening tool for visualisation of cocrystal formation of nicotinamide as coformer and different API containing carboxylic acid chain, they proposed that this technique is used to understand the thermodynamic properties of individual components and cocrystal. They visualised the formation of cocrystal under glass slide induced with temperature. The basic mechanism of Kofler technique is illustrated in Fig 2.7. Component A is the highest melting point component and component B is the low melting point. These components are subjected to temperature and allowed to melt and then the boundaries of the two melt components are brought in contact where the mixing of the two components takes place and cocrystallisation occurs at this contact zone.

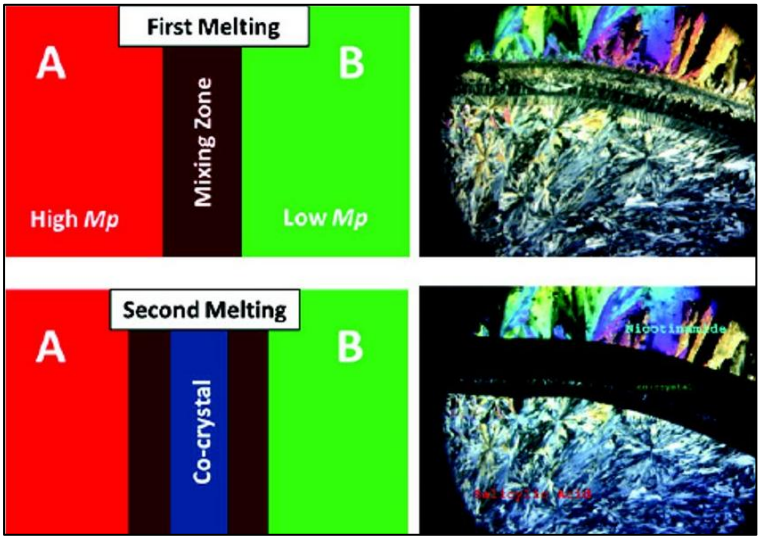

Figure 2.8 Zone of mixing in fusion mechanism for cocrystal formation

In the above Figure illustrates the pathway of cocrystal formation using thermo fusion mechanism using hot stage microscopy (HSM). Using HSM the eutectic melting profile of binary mixtures can be observed and maped. In

the above Figure higher melting component A is melted first and solidifies and then low melting component B is melted and brought in contact with component A, in the contact zone the solidified component A gets dissolved in liquid B producing a mixing zone and further when the sample is quenched cocrystals start inducing out. When these crystals are again heated till it melts a new cocrystal phase exhibiting birefringence can be observed (Nicole et al., 2012).

2.2.4.3 Eutectic or vapor phase mechanism; this theory explains the formation of cocrystals during mechanical grinding. This method has been implemented in the recent years, by the use of co-grinding of API and coformer either as dry solids (neat grinding) or by solvent drop grinding (liquid assisted grinding) (Chadwick., 2007). This technology gained the interest of the researchers as this method requires less or no solvent system for cocrystallisation so it is environmentally friendly and secondly this mechanism can be used as a screening aid to generate novel cocrystal phases which are not formed from conventional solution crystallisation. Despite evident use of this technology very little study is performed to understand the mechanism of cocrystal formation. Rastogi and group worked with solid state grinding of picric acid complexes for the formation of complexes, they postulated that vapor diffusion as mass transfer mechanism during solid-state grinding (N.B.Singh.,1965). During solvent drop grinding on the basis of the additional degree of freedom due to the molecular collision occurring during grinding seed of cocrystal is generated (Shan et al., 2002). A further mechanism of grinding is proposed explaining the eutectic effect is

the reason when the two components undergo molecular migration, the molecules can undergo gas-solid, solid-solid and solid-liquid reactions.

Recently eutectic effect is explained implementing mechanical grinding technology that during initial grinding experiment liquid phase is formed due to melt of the solid components and on further grinding this liquid and solid phase come in contact with each other and facilitate the formation of cocrystal seed (Chadwick ., 2007), binary phase diagram is also reported to explain the eutectic effect between two solid components during grinding.

2.2.4.4 Deliquescence mediated cocrystallisation; this method is based on the hygroscopic property of the cocrystal component. In this method deliquescence, mediated crystallisation has been proposed to describe the formation of cocrystals in the solution phase. Different cocrystals have shown phase transformation in presence of humidity which will further affect the stability of the API.

When two components containing deliquescent materials are selected the driving force for the cocrystallisation reaction to take place is the amount of moisture uptake by the deliquescent material at specific relative humidity, level of supersaturation of the two components and dissolution rate of the deliquescent component. Mechanism of moisture induced cocrystal is explained in below Figure 2.9.

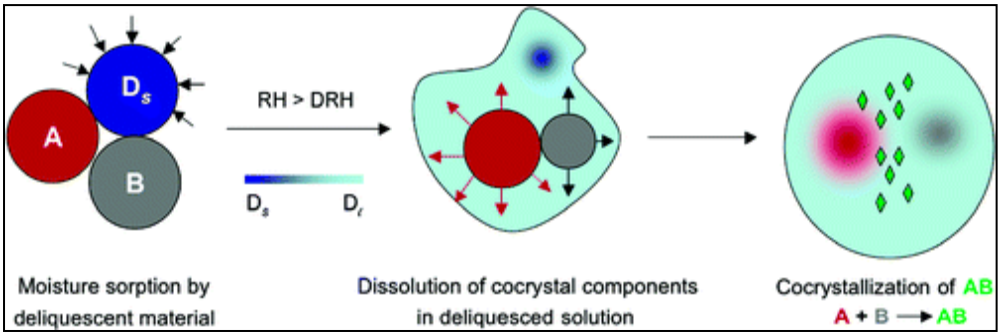

Figure 2.9 Pictogram of the mechanism of moisture in cocrystallisation, D_s deliquescent material, dissolution of cocrystal component and generation of a cocrystal of two components A and B (Jayasankar et al., 2007).

In this method, one component is highly hygroscopic in nature such as sugars, organic and inorganic salts. This component readily uptake the surrounding moisture and gets solubilised further this solution interacts with the second cocrystal component forming a thin layer, thus solution-mediated nucleation occurs due to the dissolution of the cocrystal component in the deliquescent solution (Jayasankar et al., 2007).

2.2.5 Applications of cocrystals

Various researchers based on the experimental evidence have stated that due to co-crystal formation there is an enhancement in physical and chemical performance of pharmaceutical ingredients. Applications of cocrystal formation are as follows:

A. Solubility enhancement - Cocrystallisation gained importance due to its capacity to monitor or enhance the solubility of pure APIs. This effect is observed by (Nehm, 2005) who demonstrated the phase solubility of CBZ/NIC cocrystals, which is higher than individual pure API (Rodríguez-Hornedo et al.,2008), they have studied the effect of

cocrystallisation used to enhance the solubility of poorly soluble ibuprofen. Fast dissolving curcumin is produced by this cocrystallisation approach by producing fast soluble polymorphs of curcumin (Sanphui et al., 2011). (Goud et al., 2014) group modulated the solubility parameters of sulfacetamide using cocrystal approach.

B. Improved physical stability - Caffeine, and piracetam as API are very sensitive towards moisture, they readily uptake the moisture under storage conditions and form hydrates. To enhance the physical stability of such components (Jones W, 2006),((Aitipamula et al., 2012) generated cocrystals of caffeine and piracetam with different cocrystal formers respectively.

C. Enhancement of bioavailability **-** (Dwayne T. Friesen 2008) used this process of cocrystallisation to increase the bioavailability of quercetin than pure quercetin API. (Xi Xu, 1996) used the cocrystallisation approach to enhance the bioavailability of baicalein.

D. Improvement of mechanical and compressibility of crystalline materials– Paracetamol in the commercial form I is very difficult to compress into tablets or granules so to improve this compressibility (Karki et al., 2009) produce cocrystals of paracetamol with a carboxylic acid to improve its compressibility. Mechanical properties of ibuprofen and fluriprofen were improved using cocrystallisation approach (Chow et al., 2012).

E. Enhancement of photostability - Vangala improved the photostability of nitrofurantoin (antibacterial API) which undergo degradation when exposed to sunlight by implementing the approach of cocrystallisation

with hydroxyl substituted benzoic acids (Vangala et al., 2012). Rodriguez- Hornedo used the process of cocrystallisation of CBZ/SAC to improve its photostability (Rodríguez-Hornedo et al.,2008).

F. Improving chemical stability - There are various APIs which are chemically unstable like andrographolide which gets converted into inactive metabolite during the chemical process so to overcome this hurdle (Suresh et al., 2013) used the approach of cocrystallisation to inhibit the chemical instability of andrographolide.

G. Enhancement of therapeutic activity - Due to the short residence time of APIs in the body, therapeutic activity is not reached to required amount. The example of such drug is sulfacetamide which is an antibiotic drug used for eye infection due to its low residence time in the eye region less therapeutic activity is achieved. To improve the residence time of sulfacetamide (Goud et al., 2014) and the researchers have used the process of cocrystallisation to increase its residence time in the eye region.

H. Colour tuning pigments - (Bucar et al., 2013) group analysed the mechanochemical cocrystallisation of fluorescein to synthesise new colored cocrystals.

Apart from these, cocrystallisation process has delivered various advantages to the science of solid-state chemistry by altering various physical and chemical properties of APIs.

2.2.6 Synthesis of cocrystals

Due to thermodynamic and kinetic challenges existing in formulating different APIs formulations, pharmaceutical manufacturers have started implementing

the technique of modulating crystalline API into different solid states (polymorphs, amorphous, solvates, salts, and cocrystals) to enhance physicochemical properties of individual API formulations. Screening of cocrystals has been recently a part of solid form development and design of active pharmaceutical ingredients (Clarke et al., 2011). Due to the heteromeric structure of cocrystal complex, it is very difficult to generate thermodynamically stable cocrystal moiety. The choice of cocrystal techniques is influenced by a not only number of experiments but also with a number of potential hits (Sladkova et al., 2014). Presently very few techniques are evaluated on the basis of efficiency of generation of cocrystals. As the process of cocrystallisation consists of molecular complexes between two or more components, various physical and chemical properties such as solubility, stability, and dissolution of the cocrystal components needed to be considered. Different cocrystal techniques are been reported by different research group globally to enhance the physical and chemical properties of active pharmaceutical ingredients.

Reported methods for cocrystallisation are: *Solution crystallisation* is the traditional method used for the generation of co-crystals based on the degree of supersaturation of the solute concentration in the solvent. This technique is also referred as solvent evaporation method (Bruni et al., 2012). Vangala and co-scientists have successfully generated the co-crystals of nitrofurantoin with substituted hydroxybenzoic acids. *Ultrasound-assisted crystallisation* technique sonic energy is implemented for the generation of cocrystals; it is also referred as a sonochemical reaction (Aher et al., 2010). *Spray drying technique* this technique involves the production of dry powder

by rapid evaporation of solvent due to the presence of hot air stream (Alhalaweh and Velaga 2010). *Freeze drying technique* cocrystals are formed from an amorphous state where the solvent gets sublimed (Eddleston et al., 2013). *Mechanochemical method* (Jones and Eddleston 2014,Hasa Dritan et al.,2017) Solvent-free continuous co-crystallisation (SFCC) (Dhumal et al., 2010), Thermal microscopy technique (Berry 2008) and Supercritical fluid technology (Revelli et al., 2014). In all the above-mentioned processes there are certain limitations in every technique but the common factor is the existence of external energy for the generation of co-crystals, the energy may be in the form of shear heat, sonic crystallisation, mechanochemical crystallisation and the involvement of solvent. Recently, solid state shear milling process was involved for generation of cocrystal, the limiting factor is generation of phase impurity occurs and optimisation of process parameters is difficult (Korde et al., 2018)

Various advance analytical tools like Powder X-ray diffraction (PXRD), thermal analysis- differential scanning calorimetry (DSC), thermogravimetric analysis (TGA), scanning electron microscopy (Jouyban et al.,2004), FT-IR and Raman spectroscopy are used to understand the mechanism and formation of cocrystals.

2.3 Polymorphism

In the recent years due to advances in the field of crystal engineering and supramolecular chemistry apart from drug cocrystallisation the subject of drug polymorphism has gained extensive academic and industrial attention due to the early reports presented by Aguiar and colleagues regarding the enhancement of drug dissolution and bioavailability due to drug

polymorphism of chloramphenicol palmitate (Singhal and Curatolo 2004). The structural perspective is based on the range of molecular arrangement and order of structure, in crystalline state molecules are repeatedly arranged in a definite crystal order and have similar extended molecular arrangement while in amorphous state or disordered solids they retain the similar local molecular assemblies but don't have extended range of molecular order, thus both crystalline and amorphous states exhibit similar intermolecular assembly but different in the order or arrangement of molecules. Polymorphism is defined as the crystalline material with similar chemical composition but differs in molecular conformation (Novoa 2008). Many scientists have tried to define polymorphism but in 1965, McCrone defined polymorphism as '*it is a solid crystalline phase of a given compound resulting from the possibility of at least two different arrangements of the molecules of that compound in the solid state* (Lee, 2014).

Polymorphism generally occurs due to the propensity of changing the molecular arrangement in the crystal lattice, its flexibility in the conformation of the molecules and the competition in supramolecular synthons. There are various chemical and physical properties which are affected by polymorphism such as solubility rate, dissolution properties, physical and chemical stability and bioavailability. Based on the arrangement of the molecules in the crystal lattice, the molecular flexibility, and supramolecular synthon arrangement, the process of polymorphism is further classified as conformational and pseudopolymorphism respectively.

Different analogies of polymorphism based on the supramolecular arrangements are described in the below Table 2.1 (Rodríguez-Spong et al., 2004)

Table 2.1 Definitions incorporating terms used in polymorphism

Polymorphism	-a substance with similar chemical composition but differ in the molecular arrangements and molecular conformation
Conformational polymorphism	-formed by the molecules which adopt different confirmation in the different crystal structure
Pseudo-polymorphism	-this includes crystal molecules having a solvent molecule or solvates and are classified in terms of structure as lattice channels, lattice sites, metal ions

Quantitative relationship between the mechanism of crystallisation and effect of factors responsible for polymorphism were not explored (Hulme et al., 2005). Kitamura and group based on crystallisation method and type of solvent system used , grouped these factors into two sections primary and secondary (Yu et al., 2000). Both these factors influence the thermodynamic and kinetic properties of polymorphic crystallisation. Primary factors include operational factors like temperature, supersaturation, seeding, stirring rate, cooling rate, the rate of addition if antisolvent, mixing rate of reactants on the other hand, secondary factors include interfaces, additives, solvent systems.

2.3.1 Thermodynamics and rules to predict polymorphism

When a compound exists in two or more solid forms, two factors needed to be addressed: relative thermodynamic stability of the entity or the pathway of phase transformation and factors affecting transformation and secondly the time required for the phase transformation to reach an equilibrium state (Brabander et al., 2002). The thermodynamic study will explain the pathway of polymorphism and kinetics will predict the time required to reach phase

equilibrium. They are different factors that govern solid-state phase transformation, below schematic diagram describes regarding different factors which govern solid-state phase transformation.

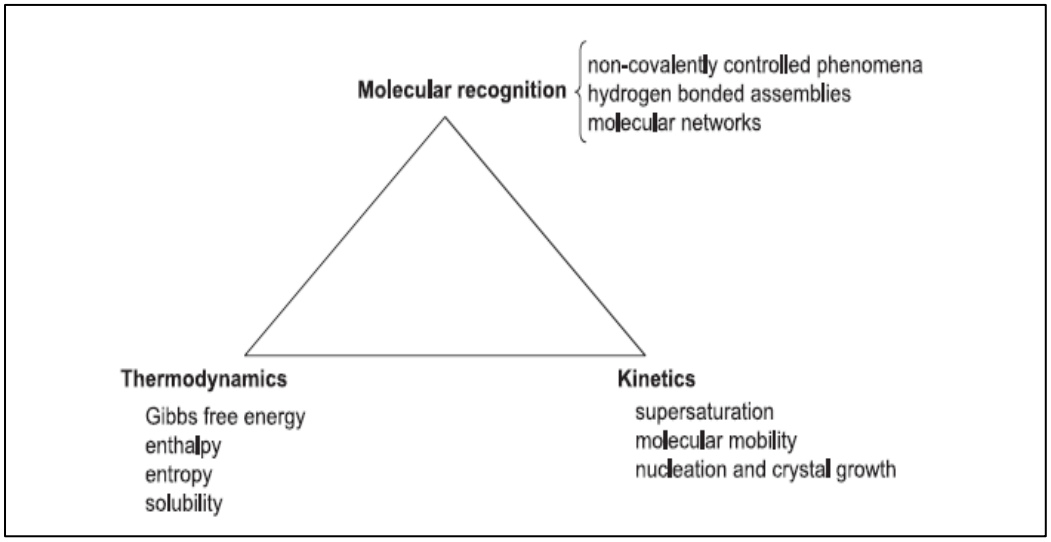

Figure 2.10 Different thermodynamic and kinetic properties governing solid states (Rodríguez-Spong et al., 2004)

Different rules and phase diagram were postulated to understand the thermodynamic stability and kinetics of polymorphism.

Phase rule

Based on the thermodynamic principle Gibbs (1876, 1878) formulated phase rule as:

$$\mathbf{F = C - P + 2}$$

Where, **F**- degrees of freedom in the system, **C**- number of components and **P**- the number of phases.

A system which is homogeneous and physically separated from the other system by a specific definite boundary then that homogenous system is referred as phase pure system. For instance, water and gas are totally homogenous and separate system so they have one phase number individually. Two different solid polymorphs which are homogeneously

distributed or form an alloy are referred to contain one phase in the solid state. Various scientists have raised certain controversies regarding homogenous systems in the field of crystal engineering when they started analysing X-ray diffraction patterns of a single crystal; they reported that the single crystals are generally inhomogeneous mixed crystals or inhomogeneous racemic mixtures (conglomerates). Others stated that in crystal two polymorphs co-exist with each other in a definite molecular arrangement. A number of components are defined as the number of individual species present in the system which may exist in the liquid, solid or gaseous state, an example for this is water that is a single component system which exists in different phases.

A number of the degree of freedom or variance is referred as the number of components like temperature, pressure and concentrations are fixed to maintain the system at equilibrium. For example, gas has two degrees of freedom and single phase whereas gases in two phase's liquid phase and gaseous phase have one degree of freedom. A system with one component and three phases have no degree of freedom, these relationships are often stated as bi-variant, mono-variant and invariant.

To control the polymorphic crystallisation thermodynamic and kinetic properties are essential properties to be considered. They are used to understand the nucleation process, crystal growth and phase conversion occurring during crystallisation process (Datta and Grant 2004). These properties are based on Gibbs free energy ΔG_c of a crystallisation process considering temperature and pressure constant (equation 1).

$$\Delta \mathbf{G_c} = \Delta \mathbf{H_c} - \mathbf{T}\, \Delta \boldsymbol{S_c} \quad (\mathbf{eq.1})$$

Where, ΔH and ΔS are related as a change in enthalpy and entropy during crystallisation process respectively. In thermodynamic point of view, a system with minimum Gibbs free energy is acting as a driving force for the formation of stable polymorphs (equation 2). Increase in rate of entropy is irreversible thermodynamics which leads to the formation of the less stable form (Brabander et al., 2002).

$$\Delta \mathbf{G_T} = \Delta \mathbf{H_T} - \mathbf{T}\,\Delta \mathbf{S_T} \quad (\mathbf{eq.2})$$

The thermodynamic system of polymorphs and the driving force responsible for the phase transformation when temperature and pressure are kept constant can be determined by the difference in Gibbs free energy. Change in the enthalpy and entropy is referred to change in lattice energy and disorder in the lattice structure respectively. In thermodynamic if ΔG_T <0, then the phase transformation occurs spontaneously as very less energy is consumed, ΔG_T =0 then the free energy between two polymorphs is similar and when ΔG_T>0 then the polymorphs are stable and spontaneous transformation is not possible (Venugopalan 2009). According to thermodynamic studies, polymorphic transformation can be considered to be enantiotropic and monographic based on the transformation of phases. There are various rules postulated by various scientists for the prediction of polymorphs and its transformations.

2.3.2 Rules for predicting polymorphs

Since entropy cannot be determined experimentally, free energy isobar cannot be predicted. Burger and Ramberger have proposed various rules for understanding and predicting the stability and nature of polymorphic systems considering temperature and free energy as parameters (Venugopalan

2009). Polymorphism as discussed before can exist in monotropic and enantiotropic systems. The most stable polymorph has lowest Gibbs free energy.

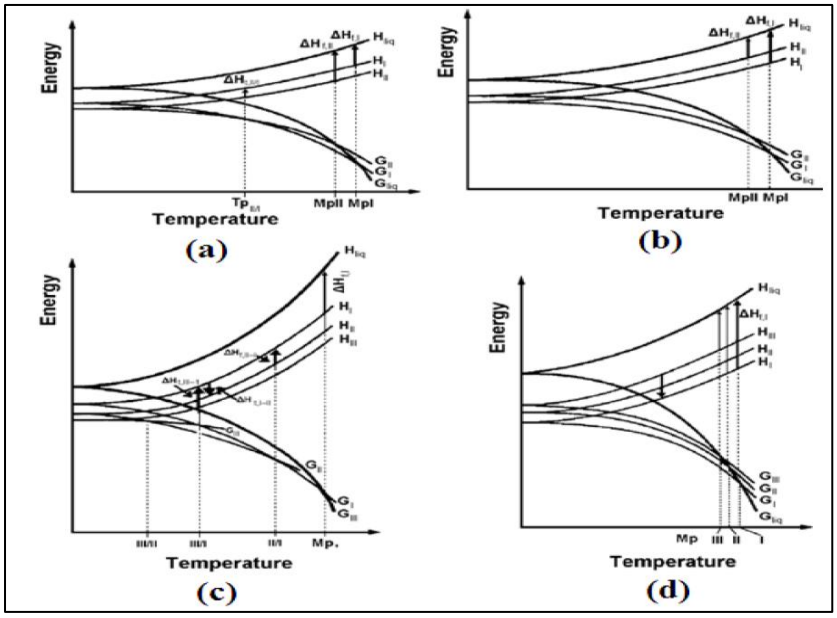

Figure 2.11 Correlation of energy and temperature of polymorphs to determine enantiotropy and monotropy (Venugopalan 2009).

In Figure, 2.11a represents a thermodynamic system with two polymorphs where form II has less Gibbs free energy till it reaches transition point (T_p) thus it is more thermodynamically stable as it crosses this transition point the Gibbs free energy of form II is higher than form I and becomes unstable up to its melting. At transition point (T_p) the two polymorphs form I and II are thermodynamically stable with equal Gibbs free energy. ΔH_t represents the enthalpy of transition where the conversion of form II to form I occurs to retain its stability .$\Delta H_{f,I}$ and $\Delta H_{f,II}$ represents the fusion enthalpy for forms I and II, respectively. Figure 2.10c represents the energy/temperature diagram for tedisamil dihydrochloride which shows three polymorphs exhibiting enantiotropic behavior. Figure 2.11b represents the monotropic system

where the Gibbs free energy of form II is greater than form I and remains unstable until melting. There is no transition point present in this system so the transformation of unstable form II to stable form I occurs but this conversion is not reversible. Figure 2.11d represents energy/temperature diagram for fluriprofen reflecting monotropic polymorphic system.

Below Table 2.2 briefs out different rules reported understanding the pathway of transformation between two polymorphs.

Table 2.2 Rules to understand the relationship between polymorphs and single component system

Heat of transition rule	The system is said to be enantiotropic when an endothermic phase transformation takes place between two crystals at a particular temperature and if that transition temperature lies below the melting temperatures of two polymorphs. The system is said to be a monotropic system when there is no thermodynamic transition point below the melting temperatures of polymorph (Venugopalan 2009).
Heat of fusion rule	The heat of fusion rule states that the polymorph with a high melting point will have a lower enthalpy of fusion then it is the enantiotropic system. If the enthalpy of fusion of higher melting point polymorph is high then the system is monotropic (Venugopalan 2009).
Enthalpy of sublimation	The system is an enantiotropic system when enthalpy of sublimation is low than high melting point polymorph. In monotropic system, high melting point polymorph show higher enthalpy of sublimation (Venugopalan 2009).
Heat capacity rule	For a pair of polymorph if heat capacity of high melting point peak is high then the system is referred as enantiotropic and if the system shows low heat capacity for high melting peak polymorph then it is monotropic (Venugopalan 2009).
Entropy of fusion rule	According to this rule, melting point is the region where the liquid state is in equilibrium with solid state and the difference in Gibbs free energy is zero. Polymorphs with high melting point peak having low entropy of fusion are the enantiotropic system. In monotropic system polymorphs with low melting point have a low entropy of fusion (Venugopalan 2009).

2.3.2 Properties of polymorphs

In the process of polymorphism has left prominent benchmark to understand the chemical and physical properties of solid state materials. They are useful in pharmaceutical industry, pigments, agrochemicals, explosives and fine chemicals in the industry (Venugopalan 2009).

- Packing properties are considered such as mass volume, density, refractive index, optical properties, electrical properties, thermal and hygroscopicity.
- Mechanical properties: Tensile strength, hardness, friability, compactability, tabletability, flow rate and blending.
- Surface properties: Surface free energy, the heat of sorption, crystal habit.
- Thermodynamic properties: Internal energy, enthalpy, melting and sublimation property, heat capacity, and the heat of fusion.
- Kinetic properties: Stability, dissolution rate, the rate of solid-state reactions.

2.4 Summary

Most of the R&D formulations are failing in the final development stage due to lack of knowledge regarding solid state chemistry, crystal attributes, supramolecular chemistry and crystal engineering. To develop a solid formulation understanding the physical and chemical properties of the solid pharmaceutical component is very important to make the formulation commercially successful. The major challenge that pharmaceutical manufacturing and processing industry facing are solubility of hydrophobic components; around 60% of the identified API molecules are reported to be

hydrophobic in nature. Thus to overcome this challenge new field of solid state chemistry has evolved. This filed is crystal engineering which deals with the design of API component with different morphological and crystal habits so that their physicochemical properties can be enhanced. To process the solid crystalline material or to manipulate the morphological properties different crystallisation and processing techniques are been postulated. In the present chapter brief introduction regarding solid state chemistry and supra molecular chemistry is explained. Introduction of multicomponent systems such as cocrystals and mono-component system such as polymorphs is elucidated. Definition to cocrystals, mechanism of cocrystallisation, designs of cocrystals, their applications, and different techniques of cocrystallisation their challenges are explained in brief. Definition to polymorphism and polymorphs their molecular arrangements is explained which was supported by explaining different thermodynamic rules to predict polymorphic transition, their properties and applications.

Chapter 3: Sub-Critical Water

3.1 Introduction

Water is referred as a universal solvent due to its proportionality during heating, its high dielectric constant and high polarity. Subcritical water (SCW) is the physical state of the water that has been heated between 100°C and 374°C (critical temperature) with sufficient pressure applied to retain the liquid state of water (Asl and Khajenoori., 2013), when water is heated above the critical temperature under high pressure and when water molecules can no further retain its liquid state than this state of water is referred as supercritical water. Water in the subcritical state is used as a tunable solvent in the food processing, extraction of chemicals from natural sources, nutraceuticals. The reason for selection of water as a solvent over other solvent system is that it is harmless and the polarity of water can be controlled by altering process conditions such as temperature and pressure. Thus this typical property of water refers it as tunable solvent (Ibanez, 2003). As the polarity of water can be monitored by controlling process parameters like temperature and pressure this water can be used for the extraction of different components with different polarity and dissolve various hydrophobic components (Ibanez, 1999).

Apart from the change in polarity of water at subcritical state the change in its surface tension, viscosity, the dielectric constant is also observed, this change in these physical properties of water enhances the effective capacity of penetrability or miscibility of water which is used to dissolve different hydrophobic components. In the present study the dielectric constant of water was tuned under high temperature and pressure conditions to alter the

morphological and induce hydrogen bonding capacity of various organic molecules which includes production of complexes molecules (cocrystals, solvates and hydrates), altering morphological properties of insoluble APIs to increase its kinetic properties (solubility, dissolution, stability) example lactose, theophylline, generation of metastable polymorph of API (paracetamol) and forming complexes between organic and inorganic molecules (API loaded hydroxyapatite). Below Figure 3.1 represents the phase diagram representing different states and regions of water at different temperatures and pressure conditions.

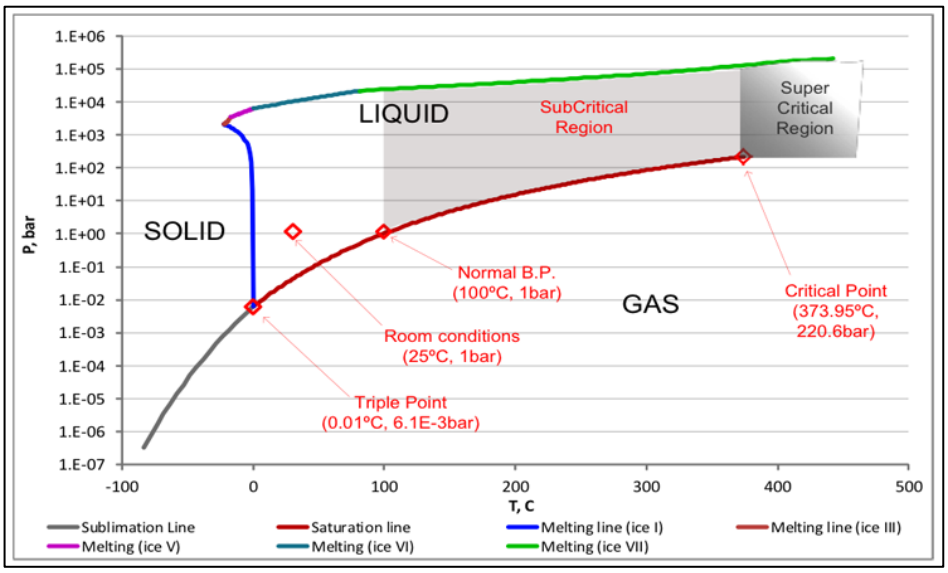

Figure 3.1 Representation of phase diagram of water as the function of temperature and pressure

In the above Figure different physical state of water is represented by different temperature and pressure conditions. From the above Figure, the subcritical region of water is between 100°C - 374°C where the vapor pressure is 1bar and 220 bars respectively. In this region due to sufficient pressure, the water retains the capacity to stay in liquid state than only this region is referred as a

subcritical region. The Figure 3.2 below represents the change in various properties of water at subcritical temperatures.

	Normal water	Subcritical water		Supercritical water	
Temp. (°C)	25	250	350	400	400
Pressure (MPa)	0.1	5	25	25	50
Density, ρ (g cm^{-3})	1	0.80	0.6	0.17	0.58
Dielectric constant, ϵ (F m^{-1})	78.5	27.1	14.07	5.9	10.5
Ionic product, pK_w	14.0	11.2	12	19.4	11.9
Heat capacity C_p (kJ kg^{-1} K^{-1})	4.22	4.86	10.1	13.0	6.8
Dynamic viscosity, η (mPa s)	0.89	0.11	0.064	0.03	0.07

Figure 3.2 Properties of water at various conditions (Toor et al., 2011)

3.2 Water structural properties at subcritical state

The life-supporting process in the evolution is based on the water due to its unique physical and chemical properties. Water structural properties are most controversially discussed in the condensed matter research. Several experiments and studies are carried out to decipher the structural orientation of water at elevated temperatures and pressure conditions (Sahle et al., 2013).

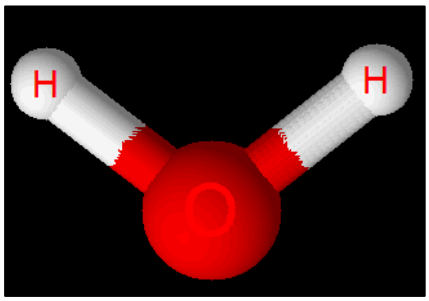

Figure 3.3 Chemical structure of water molecule.

The water stays in the liquid form when the attraction forces between the water molecules is around 23.3 kJmol^{-1} this is the enthalpy of water when it is in liquid form at 25°C, the minimum energy required to break the water hydrogen bond is equal to the heat of enthalpy the water molecule at 25°C. This separation energy is equal to half of the enthalpy of vaporisation (44

kJmol^{-1} at 25°C), this indicates that when water gets vaporised less than two hydrogen molecules are broken. Thus based on above interpretation the minimum energy required to break the water molecule in such a way that it can retain its structural electrostatic interaction is equal to 25% of hydrogen bond enthalpy (23.3 kJmol^{-1}) which is recently calculated to be 6.3 kJmol^{-1} (Smith 2006). Muller,1988 and his co-author's has proposed that if the excess heat capacity over the steam is assumed to be responsible factors for the hydrogen bond breaking this attractive energy is calculated to be 9.80 kJmol^{-1} this additional energy is due to the influence of extra energy of polarisation, cooperatively and covalence of hydrogen bond (Muller,1988).

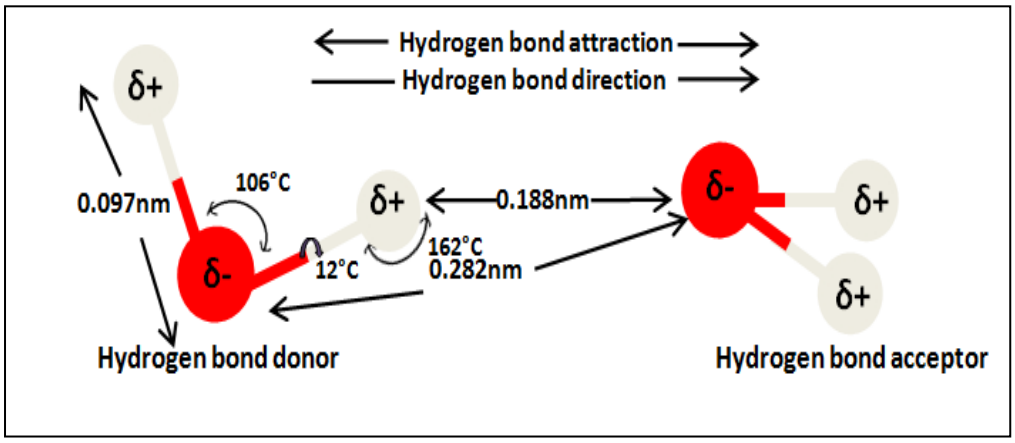

Figure 3.4 Schematic representations of dipole moments of water molecule

The most important factor which play role in understanding the polarity of water is the dielectric constant of water. As the temperature increases the polarity of water decreases and the dielectric constant or permittivity constant decreases which make water at elevated temperature to behave as organic solvents. In the subcritical region the dielectric constant of water is similar to that of organic solvents. Water at 100°C the dielectric constant is similar to organic solvent DMSO so water can solubilise all the solute molecules which

are soluble in DMSO at room temperature (Champion et al., 2007). This ability to mimic the dielectric constant of water with various organic solvents has gained importance in extraction of various hydrophobic compounds from natural sources (Charoenchaitrakool et al., 2000). Figure 3.5 represents the relationship between temperature sensitive dielectric constant of water with various organic solvents.

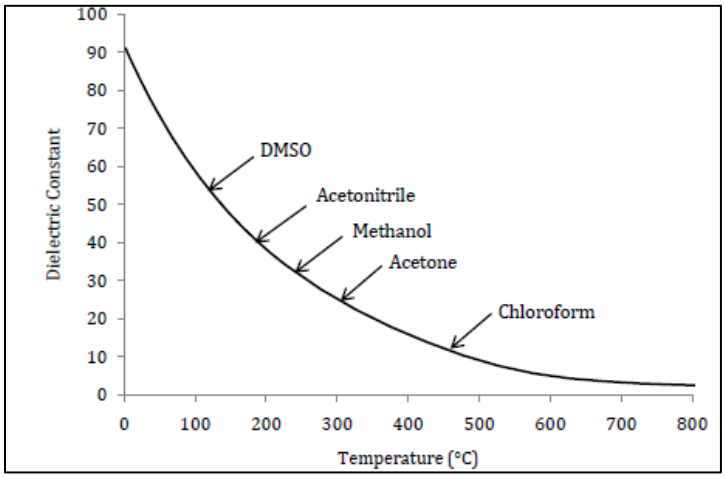

Figure 3.5 Comparison between the dielectric constant of water and organic solvents at elevated temperatures (Maghsoodi et al., 2008)

The most prominent analytical tools used to measure the site to site variation in the water structure and density fluctuations is by using X-ray or neutron scattering involving isotopic substitution (P. Postorino 1993). The spectroscopic data provided a controversial discussion regarding the local atomic structure of water (Wernet et al., 2004), this study has raised an discussion whether the structure of water at ambient conditions retain homogenous density or inhomogeneous mixture of two structural states where hydrogen bonding distorted structure surrounding less denser tetrahedral structure of water. Water is generally consists of four weak hydrogen bonds normally weaker than covalent bond but stronger than natural thermal energy. Water is generally tetrahedral structure where the

local cluster is flexible. If the hydrogen bond formed are strong than the local cluster expands leading for the decrease in the density of water resulting in increase in volume of water molecule. Optical Raman spectrometry is used by (Frantz et al., 1993) proposed that the significant tetrahedral structure of water is still retained at elevated temperature and pressure conditions. (Vasconcelos et al., 2007) had proposed that at elevated temperature and pressure number of water monomers are formed at supercritical regime, they also reported the presence of remaining higher coordinated of water like dimer and trimers. (Sahle et al., 2013) and group had investigated the microscopic structure of water at high temperature and pressure conditions using X-ray scattering experiments, they have compared the practical data with initio molecular dynamic simulations and reported that at ambient conditions the tetrahedral structure of water where four hydrogen atoms are surrounded by five oxygen motifs within the distance of 3.6 A°, with increase in temperature and pressure the number of hydrogen bonds per molecule decreases which causes decrease in the density and polarity of the water molecule, further based on the molecular simulations and experimental spectra they reported that there is clustering of motifs taking place at elevated temperature and pressure thus the water molecule is homogeneously separated at super and sub critical regime.

3.2.1 Process taking place at SCW level

They are two processes which dominate this sub-critical water process positive heat and negative heat (Duarte et al., 2006). Positive heat is driving force which is used for the formation of cavities in the media. Negative heat is used for the formation of hydrogen bonds between the solute and water molecules

where energy is consumed “ice berg formation step”. If the negative heat generated due to increase in temperature dominates over positive heat than the solubility of organic molecules in water decreases and when positive heat dominates over negative heat than the solubility of solute molecule in the water system increases (Reverchon and Della Porta 1999). Below Figure 3.6 demonstrated the effect of solubility with increase in temperature correlating with dielectric constant of water.

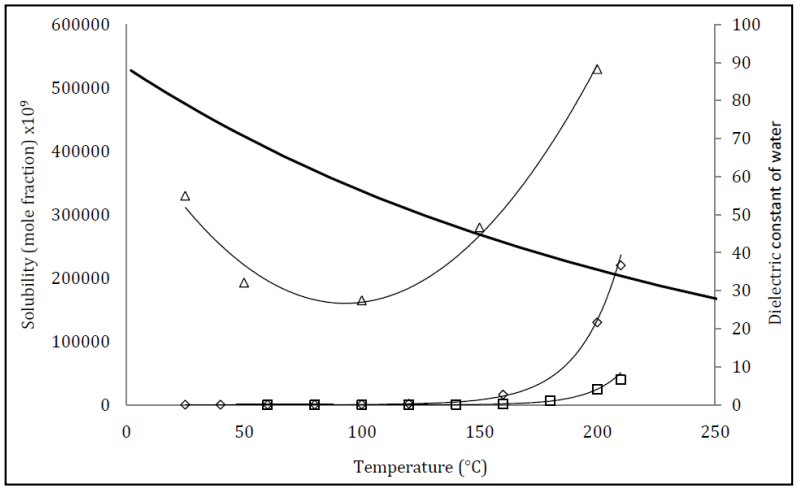

Figure 3.6 Trendline of solubility data of anthracene (diamond shape), *p*-terphenyl (square shaped) and 1, 8-cineole (triangle shape) in SCW. The effect of dielectric constant of water with increase in temperature (Reverchon and Della Porta 1999)

From the above interpretation it is suggested that after 150˚C the solubility of various hydrophobic compounds increase drastically this is related to domination of positive heat (cavity forming) over negative heat (ice-berg forming) process (Vemavarapu et al., 2002). If there is no precipitation or ice-berg formation observed in the solution it doesn’t mean that no hydrogen bonds are formed, it is due to hydrogen bonding between the water is beyond the critical point and no bonding is formed between the solute molecules in the

solvent system. Pressure as a parameter of the process has negligible effect on the solute and solvent in sub-critical levels.

3.3 Factors effecting Sub-critical water process

There are various parameters such as structure of the solute component, temperature and pressure conditions, interaction between the solute and water molecule and level of supersaturation influencing SCW process.

3.3.1 Effect of solvent conditions

The thermodynamic dissociation ability of water is based on hydrogen bonding capacity at ambient conditions and elevated temperatures (Rabinow 2004). In water hydrogen bonds of one water molecule is influenced by hydrogen bonds of other water molecule grouped around it, they are self-associating molecules. Heat of vaporisation, and change in dielectric constants are generally regulated by change in hydrogen bonding of water (P. Alessi 1996), thus little change in the hydrogen bond of water changes the entire volume of water. At low temperatures the dielectric constant of water is high and retains high hydrogen bonding capacity (P. Alessi 1996), as the temperature of water is raised the increase in thermal agitation of molecules causes reduction in the hydrogen bond strength which leads to reduction in dielectric constant of water (Duarte et al., 2006). This reduction in hydrogen bond strength and reduction in polarity leads increase in the solubility of hydrophobic compounds in water. This same principle is applied in our Microwave assisted sub-critical water process. Trend between the solubility of chemical components vs temperature is not linear as some complex molecules like benzene, toluene display liner relationship between temperature and solubility when water is heated up to 150°C under applied pressure beyond this temperature the solubility graph

shoots up drastically which is referred to further breaking of hydrogen bonds of water molecule and this region is called as “solubility minima”.

3.3.2 Effect of nature of solute

Behaviour of solute greatly affects the solubility of solute molecule in SCW (sub-critical water). Degree of conjugation, position of hydrogen bonding groups on side chain, presence of number of aromatic ring and groups on the side chain are structural factors of solute considered during SCW process.

The solute with small size increases the solubility than the complex size solute, an organic molecule with a high degree of conjugation results in higher solubility. With the increase in a number of aromatic rings in the structure increases the solubility with an increase in temperature than the molecule with linear hydrocarbon structured molecules. Complex aromatic ring structures show an increase in solubility than linear aromatic ring structures. This effect is due to the availability of delocalised pi electrons in the complex aromatic structure which results in greater interaction between SCW than hydrocarbons and cluster hydrocarbons chain structured molecules. Presence of oxygen group on the side chain increases the solubility as it takes part in hydrogen bonding process (P. Alessi 1996).

3.4 Computational model to study solubility parameter of solute in SCW

The most important parameter which is considered in SCW process is solubility of the solute in the solvent system. In particle engineering or extraction process, the material should be completely soluble in the solvent system. Very limited test and study are performed to analyse and study this solubility parameter. Some researchers proposed certain tools or model to study this solubility parameter in SCW process. Initially, Miller and group

proposed the model for solubility prediction based on the characterisation of solute and solvent but this model failed as it cannot work under elevated temperature conditions.

- **Empirical model**

This model generated the solubility study of solid materials at room temperature and constructed 1st, 2nd and 3rd order equations which can be used for the prediction of solubility in SCW process. General equation proposed in the empirical model is as follow:

$$\ln x_2(T) = \left(\frac{T_0}{T}\right) \mathrm{In} x_2(T_0) \quad \text{..... (1)}$$

Where X_2 is solubility of solid material (in moles) at temperature T (Kelvin), X_0 (T_0) is the solubility of same solid material at ambient room temperature. (Carr *et al.,* 2011b)

- **Hansan solubility model**

This model does not predict the solubility of solid materials but instead it reveals the information regarding onset of solubility of both polar and non-polar solid materials. Onset of solubility is governed by the change in hydrogen bonding, polar and dispersive forces involved in solubilising of materials in the solvent. Solubility of organic compounds is predicted by (Srinivas *et al.*, 2008) using this model.

Modified Universal Function Activity Coefficient (M-UNIFAC) model

This is most widely used model for prediction of solubility of solid materials in the solvent during SCW process. This study deals with the activity coefficient which is determined by considering the presence of functional groups on the solute side chains and the solvent system in the solution. Once the activity coefficient is predicted than the fraction of solubility is determined by

calculating the material melting properties and fugacity ratio between solute/solvent (Karásek et al., 2006). This model is applicable at elevated temperature which is positive point of implementing this model. Later on Fornari proposed the modified M-UNIFAC model in which the dielectric constant relationship between the interaction between solute and solvent systems is considered.

- **Dielectric constant model:**

This is recently proposed model which deals with the dielectric constant of water at room temperature and at elevated temperature. It give the accurate result of the change in dielectric constant of water at elevated temperature which can be correlated with the amount of solute gets solubilised in it. If a solute molecule is completely gets solubilised in water, were the molar concentration of solute varies with temperature than it becomes very easy to predict the solubility of solute in the solvent mixture like water/organic solvent, organic solvent mixture (Carr et al., 2011b).

Carr and group had worked with budesonide using SCW process, initial stages of experiment they have observed that budesonide is not soluble in water at sub-critical level (200°C) so to prevent further degradation of solute they have implemented the use of solvent mixture to further reduce the dielectric constant of water. They used 20% alcohol-water mixture to form clear solution of budesonide using SCW process. Due to presence of alcohol in the solvent system the morphology of the crystal can be altered which brings change in physical properties of the crystal. This change in morphology is observed in case of supercritical extraction process. As we

are dealing with melt induce crystallisation process it is very important to form a clear solution to obtain phase pure crystal structures.

3.5 Applications of SCW process

Particle engineering

Carr and grouped produce narrow sized particle of greseofulvin, budesonide by this process. This process took place in two steps, first is solubilising the solute in water at elevated temperature and pressure conditions and secondly spraying the saturated solution under ambient conditions. Fosters and group proposed the application of SCW process in pharmaceutical and particle engineering field. Richier et al have used this SCW process to enhance the solubility of nifedipine for tabletting formulations.

Extraction

This process is used for the extraction of hydrophobic materials from natural sources. Various studies have been performed to analyse the extraction capacity of SCW. (Smith 2006) have used for extraction of flavonoids from herbs. In this process at high temperatures and pressure conditions the diffusion rate of water increases across the cell walls of herbs and thus promotes extraction (Asl and Khajenoori, 2013). This method has proved advantage over conventional extraction process in terms of purity and extent of extraction, time of process and use of organic solvents which are toxic.

Chromatography

SCW has proved advantageous in chromatography in separation of polar and non-polar solvents. As the SCW process the dielectric constant of water is tunable various polar and non-polar components are separated using reverse phase liquid chromatographic technique (Yang et al., 2007)

Hydrolysis

Subcritical water at elevated temperatures and pressure act as catalyst as it gets ionised and used for hydrolysis process by (Yung et al., 2004). Water in ambient conditions has very less ionising capacity so it cannot break the hydrogen bonds so at elevated temperature it causes breakdown of hydrogen bonds and increase in ionisation which leads for the release of proton.

3.6 Microwave Assisted Sub-Critical Water process

Microwaves is an attarctive tool used for extraction and chemical synthesis and various studies are performed based on microwave assited organic synthesis (Giguere *et al.,* 1986). Microwaves are the electromagnetic spectrums which occur in the frequency range of 0.3 to 300GHz and wavelength between 1mm to 1m. These microwave frequencies are used in telecommunications, microwaves and various radar instruments (Kappe 2004). Microwave quantum energy can reach up to 0.0016eV, this energy is insufficient to break any covalent bonds and additionally the energy lies below the Brownian motion (Kappe 2004, Giguere 1986). Below Figure 3.7 represents the region of microwave and the relative frequency range.

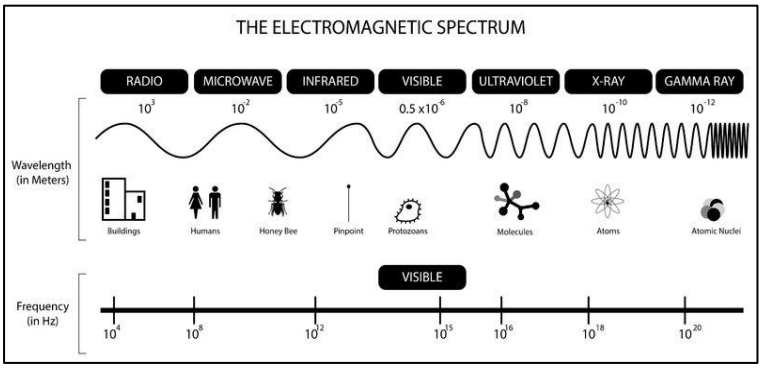

Figure 3.7 Electromagnetic spectra and distribution of frequency range (Clark, 2011)

There are various advantages of microwave heating:

- By the use of microwave heating the reaction time is reduced and further contamination of products is reduced and the yield is high.
- In the microwave reactor principle of bulk heating occurs where every molecule will simultaneously act as heat source, this kind of heating provide productive heating profile which will produce different distribution of reaction products and minimises degradation.
- The distribution of energy mass transfer is significantly high, the energy doesn't emerge equally with reaction vessels, the microwave energy only infiltrated the reacting molecules and increases heat transfer.
- Use of microwave energy in crystallisation reduces the use of solvent drastically and this is considered more environmentally friendly as compared to other technologies (Pagire et al, 2013).

Dielectric constant plays a significant role in controlling thermal behaviour of dipole carrying materials under the influence of microwave radiations. The dielectric constant is referred as physical property which changes with change in inter atomic and intermolecular interaction. The efficiency of solvents to separate electrolytes into ions is determined by calculating dielectric constant (Jouyban et al., 2004). A dielectric supports the charge by inducing polarisation in a particular electric field, like one surface develops positive charge and the other develops opposite net negative charge. This is taking place due to development of electric dipole moments between the two oppositely charged surfaces which are separated by a certain distance on a molecular level. Solvents with high dielectric constants have greater

dissociation property and solvents with low dielectric constant have capacity to form ionic pairs. Recently in most of the pharmaceutical and analytical industries there are vast studies on determining the dielectric constant of mixed solvents and their effect on the solubility of the solute molecule. Irani et al., 2017 have used the solubility of xanthine derivatives using solvent mixtures and correlating with dielectric constant (Anthony, 1966). Dielectric constant of water at room temperature is low so they have fewer ions forming capacity and water at high temperature has less dielectric constant and high polarity so its capacity of solubilising insoluble materials has enhanced (Kenneth, 1983).

3.6.1 Microwave heating mechanism

The mechanism in which material are heated is referred as microwave dielectric heating. Dielectric heating reflects the potential of the materials to consume microwave energy and transfer it into thermal energy. It is reported that only the electric part of the electromagnetic field is responsible factor for microwave heating (Strass et al., 2000, Woodward et al., 1997). Microwave heating is the coordinate mechanism originated from the overall molecule. For example, according to Debey 2013, the combination between microwave and polar molecules increases the rational speed causing an elevation in the friction forces and hence generating heat (Gabriel et al., 1998). The dielectric heating mechanism is controlled based on two main mechanism; Dipolar Polarisation and Ionic Conduction.

1. Dipolar polarisation: The dipolar polarisation required in a molecule to obtain dipolar moment such as water. When the microwave irradiations pass through the dipolar material, the dipole group start to respond to the

electric part and orient according to the electric field oscillation (Lidstrom et al., 2001, Kappe, 2004). When the electric field changes its direction, these groups will rearrange themselves according to that direction. During this reorientation process part of the energy is lost by the electric field which is absorbed by the dipole group and transformed into thermal energy. This transformation is controlled by several factors such as molecular friction and dielectric properties.

2. Ionic conduction: Tap water produces more temperature than distilled water during microwave heating; this is because of the presence solubilised ions in tap water. These ions will gain kinetic energy under the influence of microwaves and will produce more collision between molecules. This event will increase kinetic energy loss, which will transform into thermal energy.

3.6.1.1 Key attributes of microwave heating over conventional heating

There are different key attributes of microwave heating compared to conventional heating:

- ✓ Due to microwave irradiations can significantly enhance the heating process resulting in rapid crystallisation and generation of reduced particle size. In case of conventional heating longer time is required to reach the target temperature conditions, which may result in further hydrothermal degradation of organic components.
- ✓ In microwave irradiations offers rapid and volumetric heating, without the need of heat transfer surfaces or heat transfer fluids. This process is absent in conventional (conductive) heating.

- ✓ Additionally in microwave heating the microwaves directly couple with the molecules (polar) of the solution, the heat transfer is immediately stops when the magnetron is turned off, thus minimising the thermal inertia. But in conventional heating the heat transfer is continued for certain period of time even after the external heating source energy is stopped.
- ✓ In microwave heating, heat transfer is not based on thermal conductivity, which is less for conventional solvents like water, methanol or ethanol. Rather it depends on the dielectric property of the solution (Radacsi et al., 2013).

Based on the above advantages of microwave heating, microwave irradiations are used as the external heating source in the present research work. For the first time in the present research work scalable microwave assisted Sub-critical water process technology is proposed for particle engineering of pharmaceutical components. Microwave energy is used as the external heating source to treat the water from ambient conditions to subcritical temperature and pressure conditions. The scalability of this technology was performed by our industrial partner where conventional heating source was used as heating source. Due to microwave heating in the small lab scale reactor this technology was used as screening tools for different chemical components and process understanding.

RotoSYNTH microwave reactor is used as heating source for water, the instrument (Figure 3.8) is equipped with quartz tube with 30 and 50ml capacity, these tubes are covered by external covering made up of peek. The reactor tubes are coonnected by temperature and pressure valve. This

protective shield can withshand the temperature and pressure up to 250°C and 30-40 bars respectively. The complete setup is kept over magnetic stirrer which is present inside the instrument. The reaction is processed in closed container with temperature and pressure valve. Below Figure 3.8 ellustrated the design of RotoSYNTH microwave reactor with different probes and vessels.

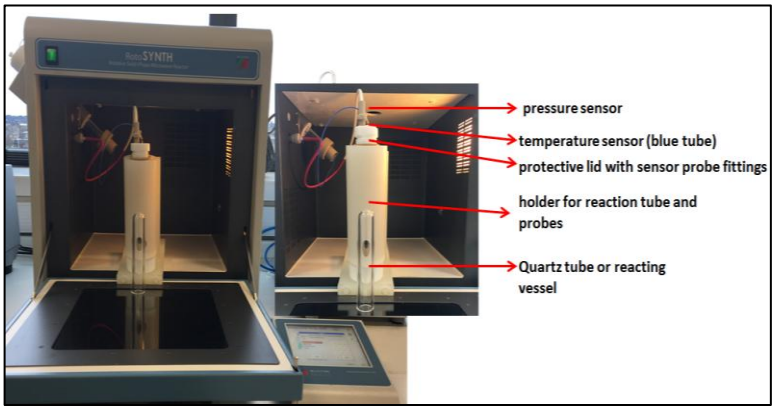

Figure 3.8 RotoSYNTH microwave reactor with pressure vessel for sub-critical water processing. (Adopted through digital camera)

In recent years various novel technologies implemented in the field of crystal engineering and process industries include the use of organic solvents which is a drawback in terms of toxicity, contamination of pharmaceutical components and non-economical. Recently Paradkar and co-workers have developed, a green pathway of crystallisation which is Solvent Free Continuous Co-crystallisation (SFCC) using hot melt extrusion, they have proved the commercial feasibility of this technology (Kelly et al., 2012), the only drawback of this technology is the thermal degradation of pharmaceutical components as they are subjected to high temperature and shear conditions. Based on the previous trials performed by various researchers on subcritical water technology they concluded that water at

subcritical level can be used as green tunable solvent to enhance the solubility of hydrophobic components. As we know pharmacokinetic effect of API formulations is potentially influenced by crystal morphological properties like particle size, shape and surface roughness, thus the present research is focussed on crystal engineering of pharmaceutical ingredients by using MASCW technology. This technology was implemented to understand the influence of various process parameters like temperature, pressure, solvent and solute concentration over morphological and kinetic properties of pharmaceutical ingredients. As discussed before change in particle morphology significantly alter various physical and chemical properties such as its solubility, stability, degradation profile, drug dissolution rate, flow property, and compressibility. For example, paracetamol is an analgesic drug and by altering the size of the particle, dissolution, flow and compressibility properties can also be changed (Champion et al., 2007). MASCW process is based on antisolvent based top-down micronisation crystallisation process. Use of water as subcritical water has various applications and advantages over conventional crystallisation technologies:

3.6.2 Advantages of subcritcal water process

- Tuning the morphological and chemical properties of particles is very easy by adjusting the process parameters like temperature, pressure, ratio of solute to solvent, type of solvent (Ibanez et al., 2003).
- In this process no high shear is applied when compared to extrusion.Thus the thermal degradation of the pharmaceutical ingredients is prevented (Bala Subramaniam 1997).

- In this process the nuceiation of the particles takes place from the molecular level up to nano/micro and macro sized particles which avoids the influence of high shear which is involved in breaking the granules into smaller particle size (Bala Subramaniam 1997).
- More efficient in terms of unit operations.

3.7 Mechanism of MASCW process

Based on the experiments performed by us a tentative mechanism of MASCW process was postulated, Figure 3.9 schematic representation of MASCW process mechanism. Initially solute solid materials are added in water according to supersaturation solubility of solute in water. Microwave energy is subjected to the solution and the temperature is raised based on the heat rate adjusted in the instrument. As the temperature increases clear solution is formed and then the saturated solution is subjected for gradual cooling. During the elevated temperature conditions the hydrogen bond strength of water is reduced and the molecules start vibrating.

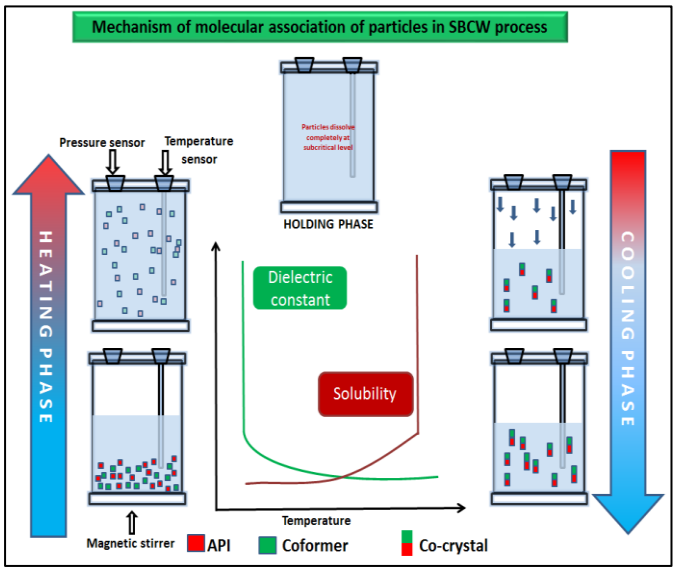

Figure 3.9 Summary of mechanism of molecular association of particles in MASCW process

The complete assembly is subjected to magnetic stirring using magnetic beads in the solution. During cooling or by rapid cooling conditions the change in the polarity of water can induce change in supersaturation of solution leading to rapid precipitation of the solute. The yield of precipitation is generally based on the solubility parameters of solute in water. The effect has been observed in the present study, when metastable cocrystals and polymorphs were generated by rapid cooling so supersaturation level of solute is solvent is altered and the precipitation starts inducing.

Previously they are few research work is reported based on subcritical water process. Adam Carr and group implemented subcritical water process for the generation of micronised budesonide, analysing solubility of griseofulvin using chromatographic oven made up of stainless steel, they have used SCW as the tunable solvent for crystallisation process (Carr et al., 2011). Recently group of Jian-Feng Chen has used this subcritical water process for generation of ultrafine clarithromycin and beclomethasone dipropionate via antisolvent precipitation mechanism (Pu et al., 2017). The instrument used them is high pressure micro reactors as heating source for water, they have used very low supersaturated solution (6 mg of beclomethasone solute in 6 ml water) for the generation of nano particles. All the studies performed on subcritical water process are performed on small scale level thus these technologies failed to gain importance commercially. In the present work using MASCW process it was successfully reported commercial feasibility of this technology by performing scaling up experiments.

The MASCW process was used for generation of cocrystal of carbamazepine, sulphamerazine and sulfamethazine as API and saccharine as cocrystal

former, carbamazepine and saccharine as novel cocrystal pair was selected for understanding the influence of various process parameters on cocrystal form and were successful in generating metastable carbamazepine saccharine form II cocrystal, further caffiene and para-hydroxybenzoic acid was selected as incongruent cocrystal pair and successfully generated CAF: 4HBA 1:1 cocrystal. This MASCW process was applied in the field of polymorphism, it was found that successsful generation of metastable form II of paracetamol with greater solubility and compresability was reported. This MASCW process was used to generate microsized particles less than 5 micron of theophylline and further analysed the enhanced aerodynamic property of MASCW treated theophylline. Further to its feasibiltity in organic molecules this MASCW technology was implemented to treat inorganic compounds like hydroxyapatite.

Chapter 4: Materials and Methods

This chapter includes detailed explanation of various chemical materials, methods and different characterisation tools used throughout this research work. The method section include summary of different methods used for crystallisation experiments and the brief description regarding the working principles and software details of different characterisation instruments.

4.1 Materials

4.1.1 Active pharmaceutical ingredients (APIs) and excipients

Standard samples of different APIs and pharmaceutical excipients are used for the present work; phase purity of all APIs and excipients is further confirmed using X-ray diffraction technique. Below Table 4.1 includes the brief description of different APIs and excipients used in the present research.

Table 4.1 Summary of list of raw materials

API name	Source / Lot no	Chemical structure
Carbamazepine (form III) (CBZ)	Sigma Aldrich/ TPL/CARB/002	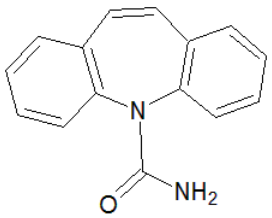 Chemical formula: $C_{15}H_{12}N_2O$ Molecular weight: 236.27 g/mol Melting point: 191-192°C
Ibuprofen (IBU)	Sigma Aldrich, UK	(a) (b)

		a) Ibuprofen monomer, b) b) ibuprofen dimer highlighting the hydrogen bonds between carboxyl groups Chemical formula: $C_{15}H_{12}N_2O$ Molecular weight: 236.27 g/mol Melting point: 76°C
Caffeine (anhydrous) (CAF)	Reagent Plus, is purchased from Sigma Aldrich, UK	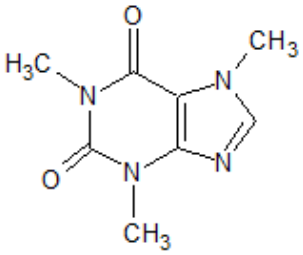 Chemical formula: $C_8H_{10}N_4O_2$ Molecular weight: 194.19 g/mol Melting point: 235°C
Theophylline anhydrous (THF)	HPLC grade purity ≥99% is purchased from Sigma Aldrich	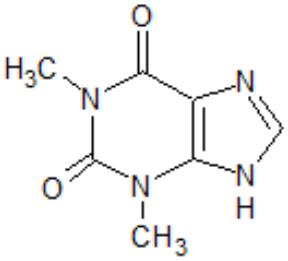 Chemical formula: $C_7H_8N_4O_2$ Molecular weight: 180.16 g/mol Melting point: 270-274°C
Paracetamol form I (PAR)	Sigma Aldrich	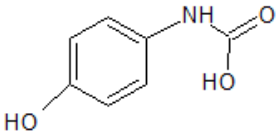 Chemical formula: $C_8H_9NO_2$ Molecular weight: 151.163 g/mol Melting point: 167°C

Sulfamerazine (SMZ)	Reagent Plus, HPLC grade purity ≥99.0% is purchased from Sigma Aldrich	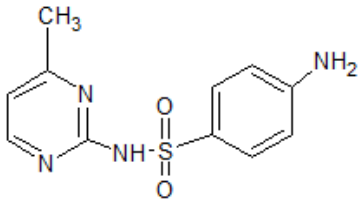 Chemical formula: $C_{11}H_{12}N_4O_2S$ Molecular weight: 264.30 g/mol Melting point: 236°C
Sulfamethazine (SMT)	HPLC grade purity ≥99.0% is purchased from Sigma Aldrich	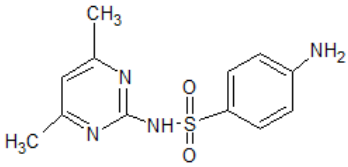 Chemical formula: $C_{11}H_{14}N_4O_2S$ Molecular weight: 264.30 g/mol Melting point: 198.5 °C
Coformers/ excipients		
Saccharine (SAC)	Sigma Aldrich (chemical purity of these chemicals is >99.9%)	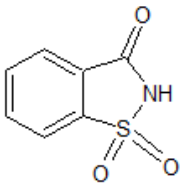 Chemical formula: $C_7H_5NO_3S$ Molecular weight: 183.18 g/mol Melting point: 226-229 °C
Para-hydroxybenzoic acid (4-HBA)	Reagent Plus, (≥ 99.0%) purchased from Sigma Aldrich, UK	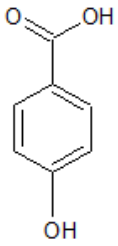 Chemical formula: $C_7H_5NO_3S$ Molecular weight: 183.18 g/mol Melting point: 226-229 °C
Calcium hydroxide ($Ca(OH)_2$)	99.995% trace metal basis is purchase from Sigma Aldrich, UK	Molecular weight: 74 g/mol Melting point: 580 °C

4.1.2 Chemicals and solvents

- *Phosphoric acid solution*, 85 wt. % in H2O, FCC, and FG is purchased from Sigma Aldrich.
- Methanol (HPLC grade purity >99%) purchased from Sigma Aldrich, UK.
- Acetonitrile (HPLC grade, purity >99%) is purchased from Sigma Aldrich, UK.
- De-ionised water used for experiments is collected from ELGA purelab ultra system providing water with purity of 18.2 MΩ / cm.
- Potassium dihydrogen phosphate, AR grade is purchased from Sigma Aldrich, UK.
- Sodium hydroxide, AR grade is purchased from Sigma Aldrich, UK
- Sodium phosphate monobasic, AR grade is purchased from Sigma Aldrich, UK.

4.1.3 Characterisation analytical instruments

Table 4.2 includes the summary of equipments used for this research work.

Table 4.2 Equipment specification

Equipment	Manufacturer	Specifications
RotoSYNTH	Milestone Helping Chemist	RotoSYNTH Rotative Solid-Phase Microwave Reactor
Spray Dryer	LabUltima	LU-228
Scanning electron microscopy	FEI, UK	Quanta 400SEM
Diffraction scanning calorimeter (DSC)	TA Instrument, UK	Q 2000
Thermogravimetric	TA Instrument, UK	Q 5000IR

analyser (TGA)		
Powder X-ray diffractometer (PXRD)	Bruker, USA	D8 powder diffractometer
Raman Spectroscopy	Renishaw, UK	Thermo Scientific
FTIR	Perkin Elmer, USA	ATR Frontier
Nuclear Magnetic Resonance (NMR)	Bruker 400	Multi-nuclear Bruker Avance 400 FT NMR Spectrometer
Dissolution apparatus (USP-II)	LabIndia, India	USP type II paddle test apparatus
UV-spectroscopy	Jasco, UK	V-730 UV-visible
HPLC	Waters	e-2695
Surface Energy Analyser	SMS, London, UK	SMS-iGC 2000
Laser diffractometer	Sympatec Instruments, UK	HELOS (H2419) & RODOS dispersion.
Rotavapor	BUCHI	Rotavapor R210 et R215
E5071C ENA series	Agilent Technologies	300kHZ-20GHz Network Analyser

4.1.4 Software

Different software used for analysis data are listed in Table 4.3

Table 4.3 List of software used for data processing

Software	Application
TA universal analysis	Thermal analysis (DSC, TGA)
PowDLL converter	PXRD pattern analysis
EVA	PXRD pattern analysis
GRAMS AI- Spectroscopy Software	Spectroscopic analysis (Raman and FTIR spectra)
ID NMR processor	NMR spectra
Cirrus Software	IGC graphical software
ACD/ Chem Sketch	Chemical structure drawing
Mercury	Chemical structure analysis

Origin 8.1	Graphical analysis of excel data
PCP Disso	Dissolution study
CITDAS	Aerodynamic properties analysis

4.2 Experimental methods

The method section is further categorised into two sections, experimental method and analytical characterisation method using different analytical tools. Initially process validation experiments is performed to understand the correlation between process parameters (temperature, pressure, supersaturation and solvent mixture) and end product physical and chemical state.

Once the process was validated further experimental designed was performed to explore the application of MASCW technology in crystal engineering.

Based on the objective to investigate the application of this new technology further experiments are categorised as below:

- Application of MASCW process for generation of congruent and incongruent stable and metastable cocrystals pairs.
- Application of MASCW process for particle engineering which includes generation of micron sized particles and analysis of kinetic and aerodynamic properties of active pharmaceutical ingredients. Investigation of MASCW technology for synthesis of metastable polymorphs
- The final study includes mechanistic understanding of hydrogen bonding between Ibuprofen and nano crystalline hydroxyapatite.

Crystal structure, polymorphic form and calculated PXRD patterns of all pharmaceutical ingredients are retrieved from Crystal Structure Database (CSD)

4.2.1 Process understanding and validation method

In this section investigation of the influence of different process parameters like temperature, pressure, solution supersaturation and dielectric solvent mixture on crystal state of end product was done. Paracetamol was selected as the model component to validate different parameter of MASCW technology. This is further categorised as below:

4.2.1. A) Investigation of effect of supersaturated concentration of paracetamol and process temperature/pressure parameters: In this study different concentrations (w/v) of paracetamol solutions in water were selected. Based on the minimum volume requirement of the instrument container, 10ml volume of water is considered as lower limit of solvent. Based on solubility of paracetamol in water different w/v supersaturated solution concentration 5%, 10%, 15%, 20%, 25% and 30% w/v of paracetamol in water were selected. All the samples were weighed accurately and processed using MASCW processes until clear solution is observed. Once the clear solution was formed the corresponding temperature and pressure conditions were recorded. Correlation between supersaturation and solubilising temperature and pressure conditions was plotted graphically using binary phase diagram. As the samples are treated at high temperature and pressure conditions percent essay of individual powdered samples, supersaturated solutions and filtered solutions was analysed using HPLC analyser. Different parameters including pH of the

supersaturated solution and percent yield is calculated for all the experiments. Once the crystal started inducing out samples were vacuum filtered using Whatmann filter paper (0.04 micron size) and air dried under ambient conditions. There were further analysed to investigate crystal form using analytical tools like PXRD, DSC and Raman spectroscopy.

4.2.1. B) Crystallisation time: In this experimental design the main objective was to prepare a saturated solution of paracetamol (similar to above experiments) using MASCW process and monitor the time required to induce crystallisation. Concentrations of paracetamol solution selected for sub-critical and conventional heating are 5%, 10%, 15%, 20%, 25% and 30% in 10 ml deionised water. Using MASCW process all the samples are processed at 140°C with heating rate of 7°C/minute at variable pressure (4.0-5.0bars) until clear solution is formed; further on cooling the time required for the crystals to induce is recorded. The experimental results was compared with the conventional heating experiments were similar supersaturated solutions of paracetamol were prepared in 10ml of water and subjected to heating and stirring using water bath at 90°C-95°C and magnetic stirrer beads respectively for four hours. The solubility and percent essay of these saturated solutions are reported. PXRD, DSC and Raman data was analysed.

4.2.1. C) Crystallisation kinetic studies: In this section the crystallisation kinetic studies of paracetamol solution using off line Raman spectroscopy have been described. Homogenous supersatured solution of 10%w/v of paracetamol is processed using MASCW technology and drop of this solution is placed on the sample slide and analysed using Raman

spectroscopy at 785nm laser power at different accumulations and time points over 24hrs. This experiment is performed to tract the crystallisation kinetics and phase identification using spectroscopy. Spectra over lay of Raman spectra are graphically plotted for every three hours' time point.

4.2.1. D) Effect of solvent mixture on dielectric constant of solution and solubility of paracetamol: In this section use of solvent mixture apart from pure water for crystallisation of API was investigated. Four different organic solvents like methanol (MeOH), ethanol (EtOH), acetone (ACE) and acetonitrile (ACN) all HPLC grade were selected to prepare 10%, 20% and 30% v/v concentration with water. Initially dielectric constant of water and solvent mixture of water-methanol, water –ethanol, water- acetone and water- acetonitrile from 0%v/v concentrations to 100%v/v concentrations was analysed. Later 10%, 20% and 30% v/v solution concentrations was selected and added 1g of paracetamol and processed using MASCW process at 130°C with heating rate of 13°C/minute under variable pressure conditions until clear solution is formed. Once these saturated solutions are cooled at room temperature change in the dielectric constant of paracetamol solutions was reported.

The equilibrium solubility of paracetamol raw in all these solvents for 24 hrs was checked at 25±3°C in triplicates. Amount of paracetamol dissolved in the respective solvent system was quantitatively determined using HPLC analyser. Based on the solubility of paracetamol in the solvent selected 1500mg of paracetamol in the solvent mixture and processed using MASCW technology was selected. Further this saturated solution was left for stirring at 300rpms for 24hrs under room temperature conditions. All the samples are

treated at 150°C with heating rate of 15°C/min at variable pressure conditions. Change in dielectric constant, pH of the solution and equilibrium solubility of paracetamol in these solvent mixtures using MASCW technology was notified and reported. Percent purity and amount of dissolved paracetamol in all the solvent mixtures is analysed quantitatively using HPLC analyser.

4.2.2 Application of MASCW process in cocrystallisation process

Under this section elucidation of the application of MASCW process in generation of stable cocrystal pairs was explored. This section is divided into three sections;

Section 1 includes the generation of CBZ: SAC (1:1) form I and form II cocrystals using MASCW process, further in this section the correlation between process parameters on cocrystal phase is reported.

Section 2 demonstrates the screening experiment used to analyse the formation of cocrystals using MASCW process, in this section SMT, SMZ as API molecules and SAC as cocrystal former was selected.

Section 3: this section included the cocrystallisation of incongruent pair; CAF and 4HBA in different stoichiometric ratios was selected and further the application of MASCW process in incongruent pair cocrystal formation was investigated.

4.2.2.1 Cocrystallisation of CBZ: SAC cocrystals

This study includes experimental design for co-crystallisation of CBZ: SAC stable form I and metastable form II cocrystal pairs using MASCW process, further methods for quantitative analysis of CBZ: SAC cocrystals using

HPLC, solubility profile of cocrystal pairs and surface properties of the powdered samples are described.

4.2.2.1.1 Crystal Structure data prediction

A) Crystal structure data of CBZ and SAC

Carbamazepine anhydrous form III (CSD Refcode CBMZPN10)

Polymorphic forms of CBZ are ranging from I to V, out of which form III anhydrous CBZ which is monoclinic crystal form is selected for the present study. This crystalline phase consists of space group $P2_1/n$, unit cell dimensions are, cell length a = 7.53Å, b = 11.15Å and c = 13.91Å and the angles are α = γ = 90 and β = 92.86°. The computationally calculated PXRD pattern and crystal structure of CBZ III are displayed in Figure 4.1 and 4.2 respectively. This PXRD pattern reflects the characteristic peaks at 2θ (°) = 13.173 and 15.32.

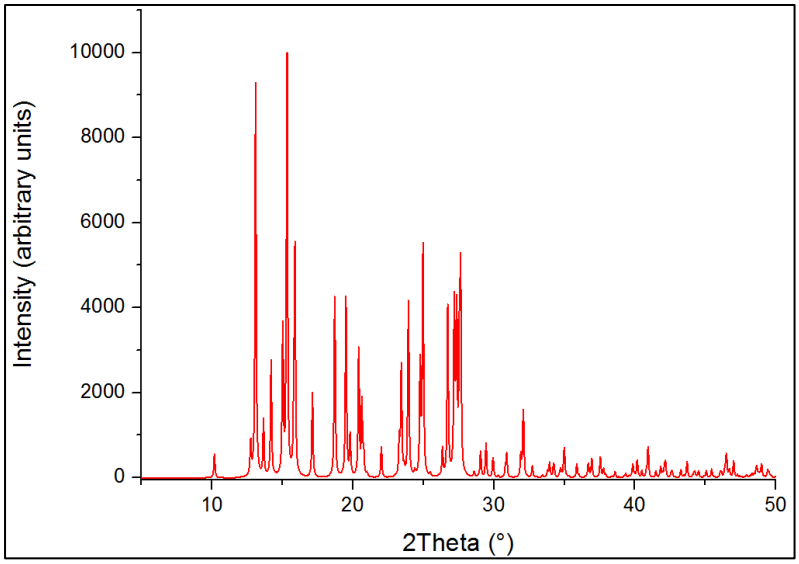

Figure 4.1 Calculated PXRD pattern of CBZ Form III (retrieved from CSD)

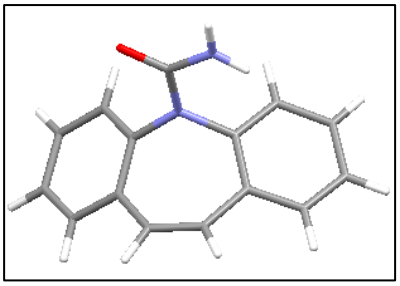

Figure 4.2 Crystal structure of CBZ III (retrieved from CSD)

B) Carbamazepine dihydrate (CSD Refcode: FEFNOTO2)

The crystal structure of CBZ dihydrate (CBZD) compromises one CBZ and two water molecules. The hydrogen bond is formed N–H…O bond by inversion of crystallographic centre, the amido groups are contributing in hydrogen bonding activity (Robin K. Harris and Caiyun Ma 2005). CBZD is present in monoclinic with space group space group $P2_1/c$, the unit cell dimensions are, cell lengths a = 10.06 Å, b = 28.71 Å, c = 4.83 Å, and angles α = γ = 90° and β = 103.45°. Calculated PXRD pattern and crystal structure of CBZD are displayed below Figure 4.3 and 4.4 respectively.

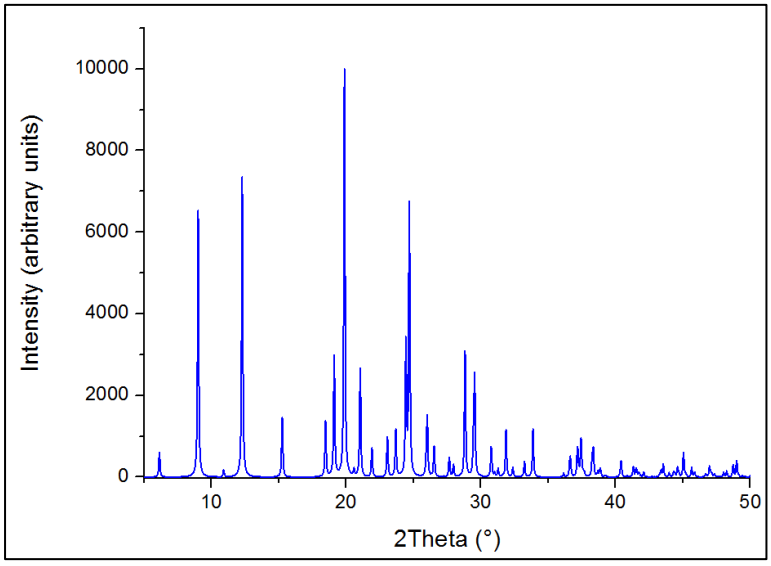

Figure 4.3 Calculated PXRD pattern of carbamazepine dihydrate (retrieved from CSD)

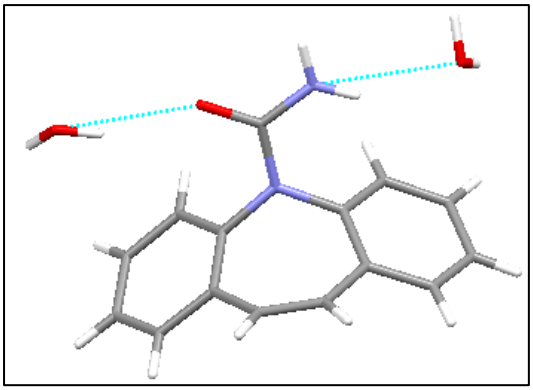

Figure 4.4 Crystal structure of CBZD (obtained from CSD)

C) Saccharin (CSD Refcode: SCCHRN)

Saccharin (CSD Refcode: SCCHRN) is arranged in planar and monoclinic crystal lattice with cell parameters as, lengths a= 9.55 Å, b = 6.91 Å, c = 11.80 Å and angels as α = γ = 90° and β = 103.9° and space group $P2_1/c$. The crystal structure represents the centrosymmetric dimer where hydrogen bond N–H···O is present between nitrogen molecule of imide group and oxygen molecule of keto group (Rahul Banerjee 2005). The below Figure no 4.5 and 4.6 represent the PXRD pattern and crystal structure of saccharin. In the calculated PXRD pattern characteristic reflections are observed in 2θ (°) = 15.99 and 25.2.

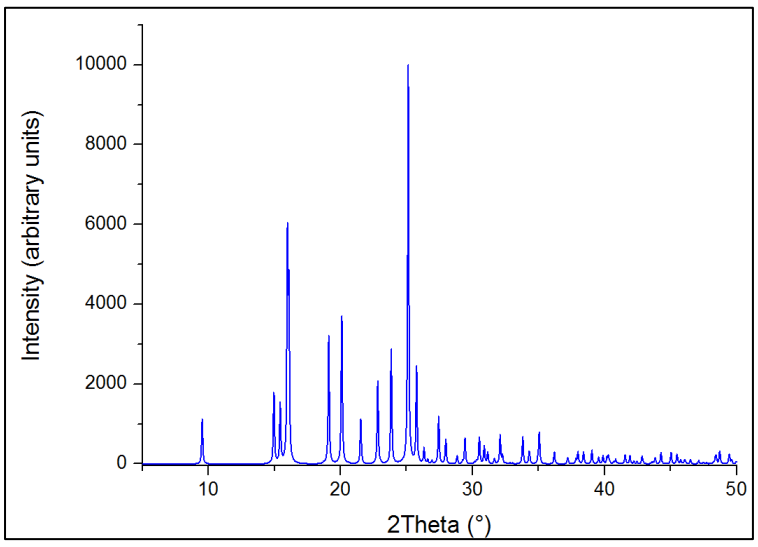

Figure 4.5 Calculated PXRD pattern of saccharin (retrieved from CSD)

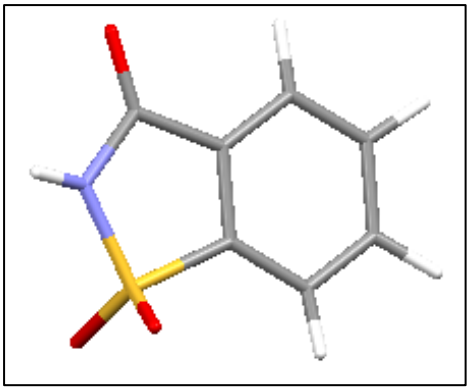

Figure 4.6 Crystal structure of saccharin (obtained from CSD)

D) CBZ/SAC cocrystal Form I (CSD Ref code: UNEZAO)

CBZ/SAC form I is triclinic crystal entity with space group of P-1 and the unit cell parameters are a = 7.514 Å, b = 10.4538 Å, c = 12.6826 Å, and angles α =83.642°, γ = 75.411° and β = 83.642°. They are arranged in 1:1 stoichiometric ratio, this form is addressed as the stable form of CBZ/SAC 1:1 cocrystal. This exhibits homosynthon between the N-H site of SAC and –COOH site of CBZ the second hydrogen bond i. e. formed between anti N-H group of CBZ and -S=O group of SAC (Porter et al., 2008). The distance of these two hydrogen bonding are d=1.75Å and d=2.47Å respectively. In the calculated PXRD pattern of this cocrystal characteristic reflections are observed at 2θ=6.88°, which is distinctive peak from CBZ/SAC form II cocrystal. Below is the schematic representation of the hydrogen bonding taking place between CBZ/SAC, PXRD pattern and crystal structure.

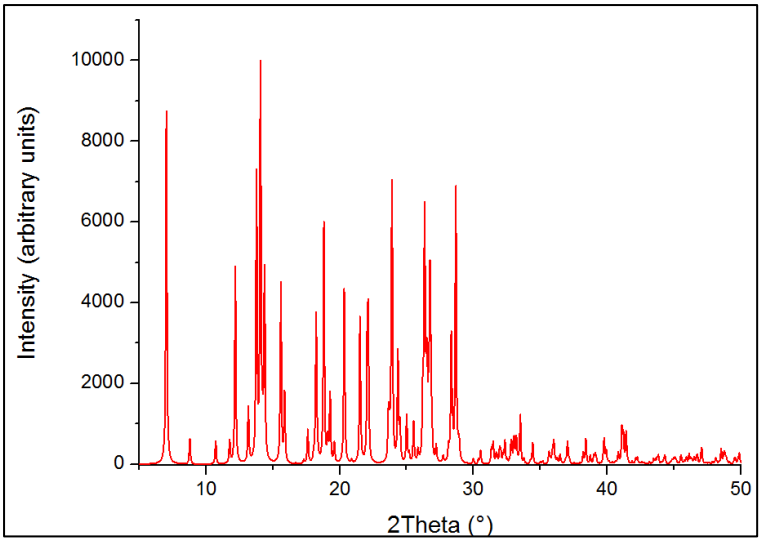

Figure 4.7 Calculated PXRD pattern of CBZ/SAC 1:1 cocrystal FI (retrieved from CSD)

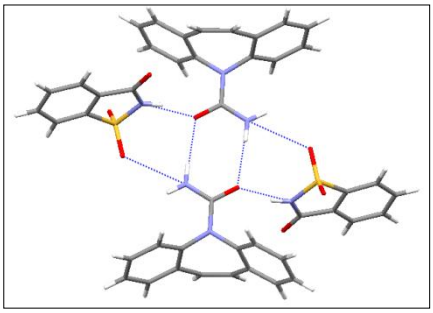

Figure 4.8 Crystal structure of CBZ/SAC 1:1 cocrystal

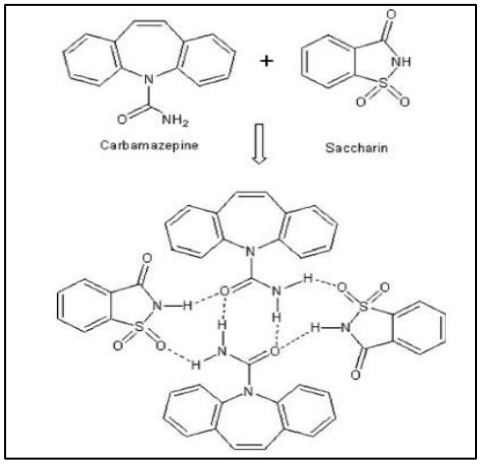

Figure 4.9 Schematic representation of CBZ/SAC 1:1 cocrystal motif (Hickey et al., 2007).

E) CBZ/SAC cocrystal Form II (CSD Ref code: UNEZAO01)

This form II structure consists of monoclinic space group *C*2/*c* with *a* = 35.72 Å, *b* = 6.84 Å, *c* = 16.11 Å, and β = 98.03°. This exists in the form of heterosynthon between CBZ and SAC. Hydrogen bond is observed between N-H group of SAC and C=O group of CBZ at d=1.76Å and second bond is observed between N-H group of SAC and carboxylic group of CBZ at d=1.97Å, the differentiating bonding is observed between the –N-H site on urea region of CBZ and S=O group of SAC at d=2.00Å. There is a characteristic distinctive peak of CBZ/SAC form II reflected at **2θ = 4.80 °** which is lacking in form I. The morphology of this form is confirmed to be needle shaped (Porter et al., 2008).

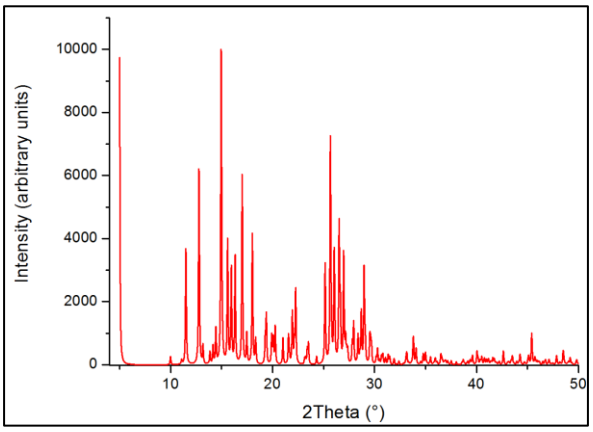

Figure 4.10 Calculated PXRD pattern of CBZ/SAC 1:1 cocrystal FII (CSD)

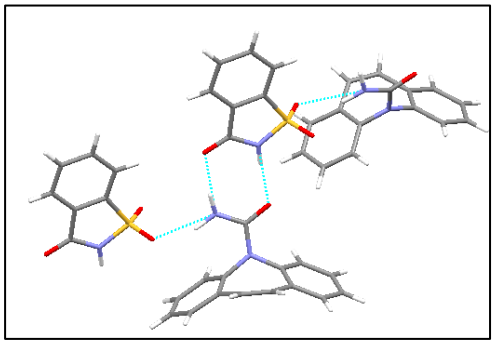

Figure 4.11 Crystal structure of CBZ/SAC 1:1 cocrystal (obtained from CSD)

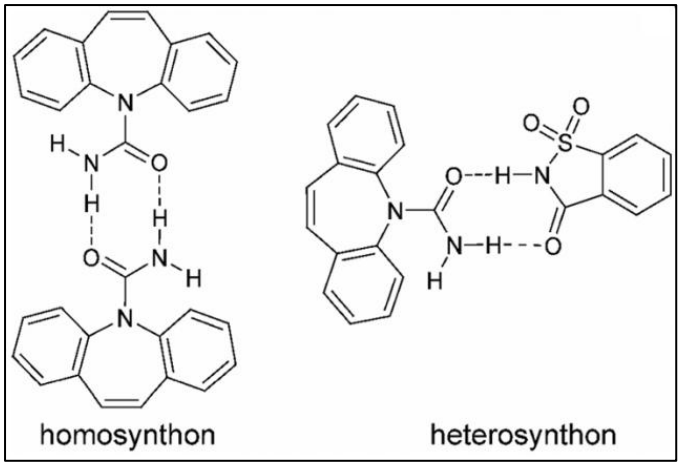

Figure 4.12 Difference between homosynthon (FI) and heterosynthon (FII) of CBZ/SAC cocrystals.

4.2.2.1.2 Crystallisation method of CBZ/SAC cocrystals

Microwave assembly used for the crystallisation is RotoSYNTH (Analytix) which consists of quartz reacting vessel with total capacity of 30mL. It has the temperature and pressure valve and the limits are up to 350˚C and 30 bars pressure respectively. Molar weight of CBZ and SAC in 1:1 stoichiometric ratios is weighed accurately using analytical balance and deionised water is used as the solvent media for cocrystallisation process. The total molar weight of CBZ /SAC 1:1 cocrystal pair is 350 mg and it is kept constant throughout the experiment. This saturated mixture solution is subjected for stirring using magnetic stirrers.

Different experiments were performed to study the effect of process parameters and concentration of solvent in the final product. For the purpose of comparison CBZ: SAC cocrystals were crystallised from methanol using conventional solution crystallisation technique. CBZ: SAC (2mmol) each is weighed and dissolved using methanol (40ml) till clear solution is formed and then the saturated solution is left for solvent evaporation to induce solution mediated crystallisation process. Below Table 4.4 represents the

experimental design where different process parameters like energy, temperature, heating rate, concentration of solvent and effect of solvent mixture as selected as variable parameters and amount of solute mixture in water as constant parameter. Microwave energy is used to increase the temperature and pressure of the solution, the solution is treated until homogenous solution of solute and solution is obtained. Once the clear solution is obtained it is further treated to confirm homogeneity and further on sudden quenching or controlled cooling crystals starts inducing out. During the cooling stage the crystals started inducing out which are vacuum filtered using wattmann filter paper (grade 1) and air dried at ambient conditions and further characterised using different analytical tools.

Table 4.4 Design of experiment for cocrystallisation using MASCW process

Constant parameter	Variable parameters			
Amt. of solute mixture (mg) (API:CF)	**Target temp (°C)**	**Vol. Of solvent (ml)**	**Microwave power (watts)**	**Rate of heating (mins)**
350 (1:1)	**110**	10	300	5
350 (1:1)	**115**	10	300	5
350 (1:1)	**120**	10	300	5
350 (1:1)	115	**10**	300	5
350 (1:1)	115	**12.5**	300	5
350 (1:1)	115	**15**	300	5
350 (1:1)	115	10	**200**	5
350 (1:1)	115	10	**300**	5
350 (1:1)	115	10	**400**	5
350 (1:1)	115	10	300	**5**
350 (1:1)	115	10	300	**2.5**

350 **(1:1.5)**	115	**12.5**	300	**5**
350 **(1:1.5)**	115	**15**	300	**5**
350 **(1:2)**	115	**12.5**	300	**5**
350 **(1:2)**	115	**15**	300	**5**
350 (1:1)	115	5ml MeOH + 5ml water	300	**5**

4.2.2.1.3 HPLC method for analysis of CBZ: SAC cocrystals

For quantitative and qualitative analysis of the raw and processed samples HPLC method is developed. In MASCW process as the samples are subjected to high temperature and pressure conditions so for quantitative analysis of CBZ in the final cocrystal samples degradation study using HPLC is performed. Based on USP standards carbamazepine further undergoes degradation to iminostilbene. The degradation study is performed using Waters e-2695 system integrated with a PDA detector (PDA 2998) connected with degasser. Waters symmetry C18 column with dimensions 4.6 x 250 mm and the particle size of the packing material is 5µm. Concentration of injection volume used is 10µL. The mobile phase selected for the separation is the combination of acetonitrile with 0.1% v/v formic acid solution, flow rate selected is 1.2 mL per minute. The temperature of the column and sample is maintained at 25˚C±2 throughout the experiment. The UV wavelengths used for detection of CBZ and iminostilbene are 219 nm, 253 nm and 285 nm. The chromatographic data is analysed using Empower 3, analysis software.

<u>Development of calibration curve for iminostilbene</u>

Calibration curve for iminostilbene is generated using six known standard concentrations of iminostilbene. Area under the curve is integrated and

calibration plot is plotted against concentration and area under curve. This graph is used to generate the slope equation. The concentrations of iminostilbene selected were 10, 20, 30, 40, 50 and 60µg/mL in acetonitrile as the solvent media. The slope equation is used to calculate the unknown concentration of iminostilbene in MASCW processed samples.

Sample preparation

Analysis of the unknown iminostilbene in MASCW processed carbamazepine is performed dissolving 250mg of processed sample in 10mL acetonitrile and subjected for stirring till clear solution is formed. The resultant solution is injected into HPLC assembly after passing through 0.45 µM nylon membrane filter. The quantification of iminostilbene in these samples is done using calibration curve equation.

4.2.2.1.4 Surface Energy Analysis method

Surface energy analysis is performed to understand the change in the surface properties of initial and final dry powdered samples. This analysis explains the change in specific surface area and surface heterogeneity which is attributed to change in particle morphology and crystal form. The instrument used for analysis is Surface Energy Analyser (SEA), UK Ltd.

CBZ/SAC form I and form II obtained from MASCW processed is analysed and in comparison with this CBZ/SAC form I obtained from solution crystallisation is used. To compare the results obtained by different batches and forms, the iGC experiments were performed at specific and constant probe surface coverage. Fixed probe surface coverage approach is applied to SEA which is next generation system.

Three separate salinised glass columns were packed with the cocrystal samples using glass wool and these are subjected for SEA analysis.

- Column temperature maintained at 30°C
- Relative humidity conditions are 0%
- The conditioning of samples to nullify the vacuum present is done for 4hrs using inert helium gas.
- Conditioning of the column before and after the experiment is done using methane injection.
- Amount of samples used are

  CBZ/SAC Form I solution crystallisation: 135 mg

  CBZ/SAC Form I MASCW processed : 110 mg

  CBZ/SAC Form II MASCW processed : 139 mg

Initially, BET surface area of the cocrystal samples were calculated and further based on the surface area of the sample further surface heterogeneity is calculated using different solvent probes.

BET surface area is calculated by injecting octane gas at different surface coverage's, area under curve (peak max) is determined using Dorris and Gray equation. Below Table 4.5 describes the experimental details used for calculating BET specific surface area. Cirrus Plus software is used to analyse the dispersive surface energy of the materials.

Based on the specific surface area results different alkanes (hexane, heptane, octane, nonane), polar and nonpolar injections were injected in the sample column to determine the surface heterogeneity of the sample. Detail description regarding the experimental conditions and solvent system for analysing surface heterogeneity of the sample is described in Table 4.5.

Table 4.5 Experimental design used to analyse the specific surface area

Flow Rate (sccm):	10					
Target Column RH (%):	0	Target Column Temperature (°C):		30		
ID	**Solvent Name**	**T. F. S. Coverage**	**Temp. (°C)**	**Flow (sccm)**	**Duration (min.)**	**FID Gain**
1	OCTANE	0.004	30	10	4	10x
2	OCTANE	0.006	30	10	4	10x
3	OCTANE	0.008	30	10	4	10x
4	OCTANE	0.01	30	10	4	10x
5	OCTANE	0.02	30	10	4	10x
6	OCTANE	0.03	30	10	4	10x
7	OCTANE	0.05	30	10	4	10x
8	OCTANE	0.055	30	10	4	10x
9	OCTANE	0.06	30	10	4	10x
10	OCTANE	0.065	30	10	4	10x
11	OCTANE	0.07	30	10	4	10x
12	OCTANE	0.075	30	10	4	10x
13	OCTANE	0.08	30	10	4	10x
14	OCTANE	0.085	30	10	4	10x
15	OCTANE	0.09	30	10	4	10x
16	OCTANE	0.095	30	10	4	1x
17	OCTANE	0.1	30	10	4	1x
18	OCTANE	0.15	30	10	4	1x
19	OCTANE	0.2	30	10	4	1x

Below Table 4.6 illustrated the method used to analyse surface heterogeneity of the samples.

Table 4.6 Experimental design to analyse surface heterogeneity

Probe Solvent	% coverage	Column temperature	Flow (sccm)	Flow time (minutes)	FID gain
Octane	0.06	30 °C	5	20	1 X
Octane	0.065	30 °C	5	20	1 X
Octane	0.07	30 °C	5	20	1 X
Octane	0.08	30 °C	5	20	1 X
Octane	0.09	30 °C	5	20	1 X
Octane	0.095	30 °C	5	20	1 X
Octane	0.1	30 °C	5	20	1 X
Nonane	0.06	30 °C	5	20	1 X
Nonane	0.065	30 °C	5	20	1 X
Nonane	0.07	30 °C	5	20	1 X
Nonane	0.08	30 °C	5	20	1 X
Nonane	0.09	30 °C	5	20	1 X
Nonane	0.095	30 °C	5	20	1 X
Nonane	0.1	30 °C	5	20	1 X
Decane	0.06	30 °C	5	20	1 X
Decane	0.065	30 °C	5	20	1 X
Decane	0.07	30 °C	5	20	1 X
Decane	0.08	30 °C	5	20	1 X
Decane	0.09	30 °C	5	20	1 X
Decane	0.095	30 °C	5	20	1 X
Decane	0.1	30 °C	5	20	1 X

4.2.2.1.5 Solubility studies

Solubility profile curves were generated based on the solubility of CBZ-SAC FI and FII in the deionised water at different temperatures ranging from 10 °C

to 45 °C. The solubility of FI and FII were measured in terms of concentration of CBZ using high performance liquid chromatography (HPLC), Waters e-2695 equipped with PDA detector (PDA-2998). The HPLC analysis is performed using Waters symmetry C18 column with 5µ column packing material and 4.6x 250mm column dimensions. The HPLC method used is an isocratic and mobile phase comprises of 30%water and 70% acetonitrile containing 0.1% trifluroacetic acid, flow rate and injection volume used is 1 mL/min and 10µL respectively.

4.2.2.2 Cocrystallisation of SMT: SAC and SMZ: SAC cocrystal pairs

MASCW technology was further explored as a screening tool for the generation of different cocrystal pairs. In the screening experiments cocrystals of SMZ: SAC and SMT: SAC is synthesised in 1:1 molar stoichiometric ratios.

4.2.2.2.1 Crystal Structure data prediction

A) Crystal structure data of SMZ (CSD Refcode- 2209208-COD)

Sulfamerazine exists in three polymorphic forms, form I, II and III (Ravindra Acharya et al., 1982) . All the three polymorphs of SMZ is a dimer via a pair of intermolecular N-H…N hydrogen bonds between two SMZ molecules. Furthermore one of the hydrogen atoms of the amide group associated with dimer is engaged in single intermolecular N-H….O hydrogen bond with the oxygen of sulfonyl group. Thus as a result of molecular association structure with extended two dimensional (2D) hexagonal networks is present in form I polymorph and one dimensional (1D) ladder network is in form II and form III. In the present study form I polymorph of SMZ with space group of P 2_1/c with cell length a 11.097, b 8.315, c 13.964 and cell angles (α 90.00 β 99.327 γ

90.00) have been used. There is no crystal structure data reported for the sulfamerazine and saccharine cocrystal pair. Below Figure 4.13 and 4.14 describes the crystal structure and calculated PXRD pattern for SMZ form I

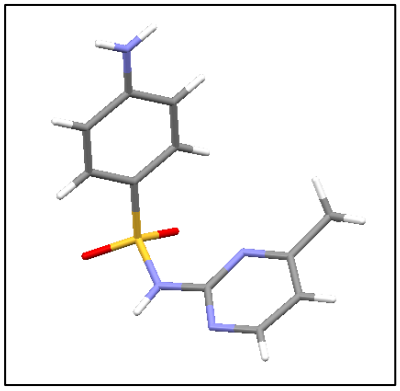

Figure 4.13 Crystal structure of: sulfamerazine (CSD -2209208-COD)

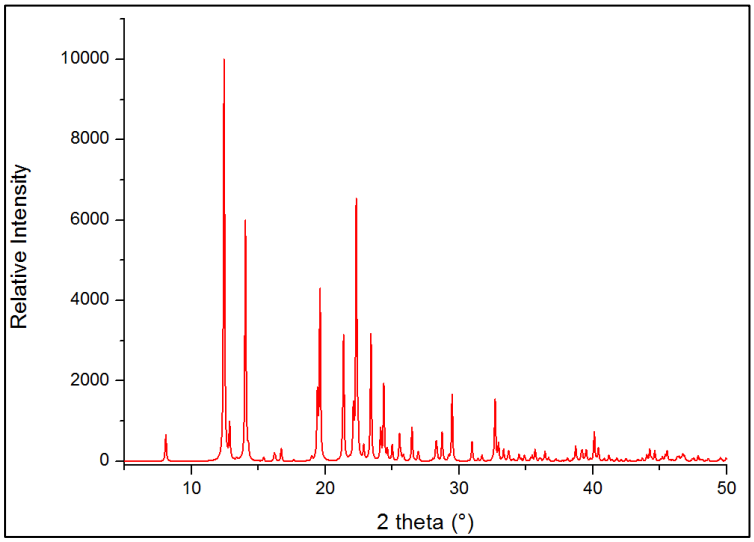

Figure 4.14 Calculated PXRD pattern of sulfamerazine form I polymorph

B) Crystal structure data of SMT and SAC cocrystal (CSD Refcode g150513a)

As the crystal structure data for sulfamethazine is not reported, therefore the calculated crystal structure data for SMT: SAC cocrystal has been used as reference. SMT: SAC in 1:1 stoichiometric ratio exists in monoclinic crystal lattice with space group of $P2_{1/n}$, bond length (a/ A° 8.0729, b/ A° 17.6015, c/ A° 14.4311) and bond angle (α/° 90, β/° 104.488, γ/° 90). Below Figure 4.15

and 4.16 represents the crystal structure of SMT: SAC 1:1 cocrystal and calculated PXRD pattern respectively (Fu et al., 2016). Crystal structure data of saccharine is described in the above section (4.2.1.1.1. a – structure-C).

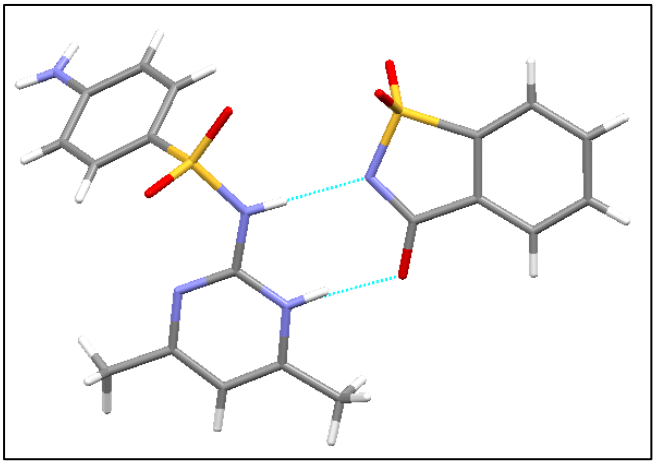

Figure 4.15 Crystal structure of: SMT: SAC 1:1 cocrystal (CSD Refcode g150513a)

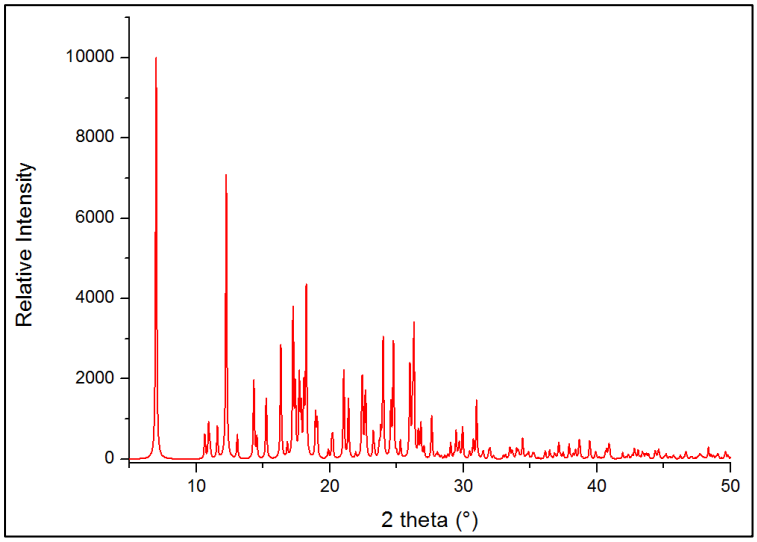

Figure 4.16 Calculated PXRD pattern of SMT: SAC 1:1 cocrystal

4.2.2.2.2 Crystallisation method for screening experiment

Equimolar concentrations of APIs SMT (278mg, 1mmol), SMZ (264 mg, 1mmol) and cocrystal former SAC (183 mg, 1 mmol) were added to 10ml of water and were subjected to high temperature and pressure under the influence of microwave energy (300watts) using MASCW technology till clear

solution is obtained. The clear solution is further aged at the targeted subcritical temperature for 1 minute to attain homogenous solution and then the solution is cooled down, upon cooling the solution is subjected for shear via stirring using magnetic stirrer and based on the supersaturation level crystals started inducing out. Below Table 4.7 explains the experimental and stoichiometric conditions of the experiment. The material is filtered using 0.22 µm PTFE syringe filter paper, dried at ambient conditions and analysed using PXRD and thermal analysis (DSC and TGA) to confirm the cocrystal formation.

Table 4.7 Experimental conditions for SMT/SAC and SMZ/SAC cocrystals

Wt. of API (mg)(1mmol)	Wt. of SAC (1mmol)	Stoichiometric ratio	Targeted-temp (°C)	Heating rate (°C/min)
SMT (278)	183 mg	1:1	135	27°/min
SMZ (264)	183 mg	1:1	135	27°/min

4.2.2.3 Application of MASCW process for generation of incongruent pair cocrystal pair (CAF: 4HBA 1:1)

In this study based on the aqueous solubility of individual component CAF and 4HBA is selected as incongruent cocrystal pair. They are process at different stoichiometric ratios using MASCW process.

4.2.2.3.1 Crystal structure data of CAF and 4HBA

A) Caffeine anhydrous (CSD Refcode NIMFEE03)

They are two polymorphs of caffeine anhydrous but one of the anhydrous crystal form is reported (Habgood and Price 2010). Caffeine anhydrous (CSD Refcode NIMFEE03) - xanthine derivative and caffeine consists of two fused

rings pyrimidinedione and imidazole. Caffeine anhydrous undergo crystallisation with five independent molecules in a monoclinic C-centered unit cell with dimensions a=43.0390 Å, b=15.0676Å and c=6.95314 Å and beta angle of 99.027° (Lehmann and Stoisser 2007). In the below Figures 4.17, 4.18 represents crystal structure and calculated PXRD pattern of t anhydrous caffeine.

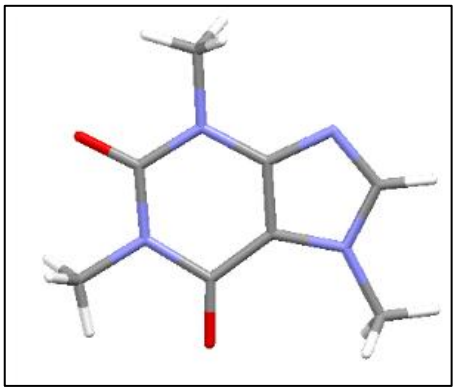

Figure 4.17 Crystal structure of: caffeine anhydrous (CSD Refcode NIMFEE03).

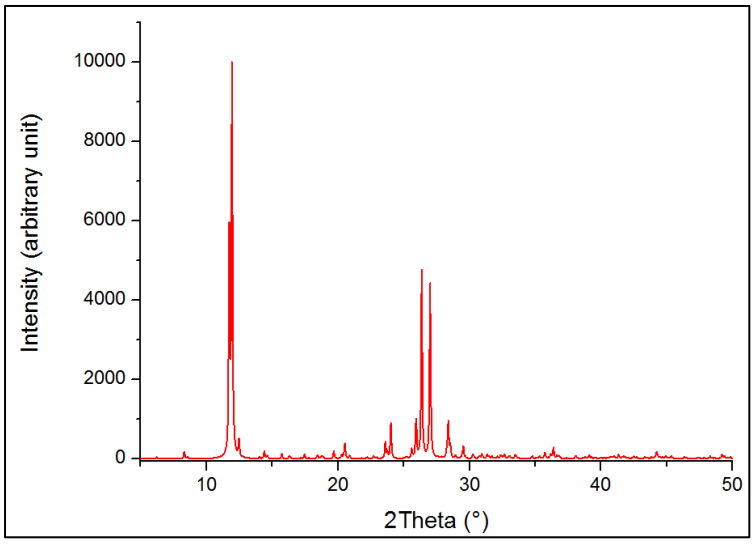

Figure 4.18 Calculated PXRD pattern of caffeine anhydrous.

B) 4-Hydroxybenzoic acid (CSD Refcode JOZZIH)

4-Hydroxybenzoic acid (4-HBA) exists in two polymorphic forms but one of the polymorphs crystal structure reported, it is the monoclinic crystal

structure with space group *P*21/*a,* and unit cell dimensions are a= 18.508 Å, b = 5.228 Å, c = 6.342 Å and angels as α = γ = 90° and β = 93.22°. This structure has hydrogen bonding site at the -OH functional group. Figure 4.19 and 4.20 represents the crystal structure and calculated PXRD pattern of 4-HBA.

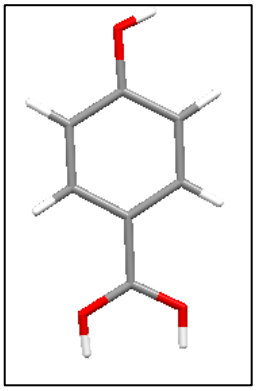

Figure 4.19 Crystal structure of 4-hydroxybenzoic acid (CSD Refcode JOZZIH).

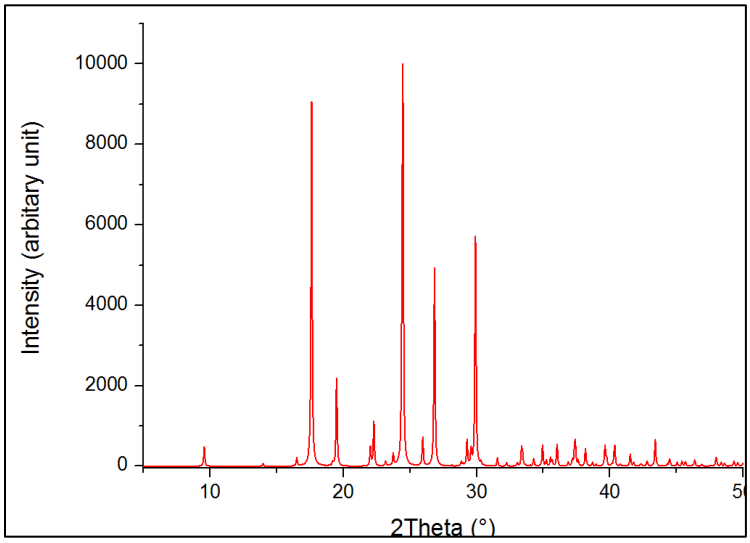

Figure 4.20 Calculated PXRD pattern of 4-hydroxybenzoic acid.

4.2.2.3.2 Experimental method of cocrystallisation

MASCW process is performed initially using water 10 mL as solvent system, microwave energy is 300W and rate of heating is 5 minutes. Molar quantity of CAF and 4HBA were weighed in different stoichiometry and subjected to

MASCW process, under the influence of elevated temperature and pressure till clear solution is obtained and the resulted supersaturated solution is further cooled using ice-water bath where the temperature is reduced suddenly. 2.5 mille moles of each starting solute components were selected based on supersaturation in the solvent system. The below Table 4.8 illustrates the brief description of experimental design of CAF/4HBA cocrystals and results obtained.

Table 4.8 Experimental design of: CAF-4HBA cocrystallisation using MASCW process.

Wt. of CAF (mg) (2.5mmol)	**Wt. of 4HBA (mg)(2.5mmoll)**	**Ratio**	**Solvent system (10 mL)**	**Temp (˚C)**
485	345	1:1	water	135
485	690	1:2	water	135
970	345	2:1	water	135
485	345	1:1	5mLMeOH +5mL H_2O	135

The cocrystal obtained is vacuum filtered using 0.22µm PTFE syringe filter paper and dried in the ambient conditions for 1 hr and further analysed using PXRD, DSC, TGA and NMR.

4.2.2.4 Application of MASCW process in particle engineering of paracetamol.

In this section MASCW process was implemented to explore its application in the field of particle engineering. This section is divided into two sections based on the application.

Section 1: In this section paracetamol was selected as lead molecule and MASCW process was implemented for generation of metastable polymorphs

of paracetamol to enhance the compressibility and kinetic properties of paracetamol powder and tablet.

Section 2: MASCW process was further explored for generation of macro sized anhydrous theophylline and analysed their aerodynamic performance using Next Generation Impactor (NGI).

4.2.2.4.1 Crystal structure database (CSD) of paracetamol

A) Paracetamol form I (CSD Refcode: HXACAN01)

Paracetamol is antipyretic drug which exists in three polymorphic forms. Paracetamol form I and II are well studied crystal structures than III which is still elusive. This is stable monoclinic form which is placed in space group $P2_{1/a}$ with unit cell dimensions cell length a = 12.930Å, b = 9.400Å and c = 7.100Å and the angles are α = γ = 90 and β = 115.9°. Below Figure 4.21 and 4.22 represents the crystal structure of Paracetamol and computationally calculated PXRD pattern of paracetamol form I (monoclinic).

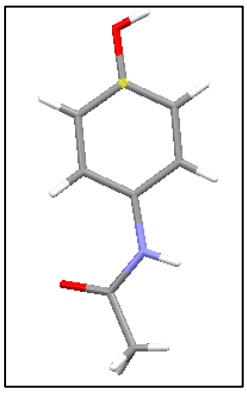

Figure 4.21 Crystal structure of paracetamol (retrieved from CSD).

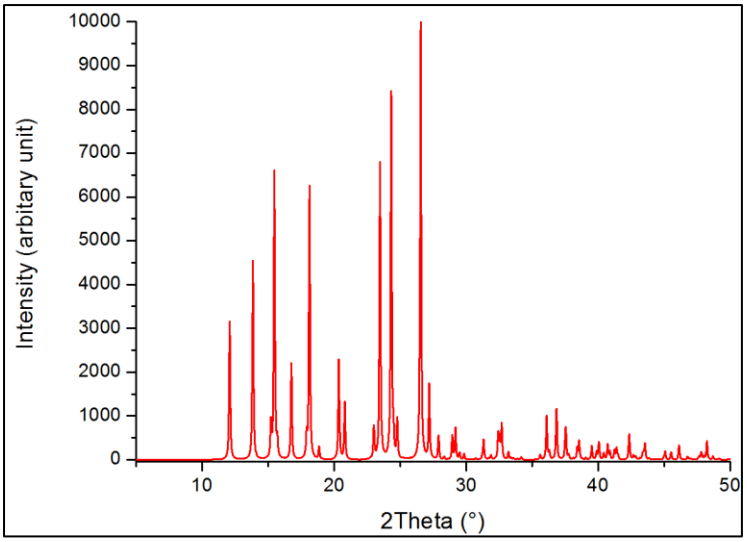

Figure 4.22 Calculated PXRD pattern of paracetamol Form I.

B) Paracetamol form II (CSD Refcode HXACAN23)

Paracetamol form II is referred as metastable phase with orthorhombic crystal structures. It is crystallized in the space group of *Pcab* with unit cell dimensions a = 7.406 Å, b = 11.837Å and c = 17.162Å and the angles are α = β = γ = 90°. Figure 4.23 represents the calculated PXRD pattern of Paracetamol form II. The crystal structure is similar in all forms as they are polymorphs they differ only in the cell dimensions and space group.

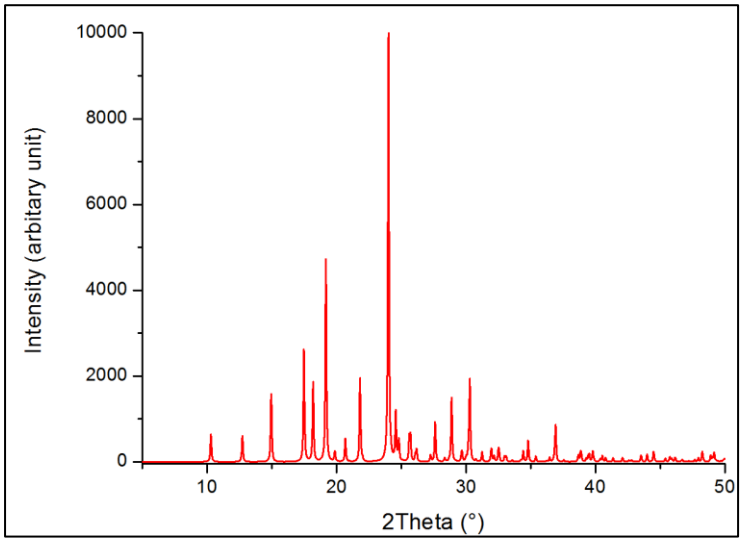

Figure 4.23 Calculated PXRD pattern of paracetamol Form II.

4.2.2.4.2 Processing method of Paracetamol

MASCW process was used to process commercially available form I polymorph of paracetamol. In this process the paracetamol was subjected to high temperature and pressure conditions until clear solution was obtained and further left it for cooling. Based on the level of supersaturation and aqueous solubility of paracetamol the crystals started inducing as the temperature decreases and the crystalline material is vacuum filtered using wattmann filter paper. The concentration of solute in the solvent system is selected considering the solubility of paracetamol in water to maintain high supersaturated concentration of paracetamol in water. Based on the literature review the solubility of paracetamol in water at 25°C is approximately 14mg/ml so initially smaller quantity of solute was used but after process due to less supersaturation concentrations crystals failed to induce, based on this observation solute concentration was optimised to 1g and based on the capacity of instrument and observations in cocrystallisation experiments 10 mL of water is considered. The supersaturation concentration is 14 times higher than the normal solubility of paracetamol in water. The heating rate to reach the target temperature is optimised to 5 minutes and is further treated at that temperature for 1 minute. At 140°C no decolouration or degradation of paracetamol took place, but when the temperature is further increased to 150°C there is decolouration of the solid materials taking place this is due to the degradation of paracetamol under the influence of high temperature and pressure conditions. Below Table 4.9 summarises the experimental conditions used to process paracetamol using MASCW technology.

Table 4.9 Experiment conditions used to process paracetamol using MASCW process.

Amt. of raw paracetamol	Experimental conditions during cooling step
1g	Controlled cooling without stirring
1g	Controlled cooling with stirring
1g	Sudden cooling with stirring
1g	Sudden cooling without stirring

4.2.2.4.3 Quantitative analysis of paracetamol using HPLC

As the samples of paracetamol are exposed to high temperatures and pressure conditions degradation analysis of paracetamol was performed using HPLC. Paracetamol in solution state undergoes oxidation to give rise to 4-aminopenol as potential degradant product. The degradation study is performed using Waters e-2695 system which is integrated by PDA detector (PDA2998) connected with degasser. The column used is waters symmetry C18 column with dimensions 4.6*250 mm and the particle size of the packed material is 5µm. Concentration of injection volume used is 10 µL.

Method: The method used to study the degradation calibration of paracetamol is gradient method where solvent A = 20mM phosphate buffer and solvent B = Acetonitrile HPLC grade. Column and the sample temperature were maintained at 25±2°C. The wavelength used to analyse paracetamol is 245nm where retention time is 3.9 and wavelength for 4-aminophenol is 230 nm where the retention time is 2.7.

Table 4.10 Summary of HPLC method (gradient)

Time (minute)	Flow rate (mg/ml)	%A Solvent	%B Solvent
0	1.50	90%	10%
10	1.50	70%	30%
12	1.50	90%	10%
15	1.50	90%	10%

Development of calibration curve for 4-aminophenol

Standard calibration curve is plotted for 4-aminophenol and paracetamol using same HPLC method of analysis. Area under the curve is integrated and the calibration plot is plotted between different concentrations and area under curve. From the slope value generated concentration of 4-aminophenol present in MASCW process paracetamol and percent purity of paracetamol present in the process samples was calculated. The concentrations used for calibrations are 5, 10, 20, 30, 40 and 50µg/mL. Phosphate buffer and acetonitrile were used for dilution of the standards and solvent to dissolve standard solute respectively.

4.2.2.4.4 Analysis of surface properties (SEA)

Surface properties like specific surface area, surface heterogeneity and acid-base values are analysed using Surface Energy Analyser (SEA). The procedures and methods used for analysis are similar to methods described in the Table 4.5 and 4.6. The analysis of the samples is performed at infinite dilutions. Approximately 100 mg of paracetamol form I and II MASCW processed and raw commercial form I is filled into salinised glass column (4mm diameter) and series of alkane gas is passed through the column to measure the change in elution obtained from all solvent systems. Fixed

probe surface coverage approach is applied to SEA which is next generation system.

4.2.2.4.5 Solubility study of paracetamol

Solubility study is performed to understand the kinetic properties of MASCW processed paracetamol samples. Paracetamol form I and II MASCW process and raw paracetamol form I is selected for this study. The particle sizes of the three samples are determined using Sympatec particle size analyser. The equilibrium solubility of the paracetamol samples were performed at constant temperature 20°C±3 against different time points using deionised water as solvent system. The time points selected for the study are 1, 2, 3, 4, 6, 12 and 24hrs. Approximately 200mg of each sample is added to 5ml of water under 300rpm stirring using magnetic stirrer. The temperature is monitored using temperature sensor on the hot plate. At every time point the supernatant liquid sample is filtered using wattmann filter paper with pore size 0.45microns and the quantitative analysis of the samples is analysed using HPLC analyser. The method used to study the concentration of the dissolved paracetamol in water is similar to the method used in quantitative analysis of paracetamol. The concentration of the dissolved paracetamol is calculated based on the slope equation derived from the calibration curve of paracetamol. All the readings are performed in triplicates.

4.2.2.4.6 Dissolution study

Intrinsic dissolution experiments were performed using a UPS II type LabIndia dissolution tester (Labin-09, India). Tablets of 500mg each paracetamol samples were prepared using IR –press at 1tones pressure for 30secs. Paracetamol raw and MASCW processed from I and from II samples

were placed at the bottom of the dissolution vessel (at least four repeats) containing 900 ml phosphate buffer (20mM) maintained at 37 ± 0.5 °C and stirred with a paddle at 50 rpm. Samples were collected periodically and further filtered. Quantification of paracetamol is performed spectrophotometrically at a fixed wavelength of 243 nm using a Jasco-V630 spectrophotometer. The percent release rate of paracetamol is calculated using PCP disso software.

4.2.2.5 Application of MASCW process for inhalation drug delivery system

In this present work MASCW process was in the field of crystal engineering for the generation of micro sized particles of anhydrous theophylline (THF) for inhalation drug delivery system. The aerodynamic performance of the MASCW process THF and spray dried THF as reference was reported.

4.2.2.5.1 Crystal Structure Data

A) Crystal structure data of Theophylline (CSD Refcode- 4505532-COD)

Theophylline is widely used antiasthmatic drug which is also known for its phase transition during pharmaceutical processing. Based on the storage conditions THF exists either as anhydrous THF or gets converted into THF monohydrate. Crystal structure of anhydrous and monohydrate THF is orthorhombic and monoclinic crystal systems respectively. In the present study anhydrous theophylline was used, this exists in two forms, stable form I anhydrous THF and metastable form I anhydrous THF (Phadnis and Suryanarayanan 1997). Crystal lattice of anhydrous THF consists of space group $Pna2_1$, cell length (A°) of a 13.087, b 15.576, c 3.863 and cell angles (°) of α90 β90 γ90 respectively. Below Figure 4.24 and 4.25 represents the

crystal structure and calculated PXRD pattern for anhydrous form I stable theophylline.

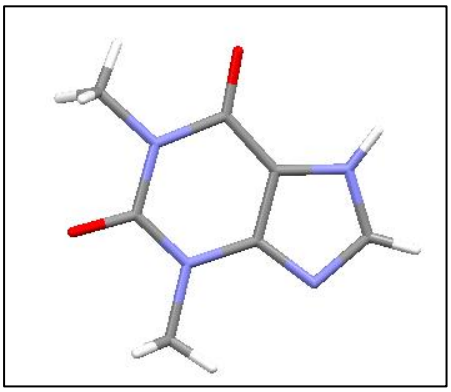

Figure 4.24 Crystal structure of: anhydrous theophylline (CSD Ref-4505532-COD)

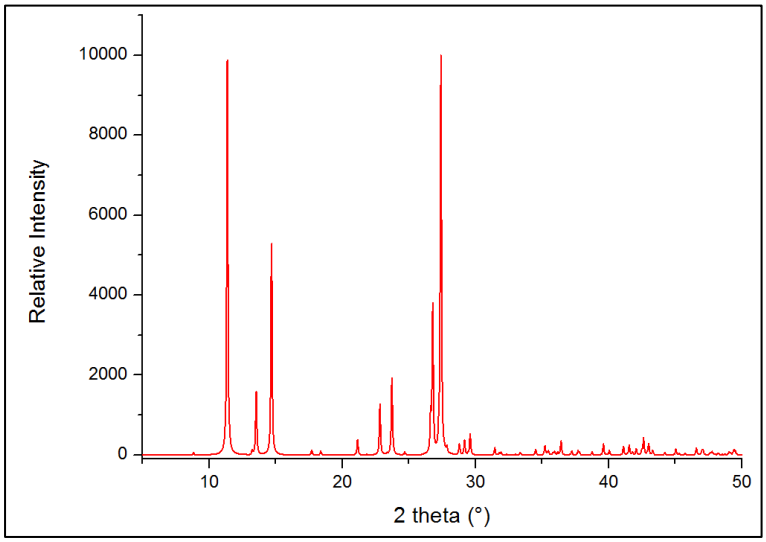

Figure 4.25 Calculated PXRD pattern of: anhydrous THF

4.2.2.5.2 Preliminary crystallisation experiments of THF

Crystallisation of theophylline is performed using various experimental conditions. Anhydrous THF (1g) in 10ml of distilled water was selected and subjected to high temperature and pressure conditions keeping microwave power (300 watts) as constant process parameter. The sample is heated till clear homogenous solution is obtained and the targeted temperature where clear solution is formed is 140°C and the heating rate is 27°C/min and is

further aged at this temperature for 1minute to attain homogenous solution and left the solution for cooling.

Different mechanisms of crystallisation were implemented to understand the effect of crystallisation techniques over particle size of the precipitated theophylline; Table 4.11 described different crystallisation conditions used to generate micro sized particles of THF. To study aerodynamic performance of any drug the mean particle size distribution (PSD) plays a significant importance in the development of inhalation drug delivery system and the PSD should be less than 5 micron according to USP standard requirements and NGI instrumental requirement. Thus the PSD of the THF samples processed using different crystallisation techniques were analysed and the one which is fulfilling the requirement for inhalation drug delivery system is selected and further large quantity of the samples were prepared to study aerodynamic performance of the powder using NGI inhaler. Methods used for crystallisation are:

I. In manual stirring the samples is stirred using magnetic stirrer during cooling stage. Based on the degree of supersaturation and shear conditions crystals started inducing out
II. Antisolvent technique is used based on the aqueous solubility of THF where MASCW solution of theophylline is poured in 50ml distilled water which is kept at ambient conditions under stirring using magnetic stirrer due to sudden decrease in the temperature and increase of shear conditions micro sized crystals induced out.
III. Implemented ultrasound induced crystallisation to produce micron sized particles, the MASCW solution of THF during cooling phase is

treated under ultrasound energy which is 100% amplitude for 3minutes.

IV. MASCW solution of THF was subjected to Ultraturrax to understand the effect of external shear of Ultraturrax over particle size of THF.

The crystals which are induced are vacuum filtered using 0.45 micron wattmann filter paper and kept for drying under ambient conditions before analysing for different crystalline properties and aerodynamic performance of THF.

Table 4.11 Experimental description of various batched of theophylline

Sample	Crystallisation techniques used
THF-S1	Raw anhydrous THF
THF-S2	Antisolvent techniques
THF-S3	Ultrasound assisted
THF-S4	Manual stirring
Lactose IG	Standard

4.2.2.5.3 Synthesis of spray dried anhydrous theophylline

Spray dryer is conventional technique used for generation of micron sized drug particle which are implemented in inhalation drug delivery system. Thus anhydrous THF was generated using spray dryer to compare aerodynamic performance results of THF obtained from MASCW technology. Based on the previous finding 0.02M solution of anhydrous theophylline in methanol (HPLC grade) (Alhalaweh et al., 2013) was used. Below Table 4.12 represents the experimental conditions used to synthesised spray dried theophylline.

Table 4.12 Experimental parameters used to crystallise THF using spray drying

Experimental parameters	
Inlet temperature -150°C	Outlet high -120°C
Outlet temperature-130°C	Cool temperature -80°C
Plate temperature -20°C	Aspirator Flow rate- 70 Nm^3/hr
Inlet high (°C)- 200°C	Feed Pump flow rate- 3ml/min

4.2.2.5.4 Method to setup the Next Generation Impactor

The Next Generation Impactor is the analytical instrument which is used to study the aerodynamic properties of the powdered materials using dry powder inhaler. This NGI consists of seven plates with a micro-orifice collector. This can be operated at inlet flow rate ranging from 30L/min to 100L/min based on the inhalation capacity of the patient. The NGI instrument consists of arrangement of three different metallic frames; bottom frame consists of the impaction cups where the material is deposited, middle plate which is sealed frame which holds nozzles and the upper most lid consists of inter stage passages which is used for the materials to flow ((United States Pharmacopeia Convention. 2004; European Directorate for the Quality of Medicines & HealthCare. 2008). Figure 4.26 demonstrated the different frames of NGI instrument. The instrument is connected to induction port preseperator. The use of pre-separator is recommended according to USP conventions, 2004 for dry powder inhaler to retain the active ingredients which are attached to larger carrier particles.

Before initialising the analysis the collection cups were coated with glycerol to prevent the bouncing of the powdered samples, the cups were placed in

the bottom frame and the NGI lid is closed, 15ml of methanol sample is placed in the central cup of pre-separator, further this pre-separator is connected to induction port which is also connected to impactor body. A suitable mouth piece is connected to the induction port to ensure there is no sample loss between the inhaler device and the induction port, a vacuum pump is connected to the NGI to attain desired flow rate. The inhalation flow rate is determined to be equivalent to 4 KPa pressure drop across the dry powder inhaler device (USP convention, 2004). This is equal to the flow rate of 60L/min. Before the use of inhaler device a calibrated electronic flow meter is used to measure the flow rate each time. The inhalation time required to attain desired flow rate and pressure drop is calculated by the following equation (European Directorate for the Quality of Medicines & HealthCare. 2008):

$$\boldsymbol{T = (60\ sec\ x\ V) / Q}$$

T = Time duration consistent for withdrawal of 4 litres of air from the inhaler

Q = Airflow which produces a pressure drop of 4 KPa

V = 4 L to be drawn through the inhaler

Based on the above equation the required time for attain flow rate of 60L/min is 4.0 secs. MASCW processed dry anhydrous THF samples (25mg) is loaded into 0.5size gelatine capsules and placed in the Foradil dry powder inhaler device, which is then connected to the induction port through an air tight connector to prevent the leakage of sample. Before starting the air flow the DPI device Foradil is pressed to break the capsule and then the drug is injected into the NGI at the flow rate of 60L/min for 4 seconds. Each experiment is performed in triplicates. Based on the particle size the sample

gets deposited in the different regions of impactor. The deposited particles at different stages are recovered by dissolving in the known volume of methanol followed by quantitative analysis using HPLC.

To study the different inhalation parameters of the samples Copley Inhaler Testing Data Analysis Software (CITDAS) is used. Using this software the fine particle fraction of drug deposited in different stages of NGI has been calculated, Mass median aerodynamic diameter and geometric standard deviation.

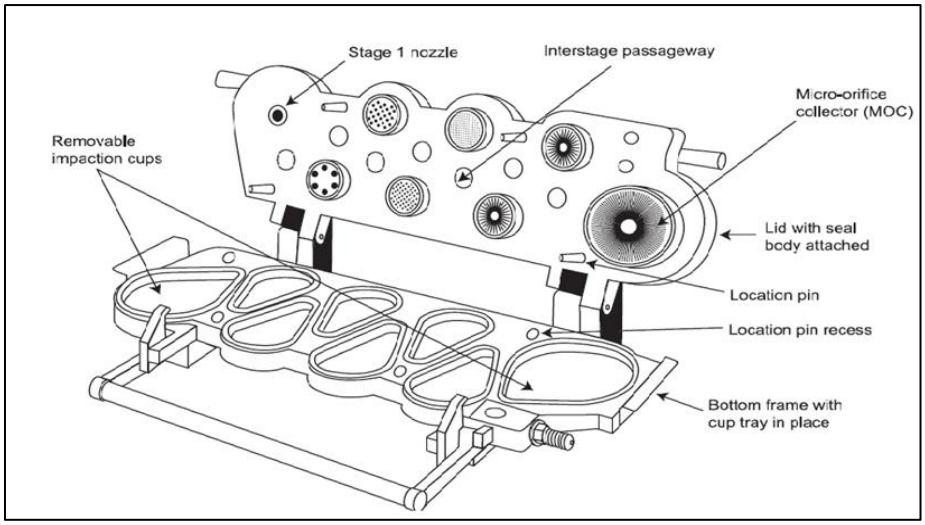

Figure 4.26 Description of the Next Generation impaction (NGI) (Zhu et al., 2015).

1. Fine particle fraction (FPF): It is the percent ration of fine particle dose (FPD) and total delivery dose for each run of NGI.

$$\boldsymbol{FPF = (FPD/Total\ delivered\ dose) * 100\%}$$

FPD- Fine particle dose is the total amount of dose deposited with particle size corresponding to a size less than 5µm.

Total delivery dose- It is the amount of drug deposited in the induction port, pre-separator and stages of NGI (Telko and Hickey 2005).

2. Mass median aerodynamic diameter (MMAD) – It is calculated from the log of effective cut-off diameter (ECD) corresponding to 50% undersized particles (on probability scale).
3. Geometric standard deviation (GSD) is calculated from the following equation (United States Pharmacopeia Convention. 2004):

$$\boldsymbol{GSD} = \sqrt{((\boldsymbol{d84.13\%} / \boldsymbol{d15.87\%}))}$$

Where d 84.13%, and d15.87% are the aerodynamic particle size at 15.87% and at 84.13% less than the stated size, respectively for the cumulative size distribution.

All the parameter values obtained for each sample are graphically plotted on Microsoft excel sheet.

4.2.2.5.5 Quantitative analysis of THF using HPLC analyser

As the samples of theophylline were processed using MASCW process due high stress conditions degradation can occur therefore quantitative analysis was performed to study the degradation of theophylline and develop a calibration method for theophylline for analysing various THF sample solutions collected from Next Generation Inhaler (NGI).

HPLC method: The quantitative analysis of THF samples are done using isocratic method, this method is based on the US pharmacopeia using Waters e-2695 system which is integrated by PDA detector (PDA2998) connected with degasser. The column used is waters symmetry C18 column with dimensions 4.6*250 mm and the particle size of the packed material is 5µm. Concentration of injection volume and flow rate used is 10 µL and 1ml/minute respectively, the solvent system involved are: solvent A = sodium acetate trihydrate (1.36g in 1L distilled water + 5ml acetic acid glacial and

solvent B = acetonitrile HPLC grade. Column and the sample temperature were maintained at 30°C. The wavelength used to analyse THF is 280nm where retention time is 5.2 for theophylline. Mobile Phase contains sodium acetate buffer and acetonitrile in 93:7 ratios respectively.

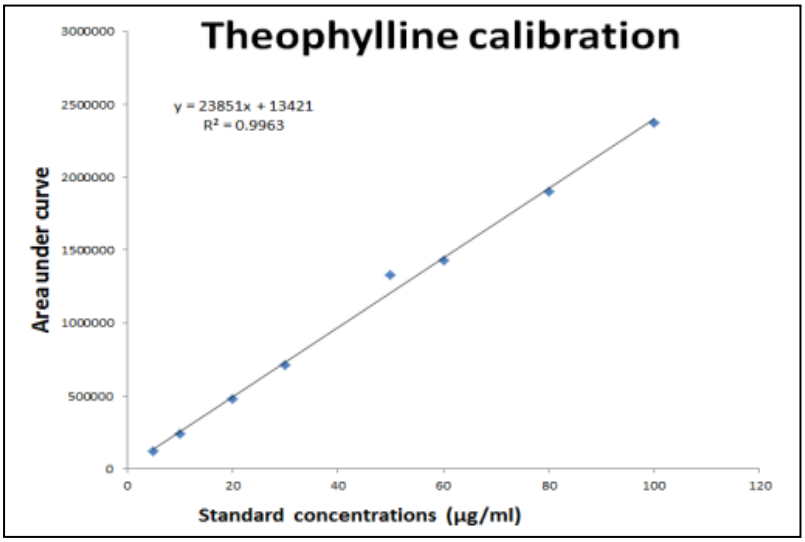

Figure 4.27 Graphical representation of calibration curve of THF

Content uniformity measurements: The content uniformity of THF and lactose IG is measured quantitatively using HPLC, as described above. Blends of THF (40mg ±0.5mg) and lactose IG is prepared my mixing using turbula mixer for 5 minutes. Relative standard deviation calculations were performed between the samples and accessed the homogeneity of blends.

4.2.2.5.6 Setup procedure to analyse surface properties of processed THF samples using SEA analyser:

The surface properties of all the raw and processed theophylline samples are analysed using Surface Energy Analyser. Using this instrument specific surface area, surface heterogeneity, thermodynamic work of adhesion between THF and lactose IG samples and thermodynamic work of cohesion within the same moieties was determined. The method used for the analysis is similar to the method used previously for the analysis of surface

heterogeneity of paracetamol samples (see Section 4.2.2.4.4). Surface properties determination was performed at infinite dilutions using Dorris and Grey equation (see Section 4.2.2.8).

Initially before performing the IGC analysis the particle size of the raw and processed samples are kept similar and analysed using Sympatec diffractometer. All experimental analysis is performed using an IGC-SEA analyser and analysis of each sample is performed in duplicate. Approximately 100mg of sample is weighed and packed in 4mm iGC salinised glass column and is analysed using series of alkanes, polar and non-polar solvents at different surface coverage's. The retained retention time is used to analyse dispersive surface energy (γSD), specific surface area, thermodynamic work of adhesion and cohesion. Before performing each of the analyses the sample loaded column is preconditioned using helium gas for 2hrs at 30°C at 10ml/min flow rate, the dead volume is calculated using methane gas purge. Solvents used non-polar solvents- heptane, octane, nonane, decane and polar solvents –ethanol, dichloromethane, ethyl acetate and chloroform. The surface coverage's used for analysis are from 0.8%, 1%, 2%, 4%, 6% and 8%. Initially alkane probes were injected at different surface coverage's to calculate specific surface area and based on the surface area results surface heterogeneity, thermodynamic work of adhesion and thermodynamic work of cohesion is calculated injecting different polar and non-polar solvent probes.

The effect of different crystallisation techniques are reported in the present study, which focused on the particle size and other characteristic properties of powdered sample. The samples generated using MASCW process are

further analysed using Sympatec diffractometer, Scanning electron microscopy (Jouyban et al.,), X-ray diffraction (XRD), Fourier transform infrared spectroscopy (FTIR), thermogravimetric analysis (TGA), and differential scanning calorimetry. The quantitative analysis of all the samples collected from NGI stages are analysed using High Performance Liquid Chromatography (HPLC).

4.2.2.6 Application of MASCW process in hydrogen bonding between nanocrystalline hydroxyapatite and Ibuprofen

In this section the application of MASCW process in the formation of complex molecules was explored, hydroxyapatite (HA) as inorganic biomaterial compound and ibuprofen (IBU) as API organic entity was selected and mechanism of hydrogen-bonded complex formation between ibuprofen and nanocrystalline hydroxyapatite was explained.

4.2.2.6.1 Nano-hydroxyapatite preparation

Nanocrystalline HA is prepared based on the method reported previously by (Kumar et al., 2004) and group. In brief, calcium hydroxide $Ca(OH)_2$ (3.704g, assay $\geq$96%, Sigma Aldrich) and phosphoric acid (3.459g, 85% wt. in water, Sigma Aldrich) were individually dissolved in 100ml of deionised water. Peristaltic pump with the rate of 3 ml/min is used to add phosphoric acid solution into calcium hydroxide solution at room temperature.

The above addition of aqueous solution of calcium hydroxide and phosphoric acid is performed using two different methods: 1) conventional mixing method, continuous addition of aqueous solution of phosphoric acid (3.459 g/100ml water) at constant addition rate of 3 ml/min using peristaltic pump into aqueous solution of calcium hydroxide (3.704g/100ml water) at stirring

rate of 300rpms using magnetic stirrer at ambient conditions, 2) MASCW process instrument used for synthesis of HA, in this method aqueous solution of phosphoric acid is added into aqueous solution of calcium hydroxide in similar stoichiometric ratios at addition rate of 3 ml/min with rotation speed of 50rpm. The resulting solutions from both the experiments is further aged at constant stirring for 2 hours and left overnight for settling. The supernatant aqueous solution is removed and the remaining suspension is oven dried at 60°C and subsequently ground using an agate motor and pestle to form powder. A 25% portion of the sample powder is further calcined for 2 hours in a furnace at 1000°C (with a heating rate of 10°C/min) in order to evaluate its thermal stability.

4.2.2.6.2 Ibuprofen and nano-hydroxyapatite complex synthesis

To synthesise IBU/HA complex using MASCW process following procedure is employed. Ibuprofen (200mg) and raw nano-HA (800mg) is dissolved in 10ml deionised water at treated at 110°C temperature and 1bar pressure with heating rate of 28°C/min under constant stirring. This experiment was performed at three different concentrations of ibuprofen (5%, 15% and 20%w/w); based on the limit of detection of complex formation 20% IBU is selected for complex formation. The reproducibility of the methods is evaluated using ATR-FTIR experiments for each sample to confirm the presence of monomeric, dimeric and attached species. An aliquot of the paste obtained is used for *in situ* and *ex situ* spectroscopic studies, the remaining sample is dried at room temperature for 24hrs and used for morphological and dissolution examinations.

4.2.2.6.3 In-vitro dissolution study of IBU and HA complex

Dissolution experiments were performed using a UPS II type LabIndia dissolution tester (Labin-09, India). Ibuprofen/HA complex, physical mixture of ibuprofen and HA or raw ibuprofen powders were placed at the bottom of the dissolution vessel (at least four repeats) containing 900 ml phosphate buffer (pH 7.2) maintained at 37 ± 0.5 °C and stirred with a paddle at 50 rpm. Samples were collected periodically and further filtered. Quantification of ibuprofen is performed spectrophotometrically at a fixed wavelength of 221 nm using a Jasco-V630 spectrophotometer.

4.2.3 Characterisation of MASCW processed samples

This section includes the brief description regarding all the analytical tools used to characterise various physical and chemical properties of raw and process pharmaceutical ingredients.

4.2.3.1 Powder X-ray diffraction (PXRD)

X-ray powder diffraction pattern were acquired using a Bruker D8 Advance Diffractometer operating at 40kV and 40mA with Cu Kα radiation. All the powder samples were analysed in the range of 0 to 30° for all organic materials and from 0 to 80° for nanocrystalline HA and ibuprofen complex. Analysis of the X-ray pattern is done using EVA programming in DIFRACplus XRD commander software. The raw files were converted into excel files using PowDLL converter and plated using OriginPro version 8. The PXRD patterns obtained were compared with the standard PXRD patterns retrieved from Crystal structure database (CSD).

4.2.3.2 Differential Scanning Calorimetry (DSC)

The DSC is performed using DSC Q2000 from TA instruments. Approximately 2-4 mg of the sample is heated in the sealed standard aluminium pan against an empty aluminium pan as reference. Inert nitrogen gas is purged at 50ml/min flow rate. All the samples were heated using ramp method with the heating rate of 10°C/min; samples were heated from 25°C as lower limit of temperature to 300°C as higher limit of temperature. The higher limit of temperature is varied based on the melting point of individual and complex samples under analysis. DSC data is analysed using the TA Universal analysis software version 4.5A. Excel sheet is exported using TA Universal analysis software and the plot is plotted using OriginPro version 8.

4.2.3.3 Thermogravimetric analysis (TGA)

Thermo-gravimetric analysis is carried out using Q500 TGA (TA instrument, UK) to determine the residual moisture content and decomposition temperature of all raw and processed samples. Standard platinum sample holders were used and the gas flow is set to 20ml/min. Samples 8-10mg is placed in the pre weighted sample holders and subjected for heating. The method used for heating is ramp method with heating rate of 10°C/minute were lower temperature range is 25°C and higher temperature is 300°C. The results obtained were analysed using TA Universal analysis software and OriginPro software is used to plot the thermogram.

4.2.3.4 Scanning electron microscopy

Scanning electron microscopy is used to analyse the crystal morphology of all raw and processed samples. Prior to analysis all the samples were mounted on dual adhesive black carbon tapes (pre-mounted on aluminum

stud) and coated with gold using sputter coater (BALTECSCD005, Japan). The sample images is collected using FEI Quanta 400 scanning electron microscope (Cambridge UK) under vacuum and XTM microscope control software V 2.3.

4.2.3.5 Particle size analysis

Particle size of all the raw and processed samples were analysed using a laser diffraction particle size analyser (Sympatec HELOS (H2419)) and RODOS dry dispersion unit, Sympatec instruments, UK. Approximately 20-30 mg of the powdered sample is fed into the analyser by ASPIROS unit, using an air pressure of 4bars at the speed of 30mm/sec for all the materials.

4.2.3.6 Fourier Transform Infrared (FTIR) spectra

Fourier Transform Infrared (FTIR) spectra were acquired using a ThermoFisher Nicolet iS50 FTIR spectrophotometer equipped with a single reflection diamond attenuated total reflection (ATR) module. Spectra were recorded in the absorbance mode from 4000 to 300 cm^{-1} at 1 cm^{-1} resolution averaging 64 scans.

4.2.3.7 Raman spectroscopy

A Raman spectrum is acquired using Renishaw Raman spectroscope (ThermoFisher), the samples were analysed under 100x objective lens and a laser radiation of 785nm is focused on the samples. Raman back scattering is collected by high numerical aperture and passed through a confocal aperture to a detector system. By using laser Rayleigh background with notch filter weak signal in the spectra were filtered and then the sample is analysed using charged coupled detector. A Renishaw Raman microscope is used to observe the samples. Samples were analysed at 50% laser power

with the exposure time of 10times/sec and the spectra accumulation of a 1s with removal of a cosmic ray.

The spectral results obtained from FTIR and Raman spectra were analysed using GRAMS/AL^{TM} Spectroscope software.

4.2.3.8 Inverse Gas Chromatography (iGC)

Inverse gas chromatography is the physical characterisation technique used to analyse the surface properties of the solid materials. In iGC the solid phase is the stationary phase and mobile phase is the gas or vapor, this technique of analysis is inverted version of gas chromatography. In iGC chromatography experiment known or constant concentration of gas (probe molecule) is injected through the solid column at different surface coverages and fixed carrier gas flow rate. The retention time of the probe is calculated by gas chromatography detector (flame ionisation detector (FID). In the present study surface properties are analysed using Surface Energy Analyser (SEA) at infinite dilutions. At infinite dilutions interactions between probe-probe is assumed to be negligible and retention is observed due to interaction between the probe and solid surface. The retention volume $V_R°$ is calculated by the following equation:

$$V_R° = \frac{j}{m} F(t_r - t_0) \frac{T}{273.15} \qquad \text{(eq.1)}$$

Where j= James- Martin pressure drop corrections

m= sample mass

F= carrier gas flow rate

t_R = gross retention time for the injected probe

t_0 = retention time for the interacting probe and

T= absolute temperature

In SMS-iGC SEA helium is used as the carrier gas. Different surface properties like specific surface area, surface heterogeneity, acid-base

constant, thermodynamic work of adhesion and cohesion is determined by injecting different polar and nonpolar solvents at different percent surface coverage's. Doris-Gray based on the principle that when serious of alkane probes are injected than the adsorption dispersive free energy of every methylene ΔG^{CH2} is determined from calculating the slope of the line by plotting adsorption free energy $-\Delta G^{ads}$ of the probes versus carbon number *n*.(Shi et al., 2011)

$$\Delta G^{CH2} = -RT.\ln(\frac{V_{N,n+1}}{V_{N,n}}) \quad \text{(eq.2)}$$

Where R= gas constant, T= absolute temperature

$V_{N,n}$ = net retention value of n-alkane probes with carbon number *n*

Determination of thermodynamic work of adhesion and cohesion is very important factor in post processing and stability determination of pharmaceutical ingredients. Thermodynamic work of adhesion can be defined as the interactions between two components. These interactions may be weak van der Waals interactions, electrostatic and capillary forces. The influence of each force in overall adhesion is dependent on several physical factors such as surface interfacial free energies, mechanical properties, morphological properties and environmental conditions. Thermodynamic work of adhesion can be determined from dispersive (γ^d) and specific surface (γ^{sp}) energy values for different components:

$$W_{AD} = 2.(\gamma 1^{d}.\gamma 2^{d})^{\frac{1}{2}} + 2.(\gamma 1^{sp}.\gamma 2^{sp})^{\frac{1}{2}} \quad \text{(eq.3)}$$

Thermodynamic work of cohesion is the interaction between the like components. This can be determined dispersive and specific surface energy values of the materials.

$$W_{COH} = 2.(\gamma 1^{d}.\gamma 2^{d})^{\frac{1}{2}} + 2.(\gamma 1^{sp}.\gamma 2^{sp})^{\frac{1}{2}} \quad \text{(eq.4)}$$

All the samples are characterised in identical conditions: at 30°C temperature of the column and 0% RH (relative humidity). Carrier gas flow rate of 10 sccm (standard cubic centimetres per minute) is employed in all the experiments.

4.2.3.9 ^{1}H- Nuclear magnetic resonance:

^{1}H-NMR experiments were recorded at 400 MHz using a Bruker Avance III 400 spectrometer. Measurements were collected at room temperature for solution of CAF: 4HBA cocrystal sample in d6-DMSO (NMR grade) and scanned for 128 scans. Fitting of the NMR peaks is carried out using Bruker Top Spin 3.2 software, and data analysis is carried out by a successive approximation method based on fixed-point iteration algorithm.

Chapter 5: MASCW process understanding and validation

In this chapter, the effect of different process parameters like temperature, pressure, solute-solvent concentrations and solvent mixture on crystallisation of paracetamol is investigated. Further, effect of solvent mixture on dielectric constant and equilibrium solubility of paracetamol is reported.

5.1 Introduction

Before exploring the application of newly developed MASCW process technology, the effect of different process and experimental parameters on crystal attributes (morphology, particle size, surface texture and chemical phase) was investigated initially. To perform process validation pca raw (form I) is selected as the model API moiety as it is less soluble in water (solubility 13±2 mg/ml). Paracetamol or acetaminophen is very popular drug moiety used as an analgesic and antipyretic component. Paracetamol exists in two polymorphic forms, monoclinic form I and orthorhombic form II polymorphs recently form III metastable polymorph is characterised by (Etienne Joiris 1997). Monoclinic form I is the stable commercially available polymorph which exhibits poor tabletability under compression thus process scientist started implementing novel technologies for generation metastable orthorhombic form II polymorph of pca which retains higher tabletability under compression. Recently William Jones and team has used the sonocrystallisation technique for generation of form II pca with greater compressibility property (Dejan-Kresimir Bucar,2017). Marc-Antoine and group have elucidated the crystal structure of elusive polymorph form III of paracetamol (March-Antoine et al., 20111)

For development of robust process in the laboratory knowledge and understanding regarding the solubility curve, stability of the supersaturated solution at the vicinity of the equilibrium point is required. The crystallisation of the crystal phase is explained based on the metastable zone width, which is required for process optimisation and scale-up of the crystalliser. The metastable zone width is the point where primary nucleation occurs. Below Figure 5.1 describes the between the supersaturated and saturated solubility curve.

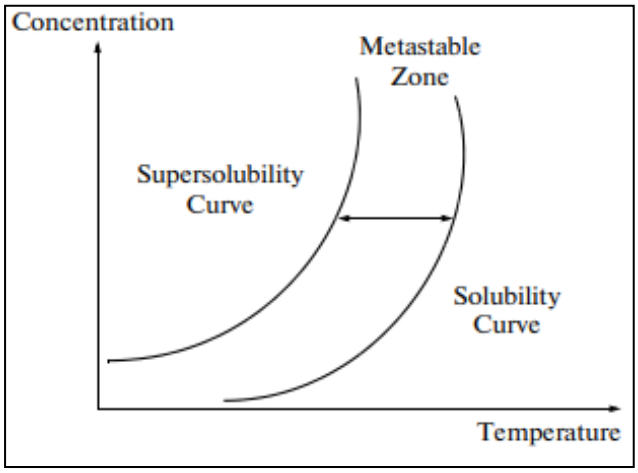

Figure 5.1 Solubility curve and MSZW

The solute molecule will remain stable in the solution until sufficiently high supersaturation level is not developed to induce immediate nucleation. The extent of this supersaturation is referred as MSZW. This MSZW is typically influenced by the saturated temperature, rate of supersaturation, mixing and solution history. Understanding the nucleation mechanism as an indicator of metastable zone width is important for scale-up and understanding the influence of process parameters (Somnath S. Kadam et al., 2012). In the

present study supersaturated solubility curve was generated based on the target temperature and pressure where clear solution is formed.

5.2 Results

The result section is divided into four sections based on the objective of the study.

5.2.1 Development of temperature and solubility curve using MASCW technology.

The detailed methods and experimental conditions for this study are described in (Section 4.2.1.A). The effect of supersaturation concentration of pca in water (10ml) over the solubility of pca in water under MASCW treatment conditions was investigated. The change in the pH of the solution after processing and percent purity of crystallised solid material is calculated using HPLC. Below Table 5.1 summarises the experimental results of different saturated concentrations of pca and their melting points.

Based on the result table it is observed that as the concentration of pca in solution increase the target temperature where the clear solution is formed also increases along with pressure, thus the temperature and pressure conditions where the clear solution of pca is formed is based on pca supersaturated solution concentration. Table 5.2 represents the experimental images of all batches at different temperatures and marking the temperature where the clear solution is formed.

Decrease in the pH of the pure water pre-treated in the MASCW process reactor and pure water at room temperature is observed. This decrease in pH can be attributed to the molecular arrangement or hydrogen bonding

dissociation of the water molecule in the sub-critical state. Thus once the water molecules are treated under sub-critical conditions, for the water molecule to retain its structure it takes some time. Slight pink decoloration of pca solution is observed after treating under a high temperature above 140°C and solution concentration above 25%w/v this is due to solution state degradation of pca into p-aminophenol.

Quantitative analysis of the crystallised material is done by calculating percent purity using HPLC analyser. It is noticed that range of degradation of pca after MASCW treatment is within the acceptable range which is not less than 97% and not more than 102% purity according to USP standard monograph for pca tablets. As these supersaturated solutions are placed at room temperature for 24hrs the total amount of pca solute remaining in the solution after filtration was determined, this data is reported in the Table below as FSC (filtered solution concentration). In the below Table 5.2 represents the images of all the experimental batches at different temperature conditions, it is observed that the temperature at which clear solution is formed increase as there is increase in the concentration of pca in water, this is attributed that the solubility of the solute in solution depends on solute- solution concentration. Figure 5.2 represents the binary phase diagram correlating percent concentration of pca solution, temperature and pressure of MASCW reactor.

Table 5.1 Summary of solubility vs temperature data

T (°C)	P	S (mg)	pH	% Y	% P	FSC	SC	form	Image	Observations	Exp-plot
35	-	-	6.96 blank	-	-				-	-	-
150	4.2-4.5	-	6.69	-	-				-	-	-
125	1.6-1.8	500	5.72	71.6	100.25	26.41	462.95	**FI**		clear solution is formed at 125°C, no decolouration observed	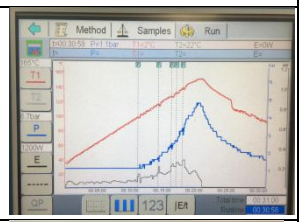
132	3.0-3.1	1000	5.64	68.0	98.98	119.14	982.39	**FI**	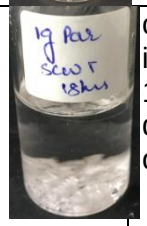	clear solution is formed at 132°C, no decolouration observed	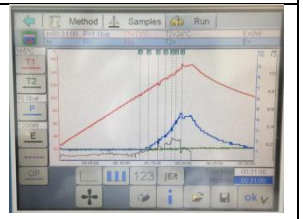
138	3.1-3.4	1500	5.56	70	99.44	129.27	1217.85	**FI**		clear solution is formed at 138°C, no decolouration observed	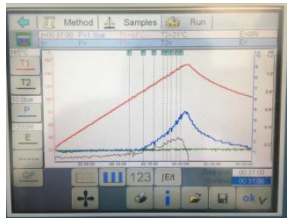

145	3.8-4.2	2000	5.42	77.5	102.93	127.25	1563.17	**FI**		Very slight pink colouration is observed. After 30mins precipitation is observed	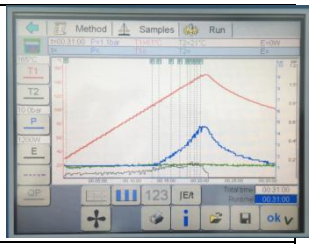
148	4.3-4.5	2500	5.35	86	98.66	188.99	1850.13	**FI**		Intensity of pink colouration further increased. After 15minutes precipitation is observed	
151	4.9-5.2	3000	5.21	92.3	99.74	231.11	2250.05	**FI**		Sudden crystallisation occurred once the solution is transferred to vial. Pink coloration is observed	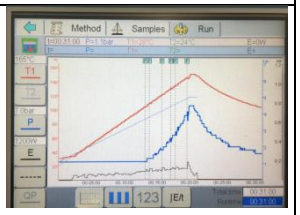

T= temperature at which clear solution is observed, **P**= Pressure at the corresponding temperature, **S**= solubility of pca

%Y= percent yield after 24hrs, **% P**= percent purity of pca, **pH**= pH of the supersaturated solution

FSC= filtered solution concentration (mg/10ml water)

SC= solution concentration- amount of pca dissolved after processing (mg/10ml water)

Table 5.2 Pictographic representation of: correlation between solubility of different pca concentrations vs corresponding temperature conditions.

T(°C)	Percent supersaturation (g/ml)					
	5%	10%	15%	20%	25%	30%
100	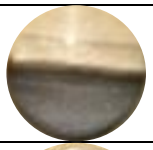	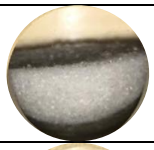	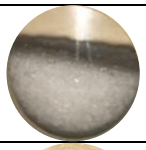	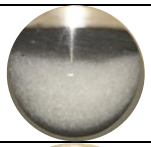		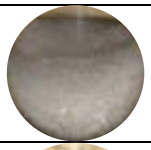
110		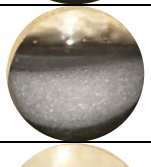	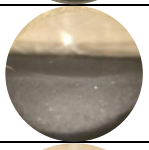	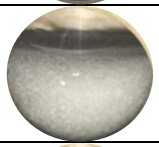		
120	 CS 125°C		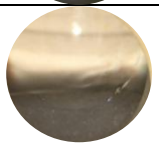	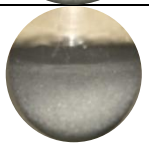	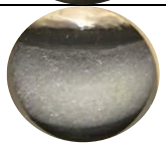	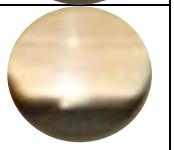
130	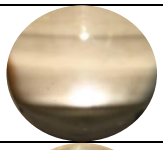	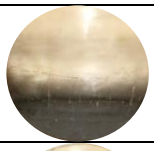	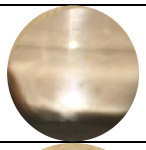	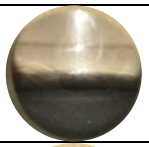	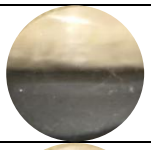	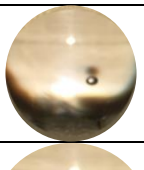
135	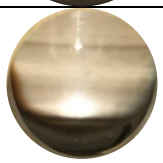	 CS 132°C	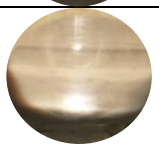	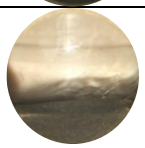	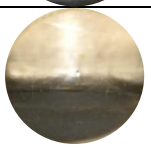	
140	-	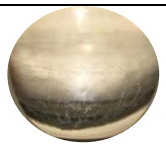	 CS 138°C			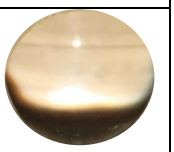
150	-		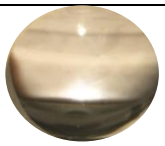	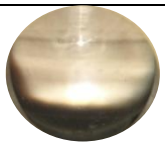 CS 145°C	 CS 148°C	 CS 151°C

CS- clear solution is observed

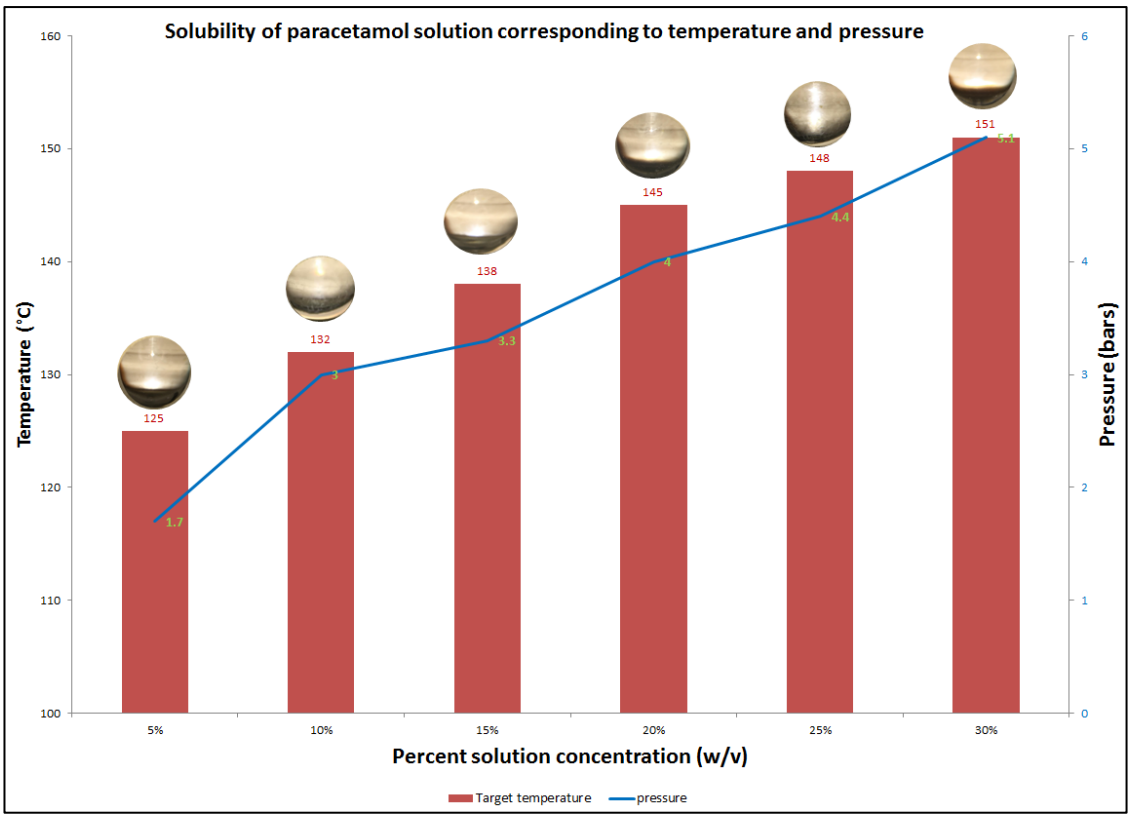

Figure 5.2 Binary phase diagram of concentration of the solution and corresponding temperature and pressure

5.2.1.1 PXRD data

Based on the PXRD data all the samples process using MASCW process are the form I polymorphs as they are rightly similar to form I standard PXRD pattern of form I raw pca. As the samples are present in the solution for more than 24hrs there is present of hydrate peak at (7.5 2θ°) which is the characteristic peak of pca dihydrate (Liming Yang 2008). Further to confirm the crystal form Raman spectroscopy is performed. Below Figure 5.3 represents the PXRD overlay all process samples against pca form I and form II patterns.

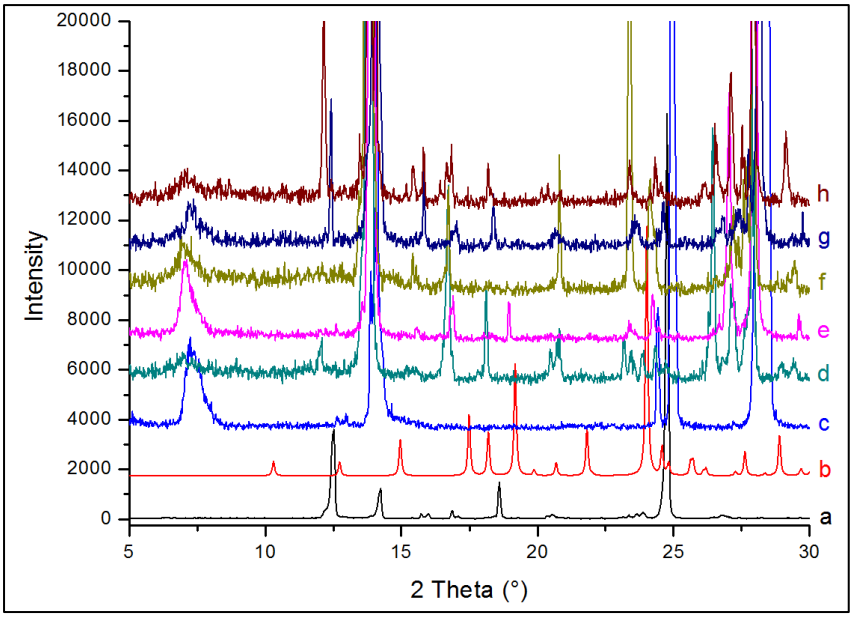

Figure 5.3 PXRD overlay of : a) Raw form I pca, b) form II pca, c) 5% pca, d) 10%pca, e)15%pca, f) 20%pca, g) 25%pca, h-30%pca

5.2.1.2 Raman data

Below Figure 5.4 shows the overlay of Raman spectra of all pca batches against form I raw pca. Based on the presence of characteristic peaks at 837 cm^{-1}, 1234 cm^{-1} and absence of a peak at 1220, 1245 and 1623cm^{-1} it is confirmed that the formation of form I and absence of form II polymorph of pca. The dome-like spectral pattern of processed samples is due to the presence of water molecule or presence of amorphous fraction of pca.

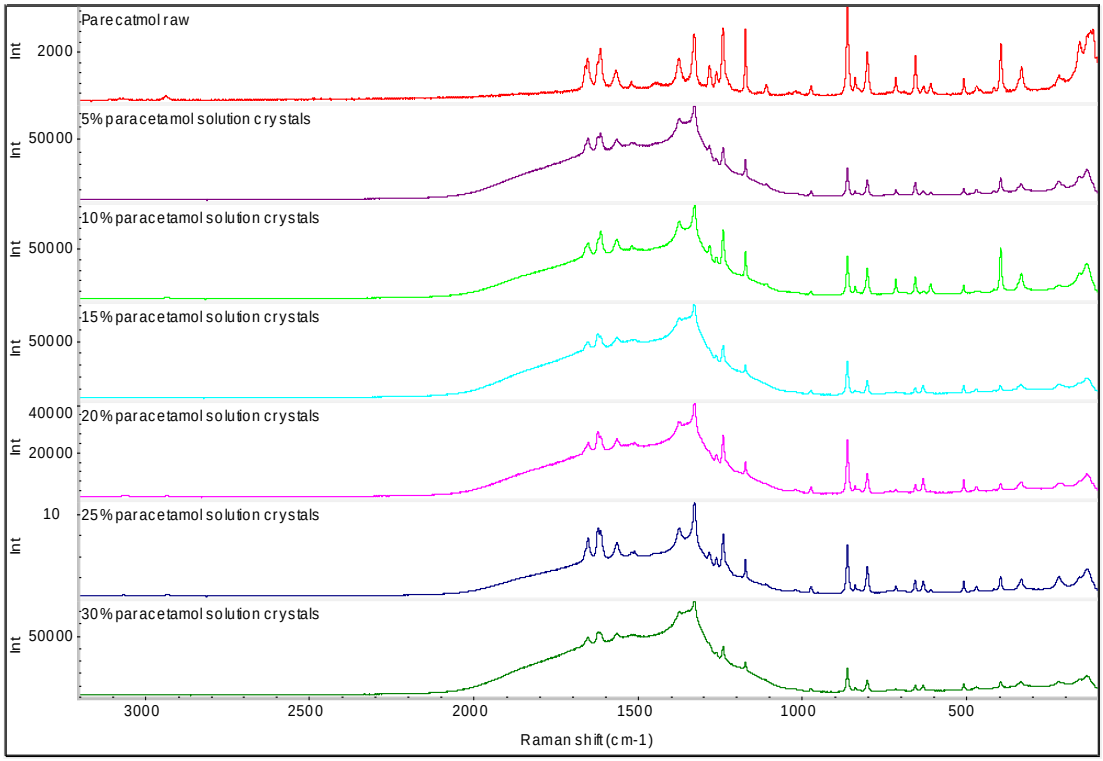

Figure 5.4 Overlay of Raman spectra of Pca form I raw and MASCW processed pca samples of different solution concentrations

5.2.2 Monitoring crystallisation time and pca supersaturated solution concentration using MASCW process

In this section, the time required for the crystallisation to occur in different solution concentrations of pca is monitored. A brief description of experimental method is explained in Section (4.2.1.B). Below Table 5.3 summarises the results obtained from both conventional heating and MASCW process.

It is observed that, when 5%w/v and 10%w/v saturated solution of pca are processed using MASCW process at 140°C the time required for the crystals to induce out is 30-hrs and 24-hrs respectively, as compared to conventional heating experiments the crystals started inducing out relatively faster within

2-hrs and 8-min respectively. This result is attributed to the eutectic molecular association or hydrogen bonding between water and solute molecules is very strong and stable that it takes a longer time to crystals to induce out. Water when treated at sub-critical state it takes long time to retain its molecular dynamics. At sub-critical state of water more number of hydrogen bonds are broken therefore water volume is increased and during cooling conditions to retain its physical molecular dynamic water molecules tend to form weak hydrogen bonds with the solute molecules. When stirring is applied to the supersaturated solution of pca, sudden generation of metastable form II phase of pca occurs which proves the theory of crystallisation pathway that stable polymorphs are formed after generation of metastable phase which further in presence of crystallisation medium (water) gets converted to stable form I polymorph.

When similar experiments were performed using conventional heating method it is observed that in 5% and 10% w/v solution concentration of pca takes 2-hrs and 8-mins respectively and concentration above 15%w/v doesn't form a clear solution and on further heating pink coloration was developed due to degradation of pca. In MASCW process clear solutions are formed at all the concentrations but faint pink coloration was observed in 25 and 30%w/v solution concentration of pca due to degradation of pca. All the saturated pca solutions obtained from MASCW process acidic pH compared to conventional heated pca solutions. Based on the previous finding pca is stable at acidic pH range between 4 to 5 and on further increase in pH oxidation of pca into 4-aminophenols occurs (Liming Yang 2008). Based on the HPLC analysis higher solution state degradation of pca in conventional

heating was observed than MASCW process (refer Figure 5.9), this is attributed to the supersaturated solution concentrations of pca and type of heating conditions.

This solubility curve can be compared with the MSZW where supersaturated solubility is obtained at 30%w/v of pca in SCW, upon further increase in the concentration degradation of pca solution occurs. Compared to the conventional heating supersaturated solubility is less than 15%w/v of pca in water at (95°C), and upon increase in the concentration no clear solution is formed. The longer solution stability of 10%w/v of pca in SCW can be correlated to the larger MSZW of microwave heated SCW and no equilibrium saturation is obtained at 10%w/v pca concentration.

Table 5.3 Summary of crystallisation time vs solution concentration for MASCW process and conventional heating experiments

Microwave-assisted sub-Critical water process						Conventional heating process						
Wt (mg)	pH	T (mins)	%P	Images	Observation	T (°C)	S (mg)	T (mins)	pH	% P	Image	Observation
500	5.88	30hrs	96.72		clear solution gets converted to pink colour after 24hrs	95-100	500	120	6.06	95.35		after 90 mins small crystal starts inducing
1000	5.67	24hrs	98.98		clear solution	95-100	1000	8	6.24	92.54		small crystals started inducing out in 8mins
1500	5.53	6hrs	99.44		clear solution formed	95-100	1500	5	6.50	96.05		ICO, no clear solution is formed
2000	5.47	25mins	102.93		clear solution formed	95-100	2000	3	6.52	98.86	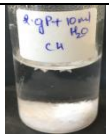	ICO, no clear solution is formed
2500	5.22	13mins	98.66		clear solution formed	95-100	2500	2.5	6.50	97.22		ICO, no clear solution is formed
3000	5.09	8mins	99.74		immediate crystallisation-	95-100	3000	2	6.39	96.72		ICO, no clear solution is formed

T= time required to induce crystals, **ICO**= immediate crystallisation observed, **FC**= filtration solution concentration

Thus based on the aqueous solubility of pca in water (14mg/ml), higher supersaturated stable solutions concentration (100mg/ml) of pca is generated using MASCW process compared to conventional heating techniques. This proves the significance of this technology for generation of stable supersaturated solutions and enhancement of solubility of hydrophobic components.

This investigation provided us a new pathway of processing as when the supersaturated solutions are stable for 1-day, the crystallisation kinetics using PAT tools like Raman spectroscopy can be used. During crystallisation the crystal phase can be manipulated by addition of certain additives.

Table 5.4 Summary percent purity of pca solutions using SCWT and conventional heating

Sol. concentration (w/v)	%purity of MASCW treated samples	%purity of conventional heating
5%	96.72 ± 0.86	95.35 ± 0.36
10%	98.98 ± 2.58	92.54 ± 0.09
15%	99.44 ± 0.22	96.05 ± 0.18
20%	102.93 ± 0.30	98.86 ± 0.38
25%	98.66 ± 1.91	97.22 ± 0.16
30%	99.74 ± 0.12	96.72 ± 0.42

5.2.2.1 SEM images

Morphological properties like crystal shape, surface smoothness and crystal habit of all pca powdered samples is analysed using SEM analyser. Below Figure 5.5 represents the SEM images of MASCW treated and conventionally treated pca powdered samples collected from different solution concentrations at 1000X magnifications. MASCW processed samples displayed smother surface.

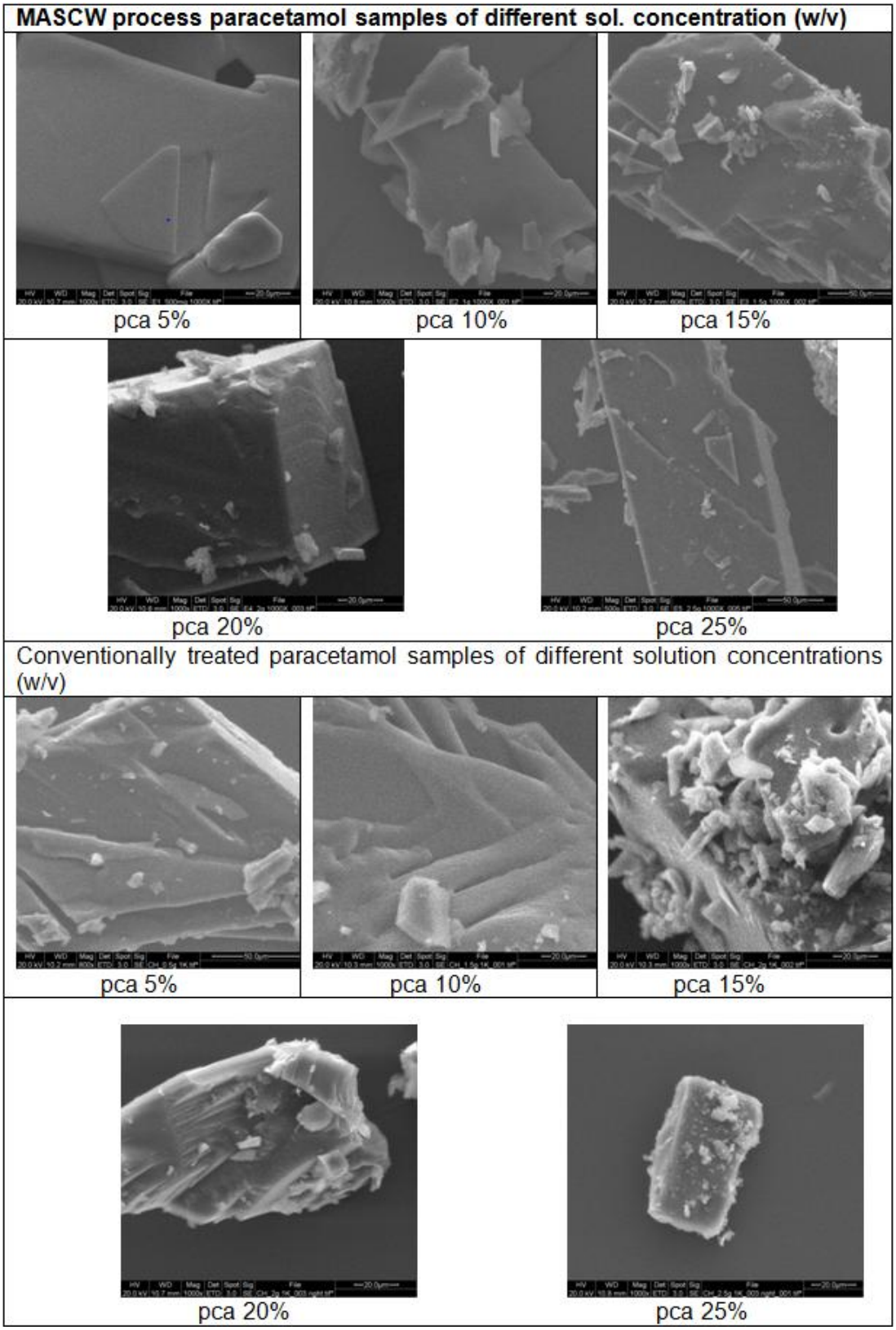

Figure 5.5 SEM images of paracetamol crystallised from the MASCW process and conventional heating.

5.2.3 Crystallisation kinetic data

In this study, the crystallisation pathway of 10%w/v supersaturated solution of pca over 24-hrs using off-line Raman spectroscopy is studied. In this study 10% (w/v) of pca solution is prepared using MASCW process and left for cooling to ambient conditions. Once the solution temperature comes to ambient conditions a drop of 100µL volume is placed on the sample holder and further crystallisation kinetics is monitored under Raman spectroscopic analyser. Below Figure 5.6 represents the Raman spectral overlay of pca solution over 24hrs.

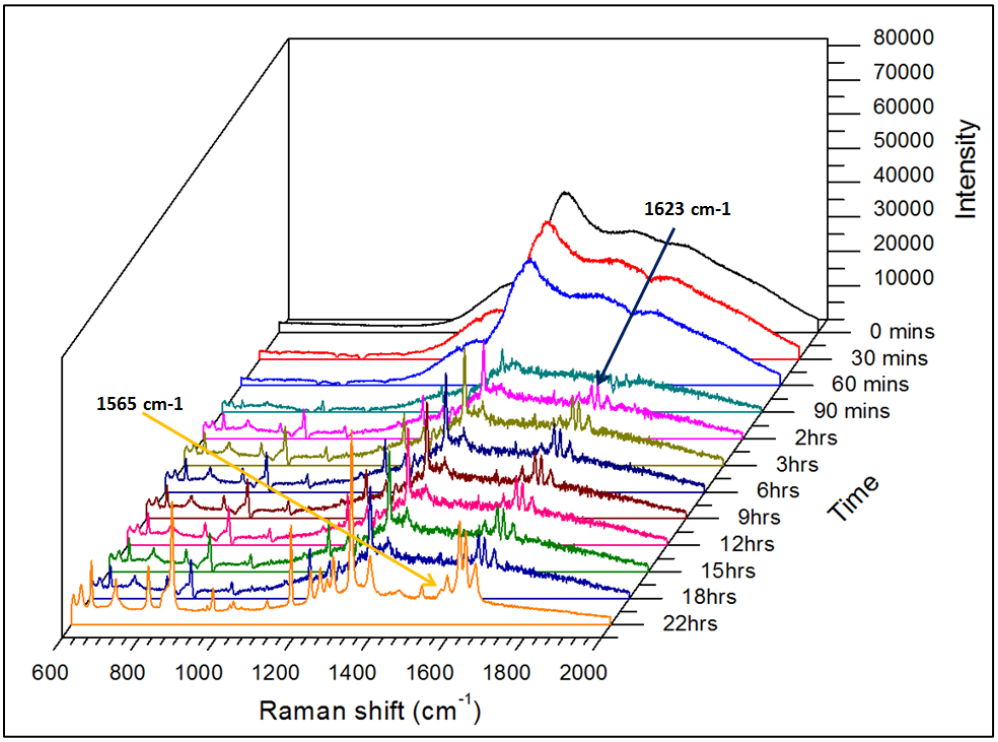

Figure 5.6 Overlay of Raman spectra spotting the characteristic peak of pca form II (1623cm^{-1}) and form I (1565 cm^{-1}) polymorph.

In the above spectral overlay, initial spectra red, blue and green represent the spectra for blank water + pca in solution and 30-mins and 45-mins respectively, no crystallisation is observed till 90-mins and after 90-mins

crystals started inducing out as spectral peaks were tracked. On analysing the peaks it is found that the peaks at 1623, 1120 and 1245 cm^{-1} resembles the characteristic peaks of metastable form II pca. It is confirmed that form I and form III polymorphs of pca is absent due to absence of characteristic peaks at 837cm^{-1}, 1234 cm^{-1}, 1565 cm^{-1} for the form I and absence of a peak at 1321cm^{-1} which is the characteristic peak of form III polymorph of pca. The intensity of from II characteristic peaks went on increasing at further accumulation for 18-hrs, after 18-hrs at 22nd hour of spectral scan presence of both form I and form II polymorphs of pca is observed.

In the above experiment polymorphic transformation of paracetamol from metastable form II to stable form I polymorph is tracked using off-line spectroscopic technique. This transformation of metastable polymorph to stable polymorph is absent in case of conventional heating experiment.

5.2.4 Effect of the solvent mixture on the dielectric constant of solution and crystallisation of paracetamol

In this section, the change in the dielectric constant of solution using solvent mixture and in presence of solute (pca 1g), for method refer to section (4.2.1.D) is analysed. Below Table 5.5 demonstrates the change in dielectric constant of water by addition of different concentrations of solvent systems at ambient conditions.

Table 5.5 Dielectric constant values of different solvent mixtures at RT

	Dielectric constant			
Percent solvent mixture (v/v%) in water	**MeOH**	**EtOH**	**ACE**	**ACN**
0 (water pure)	77.49 ± 0.04			
10	73.57 ± 0.14	71.68 ± 0.11	73.35 ± 0.03	74.99 ± 0.03
20	69.68 ± 0.08	66.62 ± 0.26	68.74 ± 1.31	70.06 ± 0.10
30	66.35 ± 0.26	62.14 ± 0.66	64.51 ± 0.76	67.52 ± 0.04
40	60.04 ± 0.19	47.57 ± 0.96	58.86 ± 0.43	64.13 ± 0.04
50	53.60 ± 1.77	45.88 ± 0.29	52.69 ± 1.28	60.05 ± 0.03
60	48.17 ± 0.10	37.03 ± 0.19	47.01 ± 0.09	54.74 ± 0.03
70	42.73 ± 0.05	29.12 ± 0.21	40.95 ± 0.10	50.39 ± 0.02
80	37.22 ± 0.70	21.77 ± 0.11	34.99 ± 0.12	46.14 ± 0.02
90	30.40 ± 0.29	14.50 ± 0.09	29.10 ± 0.08	41.80 ± 0.03
100	25.10 ± 0.09	8.67 ± 0.06	22.34 ± 0.06	37.53 ± 0.02

It is observed that the dielectric constant of every solvent decreases with increase in organic solvent concentration thus increasing the solubility parameter of solute in the solvent mixture. Below Figure 5.6 represents the above data graphically.

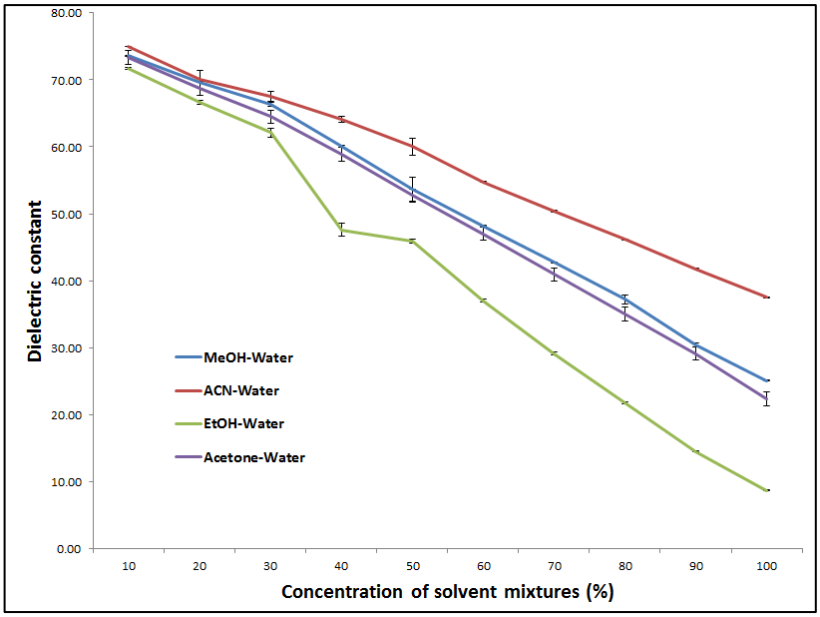

Figure 5.7 Graphical presentation of the dielectric constant of solvent mixtures from 10 to 100%v/v concentrations

Based on the above graph ethanol pure solvent and solvent mixture retains minimum dielectric values so theoretically the solubility capacity of this solvent mixture is high compared to other solvent mixtures. Later based on the above study added 1g of pca in pure water was added and individual solvent mixtures of total volume 10 ml and processed using MASCW process and checked the change in the dielectric constant of water after MASCW treatment and due to the addition of pca. Below table 5.6 represents the dielectric constant of pure solvents, pure water, and solvent mixtures after MASCW treatment.

Table 5.6 Summary of the dielectric constant of the pure solvents and solvent mixtures with paracetamol solute after MASCW treatment

Solvent mixtures (v/v)	Paracetamol (mg)	Dielectric constant (ε'')
Water	-	77.42±0.09
MeOH 100%	-	23.22 ±0.09
M+W (10%)	-	73.30±0.03
M+W+P (10%)	1000	66.19±0.07
M+W (20%)	-	68.60±0.10
M+W+P (20%)	1000	51.87±2.05
M+W (30%)	-	63.35±0.11
M+W+P (30%)	1000	40.84±1.18
EtOH 100%	-	8.27±0.16
E+W (10%)	-	72.31±0.01
E+W+P (10%)	1000	68.17±0.04
E+W (20%)	-	65.78±0.37
E+W+P (20%)	1000	60.84±0.23
E+W (30%)	-	56.46±0.36
E+W+P (30%)	1000	50.74±0.60
ACN raw	-	34.31±0.15
ACN+W (10%)	-	74.87±0.30
ACN +W+P (10%)	1000	63.16±0.99
ACN +W (20%)	-	68.12±1.33
ACN +W+P (20%)	1000	59.49±0.31
ACN +W (30%)	-	66.90±0.71
ACN +W+P (30%)	1000	53.98±0.40
Acetone 100%	-	19.62±0.10
ACE+W (10%)	-	72.73±0.17
ACE+W+P (10%)	1000	59.46±1.35
ACE+W (20%)	-	66.94±0.68
ACE+W+P (20%)	1000	54.93±0.29
ACE+W (30%)	-	61.19±1.20
ACE+W+P (30%)	1000	48.60±0.30

Based on the above tabular data it is observed that the dielectric constant values of blank solvent mixtures is further reduced due to the presence of pca this is because of the hydrogen bond association of pca molecules with solvent molecules. The dielectric constant of solvent mixture solutions was analysed before and after MASCW processing and by addition of pca as a solute molecule. Below Figure 5.8, 5.9, 5.10 and 5.11 represents the bar

graph for change in dielectric constants of the solution with and without pca moiety.

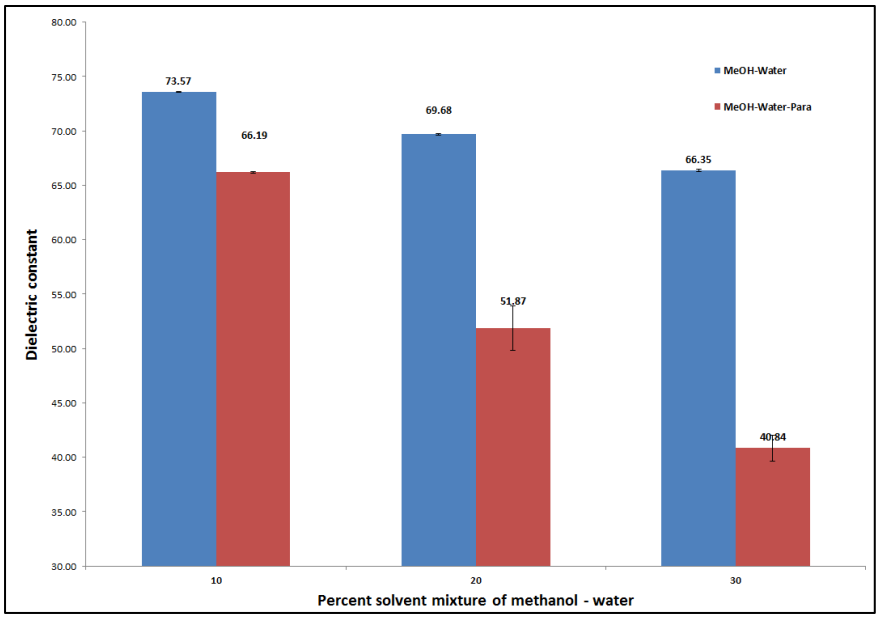

Figure 5.8 Dielectric constant values for: water-MeOH blank and water-MeOH-pca solution at 10, 20 and 30% v/v concentration of MeOH -water.

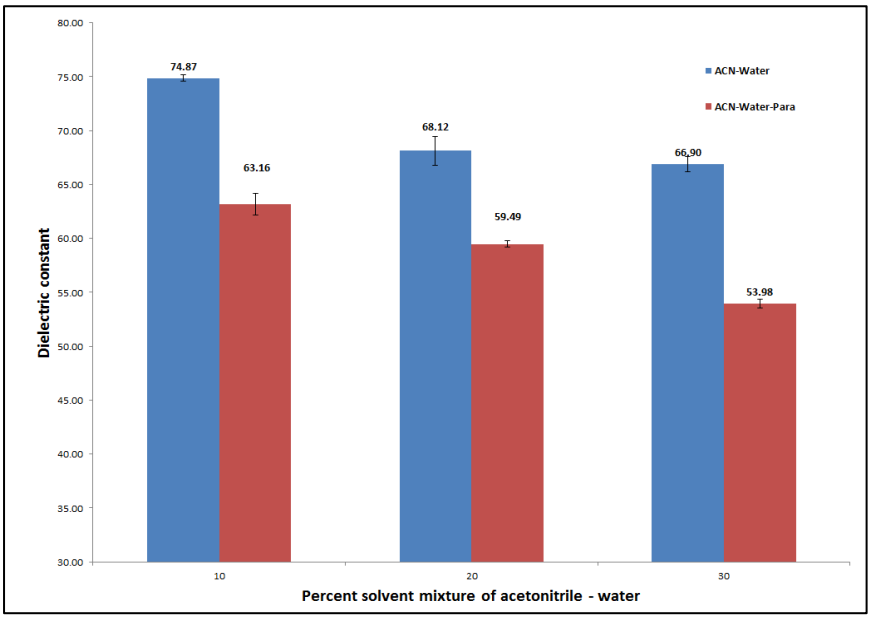

Figure 5.9 Dielectric constant values for water-ACN blank and water-ACN-pca solution at 10, 20 and 30% v/v concentration of ACN-water.

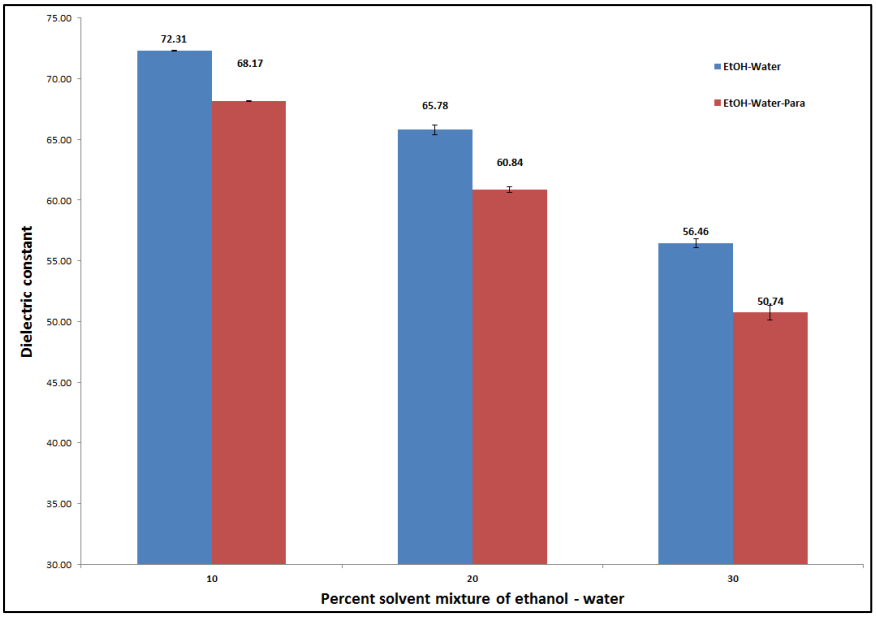

Figure 5.10 Dielectric constant values for water-EtOH blank and water-EtOH -pca solution at 10, 20 and 30% v/v concentration of EtOH -water.

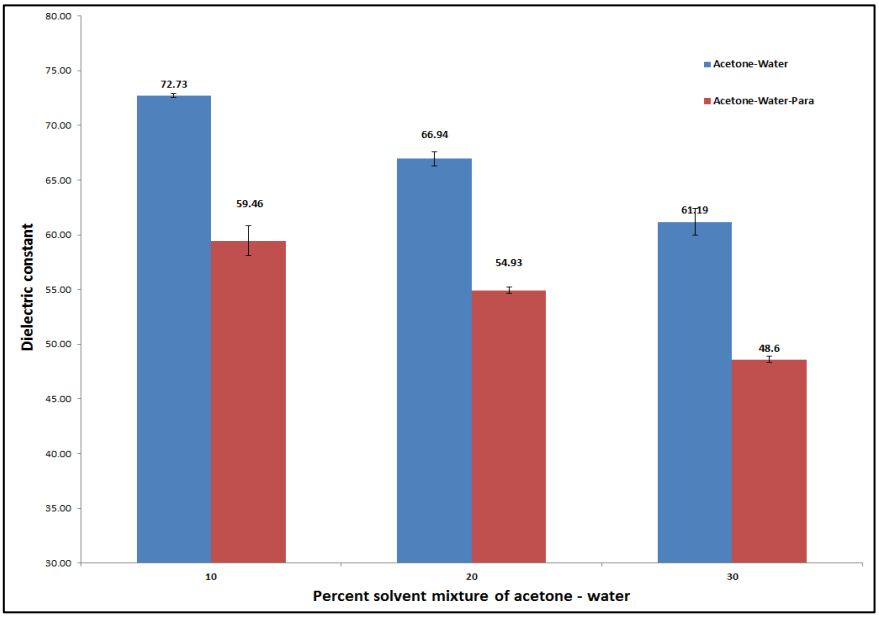

Figure 5.11 Dielectric constant values for water-ACE blank and water-ACE –pca solution at 10, 20 and 30% v/v concentration of ACE -water.

When pca is added to the solvent mixture the dielectric constant values of methanol-water drastically reduced compared with another solvent system. This can be attributed to hydrogen bonding association between methanol-

water and pca. After investigating the change in the dielectric constant of water further investigation of the effect of a change in dielectric constant of solvent mixtures on equilibrium solubility of pca before and after MASCW treatment is studied. Below Table 5.7 represents the equilibrium solubility of pca in all the solvent mixtures under MASCW treated and untreated conditions.

Table 5.7 Equilibrium solubility of: paracetamol in solvent mixtures when treated using MASCW process and conventional temperatures and percent purity of MASCW process paracetamol solid samples.

Solvent mixture	ES UT(1ml)	ES T(1ml)	%P of MASCW treated
Water	13.52	15.57	99.44
MeOH 100%	191.28	-	
M+W+P (10%)	17.37	19.76	94.21
M+W+P (20%)	23.01	37.05	94.39
M+W+P (30%)	34.26	58.74	96.17
EtOH 100%	130.80		
E+W+P (10%)	19.51	39.46	97.38
E+W+P (20%)	27.12	58.63	99.37
E+W+P (30%)	46.71	82.57	99.06
ACN raw	20.69		
ACN +W+P (10%)	24.57	28.03	94.86
ACN +W+P (20%)	48.56	53.16	95.61
ACN +W+P (30%)	84.59	85.96	95.99
Acetone 100%	71.56		
A+W+P (10%)	25.11	31.44	96.09
A+W+P (20%)	47.82	53.06	94.72
A+W+P (30%)	80.54	85.28	97.02

ES UT= Equilibrium solubility of untreated pca solutions

ES T= Equilibrium solubility of treated pca solutions

Below Figure 5.12 represents the solubility variation of all the solvent mixture with and without MASCW treatment.

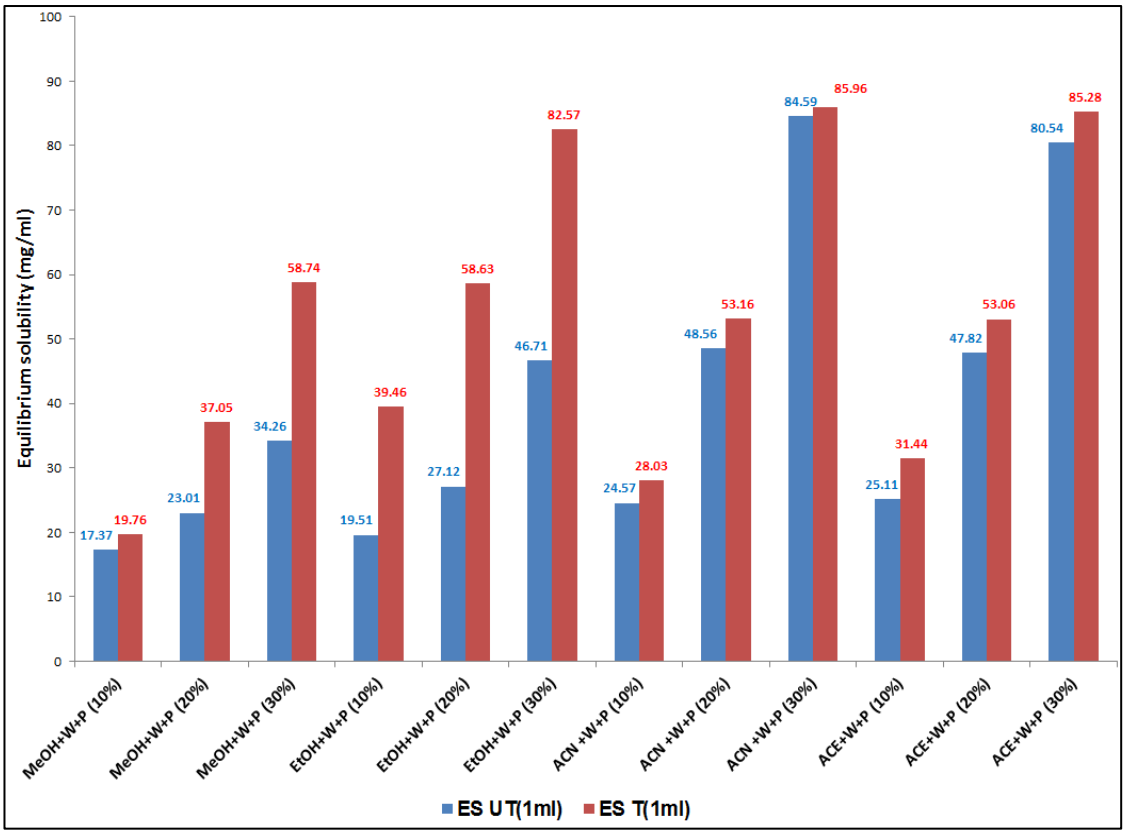

Figure 5.12 Equilibrium solubility (mg/ml) of pca in untreated and MASCW treated solvent mixtures.

Based on the above graph it is observed that the solubility of pca increases in MASCW treated batches compared to ionisation capacity and supersaturation limits of the individual solvent system before and after MASCW treatment. The increase in the solubility of the pca is large in case of methanol and ethanol solvent mixtures and percent purity of pca solid material crystallised from these solutions are in the acceptable ranges according to USP standards.

Investigation of crystal form of pca crystallised from the above solvent mixtures using PXRD, DSC and Raman spectroscopy is performed. Below Figure no 5.13, 5.14 and 5.15 represents the PXRD, DSC, and Raman data for all the batches respectively.

5.2.4.1 PXRD data

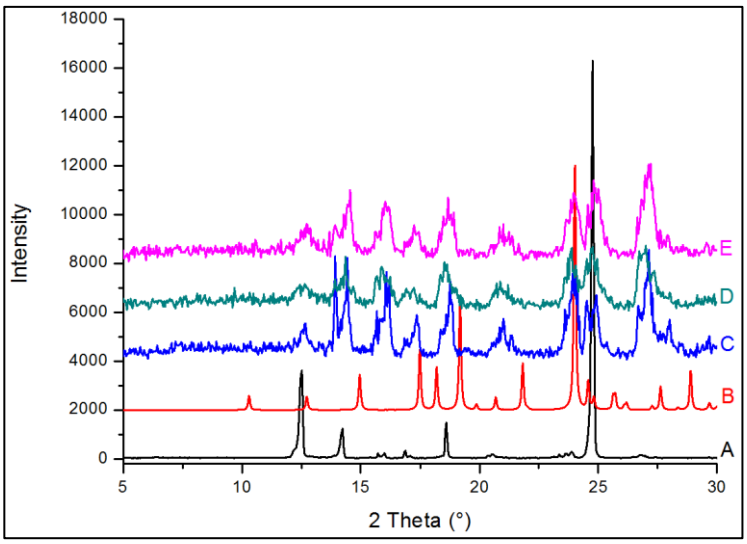

Figure 5.13 PXRD pattern of A- Par raw form I, B- Par form II, C- 10% ACE-water, D-20% ACE-water, E- 30% ACE-water

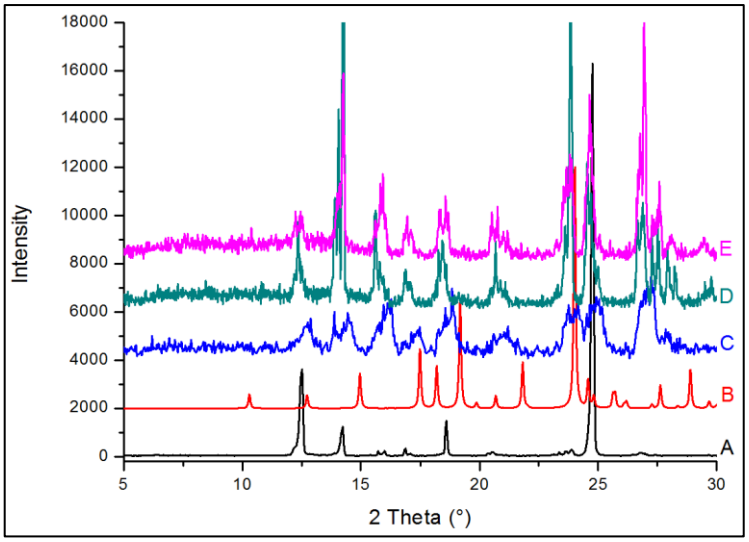

Figure 5.14 PXRD pattern of A- Par raw form I, B- Par form II, C- 10% ACN-water, D-20% ACN-water, E- 30% ACN-water

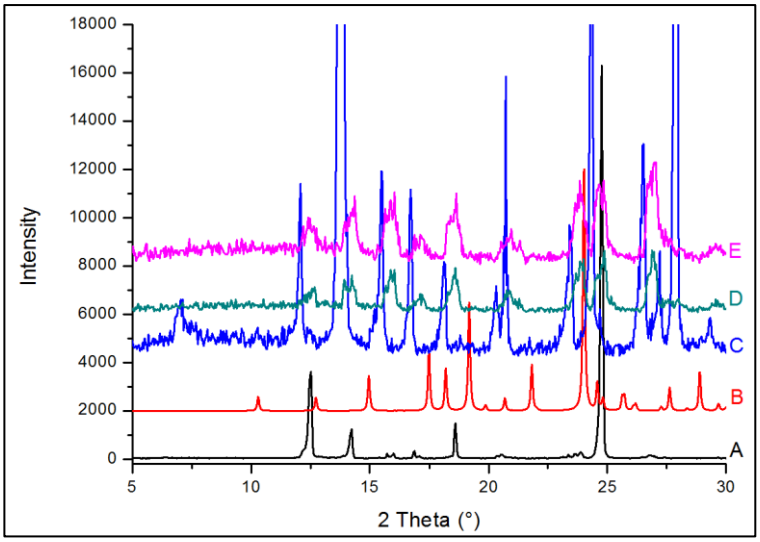

Figure 5.15 PXRD pattern of A- Par raw form I, B- Par form II, C- 10% EtOH-water, D-20% EtOH-water, E- 30% EtOH-water

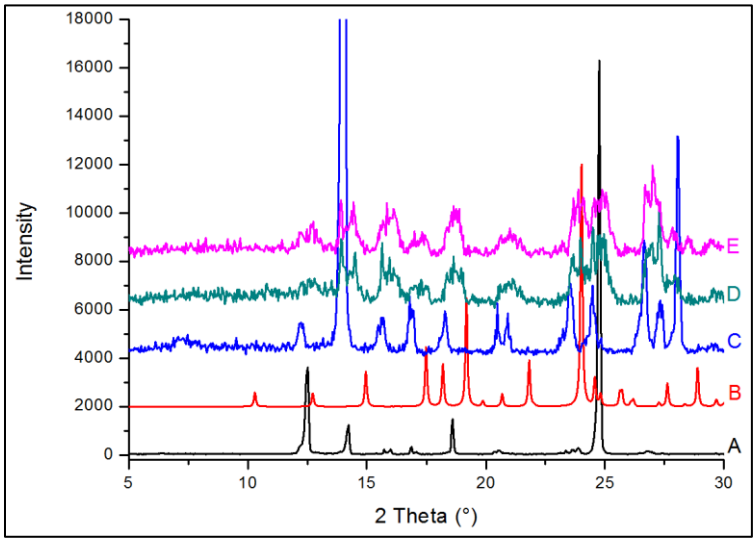

Figure 5.16 PXRD pattern of A- Par raw form I, B- Par form II, C- 10% MeOH-water, D-20% MeOH-water, E- 30% MeOH-water

5.2.4.2 DSC data

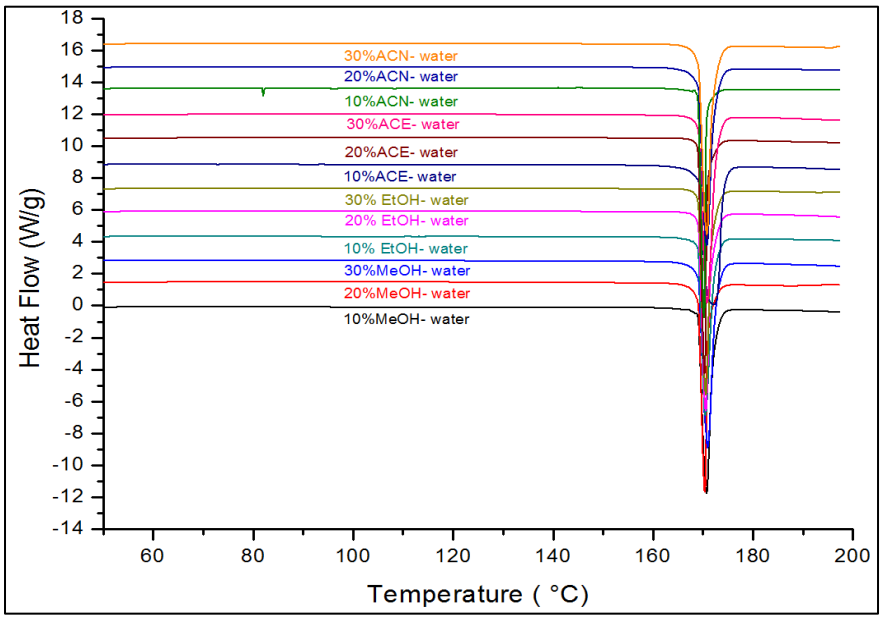

Figure 5.17 DSC thermogram overlays of all pca crystals obtained from all solvent mixtures.

In all the above DSC overlay of thermograms of all solvent mixture, reveals the presence of single endotherm at 169±2°C representing characteristic peaks of form I polymorph of pca. Thus based on DSC data it can confirm that form I stable polymorph of pca is formed. Based on the above thermogram no hydrate formation is observed.

5.2.4.3 Raman data

Raman spectroscopic analysis is performed to investigate the phase purity of pca processed batches. Based on the Raman data characteristic spectra of form I pca polymorph at wavelength 837 cm^{-1}, 1234 cm^{-1} and 1565 cm^{-1} is observed. A characteristic peak of form II polymorph is not observed, thus it is confirmed that all the processed samples are the pure form I pca. Below

Figure 5.18, 5.19, 5.20 and 5.21 represent the Raman spectra for all pca batches.

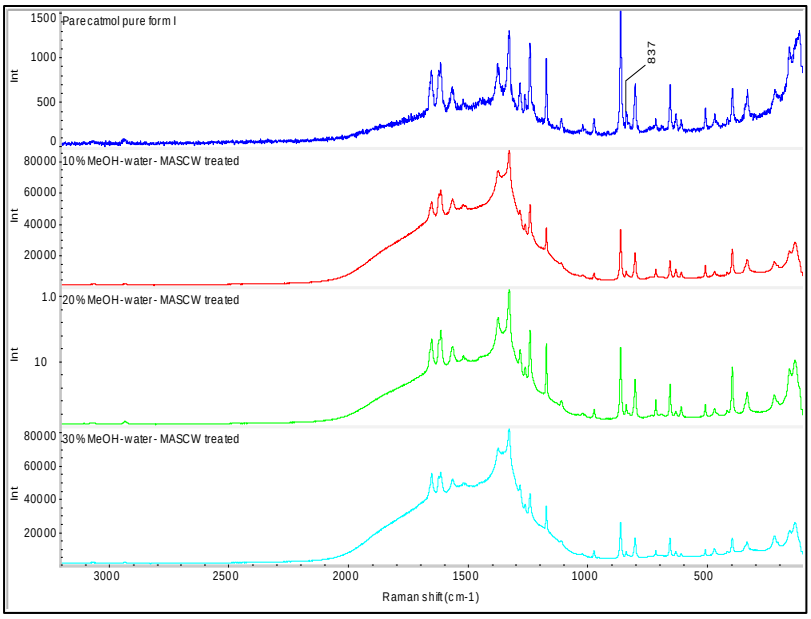

Figure 5.18 Raman spectra overlay for raw pca form I, solid materials obtained from 10%, 20% and 30% MeOH-water solvent mixtures

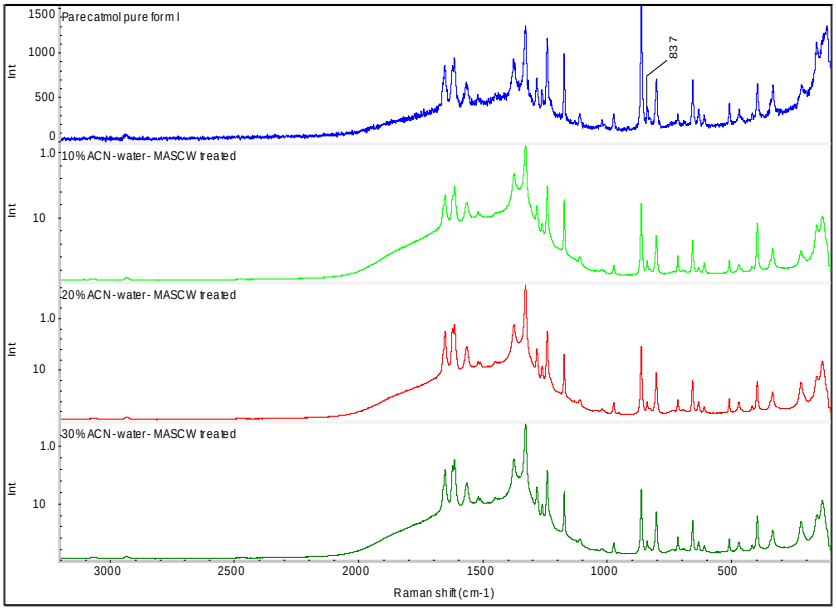

Figure 5.19 Raman spectra overlay for raw pca form I, solid materials obtained from 10%, 20% and 30% ACN-water solvent mixtures

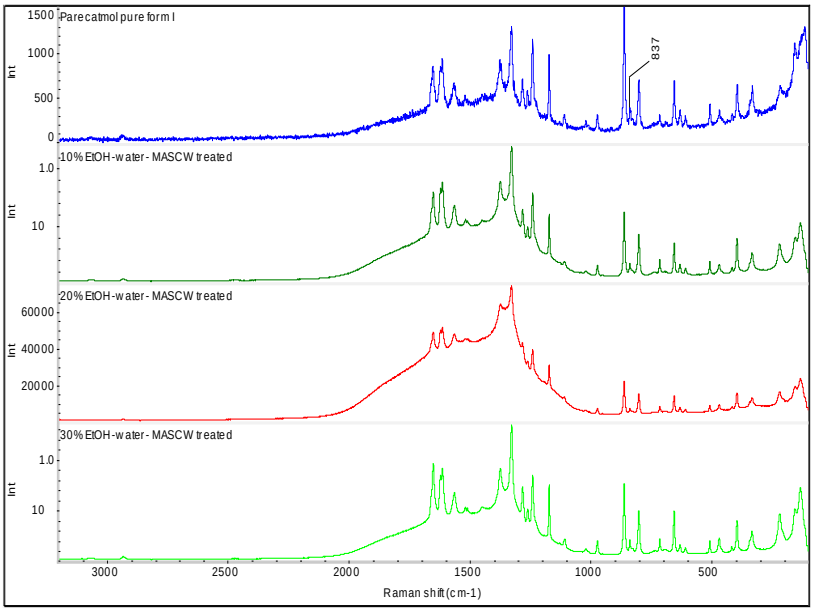

Figure 5.20 Raman spectra overlay for raw pca form I, solid materials obtained from 10%, 20% and 30% EtOH-water solvent mixtures

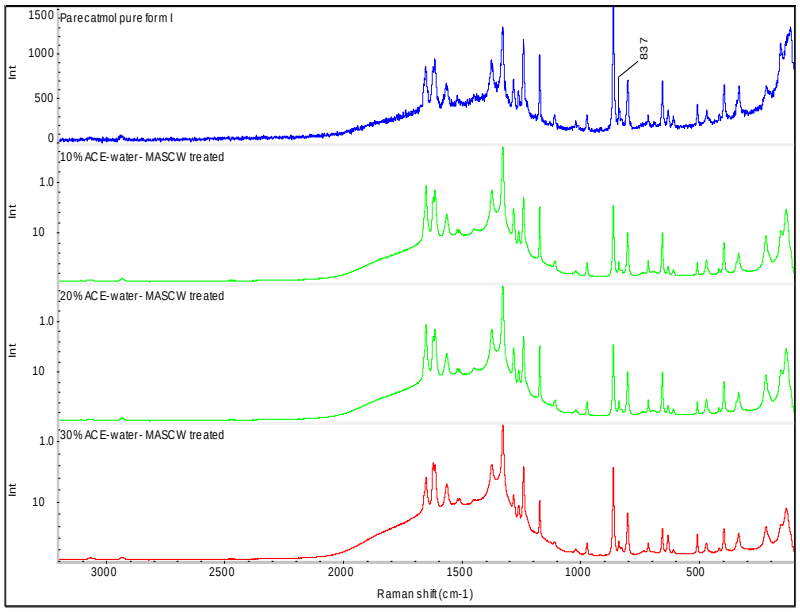

Figure 5.21 Raman spectra overlay for raw pca form I, solid materials obtained from 10%, 20% and 30% ACE-water solvent mixtures

5.2.5 Conclusion

The effect of different process and experimental parameters on morphological and chemical properties of pca polymorphism was reported. Correlation between solution concentrations of pca and the processing temperature where the clear solution is formed is derived, further quantitative analysis of the process samples is analysed by calculating percent purity using HPLC analyser. Crystallisation kinetics of MASCW processed pca solution is analysed using Raman spectroscopy. Comparative studies were performed to investigate the crystallisation time for MASCW process and conventional heating pca solutions. Experimental correlation data is generated to explain the correlation between the dielectric constant of solvent system and solubility of pca in the solvent system using water itself and by using solvent mixtures of different organic solvents at varied temperature conditions. Further, the solution state stability of pca solute in all solvents mixtures at different temperature conditions is reported using HPLC analyser.

Thus, based on all the above experiment conditions investigation between effect of different process parameters and solvent mixtures on crystallisation of pca solute is analysed.

Chapter 6: Application of MASCW technology in cocrystallisation process

In this chapter, application of MASCW process for the generation of congruent and incongruent cocrystal pairs is explored. Based on congruency theory between API and coformer this chapter is further categorised into two sections: section 1: Includes screening experiment to understand the effect of different process parameters in the cocrystallisation process, this includes formation of congruent cocrystal pairs of CBZ: SAC, SMT: SAC and SMZ: SAC in 1:1 stoichiometric ratio. In the second chapter, CAF and 4-HBA pair is selected as incongruent cocrystal pair and application of solvent mixture in MASCW technology is studied to form pure anhydrous cocrystal phase of CAF: 4-HBA in 1:1 stoichiometric ratio.

6.1 Introduction

Cocrystals are the complex molecules consists of two or more chemical moieties combined together via non-covalent interactions. Cocrystal complex consists of active pharmaceutical ingredient and co-crystal former also called coformer which undergoes chemical interactions to form a single co-crystal complex with enhanced physicochemical properties as compared to individual components. To generate phase pure cocrystal pairs with enhanced physical and chemical properties various pharmaceutical process industries and research groups have developed various novel techniques of cocrystallisation, all the new technologies of crystallisation retain certain potential limitations like use of different organic solvents which may cause side effects, generation of unstable cocrystals, phase impurities in co-crystal and solvate formation due to use of solvent systems (formed when

mechanochemical method is used). Recently Padrela and co-workers, 2015 have proposed the new mechanism of cocrystallisation using supercritical solvents, these solvents include ethanol, supercritical carbon dioxide. (Padrela et al., 2015), this technology is based on the principle of antisolvent crystallisation using organic solvents as the bridging liquid to provide molecular mobility and form covalent bond between the two reacting components, this technique is subjected to organic solvents for the production of co-crystals and very stringent process parameters are used. This technology also contains certain limitations such as phase impurities, use of organic solvent so it's not a green technology; due to stringent process conditions the crystallinity and chemical stability of active ingredients is reduced. Therefore to surmount all such challenges during the processing of pharmaceutical ingredients it is very much desired to develop new novel crystallisation technology which is preferably green. In the present chapter MASCW technology is implemented as the screening tool for the generation of stable cocrystals, for this congruent cocrystal pairs with almost similar solubility in water were selected. CBZ is generally used for the treatment of epilepsy and neuropathic pain. SAC is referred as an artificial sweetener which is a substituent added in the formulation as a pharmaceutical excipient for the purpose of taste masking. Carbamazepine and saccharin exist in the form of two polymorphs, form I and II. Form II is the metastable form which gets converted into a stable form I polymorph in a very short period of time (Porter et al., 2008), CBZ has the propensity to form dihydrate when subjected to crystallization (Hickey et al., 2007). It is proposed that the scalability of CBZ/SAC by solution crystallisation has resulted in the

formation of CBZ dehydrate, which is stable in presence of water. For the first time, the metastable cocrystal polymorph of CBZ/SAC is proposed by Matzger's group (Porter et al., 2008). CBZ/SAC form I is generated recently using antisolvent crystallisation method (Wang et al., 2013). Reddy and co-workers proposed the potential of the rotary evaporator for the generation of CBZ/SAC form I and II (Bag et al., 2011). Ragar and Hilfiker used ultrasound technique for the generation of CBZ/SAC cocrystals (Hilfiker 2006). Certain researchers have proposed the generation of metastable form by using higher moles of saccharin. Recently Aher *et al* have proposed phase diagram for generation of metastable form by using an excess amount of cocrystal former in case of caffeine/maleic acid cocrystals. (Aher et al., 2010)

In the present chapter, formation of CBZ: SAC form I and form II cocrystal phase and formation of SMT and SMZ cocrystal with SAC as coformer is reported. The effect of different process parameters like temperature, level of supersaturation, microwave energy and heating rate over the end cocrystal phase is elucidated using CBZ: SAC as cocrystal components.

6.2 Results and Discussion

The result section is divided into two sections where the first section represents the process understanding using CBZ: SAC as cocrystal pair and the second section corresponds to screening experimental data for SMZ: SAC and SMT: SAC cocrystal pairs.

6.2.1 Preliminary experiments of cocrystallisation

This section includes the results obtained by varying different process parameters of MASCW technology and generation of CBZ: SAC form II

metastable phase using a solvent mixture. Different characterisation tools are used to analyse phase purity and form of cocrystal pairs.

6.2.1. a) PXRD data

PXRD instrument is used to identify the cocrystal form produced between CBZ: SAC cocrystal pair by varying different process parameters.

The below Table 6.1 represents the brief overview and experimental variables and the PXRD results of the solid complex obtained, CBZ and SAC were selected in 1:1 stoichiometric ratio, for a method of crystallisation see section (4.2.2.1.2).

In the MASCW process the heating temperature or the sub-critical temperature is altered initially keeping the concentration of solute in 10ml solvent and other parameters constant, at lower temperature range 110°C no clear solution is formed and further as the temperature is increased to 115 and 120°C formation of clear solution is observed, below Figure 6.1 represents the PXRD pattern of CBZ: SAC cocrystal pair at two different temperatures.

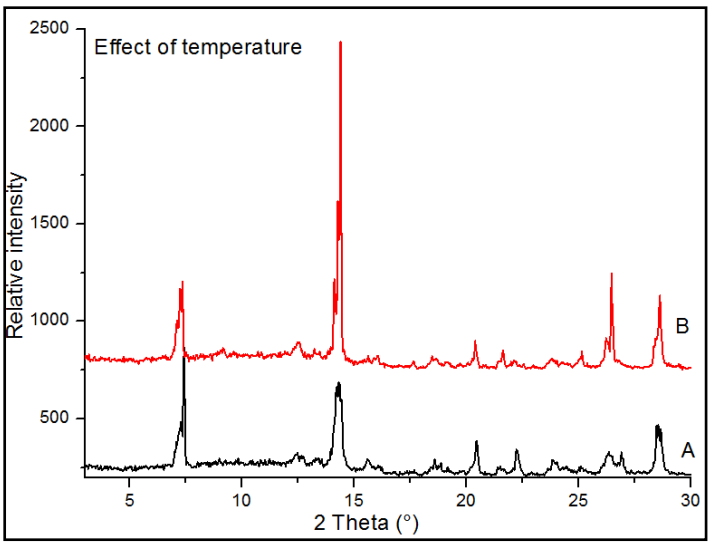

Figure 6.1 PXRD patterns of batches carried out at A-115°C and B-120°C

Table 6.1 Result summary of: cocrystal phase obtained by altering different process parameters.

Constant parameter	Variable parameters				
Amt. of API:CF solute mixture (mg)	**Target temp (°C)**	**Amount of solvent (ml)**	**Microwave power (watts)**	**Rate of heating (mins)**	**PXRD results**
350 (1:1)	**110**	10	300	5	No clear solution formed
350 (1:1)	**115**	10	300	5	cocrystal form I
350 (1:1)	**120**	10	300	5	cocrystal form I
350 (1:1)	115	**10**	300	5	cocrystal form I
350 (1:1)	115	**12.5**	300	5	cocrystal form I + CBZD
350 (1:1)	115	**15**	300	5	cocrystal form I +CBZD
350 (1:1)	115	10	**200**	5	target temperature is not obtained (no clear solution)
350 (1:1)	115	10	**300**	5	cocrystal form I
350 (1:1)	115	10	**400**	5	cocrystal form I
350 (1:1)	115	10	300	**5**	cocrystal form I
350 (1:1)	115	10	300	**2.5**	cocrystal form I
350 **(1:1.5)**	115	**12.5**	300	**5**	cocrystal FI + CBZD
350 **(1:1.5)**	115	**15**	300	**5**	cocrystal FI+ CBZD
350 **(1:2)**	115	**12.5**	300	**5**	cocrystal FI + CBZD
350 **(1:2)**	115	**15**	300	**5**	cocrystal FI+ CBZD
350 (1:1)	115	5ml MeOH and 5ml H20	300	**5**	**cocrystal form II**

Based on the PXRD patterns of CBZ: SAC cocrystal pair at two different temperatures, they rightly match with the form I stable phase of CBZ: SAC cocrystal (Rodríguez-Hornedo et al.,2008).

Next parameter which is analysed is the effect of solvent concentration on the end product, below Figure 6.2 represents the PXRD pattern of MASCW processed samples at different solvent concentrations. Based on the specification and minimum requirement of the instrument the minimum amount of solvent which needs to be used based on the concentration of solute is 10ml, therefore 10ml water as the minimum volume of solvent is maintained.

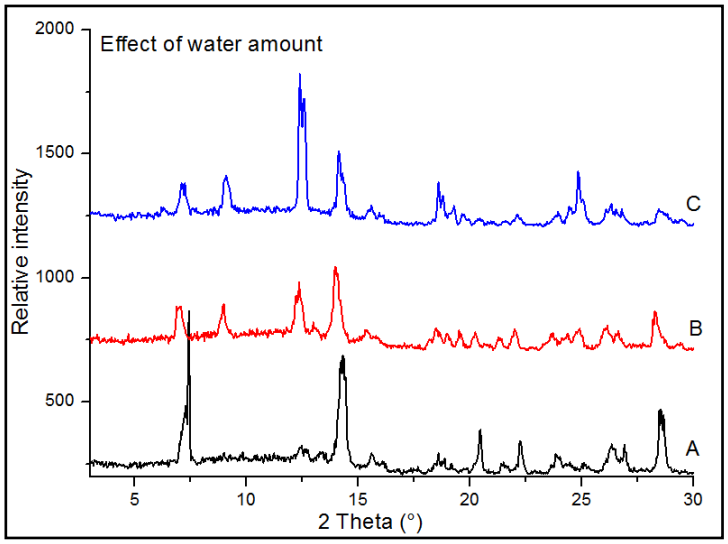

Figure 6.2 PXRD data of experiments carried with A- 10mL, B- 12.5mL and C- 15mL water as solvent system.

Based on the above PXRD data it is concluded that as the concentration of solvent system is varied, phase purity and crystal form of the cocrystal complex also changed. At 10ml water volume form I CBZ: SAC cocrystal phase is obtained and when 12.5 mL and 15 mL solvent concentration is used formation of CBZ/SAC form I cocrystal along with CBZ dihydrate as impurity is observed. Based on the previously published data the impure

phase formed is coinciding with CBZ dihydrate phase (Robin K. Harris and Caiyun Ma 2005). At the 2θ° scale the peak present at 7.5 theta degrees represents dihydrate peak which is obtained at 12.5 and 15 mL of solvent volume. Further formation of dihydrate is confirmed using thermal analysis study.

The third process parameter which is altered is the microwave power; this data is used to understand the effect of microwave energies on the end product. Below Figure 6.3 represents the PXRD patterns of CBZ: SAC cocrystal sample at different microwave energies.

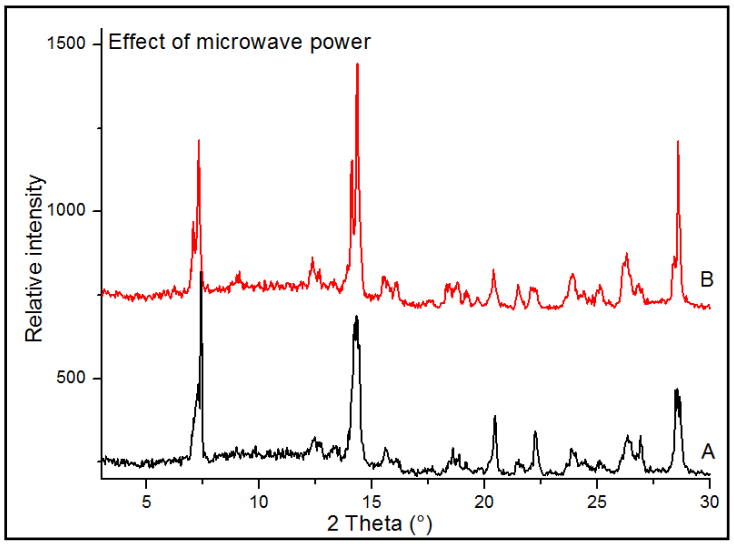

Figure 6.3 PXRD patterns of batches carried out at A-300W and B-400W.

Based on the above PXRD pattern it is observed that the microwave power does not have any effect on the end product phase purity and only affect the rate of heating. When 200 watts microwave energy is used no clear solution is formed as the targeted temperature of 115°C did not reach so further the experiments were performed at 300 and 400 watts of energy. At two different microwave powers, formation of phase pure form I cocrystal of CBZ and SAC occurred.

The fourth parameter is the rate of heating, it the time required to reach the targeted temperature (temperature where the clear solution is formed). Two different heating rates were selected to reach the targeted temperature of 115°C and they are 23°C/min and 46°C /min respectively. Below Figure 6.4 represents the PXRD pattern of CBZ: SAC sample at two corresponding rates of heating.

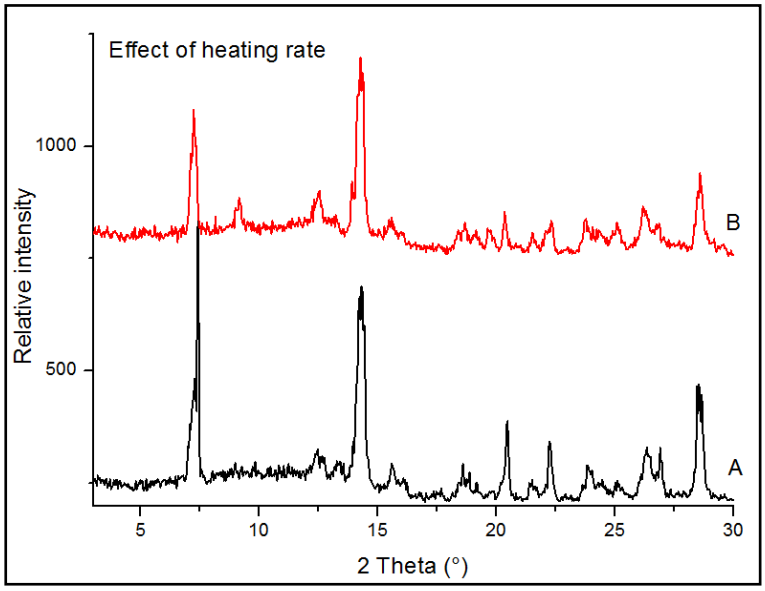

Figure 6.4 PXRD patterns of samples processed at different heating rates A) 26 °C/minute and B) 46 °C/minute.

Based on the PXRD pattern obtained it is concluded that the rate of heating doesn't affect the cocrystal phase, as generation of form I cocrystal of CBZ: SAC cocrystal pair took place. Later the effect of the stoichiometric ratio of solute and volume of water at constant temperature, microwave energy, and heating rate is investigated. Below Figure 6.5 represents the PXRD pattern of CBZ: SAC at different stoichiometric ratio in 12.5ml and 15ml water as solvent system respectively.

Based on the below PXRD pattern the formation of CBZ/ SAC form I cocrystal and CBZ dihydrate as an impurity in all the samples is observed.

This result proves that the concentration of coformer (CF) has no correlation with solvent volume to prevent the formation of dihydrate.

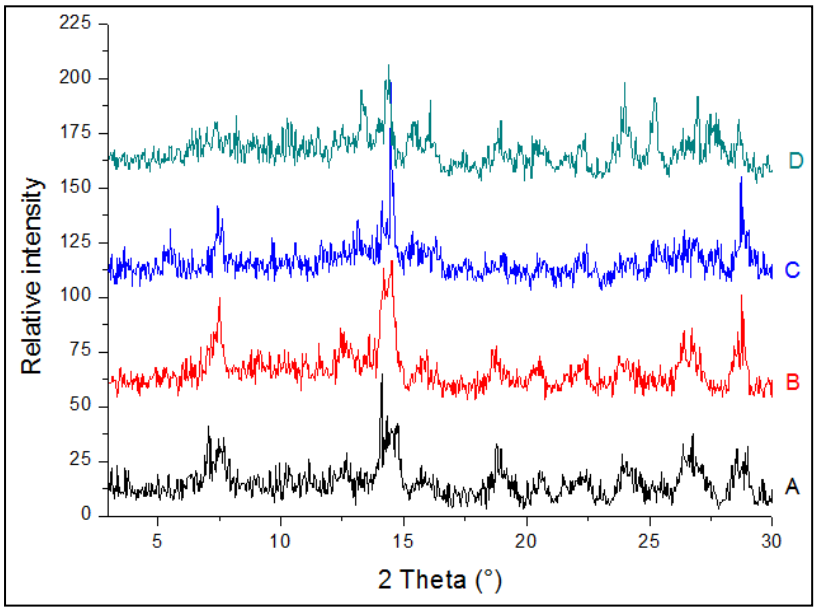

Figure 6.5 PXRD pattern of: A) CBZ: SAC 1:1.5_12.5ml water, B) CBZ: SAC 1:1.5_15ml, C) CBZ: SAC 1:2_12.5ml water and D) CBZ: SAC 1:2_15ml water

Based on the results obtained in the previous experiments using water as a solvent system generation of CBZ/SAC form I pure stable phase is obtained but no metastable form II is generated. Thus dielectric constant of solvent system plays an important role in monitoring crystallisation pathway so to investigate the effect of change of dielectric constant on crystal form the use a mixture of solvents as the solvent system is used to further reduce the dielectric constant of the solvent system. Recently various research group has shown their interest in generating from II metastable phase of CBZ: SAC cocrystal and to prevent CBZ dihydrate formation, (Hilfiker 2006) demonstrated the process of solvent mixture to prevent the formation of CBZ dihydrate. (Childs et al., 2008) they have crystallised cocrystal of CBZ/SAC using water as a solvent but they have used different molar ratios of CBZ

and SAC and were successful in producing form I cocrystal and preventing the formation of dihydrate by increasing the molar concentration of coformer. In the present study, solvent mixture of methanol-water (50-50) in total 10 mL for the crystallisation is used. Below Figure 6.6 represents the PXRD patterns of form I and form II cocrystal phases of CBZ: SAC 1:1 cocrystal pair.

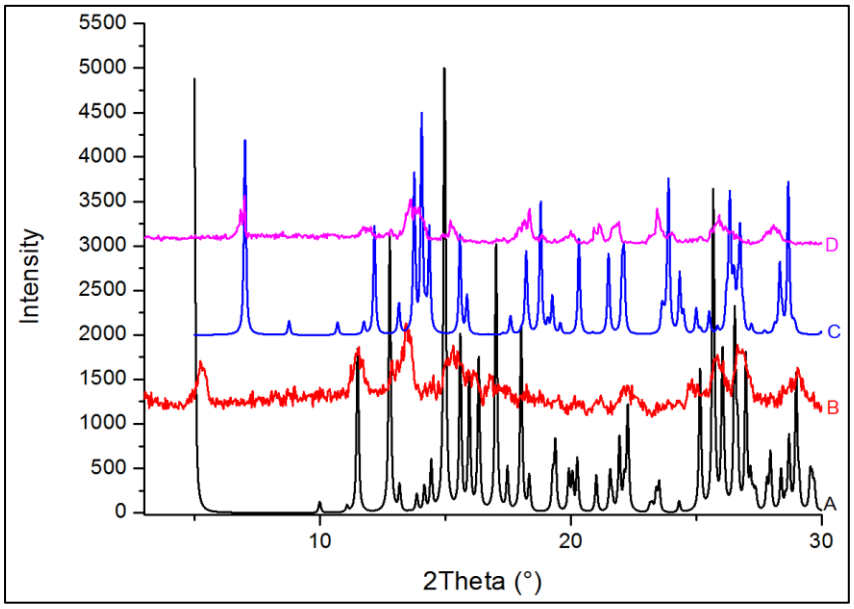

Figure 6.6 PXRD pattern of A- CBZ/SAC FII CSD data, B- CBZ/SAC FII MASCW processed, C- CBZ/SAC FI CSD data and D-CBZ/SAC FI MASCW processed.

Based on the PXRD pattern generated sample B correlates with the standard CSD pattern of form II cocrystal phase of CBZ: SAC. Based on the CSD data characteristic peak at 5 2(θ°) represents the formation of metastable form II phase of CBZ: SAC cocrystal. This peak is observed in the sample which is treated by continuous stirring and solvent mixture. In this process of cocrystallisation by continuous stirring of the sub-critically treated solution external stress is applied which prevents the formation of stable crystal phase and gets precipitated out as metastable phase.

Below Table 6.2 represents the summary of experimental results obtained during crystallisation of CBZ: SAC 1:1 cocrystal pair using solvent mixture under different crystallisation techniques.

Table 6.2 Summary of CBZ: SAC cocrystal phase obtained during crystallisation and the technique used.

Wt of CBZ/SAC(1:1) molar ratio	5ml MeOH + 5mL water as solvent mix	PXRD and DSC data results
350mg	5 mL MeOH + 5 mL Water	Form I pure on controlled cooling.
350mg	5 mL MeOH + 5 mL Water	Form II pure on sudden shear-induced cooling.

Formation of CBZ/SAC form II phase pure cocrystal were generated successfully when solvent mixture of methanol water is used as solvent system. Further, during the cooling step the processed solution is suddenly cooled accompanied by continuous stirring so the crystals started inducing out in the form of solid mass, but with controlled cooling and no stirring form I cocrystal formation took place.

To confirm the results obtained from the PXRD analysis further characterisation is performed thermal analysis using DSC analyser and spectroscopic analysis.

6.2.1. b) DSC thermogram

Diffraction scanning calorimetric analysis is performed for all the samples to study the phase transformation, the presence of any residual water content and understand and reveal the crystallinity of the cocrystal complex formed. Below Figure 6.6, 6.8, 6.9, 6.10 and 6.11 represents the thermogram

obtained for CBZ: SAC 1:1 cocrystal when different parameters like target temperature, amount of solvent, microwave power, heating rate and solute stoichiometric ratio vs solvent volume were analysed respectively.

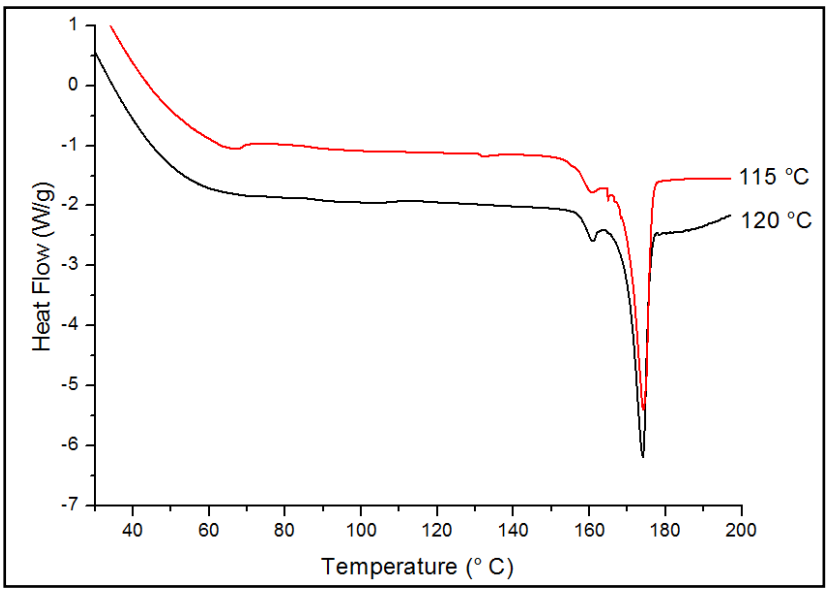

Figure 6.7 DSC thermograms of batches carried at different process temperatures.

Based on the literature value the melting point of CBZ, SAC and CBZ: SAC form I cocrystal is 189-193°C, 228°C and 175-177°C respectively. In the above thermogram obtained at different process temperatures a distinct endotherm at 176°C is observed which is attributed to form I cocrystal of CBZ: SAC cocrystal pair and a small endotherm at 160°C is the phase transition taking place between metastable form II to form I under high-temperature conditions (Rodríguez-Hornedo et al.,2008).

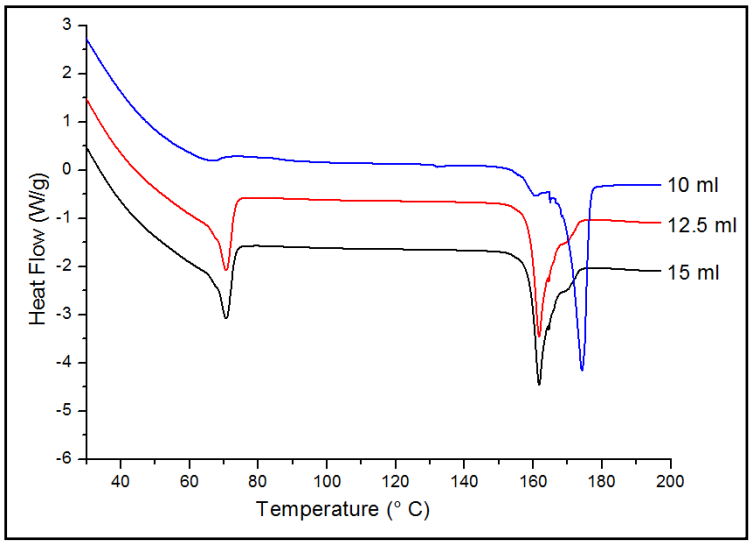

Figure 6.8 DSC thermograms of experiments performed at different amount of water.

In the above thermogram at different solvent concentrations, formation of CBZ: SAC form I cocrystal dihydrate at 12.5 and 15ml volumes of water is observed. In 10ml the endotherm is corresponding to form I cocrystal whereas in 12.5 and 15ml samples endotherm shifted towards lower degrees due to phase impurities and the broadness of the endotherm is attributed to the bounded water impurities.

Below Figure 6.9 and 6.10 represents the thermogram for CBZ: SAC cocrystal at different microwave energies and heating rate. In both the experiments generation of CBZ: SAC form I cocrystal took place. At the fast heating rate, some impurities of cocrystal and CBZ starting material based on the melting points is observed, in this thermogram presence of broad endotherm between 60-110°C is observed which corresponds to a bound water molecule.

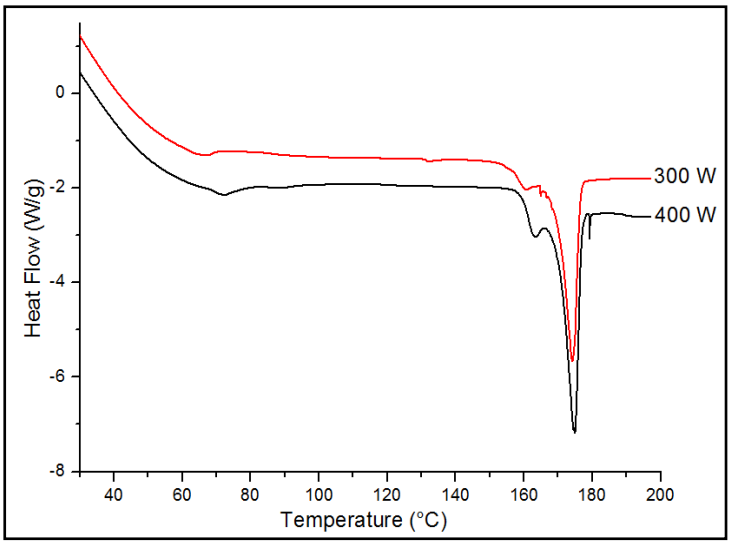

Figure 6.9 DSC endotherm of batches carried out at 300W and 400W.

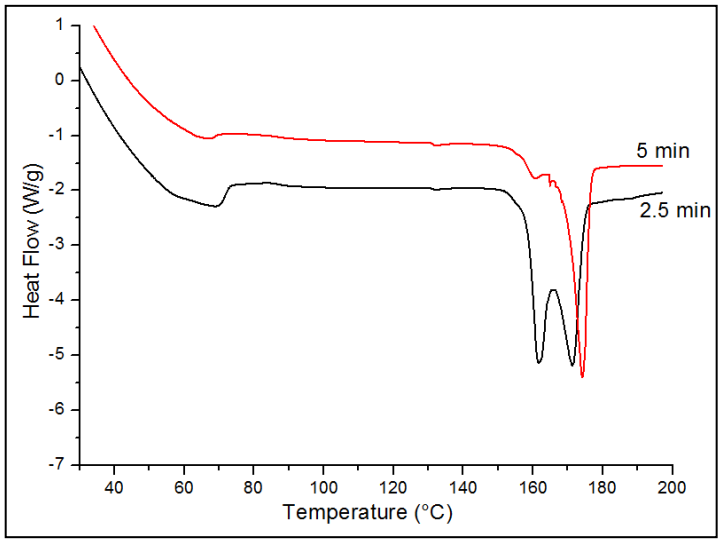

Figure 6.10 DSC thermograms of two cocrystal batches at different heating rates.

Based on the thermogram below (Figure 6.11) a minor broad endothermic event between 80-110°C is observed which is attributed to residual moisture and further phase transition endotherm from form II to form I in the region between 160-165°C and 173-175°C occurred respectively.

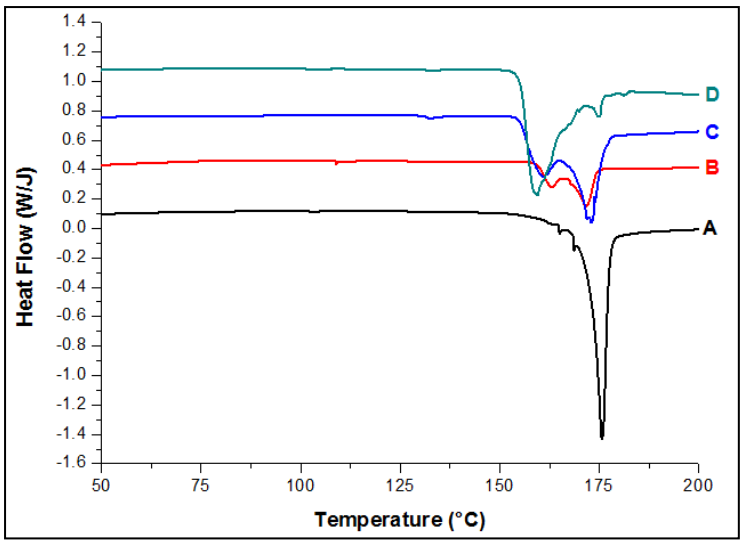

Figure 6.11 DSC thermograms of A) CBZ: SAC 1:1.5_12.5ml water, B) CBZ: SAC 1:1.5_15ml water, C) CBZ: SAC 1:2_12.5ml water and D) CBZ: SAC 1:2_15ml water

Figure 6.12 represents the DSC thermogram for CBZ: SAC form II cocrystal processed using a solvent mixture.

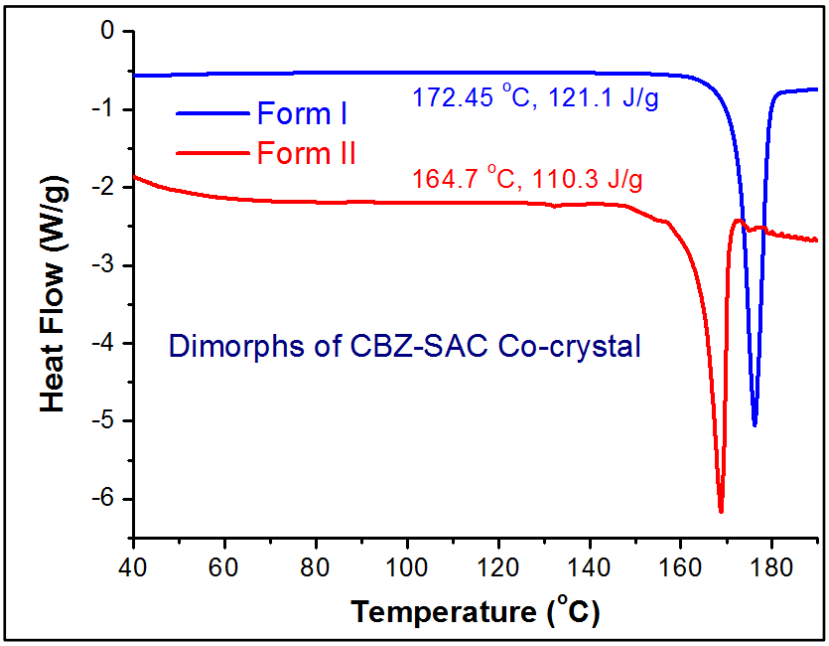

Figure 6.12 DSC thermograms of CBZ/SAC Form I and FII processed by MASCW.

Based on the above DSC thermogram comparison of two different cocrystal samples is represented. The melting endotherm at 164.7°C represents to

form II cocrystal of CBZ: SAC which is a metastable phase and melting endotherm at 172.45°C represents to form I stable cocrystal phase.

6.2.1. c) HPLC analysis

Quantitative analysis of MASCW processed CBZ: SAC cocrystals were done as there are subjected to high temperature and pressure conditions and during performing experiments certain coloration of the supersaturated solution after microwave treatment is observed. CBZ undergoes oxidation reaction in presence of solvent system to give rise to iminostilbene. The initial steps consist of the preparation of calibration curve for various concentrations of iminostilbene and from the equation received from the graph the percentage concentration of iminostilbene present in an unknown sample of CBZ/SAC cocrystals process in MASCW process. The calibration curve for iminostilbene is displayed below in Figure 6.13

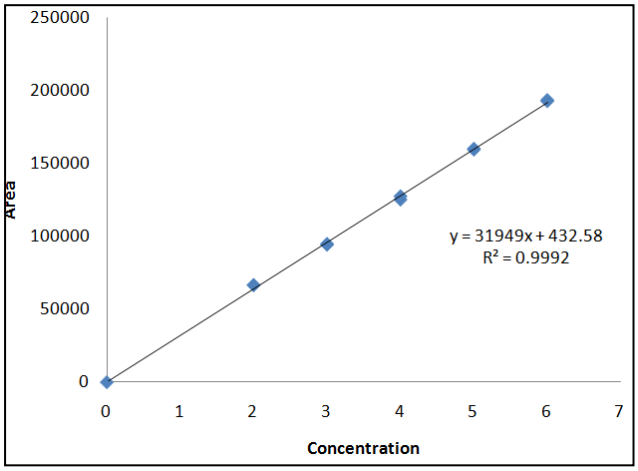

Figure 6.13 Calibration curve for iminostilbene

Both CBZ standard and iminostilbene standards were isolated using the isocratic method, below Figure 6.14 represents the chromatogram representing two different separated peaks for CBZ and iminostilbene respectively.

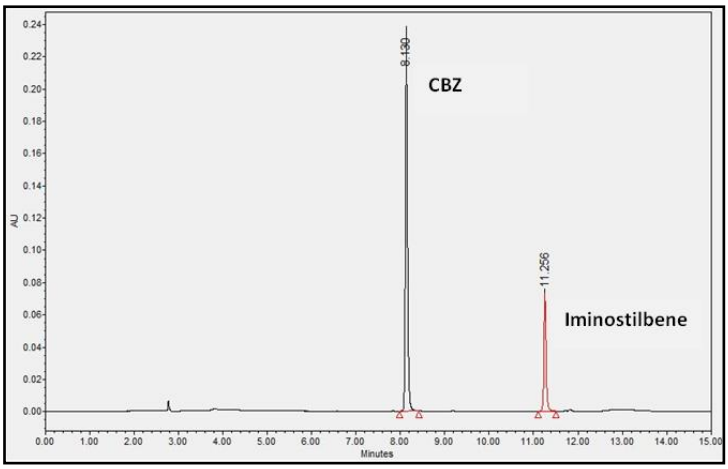

Figure 6.14 Chromatogram representing the separation of CBZ and iminostilbene.

Below Table 6.3 represents the percent essay of iminostilbene for all the samples processed at different process parameters and form I and form II polymorphs of CBZ: SAC cocrystals.

Table 6.3 Percent degradation of MASCW processed CBZ: SAC cocrystal samples using different parameters

Processing variable	**Process parameters**	**% iminostilbene**
Solvent amount	10 mL	0.1366
	12.5 mL	0.2136
	15 mL	0.1518
Temperature	110 °C	0.2958
	115 °C	0.1366
	120 °C	0.1993
Microwave power	200 W	0.1790
	300 W	0.1366
	400 W	0.1947
CBZ/SAC form I cocrystal	-	0.1122
CBZ/SAC form II cocrystal	-	0.1024

Based on the degradation study performed, it is observed that samples which were treated at an elevated temperature, high microwave power and

for a prolonged period of time contain a higher concentration of iminostilbene as potential degradant. Above table showed an acceptable amount of degradation according to USP guidelines. Thus based on the degradation study the optimum process parameters quantified for this cocrystallisation experiment is temperature 115°C, 300W power, 10mL solvent system and 5 minutes heating rate to reach the target temperature.

6.2.1. d) Scanning electron microscopy

As all the cocrystals samples were exposed to high temperature and pressure condition using water as the solvent system, change in the morphological properties of cocrystal samples processed using MASCW process and solution crystallisation is reported in the below Figure 6.15 and 6.16 respectively. Change in the crystal habits of two different form of CBZ: SAC form I and form II cocrystals is reported (see Figure 6.17).

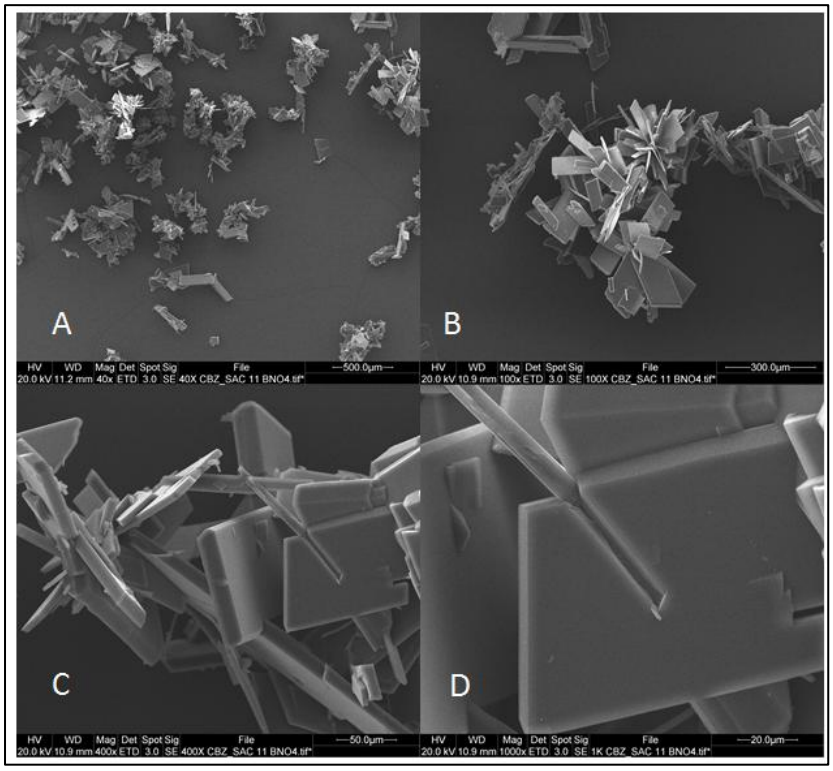

Figure 6.15 SEM images of CBZ/SAC cocrystal form I process from MASCW at optimum process parameters; A-40X, B-100X, C-400X and D-1000X magnifications.

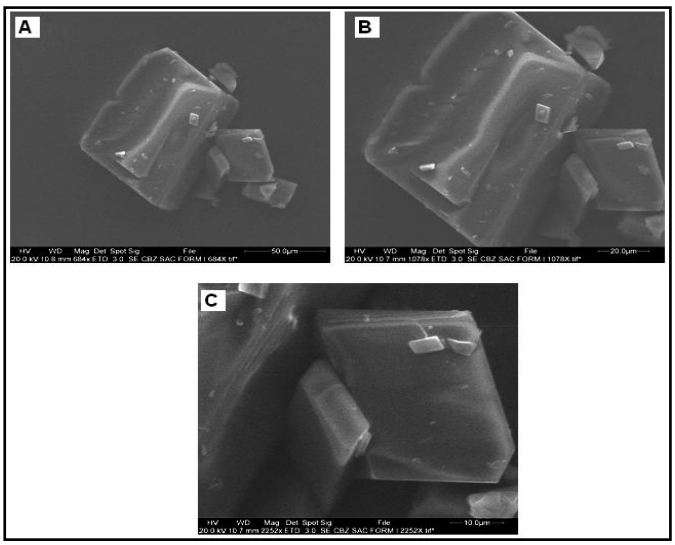

Figure 6.16 SEM images of CBZ / SAC co-crystal Form I obtained from solution crystallisation method A) 700X, B) 1000X and C) 2250X magnifications.

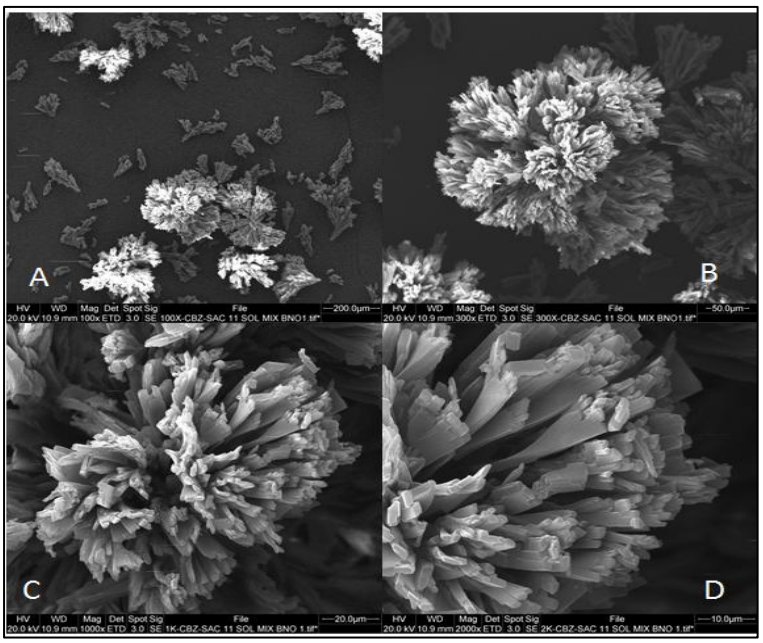

Figure 6.17 SEM images of CBZ/SAC cocrystal form II process from MASCW at optimum process parameters: A-100X, B- 300X, C-1000X, and D-2000X magnifications.

SEM images of MASCW processed samples are compared with reference i.e. CBZ/SAC form I produced from conventional solution crystallisation process. The samples processed by MASCW show smooth surfaces plate-like structure with minimum crystal defects. The CBZ/SAC form II cocrystals produced from a MASCW process show very drastic change in the morphology. This may be due to the growth of secondary nuclei which are based on primary nuclei. The plate-like crystal morphology of CBZ/SAC form I is previously reported in the literature (Rodríguez-Hornedo et al., 2008; Porter et al., 2008; Shariare et al., 2012). Shariare and co-workers proposed the change in the crystal structure due to change in the solvent system so the change in the crystal structure can be attributed to the process methods and the solvent system used. The cocrystal form II size is relatively smaller than form I cocrystal which can be correlated to the process parameters and phase properties.

6.2.1. e) Surface Energy Analysis (SEA)

Based on the SEM images the change in the crystal habit of MASCW processed cocrystal samples were observed compared to conventional solution crystallisation samples, therefore to study the change in the surface properties we have reported dispersive surface energies of all the samples at different surface coverage's (methods see Section 4.2.2.1.4). Various literature reviews are present which represent the change in the surface energy with the morphology, Peter York, and group demonstrated the

solubility variations observed with difference in morphology of Ibuprofen crystals, they demonstrated that plate-shaped crystals generated from ethanol have higher solubility and needle-shaped crystals obtained from hexane solvent (Shariare et al., 2012). (Heng et al., 2006) has represented the change in the surface energy with the presence of impurities in paracetamol crystals. All the samples selected retain similar particle size distribution. Figure 6.18 represents the dispersive surface energies of CBZ: SAC form I cocrystal solution crystallised, CBZ: SAC form I and form II MASCW processed cocrystal samples.

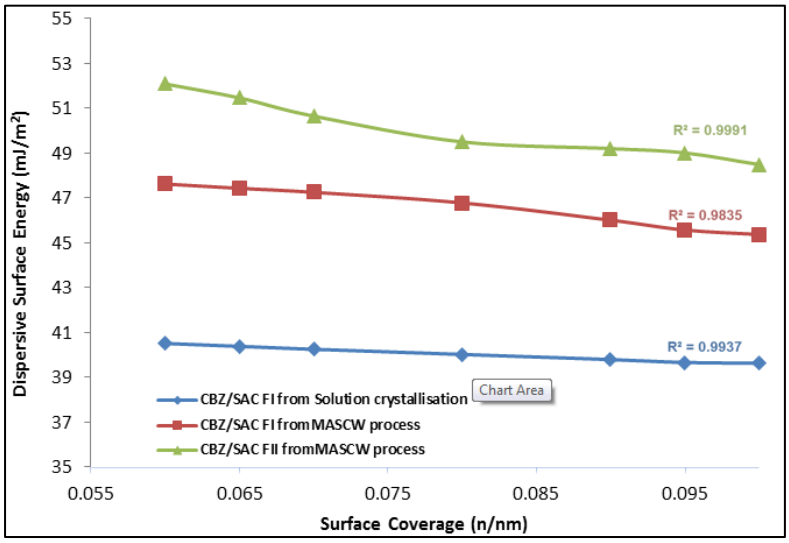

Figure 6.18 Dispersive surface energy plot for CBZ/SAC cocrystal FI and FII obtained from the MASCW process and CBZ/SAC FI obtained from solution crystallisation.

The above plot reading is based on different percent surface coverage of samples obtained when series of alkane gas molecules are passed through the sample column. The dispersive surface energy is calculated by using Dorris/Gray approach with peak max as result parameter using SMS Cirrus Plus analysis software. Figure 6.16 represents that the crystals obtained using MASCW process have greater surface energy than the crystals

obtained from solution crystallisation. CBZ/SAC FII as discussed before as metastable phase retain highest surface energy than the FI crystals obtained from the same MASCW process. The surface energy is the analysis of the type of interaction between the molecules on the surface and bulk region, it indicates the presence of active sites on the surface and the bulk of the sample. They showed the retention of probe solvents on the bulk and surface of the material which depends on the interactions between the sample materials and the solvent probes passed through it. In the present study non-polar solvents displayed higher surface energy values which indicate the presence of less polar functional group on the surface and bulk of the sample mass. Less surface energy for the crystals obtained from solution crystallisation is observed which indicates the presence of more polar functional groups on the bulk and surface of the sample materials. The change in the surface energies is attributed to crystal habit and presence of active sites on the surface of the cocrystals.

6.2.1. f) Solubility data

Due to the variation observed in the different forms of CBZ: SAC cocrystals investigation of solubility properties of the cocrystal is performed by studying the equilibrium solubility of the samples at different temperature conditions. Figure 6.19 represents the solubility profile of CBZ: SAC form I and form II at different temperature conditions.

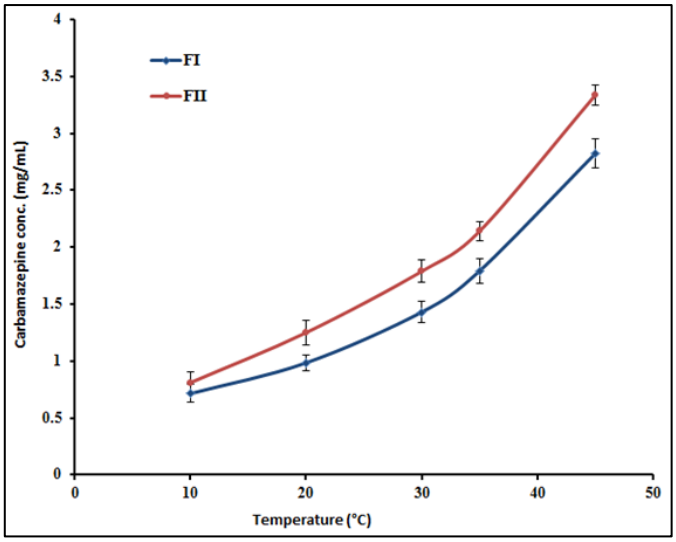

Figure 6.19 Solubility vs temperature profile for CBZ: SAC form I and form II cocrystal phase.

Based on the solubility vs temperature curve an increase in the solubility of metastable form II phase of CBZ: SAC cocrystal compared to form I is observed. This increase in the solubility is attributed to the surface energy of metastable form II phase, crystal habit and dimorphic crystal lattice arrangement of cocrystal components.

6.2.2 Screening experiment: cocrystallisation of SMT: SAC and SMZ: SAC cocrystal pairs

In this section, MASCW process as the screening tool is implemented for the generation of SMT: SAC and SMZ: SAC cocrystal pairs in 1:1 stoichiometric ratio using water as the solvent system. The process parameters selected for these experiments are optimised in our previous studies (for method see Section 4.2.2.2.2). Previously (Fu et al., 2016) and the group had produced cocrystal complexes of sulfamethazine and saccharine in 1:1 stoichiometric ratio to study the formation of cocrystal salt or cocrystal based on the intermolecular interaction sites.

6.2.2. a) PXRD data

The PXRD analysis is performed on all the samples processed using MASCW technology. Below Figure 6.20 represents the comparison of PXRD pattern for SMT and SAC cocrystals with starting materials and CSD standard PXRD pattern.

Based on the PXRD data it is observe that the XRD peaks of SMT: SAC 1:1 cocrystal sample is different from the raw starting materials and similar with the distinct characteristic peaks of SMT: SAC 1:1 CSD (XOBCOH) reference standard. According to the standard CSD pattern, two distinct peaks at 7.5 θ° and 12.5 2θ° can be distinguished which attributes to cocrystal phase. These two characteristic peaks are present in the processed sample of SMT: SAC cocrystal pair in 1:1 stoichiometric ratio (Fu et al., 2016). Thus formation of SMT: SAC 1:1 cocrystal is confirmed.

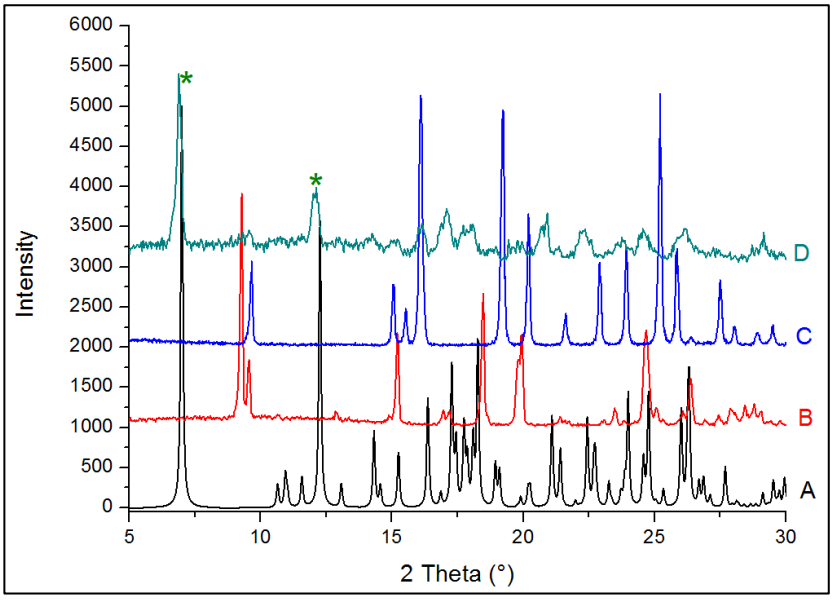

Figure 6.20 PXRD patterns of : A) SMT_SAC 1:1 CSD-(XOBCOH), B) SMT raw, C) SAC raw and D) SMT: SAC 1:1 cocrystal

In a similar manner, SMZ: SAC 1:1 cocrystal pair is selected and processed using the MASCW process to study the formation of cocrystal solid phase.

Figure 6.21 represents the comparison of PXRD pattern for raw and processed samples of SMZ and SAC.

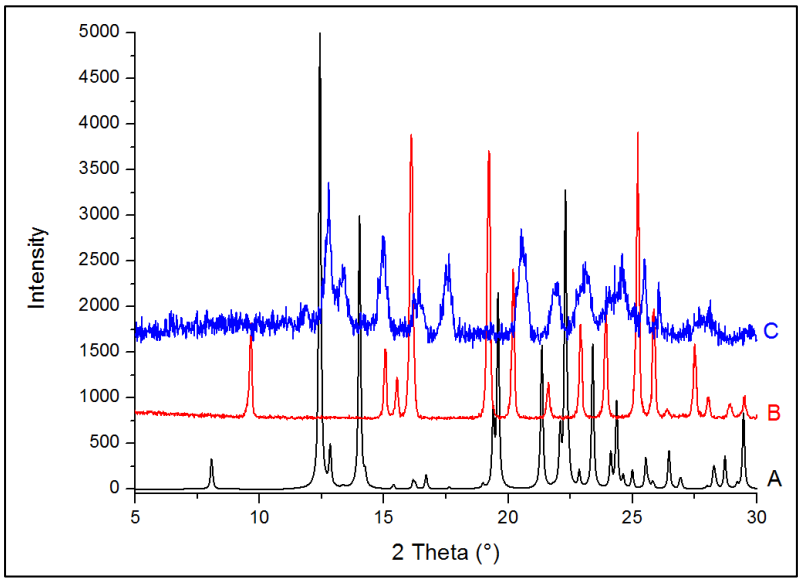

Figure 6.21 PXRD patterns of A) SMZ raw, B) SAC raw and C) SMZ: SAC 1:1 cocrystal

From the above PXRD pattern, new peaks at 17.5 and 19.2 2θ° is observed which may be corresponding to the formation of a new phase which could be cocrystal phase. Characteristic peak of SMZ and SAC raw materials are disappeared, which can be attributed to the interactions between SMZ and SAC during crystallisation or processing. To confirm the presences of new solid phase DSC analysis was performed.

6.2.2.b) DSC data

Based on the data obtained from PXRD studies thermal analysis of the processed samples is conducted to confirm the presence of any water molecule and new solid phase transitions. Below Figure 6.22 summarises the DSC endotherm of SMT, SAC raw materials, the physical mixture in 1:1 stoichiometric ratio and processed samples.

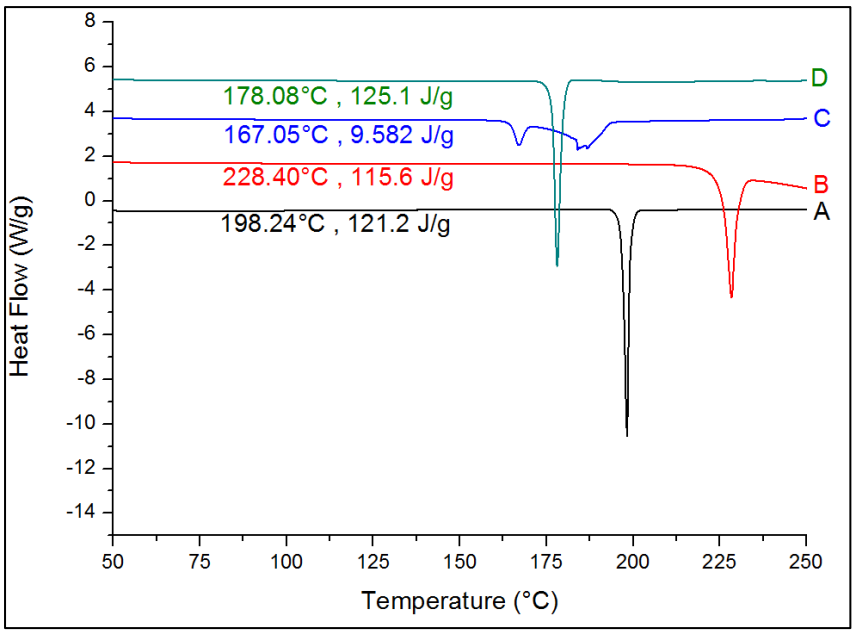

Figure 6.22 DSC endotherms of A) SMT raw, B) SAC raw, C) SMT/SAC 1:1 physical mixture and D) SMT/SAC 1:1 cocrystal

Based on the DSC endotherm it is observed that the melting endotherm of processed samples is less than the melting points of raw materials, which confirms the new phase generation. In the physical mixture, very small endotherm at 167°C is observed further followed by broad degradation peak which can be attributed to phase impurities. Based on the previous literature findings the melting endotherm between 175°C and 179°C corresponds to cocrystal phase of SMT: SAC 1:1 cocrystal (Padrela et al., 2010).

The similar ramp method is used to analyse the formation of SMZ: SAC 1:1 cocrystal phase, Figure 6.23 represents the DSC endotherm of SMZ, SAC raw, physical mixture and processed samples.

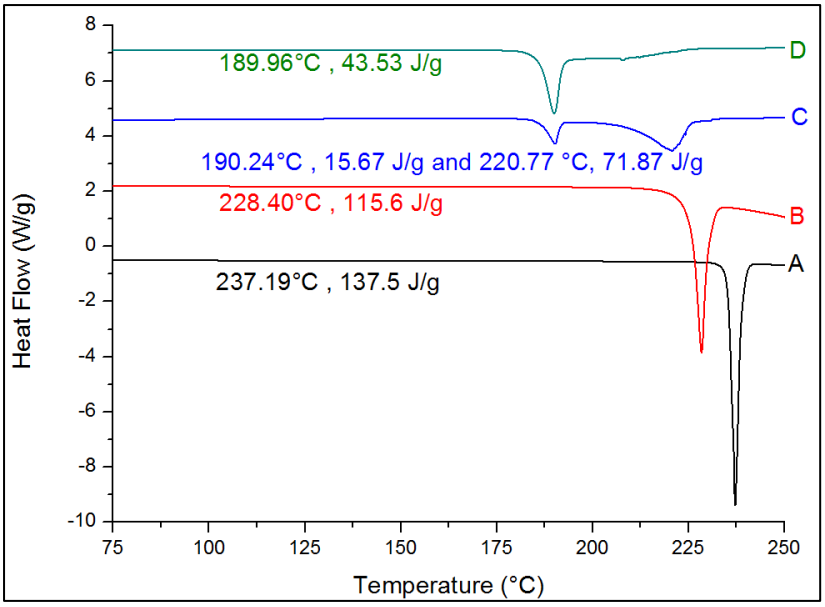

Figure 6.23 DSC endotherms of A) SMZ raw, B) SAC raw, C) SMZ/SAC 1:1 physical mixture and D) SMZ/SAC 1:1 cocrystal

Based on the above DSC patterns, the processed samples show new melting peak at 189.96°C which does not correlate to melting endotherms of starting materials. In the physical mixture, small melting event at 190.24°C is observed followed by a broad melting event at 220.77°C which can be attributed to the cocrystal peak and saccharin impurities. Thus based on the melting points, in the processed samples the melting point is lower than raw materials. Therefore generation of new crystal phase is confirmed which may be cocrystal. The absence of any broad or distinct endotherm between 60°C -110° C further confirms the absence of hydrate formation.

6.2.3 Cocrystallisation of CAF – 4-HBA acid using MASCW process

6.2.3.1 Introduction

In the present chapter, application of MASCW process and solvent mixture is explored for the generation of incongruent cocrystal pair of caffeine (CAF) and para-hydroxybenzoic acid (4HBA) in 1:1 stoichiometric ratios. Various studies have been performed for the generation of cocrystals with enhanced

properties but the real challenge lies when the predicted results are not reflected experimentally when the stoichiometric ratios of the starting two components are not similar to the stoichiometric ratios of cocrystals formed. Aitipamula's group have analysed the study to predict the hidden cocrystal hydrates of caffeine and piracetam with 4-hydroxybenzoic acid (Aitipamula et al., 2012), they revealed the presence of CAF-4HBA (1:1) hydrate. The findings were able to generate 1:2 and 2:1 cocrystals of CAF/4HBA which is earlier studied by McGillivray's group, 2009. Recently (Dejan-Kresimir Bucar 2008) have used cocrystallisation of caffeine with regioisomers of hydroxybenzoic acids (2, 3 and 4) to understand the product variability which is referred as an incongruent pair. The hydroxybenzoic acids have the capacity to form three different components of cocrystals with caffeine with different crystal properties. Recently, Price's group tried to study the cocrystallisation of CAF/4HBA in 1:1, 1:2 and 2:1 stoichiometric ratios based on its lattice energy and capacity to form hydrogen bonding between these two cocrystal components, this group has postulated that based on the crystal lattice energies and arrangements formation of CAF/4HBA in 1:1 is practically not possible (L. Sarah Price, 2014). Caffeine has in total three sites of a functional group which retain hydrogen bonding capacity, N-atom on imidazole, the other two are based on oxygen atom present on carbonyl group of urea and an amide moiety (Dejan-Kresimir Bucar 2008). So various studies were performed to study the heterosynthon in caffeine based cocrystallisation, (Dejan-Kresimir Bucar 2008) is able to produce CAF/4HBA 1:2 and 2:1 cocrystals but failed in generation of 1:1 cocrystal of CAF/4HBA due to formation of concomitant impurities of 2:1 CAF/4HBA cocrystal, there

were successful in reporting the formation of hydrates of CAF and multi-substituted HBA cocrystals when water and organic solvent (acetonitrile) is used as solvent media for cocrystallisation. Based on this screening experiment performed by (Dejan-Kresimir Bucar 2008) it is proved that it is practically difficult to produce 1:1 cocrystal of CAF/4HBA due to its incongruence. Hence, the present study aims in the production of anhydrous phase of CAF/4HBA cocrystal in 1:1 stoichiometry using MASCW process, (for method see Section 4.2.1.3.2). For the reference purpose, CAF/4HBA cocrystal at different stoichiometric ratios was produced using slow evaporation solution crystallisation.

6.3.2.2 Results and discussion

6.3.2.2. a Summary of experimental data

As discussed by (Dejan-Kresimir Bucar 2008) the unpredictable enormous behavior of 4HBA with CAF, when 1:1 stoichiometric ratio of CAF/4HBA is subjected to crystallisation they induce out as CAF/4HBA 2:1 cocrystals instead of 1:1 cocrystals. CAF/4HBA in 1:1 molar ratios was subjected to MASCW process and analysed the resultant product stoichiometry using X-ray diffraction analysis. Below Table 6.4 summarises the results obtained at different experimental conditions.

Table 6.4 Experimental design of CAF/4HBA cocrystallisation

Weight of CAF (mg) (2.5mmol)	Weight of 4HBA (mg)(2.5mmol)	Stoichiometry	Solvent system (10 mL)	Temp (˚C)	Result (PXRD)
485	345	1:1	water	135	Mixture of 1:2 and 2:1cc
485	690	1:2	water	135	1:2 cc
970	345	2:1	water	135	2:1 cc
485	345	1:1	5mLMeOH +5mLH2O	135	1:1 cc

Generation of cocrystal pairs at different stoichiometric ratio is analysed and observed the formation of either 1:2 or 2:1 stoichiometric ratio of CAF/4HBA. When 1:1 molar ration of CAF/4HBA is subjected to processing based on PXRD data concomitant mixture of 1:2 and 2:1 stoichiometric ratios of CAF/4HBA is observed.

6.3.2.2. b PXRD data

Using solution crystallisation technique and methanol as the solvent system generation of CAF/4HBA cocrystals in different stoichiometric ratios is reported. The below Figure 6.24 summarises the PXRD results of CAF/4HBA cocrystals with different stoichiometric ratios.

Based on the solution crystallisation PXRD result when 1:1 molar concentration of CAF and 4HBA is subjected to solution crystallisation using methanol as solvent, concomitant impurities of 2:1 CAF/4HBA cocrystals have induced out. CAF/4HBA 1:2 and 2:1 cocrystal results are in similar stoichiometric ratios as the initial molar ratios of caffeine and 4-hydroxybenzoic acid. These results are in good agreement with results obtained previously by various research groups.

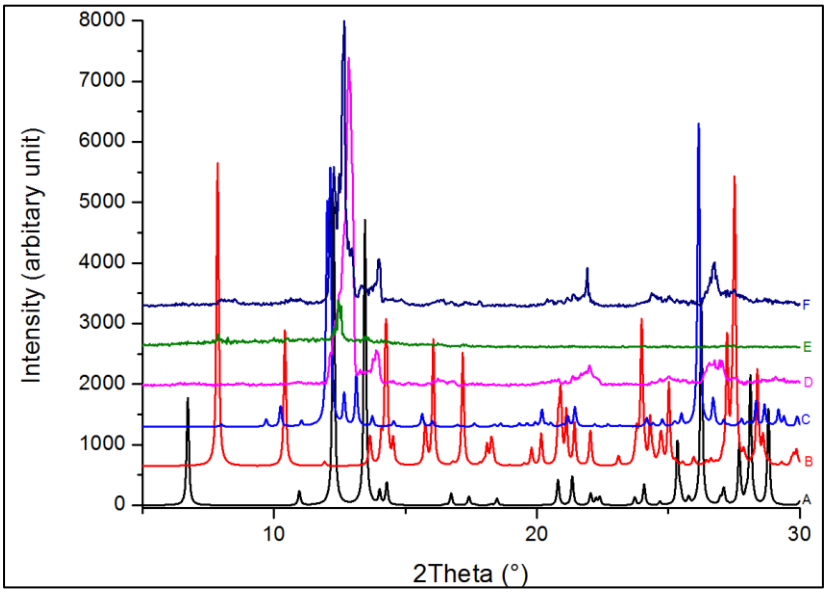

Figure 6.24 PXRD patterns of solution crystallisation pattern of CAF/4HBA cocrystals A-CAF-4HBA (1:1) CSD, B-CAF-4HBA (1:2) CSD, C-CAF-4HBA (2:1) CSD, D- CAF-4HBA (2:1) solcryst, E-CAF-4HBA (1:2) solcryst and F-CAF-4HBA (1:1) solcryst.

Below Figure 6.25 represents the PXRD patterns of CAF-4HBA cocrystal pairs at different stoichiometric ratios using water as the solvent system.

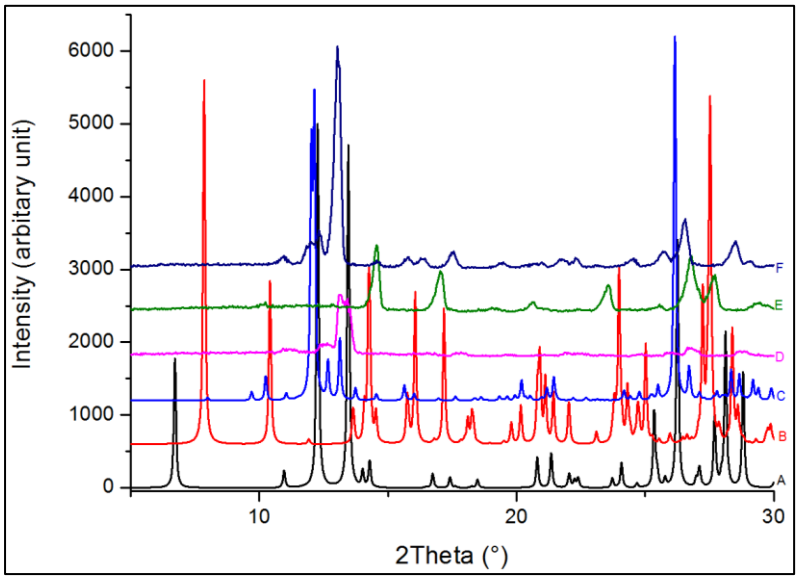

Figure 6.25 PXRD patterns of MASCW process batches of CAF/4HBA cc A-CAF-4HBA (1:1) CSD, B- CAF-4HBA (1:2) CSD, C- CAF-4HBA (2:1)CSD, D-CAF-4HBA(1:1)-SCWP, E-CAF-4HBA(1:2)-SCWP and F-CAF-4HBA (2:1) – SCWP.

Below Figure 6.26 represents the formation of 1:1 cocrystal pair of CAF-4HBA using a solvent mixture (50%methanol + 50% water) as the solvent system.

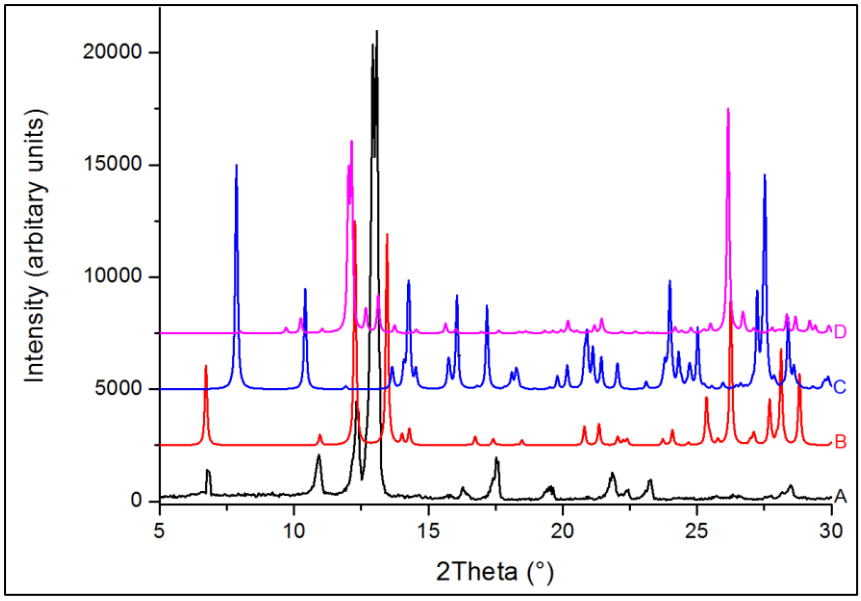

Figure 6.26 PXRD patterns of CAF/4HBA 1:1 cocrystals produced from a MASCW process using a solvent mixture (50%-50% MeOH-water) as a solvent. A-CAF/4HBA 1:1 cocrystals produced from MASCW, B- CAF-4HBA (1:1) CSD, C- CAF-4HBA (1:2) CSD, D- CAF-4HBA (2:1) CSD.

As concomitant impurities of 2:1 CAF/4HBA when 1:1 molar concentrations of two components were obtained when subjected to solution crystallisation. The effect of the MASCW process in the molar ratios of initial components and final cocrystal product was studies using 10 mL water as the solvent system. Figure 6.25 represents the PXRD results of CAF/4HBA cocrystals obtained using MASCW process using water as the solvent system. As a result, this experiment failed as there is no 1:1 stoichiometric ratio of CAF/4HBA cocrystals is formed, same results similar to solution crystallisation observed in this process as well.

These results made us consider the dielectric constant of solvent at elevated temperatures so a solvent mixture (5 mL water + 5 mL methanol) as a solvent system was used so the dielectric constant is further reduced at elevated temperatures which increase its polarity. Figure 6.26 represents the

PXRD patterns of CAF/4HBA 1:1 cocrystal obtained using MASCW process using solvent mixtures as the solvent system. The peak at 6.8 2θ degrees is the characteristic peak which corresponds to 1:1 stoichiometric ratio of CAF/4HBA cocrystal. The PXRD pattern of CAF/4HBA 1:1 cocrystals very correctly matches with CAF/4HBA 1:1 cocrystal pattern generated from crystal structure data (CSD).

6.3.2.2. c Thermal analysis data

Thermal analysis using DSC and TGA is performed to the hit sample of CAF-4HBA 1:1 produced from a MASCW process using the solvent mixture to analyse the presence of hydrate due to the hygroscopic property of caffeine and hydroxybenzoic acid.

Based on the DSC analysis the endotherm observed at melting point 150.99˚C corresponds to the melting point of CAF: 4HBA 1:1 ratio observed by Aitipamula's and group. The absence of broad endotherm between 70°C-110°C further confirms the absence of residual water molecule. The TGA thermogram contains only single linear event and doesn't show any loss in weight at 70°C-110°C which confirms the absence of water molecule. The only event present is around 150°C corresponds to the melting of CAF: 4HBA co-crystal. Molecular association of hydrogen bonds involved in cocrystals of CAF-4HBA 1:1 stoichiometry is further confirmed by using ^{1}H NMR which provided the complete description regarding stoichiometric ratios of CAF and 4HBA based on the proton molecules.

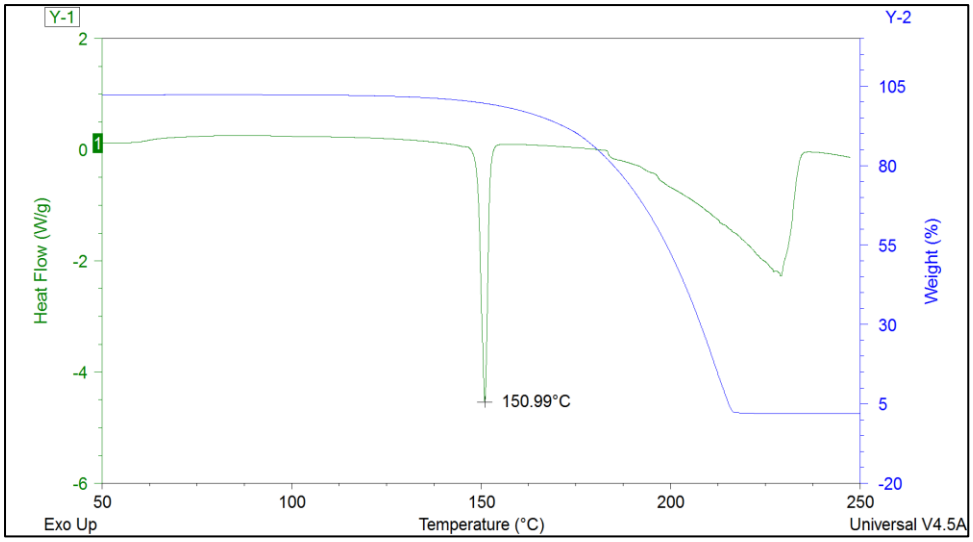

Figure 6.27 Overlay of DSC and TGA thermogram of CAF/4HBA 1:1 processed using MASCW process.

6.3.2.2. c ^{1}H-NMR- spectra

Successful determination of CAF: 4HBA cocrystal complex by thermal and X-ray diffraction then is monitored by ^{1}H-NMR, processed cocrystal pair of CAF: 4HBA is dissolved in d6-DMSO solvent before analysis, based on the integrated area ratios extracted from deconvolution of experimental ^{1}H-NMR spectra (peak fitting) that particularly considering the signal fraction of protons in CAF and 4HBA molecules were determined.

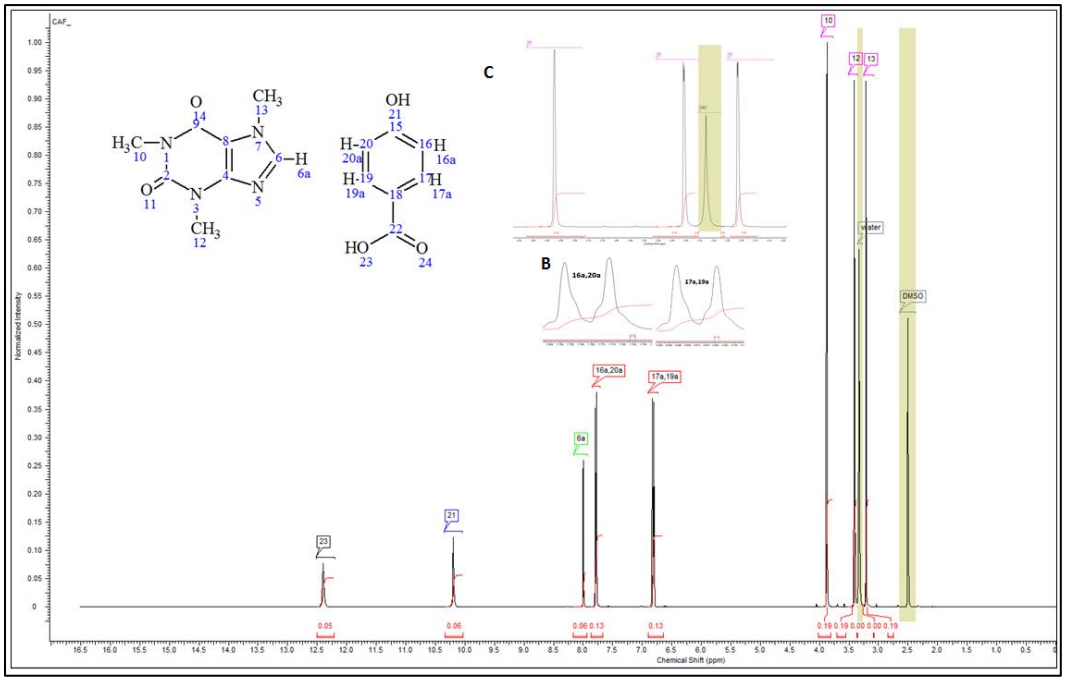

Figure 6.28 NMR spectral comparison of CAF: 4HBA 1:1 cocrystal in d6-DMSO

Upon inspection of 1H-NMR spectra for CAF: 4HBA cocrystal, it is observed that all the chemical shifts representing the protons of either CAF or 4HBA are well separated. Based on the peak picking analysis; 4-HBA is present in three different proton environments based on the chemical structural environment, peak at 12.5 ppm can be labelled as 23 represents the proton corresponding to –COOH group of 4-HBA, peak at 10.3 ppm labelled as 21 correspond to –OH group of 4HBA, peak at 7.8 and 6.8 labelled as 16a, 20a and 17a, 19a respectively corresponds to four aromatic –CH protons of 4HBA. CAF is present in chemically four different environments and 10 protons are present in total based on the molecular structure; peak at 8 ppm labeled as 6a corresponds to one hydrogen atom of imidazole C-H, and peaks between 3 to 3.8 ppm represent three –N-CH_3 protons which belong to 1, 3 and 7 nitrogen atoms. Peaks at 2.5 and 3.3 ppm represents to solvent (DMSO) residual peak and water respectively.

Next, the peak integration was evaluated for each of these chemical shifts using peak area values. As per NMR spectra, peak area for one proton (0.04), the integrated area ratios for (–COOH: -OH: -CH) groups of 4HBA are (1:1:4) and integrated area ratios of (–H: -N-CH3) groups of CAF are (1: 9) was determined. Finally upon considering the peak area ratios of all hydrogen's present in CAF and 4HBA, it is in excellent agreement with 1:1 stoichiometry.

6.2.4 Conclusion

Microwave assisted subcritical water process have successfully demonstrated the potency to generate cocrystal (metastable phase) with minimum degradation with enhanced surface free energy and solubility compared to cocrystals generated from conventional solution crystallisation process. Demonstration of the effect of different process parameters and phase purity of end products was reported. The generation of further two cocrystals of SMT: SAC and SMZ: SAC using water as solvent system was reported, thus MASCW process is novel green technology which can be used as high throughput screening tool as it is less time consuming, efficient in controlling the process parameters and cause minimum chemical degradation to the processed samples.

For the first time in this research work, the application of MASCW process for generation of incongruent pair cocrystals of CAF: 4HBA in 1:1 stoichiometric ratio is explored.

Chapter 7: Application of MASCW process in polymorphism

In this chapter, application of the MASCW process in particle engineering of pharmaceutical ingredients is investigated. This chapter is further divided into two sections- 1) less compressible pharmaceutical ingredient like paracetamol (pca) and processed using MASCW technique for the generation of the metastable polymorphic phase of pca with enhanced compressibility and physicochemical properties.2) In the second section, application of the MASCW process for the generation of micro-sized theophylline particles with stable physicochemical and enhanced aerodynamic properties is investigated.

7.1 Generation of metastable paracetamol form II polymorph using MASCW process

7.1.1 Introduction

Two chemical compounds which are chemically similar but differ in the crystal lattice arrangement than they are said to exhibit polymorphism (Williams, 2006). Most of the chemical entities virtually exhibit polymorphism; they exhibit different crystal structure arrangement in terms of unit cell spacing, angles or crystal system but are similar in the chemical composition. Polymorphism has gained its importance in the pharmaceutical industry because of different polymorphs of same chemical component exhibit different physical and chemical properties such as stability, melting point, process compatibility, solubility, particle flow. (Burley et al., 2007). In the pharmaceutical industry, they are various groups of APIs which exhibit polymorphism up to 10 polymorphs. Groups such as barbiturates, steroids, and sulphonamide exhibit polymorphism (Tsapatsaris et al., 2014).

Controlled polymorphism is the new approach used in industry to obtain suitable polymorphs with advanced physicochemical properties. The most difficult task considered by researchers in the study of polymorphism is understanding and identification of thermodynamically stable polymorph. Most of the process parameters and experimental conditions are considered while identification and synthesis of polymorphs, parameters need to be considered are degree of supersaturation during crystallisation, solvent properties, process temperature and pressure. In recent years very good understanding of polymorphs have been developed via computational structural data study (Perrin et al., 2009). This process of polymorphism is exemplified by Acetaminophen (4-acetaminophen; paracetamol) which is rigorously studied antipyretic pharmaceutical ingredient which exhibits polymorphism. Paracetamol exists in three polymorphic crystal structures, pca form I is most stable and form III is most metastable crystal form. The relative thermodynamic stability of pca polymorphs in I>II>III and the inter conversion of the transformation of these polymorphs follow reverse order kinetics (Matthew L. Peterson 2003). Various studies have been performed to understand and isolate the polymorphic crystal structures of pca to generate metastable phase. (Matthew L. Peterson 2003) and group demonstrated the production of a trihydrate of polymorphs form I and II by ice-cold aqueous suspension approach. They demonstrated that the trihydrate form of polymorph is more metastable lath-shaped crystalline structure. Polymorphs of pca exhibit enantiotropic behavior which undergoes a phase transformation from metastable phase to stable phase. The most thermodynamically stable polymorph of pca is the monoclinic form I and

metastable form II which is orthorhombic form in ambient conditions. Despite various methods and studies the crystal structure of pca form III is difficult to isolate, it is postulated to be very unstable based on the crystal lattice energy (Etienne Joiris 1997). In the formulation aspects, pca is commonly used for the manufacturing of tablet dosage forms, commercially available stable polymorph form I is very poorly compressible due to its low densification property and crystal lattice arrangement (Etienne Joiris 1997). Pca monoclinic form generally represents high elastic deformation, particle fragmentation resulting tablet capping problem so it became very important to produce a metastable form of pca with enhanced compressibility property so the addition of external binders and pharmaceutical excipients can be avoided. And to avoid granulation step prior to compression Burley's group is able to isolate metastable form I and II of pca by implementing Oswald's rule of states (Burley et al., 2007). They proposed that in the process of crystallisation the system transforms from state of high energy to state of low energy via a minimum change of free energy so this study confirms than less stable polymorphs should get isolated first. This process is explored by using hot stage microscopy; they have produced by the heating glassy state rather than cooling the solution. Martino and group studied the molecular mobility of pca amorphous form using DSC instrumental analysis and proposed that the metastable forms are generated from the melt (Piera Di MARTINO 2000). Compression behavior of orthorhombic form of pca is studied and analysed by Joiris and co-workers. They have recrystallised the monoclinic form of pca and proposed that orthorhombic form II has higher compressibility due to its sliding structural planes (Etienne Joiris 1997). Gary Nichols proposed that

quantitative crystallisation of pca form II is possible only using polycrystalline material from fused form I. It is stated that form II orthorhombic polymorph undergoes plastic deformation and which is suitable for direct compression into tablets (Frampton 1998). The only method used for crystallisation of form II polymorph is by seeding the supersaturated solution of monoclinic form I with orthorhombic form II (Frampton 1998). Various studies were performed to generate cocrystals of pca which have enhanced compressibility properties than commercially available stable form I pca. Cocrystals of pca with trimethylglycine in 1:1 stoichiometry is generated which retains good compressibility property, later trimethylglycine replaced by oxalic acid as a coformer based on the compressibility property (Maeno et al., 2014). Crystal structure determination of pca form III is performed by Perrin and group using crystal structure prediction and powder X-ray diffraction technique (Perrin et al., 2009). Due to high requirement and greater need of metastable form II of pca in industrial level MASCW technology was implemented to generate stable pca form II polymorph. Further, this technology is transferred to the scalable level with our industrial partner where pca is used as the model component for generation of stable metastable phase with enhanced physicochemical properties.

7.1.2 Results and discussion

7.1.2.1 MASCW crystallisation of commercial paracetamol

Using MASCW technology generation of form I and form II polymorphs of pca was successfully performed in the lab scale as well as industrial scale. Below Table 7.1 represents the experimental conditions and phase obtained during crystallisation.

Table 7.1 Experimental results of MASCW treated pca

Wt. of pca commercial grade	Solvent volume water	Temperature (°C)	Cooling conditions	Results (PXRD)
1g	10mL	140	Controlled cooling without stirring	Pure form I
1g	10mL	140	controlled cooling with stirring	Form I+ form II impurities
`1g	10mL	140	Sudden cooling with stirring	Pure form II
1g	10mL	140	sudden cooling without stirring	Pure form I

Based on experimental data formation of form I stable and form II metastable phase of pca is reported at different experimental conditions. When 10% w/v supersaturated solution of pca is processed using MASCW technology and implemented different crystallisation techniques different pca polymorphs were identified. When the supersaturated solution is not disturbed during controlled cooling and sudden cooling form I polymorph is obtained. When the solution under controlled cooling step is disturbed by applying external shear than immediate crystal start inducing which results form I polymorph with form II impurities. To obtain pure metastable polymorphic phase the supersaturated solution is suddenly cooled by applying shear (stirring) immediate crystals start inducing resulting generation of form II orthorhombic polymorphic phase of paracetamol. The generation of metastable form II phase of pca is attributed to the supersaturation level of the solution and importantly the water hydrogen bonding property, when sub-critically treated solution of pca in water is disturbed during the cooling step we are inhibiting water to retain its hydrogen bonding structure and based on the dielectric energy difference of the solution and solubility of pca in water generation

metastable phase of pca is occurred. The phase purity of the processed pca is further confirmed using spectroscopic studies.

7.1.2.2 PXRD data

Below Figure 7.1 represents the PXRD patterns of pca samples MASCW processed and raw commercial pca form I as the reference.

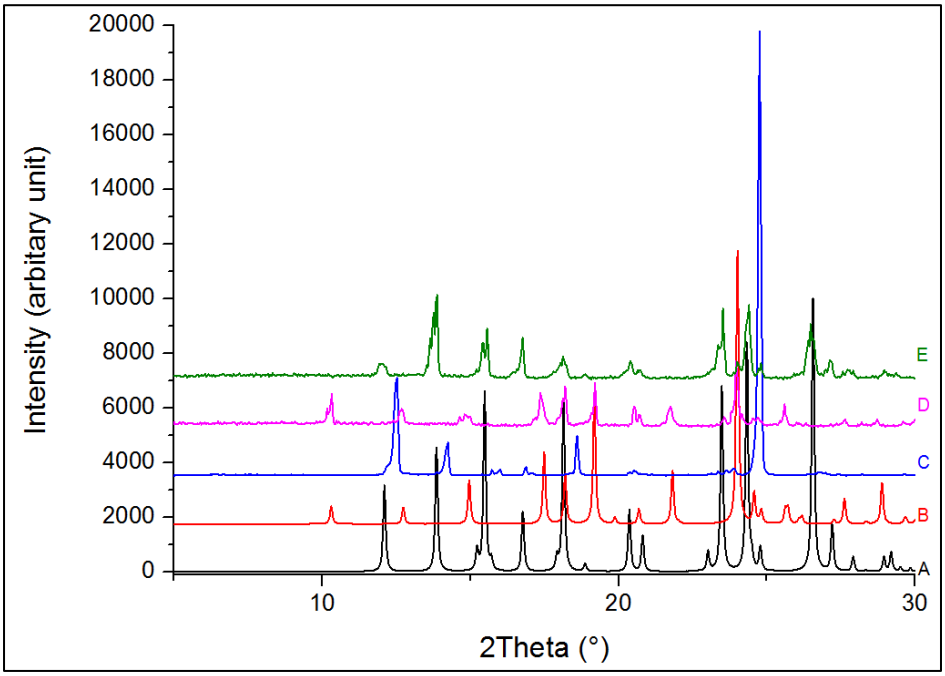

Figure 7.1 PXRD patterns of: A- pca FI CSD, B- pca FII CSD, C-pca-raw, D- pca FII MASCW processed and E – pca FI MASCW processed.

Based on the PXRD patterns MASCW processed samples of pca are in good agreement with pca FII CSD calculated patterns and pca FI calculated pattern. Characteristic peak at 10 theta degrees in pca form II CSD pattern (D) is in good agreement with PXRD pattern D. Pattern E which is MASCW processed samples proved to be pca form I similar to starting material and pattern A. Only difference in the process between D and E is the batches (D) which is subjected to continuous stirring and rapid cooling step whereas batch E is subjected to control cooling without stirring action. The decrease

in the crystallinity can be attributed to decrease in particle size and generation of amorphous fraction of processed samples.

7.1.2.3 Raman spectroscopic data

Based on the previous literature studies pca exists in three polymorphic phases form I,II and III out of which form II and III are the metastable phase and were studied using DSC coupled with Raman spectroscopy (Kauffman et al., 2008) . Figure 7.2 represents the base line corrected and normalised Raman spectra of raw and processed pca samples.

A)

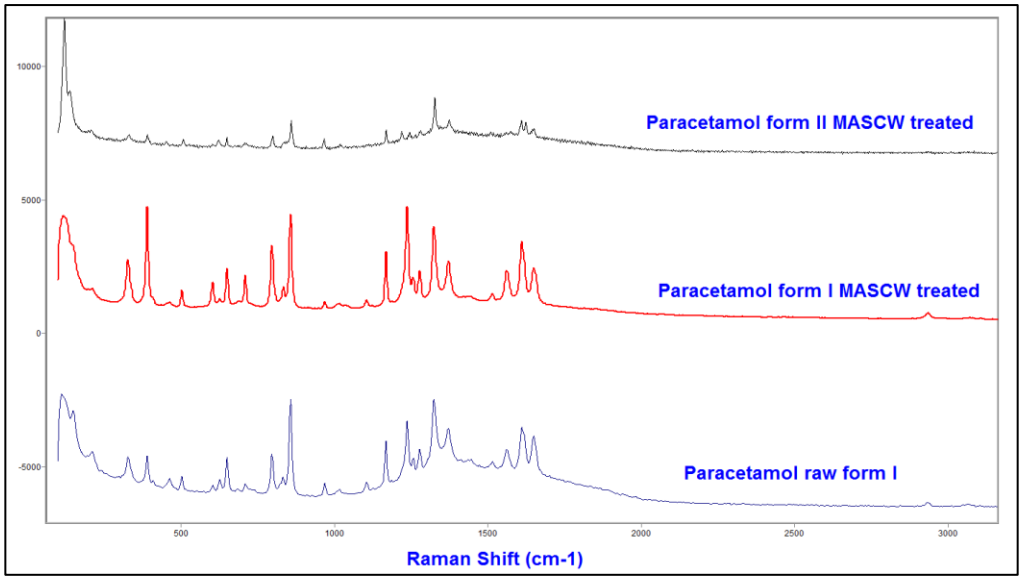

B)

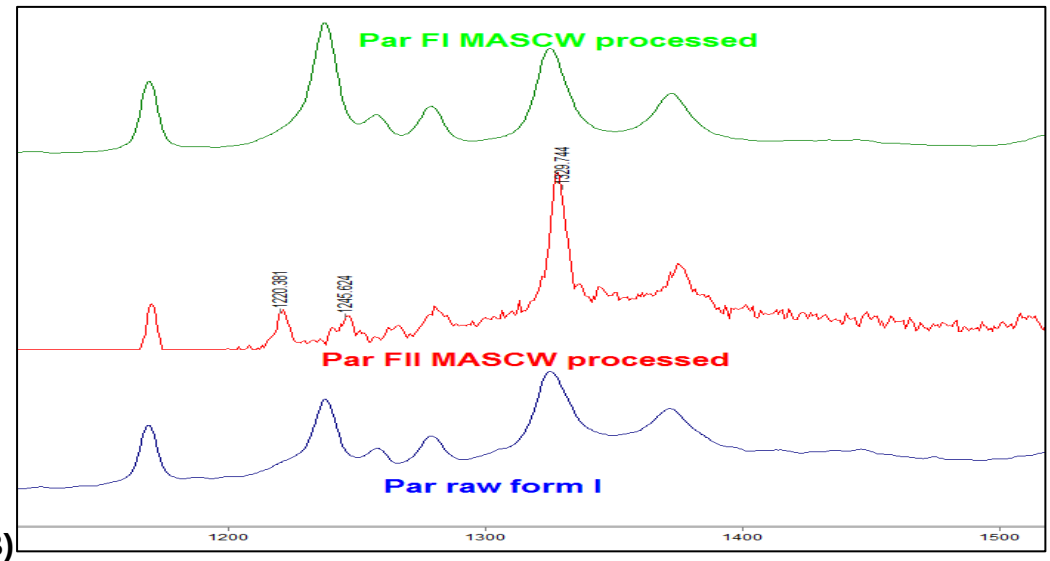

Figure 7.2 A) Full range spectra of pca raw form I, MASCW processed form I and MASCW processed form II and B) Zoomed spectral region marking the charecteristic distinct peak marking of form II polymorph of pca .

Form I polymorph exhibits its characteristic spectral peaks at 1234 and 1325 cm^{-1}, form II display a weak peaks at 1220 and 1245 cm-1and a strong peak at 1329cm-1 and based on the literature study form III polymorph of pca show well resolved peaks at 1500-1700cm^{-1} range. From the above spectral data it is confirmed that form III polymorph is absent as there are no characteristic peaks representing form III polymorph. PCA form I obtained from MASCW process rightly coincides with the characteristics peak of form I polymorph. In the form II polymorph characteristic peaks at 1220 and 1245 cm-1 is observed. Comparatively strong peak at 1329 cm-1 which correctly correlates with literature values for form II pca (Kauffman et al., 2008) is identified. Thus based on the Raman spectra it is concluded that successful generation of form II polymorph of pca which is phase pure has occurred using this technology. Table 7.2 represents the measured peak positions of form I, II and III of pca polymorphs.

Table 7.2 Measured peak positions of all polymorphs of pca

Form I (cm^{-1})	Form II (cm^{-1})	Form III (cm^{-1})
654	650	650
837	-	-
854	862	862
-	**1220**	-
1234	-	-
-	**1245**	1245
1565	1576	1561
1615	1611	1611
-	**1623**	-
1650	1650	1646

7.1.2.4 Differential Scanning Calorimetry

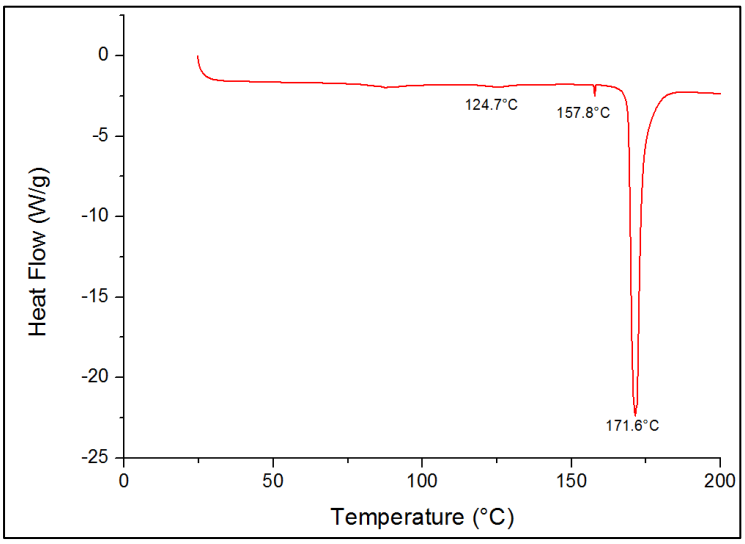

Figure 7.3 Practical DSC thermogram of pca FII processed.

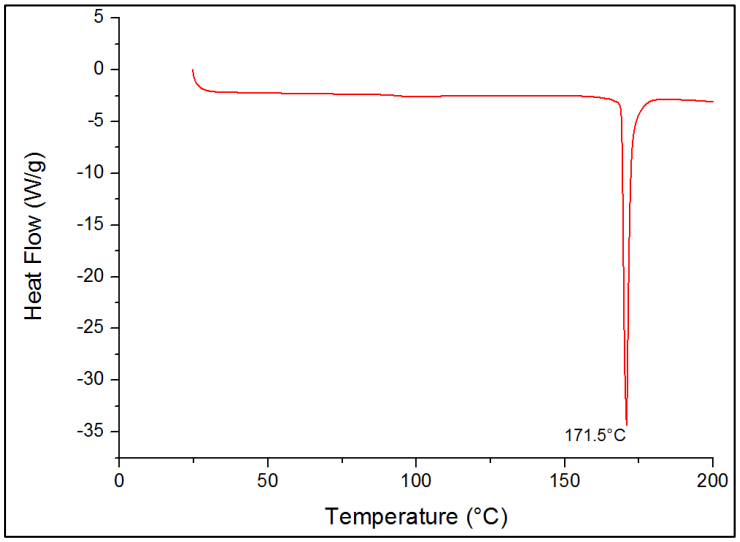

Figure 7.4 Practical DSC thermogram of pca FI processed.

Thermogram of form I pca show single endothermic peak at 171°C (onset 168°C) refer Figure 7.4 which is similar to the DSC data generated by Gary and co-workers (Frampton 1998). FII pca gave thermogram with three endothermic peaks at 128°C (weak broad peak), 157°C (weak sharp peak) and 171.6°C (strong and sharp peak) refer Figure 7.3. All these three events are similar to the events observed in previous publications. The thermally induced events for FII thermogram is interpreted as a solid state conversion

of FII to FI as the temperature is increased. As the crystals are obtained from melt solution crystallisation it may have many structural defects and may thermally promote the conversion of FII to FI. As reported before that FII generated from melt crystallisation generally produces sharp peak at 157°C.

Based on the Raman spectra, XRD pattern and DSC thermogram it is found that phase pure form I and form II polymorph of pca was generated and further thermal study provides the absence of water molecule in pca processed samples.

7.1.2.5 Degradation study of MASCW processed pca samples

As the pca raw material is subjected to high temperature and pressure conditions and decolouration of samples is observed when treated at high temperature. To quantitatively analyse the percent purity of pca samples degradation studies using HPLC analyser is done. Initially calibration curve for potential degradant of pca i.e. 4-aminophenol is determined at different concentrations. The slope equation obtained by plotting a calibration graph between concentration and area under curve is used to analyse the unknown concentration of 4-aminophenol present in MASCW processed pca samples. Below Figure 7.5 represents the chromatogram of elution peaks of pca and 4-aminophenol separately; this confirms the sensitivity of the method developed. Figure 7.6 represents the calibration curve obtained for 4- amino phenol raw.

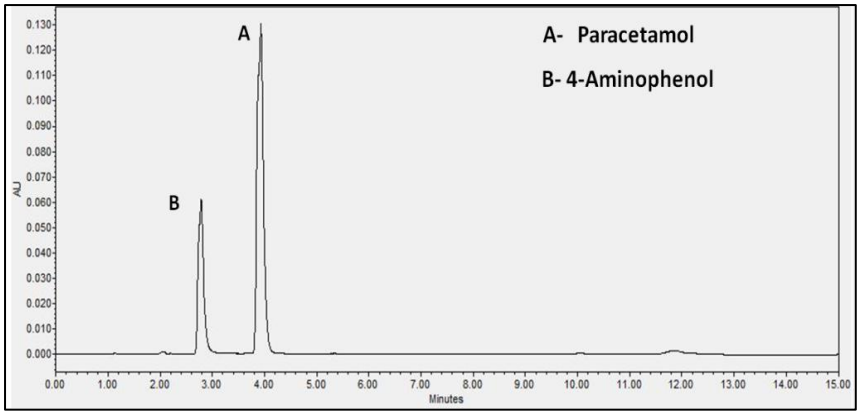

Figure 7.5 HPLC chromatogram of: distinctive peaks of pca and 4-aminophenol raw

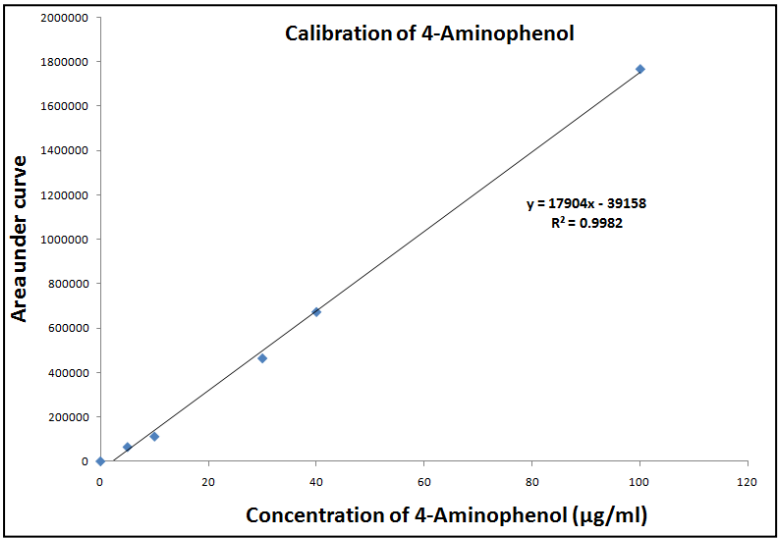

Figure 7.6 Calibration curve plot of: 4-aminophenol.

Based on the calibration curve obtained and slope equation percent essay is calculated to various MASCW processed samples of pca. Analysis of degradation profile of all pca samples which are MASCW treated and conventionally heated is performed. Below Table 7.3 summarises the degradation profile of pca using MASCW process and conventional heating process.

Table 7.3 Percent assay of pca treated at high temperatures

Name of sample	Percent assay (%)
Para MASCW treated	99.50±0.29
Para conventional heating	96.23±0.46

Based on the HPLC analysis very negligible amount of degradation is observed in MASCW process pca samples as compared to conventional heating process. As per literature review it is concluded that upon storage in solution state, potential degradant product of pca which is 4-amino phenol undergo further oxidation to give rise to quinoeimine derivatives which are under detection limit using HPLC technique. According to literature the pink colorations to pca sample in solid state or darkening of solution is due to quinoeimine (Francois Dietlin 1998), (Jouyban et al.,2004).

7.1.2.6 Scanning Electron Microscopy

Due to the exposure of pca samples to high pressure and temperature conditions using water as solvent system SEM analysis was performed to study the change in morphology and crystal habits of the processed samples. Figure 7.7 represents the SEM images of pca raw and MASCW treated at different magnifications.

Based on the SEM images it is observed that the morphological changes were observed when raw pca is treated by MASCW process to give rise to plate like orthorhombic structures on continuous stirring using magnetic stirrer, this structure represents the form II polymorphic structure of pca and when the supersaturated solution is left for cooling without stirring large prism shaped agglomerated of pca were obtained which coincides with the monoclinic crystal structure of form I pca. The particle size of form II pca is

reduced as compared to form I pca which is attributed to implementation of shear while crystallisation is taking place.

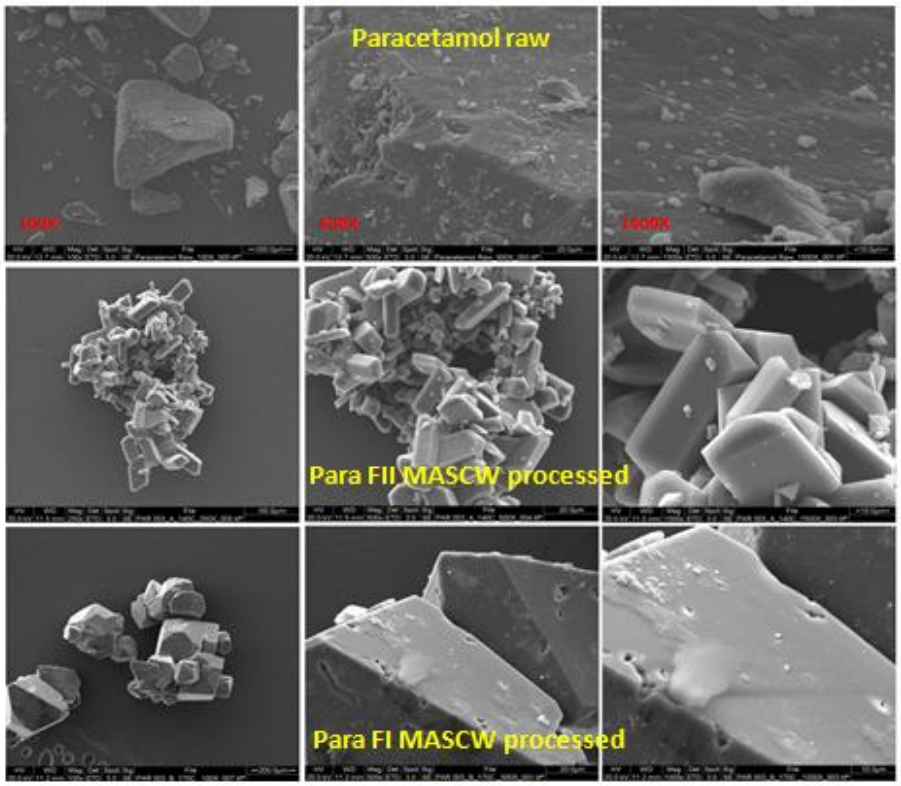

Figure 7.7 SEM images of pca raw, pca FII MASCW processed pca FI MASCW processed.

7.1.2.7 Surface Energy Analysis

Based on the SEM data as the morphological properties like crystal habit, surface roughness, size of processed pca are changed, further investigation of change in the bulk surface properties is performed using MASCW processed form I, form II and raw paracetamol samples (reference). All the samples selected retain similar particle size distribution. Initially BET surface area is determined and based on the BET results further surface heterogeneity of all the samples were calculated using Dorris and Gray peak max equation.

Table 7.4 BET surface area of raw and processed pca

Sample name	Sample mass (mg)	BET Surface area (mJ/m^{-2})
pca raw FI	148	0.7838 ± 0.05
pca FI	373	0.9911 ± 0.65
pca FII	138	1.7725 ± 0.04

The surface area of pca form II polymorph is higher than pca form I processed and raw samples. Even though the particle size of all the samples are similar the surface area of MASCW processed form I polymorph is greater than raw form I polymorph of pca this is due to crystal habit and increase number of active sites of the processes form I pca and polymorph form II is metastable phase it retains higher specific surface area. Below Table 7.5, 7.6 and 7.7 represents the tabular format of dispersive surface energy, acid-base surface energy and total surface energy of paracetamol raw, paracetamol form I and form II respectively.

Table 7.5 Summary of Dispersive surface energy (γ_s^D), acid base surface energy (γ_s^{AB}) and total surface energy (γ_S^T) of paracetamol raw unprocessed.

User specified coverage (n/nm)	γ_s^D (mJ/m^2) (Dorris-Gray)	γ_s^{AB} (mJ/m^2)	γ_S^T (mJ/m^2)
0.008	43.63 ± 0.68	4.73 ± 0.23	48.36 ± 0.91
0.01	43.13 ± 0.04	4.52 ± 0.16	47.66 ± 0.20
0.02	41.11 ± 0.16	3.92 ± 0.06	45.03 ± 0.21
0.04	38.23 ± 0.34	2.71 ± 0.08	40.94 ± 0.42
0.06	37.09 ± 0.13	1.40 ± 0.05	38.50 ± 0.18
0.08	35.21 ± 0.89	1.70 ± 0.04	36.91 ± 0.92
0.1	35.75 ± 0.13	1.67 ± 0.10	37.42 ± 0.23

Table 7.6 Summary of Dispersive surface energy (γ_s^D), acid base surface energy (γ_s^{AB}) and total surface energy (γ_S^T) of paracetamol form I MASCW processed.

User specified coverage (n/nm)	γ_s^D (mJ/m^2) (Dorris-Gray)	γ_s^{AB} (mJ/m^2)	γ_S^T (mJ/m^2)
0.008	50.61 ± 1.45	8.40 ± 0.11	59.00 ± 1.56
0.01	51.77 ± 0.31	8.31 ± 0.07	60.08 ± 0.24
0.02	51.18 ± 0.09	8.01 ± 0.03	59.19 ± 0.13
0.04	49.45 ± 0.28	7.28 ± 0.23	56.73 ± 0.52
0.06	49.50 ± 0.40	7.17 ± 0.24	56.67 ± 0.64
0.08	50.09 ± 0.80	7.25 ± 0.18	57.34 ± 0.98
0.1	51.02 ± 0.28	7.17 ± 0.23	57.94 ± 0.15

Table 7.7 Summary of Dispersive surface energy (γ_s^D), acid base surface energy (γ_s^{AB}) and total surface energy (γ_S^T) of paracetamol form II MASCW processed.

User specified coverage (n/nm)	γ_s^D (mJ/m^2) (Dorris-Gray)	γ_s^{AB} (mJ/m^2)	γ_S^T (mJ/m^2)
0.008	64.35 ± 0.16	9.02 ± 0.04	73.37 ± 0.11
0.01	65.23 ± 0.16	9.15 ± 0.21	74.38 ± 0.37
0.02	67.20 ± 0.27	9.64 ± 0.13	76.84 ± 0.40
0.04	64.74 ± 0.02	8.77 ± 0.02	73.50 ± 0.00
0.06	61.90 ± 0.53	8.05 ± 0.00	69.95 ± 0.53
0.08	60.14 ± 0.64	7.56 ± 0.06	67.70 ± 0.59
0.1	59.31 ± 0.45	7.07 ± 0.11	66.38 ± 0.56

Below Figure 7.8a, 7.8b and 7.8c represents the graphical comparison of dispersive surface energy, acid base surface energy and total surface energy of paracetamol raw, paracetamol processed form I and form II respectively.

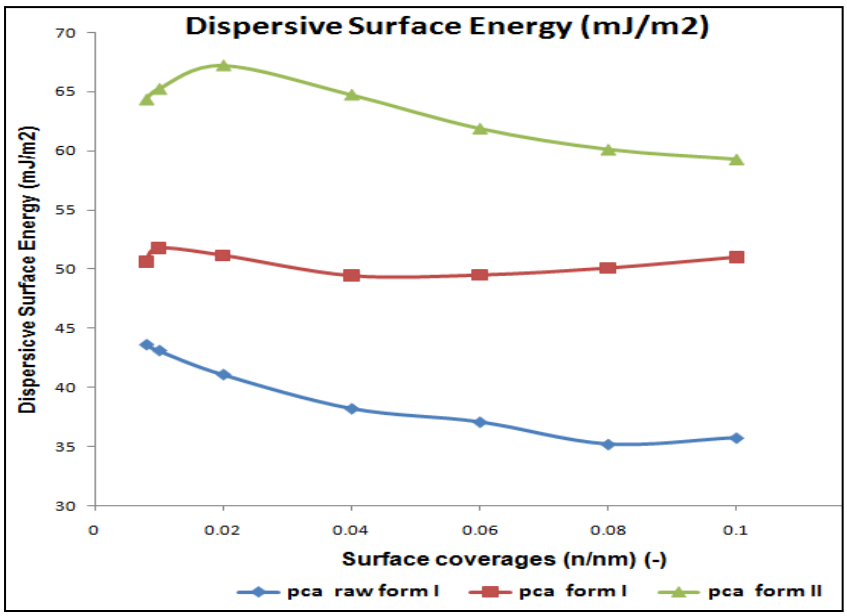

Figure 7.8a Comparative profile of dispersive surface energies of pca raw form I, MASCW processed form I and form II

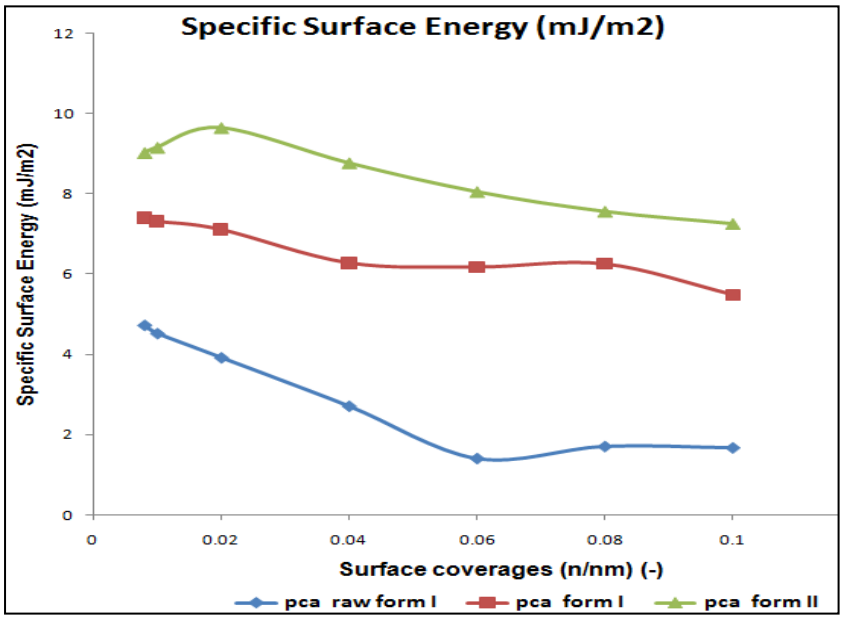

Figure 7.8b Comparative profile of dispersive surface energies of pca raw form I, MASCW processed form I and form II

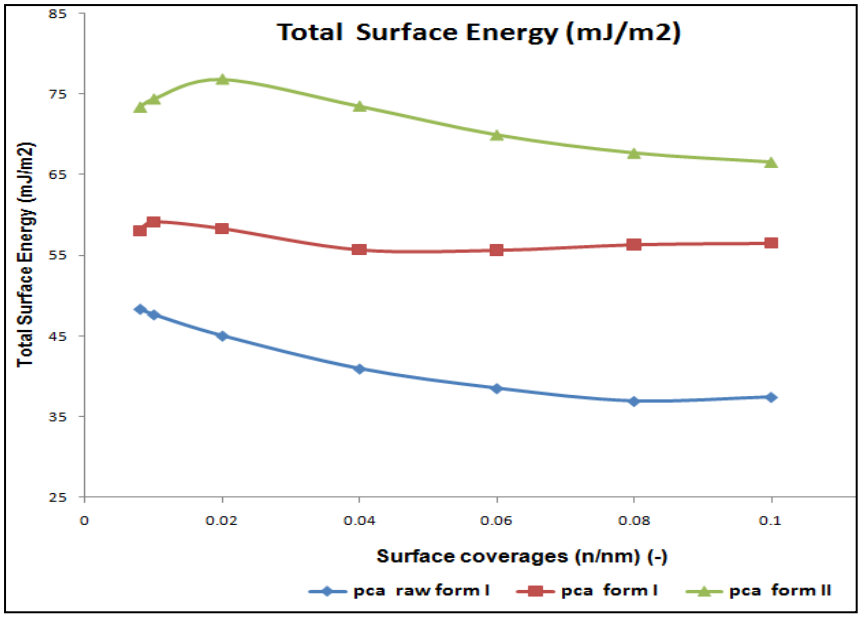

Figure 7.8c Comparative profile of total surface energies of pca raw form I, MASCW processed form I and form II

The dispersive, specific and total surface energy readings of pca form II polymorphs is greater than form I processed and raw form I pca which can be attributed to the surface morphologies and crystal habit. Based on the literature review the particles with greater surface area and surface energy display greater kinetic properties thus in the results obtained form II polymoprh displayed higher surface energy than form I polymorph. The increase in the surface energy of paractamol form II polymorph can be attributed to planar deformation of crystals and prescence of charged moities on the surface of the particles. Due to increase in the charges molecules on the surface of form II polymorph further solubility and intrinsic dissolution experiments were performed to analyse the differece in the kinetic properties of pca processed and raw samples.

7.1.2.8 Solubility analysis of MASCW processed pca samples

Based on the morphological and surface energy results of the processed pca samples equilibrium solubility experiments were performed to analyse the aqueous solubility of pca raw and processed at constant temperature and different time points. Below Figure 7.9 represents the solubility profile of pca from I and II processed and raw form I samples (refer Section 4.2.2.4.5).

Table 7.8 Summary of aqueous solubility of pca form I and II MASCW treated versus commercial pca sample form I.

Time points (hrs)	Solubility (mg/ml)		
	pca-raw FI	pca-MASCWT-FI	pca-MASCWT-FII
0	0	0	0
1	13.70 ± 0.25	14.02 ± 0.50	14.10 ± 0.30
2	13.90 ± 0.04	14.23 ± 0.15	14.34 ± 0.15
3	13.91 ± 0.23	14.26 ± 0.26	14.46 ± 0.18
4	14.10 ± 0.15	14.33 ± 0.15	14.56 ± 0.02
6	14.26 ± 0.01	15.19 ± 0.03	15.46 ± 0.01
12	14.37 ± 0.94	15.06 ± 0.09	15.63 ± 0.42
24	14.57 ± 0.69	15.40 ± 0.86	16.26 ± 0.19

Based on the solubility data obtained there is increase in the solubility of MASCW processed pca samples compared to raw material. Paracetamol form II polymorph displayed higher (12%w/v) solubility compare to pca raw material, followed by form I MASCW processed sample showed (6%w/v) increase in solubility compared to raw form I sample. This increase in the solubility correlates with the increase in the surface energies, polymorphic form and morphological properties of MASCW processed samples.

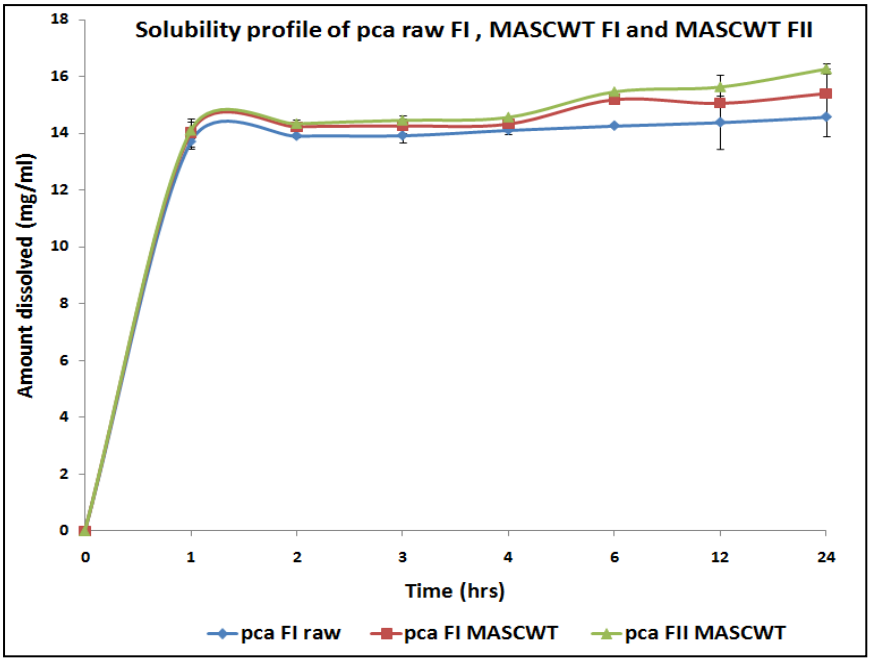

Figure 7.9 Solubility profile of raw and MASCW process pca in water at ambient conditions.

7.1.2.9 Drug dissolution data

The dissolution profile of pca raw and MASCW treated samples of form I and form II pca polymorph is analysed using intrinsic dissolution apparatus (USP II apparatus). All the samples are shifted trough 35 µm sieve and particles size distribution is determined using Sympatec particle size analyser (Table 7.9).

Table 7.9 PSD of pca raw form I, MASCW processed form I and form II

Sample code	X_{10} (µm)	X_{50} (µm)	X_{90} (µm)
pca raw form I	1± 0.03	5.92 ± 0.11	21.34 ± 0.39
pca form I	1.74 ± 0.08	15.42 ± 0.61	28.52 ± 0.20
pca form II	3.42 ± 0.17	9.66 ± 0.32	19.78 ± 0.37

Figure 7.10 describes the drug release profile for pca form I raw and MASCW generated pca form I and II powdered samples. Below table no 7.10 IDR dissolution data for pca samples.

Table 7.10 IDR dissolution data for pca raw, processed F I and F II

	Percent release of pca samples		
Time (mins)	PCA raw form I	PCA form I	PCA form II
0	0.00 ± 0.00	0.00 ± 0.00	0.00 ± 0.00
5	0.43 ± 0.01	0.50 ± 0.11	0.50 ±0.03
10	2.34 ± 0.14	2.28 ± 0.00	4.69 ± 0.12
15	4.18 ± 0.10	3.98 ± 0.01	8.87 ± 0.18
30	10.02 ± 0.00	9.26 ± 0.11	23.02 ± 0.26
45	14.44 ± 0.33	13.19 ± 0.18	34.34 ± 0.61
60	18.97 ± 0.46	17.36 ± 0.46	46.64 ± 0.43
90	27.62 ± 0.98	25.56 ± 0.62	69.16 ± 0.37
180	41.44 ± 0.76	52.18 ± 2.52	69.58 ± 1.05
360	55.11 ± 0.41	61.66 ± 1.40	88.43 ± 0.15

In the below Figure 7.10 it is observed that form I pca and MASCW processed form I polymorph sample display negligible release difference up to 90mins time points but latter MASCW processed form I sample displayed increase in release rate followed by form I raw sample. The interesting profile is shown by MASCW processed form II polymorph with higher release rate from 10mins time point and after 360 mins it showed 60% increase in release rate compared to raw and form I processed samples. This enhancement in

the release rate can be attributed to surface energies, metastable phase of pca form II.

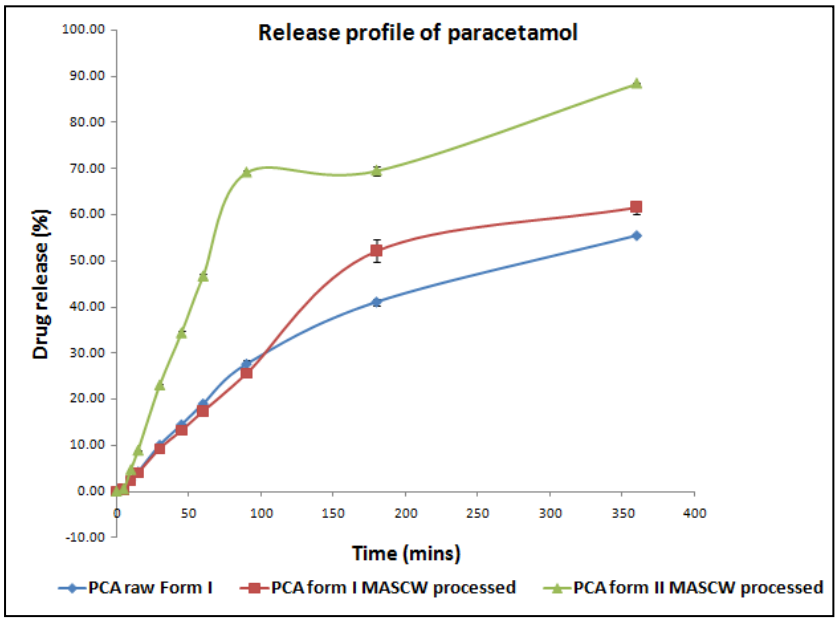

Figure 7.10 Drug release profile of pca raw and MASCW processed.

To further confirm the stability of pca form II in phosphate buffer (dissolution media) stability analysis of pca in phosphate solution is performed to track the polymorphic transformation of metastable pca form II to form I using Raman spectroscopy for 22hours (refer Figure 7.11 (a) and (b).

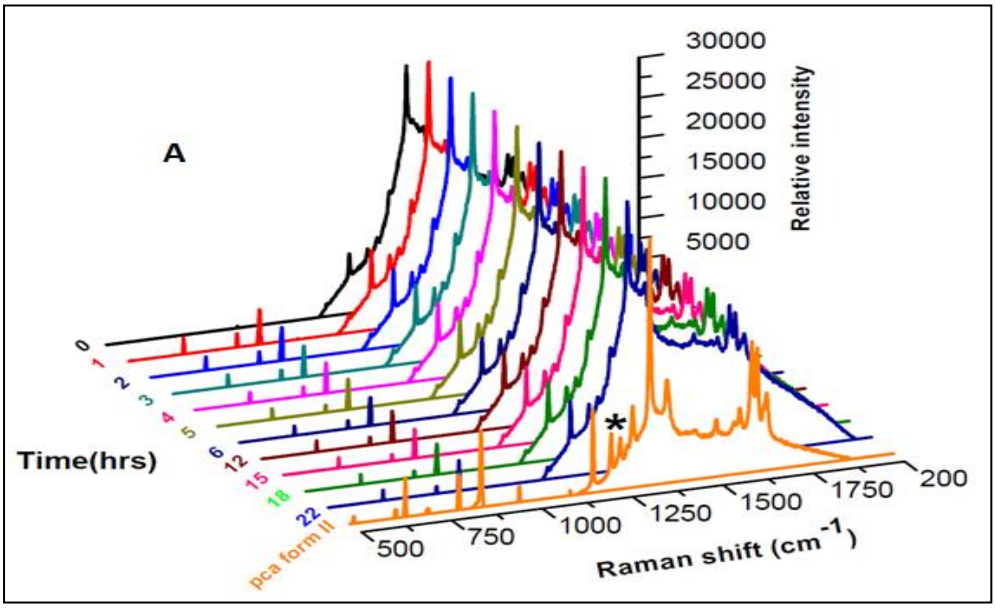

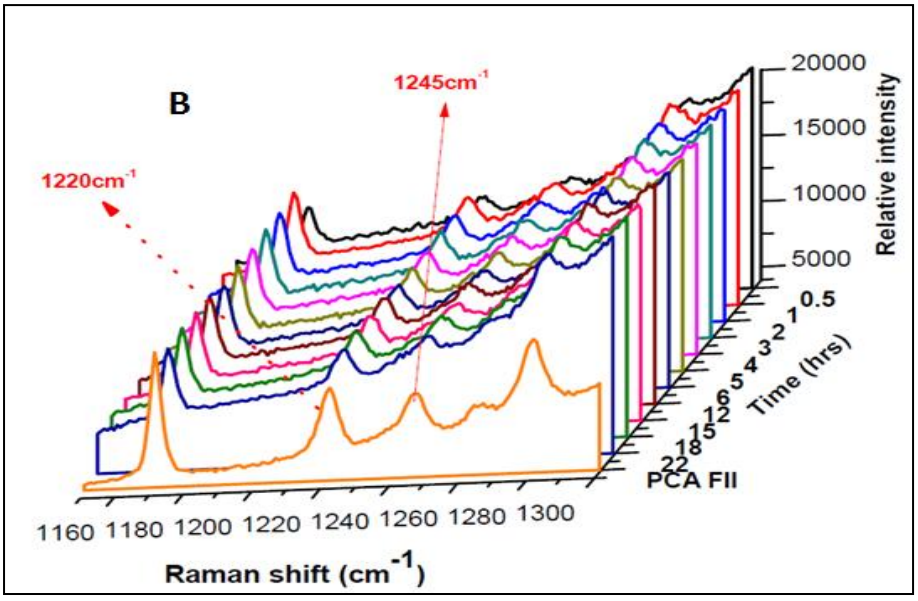

Figure 7.11 Raman spectral data for pca form II suspension a) full range spectra and B) magnified view of Raman shift between (1150-1300cm^{-1}) highlighting presence of pca form II characteristic peak at 1220 and 1245cm^{-1}

As previously discussed in Raman crystallisation kinetics data regarding the characteristic peak of form II pca at 1220 and 1245cm^{-1} and form I peak at 1234 and 1325 cm^{-1} respectively. Based on the above Raman data reflects the presence of form II pure spectral peaks and absence of form I peaks throughout the experiment for 22hours proving the stability of form II polymorph of pca in solution over 22hours.

7.1.3 Conclusion

Therefore the application of MASCW technolgy for the generation of phase pure stable metastable orthorhombic polymorph of paracetamol is reproted. This results was supported by performing dissolution data which displays enhanced intrinsic dissolution profile of orthorhombic polymorph using USP-II dissolution apparatus. Effect of crystallisation technique for the generation of metastable phase is investigated.

7.2 Pharmaceutical analysis and in-vitro aerodynamic characterisation of inhaled theophylline formulations generated by Microwave Assisted Sub-Critical water process

In this present work MASCW process is implemented to explore its application in the field of crystal engineering for the generation of micro sized particles for inhalation drug delivery system. Anhydrous theophylline (THF) is selected as the model component to investigate the aerodynamic performance of MASCW processed samples.

7.2.1 Introduction

Theophylline (THF) is very well established antiasthma drug administered through oral and intravenous routes. Due to its low solubility in water it has restricted its clinical application. The prominent drawbacks of this API are related to its narrow therapeutic index and certain side effects, i.e. nausea, dizziness, headache and vomiting (Banner 1994). Various studies have reported regarding THF that at lower plasma concentration it has significant anti-inflammatory effect in chronic pulmonary disease (Barnes 2005). With the aim to attenuate the side effect and exploit the anti-inflammatory advantages of THF different potential formulations are developed, among these the most successful formulation is inhalation drug delivery system using dry powder inhaler (DPI) (Zhu et al., 2015). Thought this route of administration scientist has reported good aerosolisation and cell results, the only disadvantage of this delivery system is that the dose is limited to few micrograms (Zhu et al., 2015).

For the inhalation drug delivery system particle size, morphological and structural configuration of API play very prominent role in the therapeutic

behaviour of the substance especially in respiratory drug delivery system. Therefore, production of micro- and nano- sized particles with controlled properties is very important steps during formulation of inhalable pharmaceutical actives and excipients. Various studies and techniques are been reported which are implemented for generation inhalable drugs with enhanced aerodynamic properties (Alhalaweh et al., 2013; Korang-Yeboah et al., 2016). All the technologies used retain certain drawback like use of organic solvent in case of antisolvent crystallisation process, solution state degradation of API in solution crystallisation, use of carbon dioxide at supercritical temperatures in case of supercritical fluid technology in the present study keeping in mind the drawbacks related to process and API water is used as green solvent for crystallisation implementing MASCW crystallisation process as quick crystallisation technique with negligible chemical degradation.

In the present work nano- and micro- sized THF particles were generated and its aerodynamic properties was analysed using Next Generation Impactor (NGI) and Foradil as dry powder inhaler. Anhydrous theophylline was processed using MASCW process, once the clear theophylline solution was formed the recrystallisation of the particle was done using different crystallisation techniques like manual stirring, antisolvent technique, effect of external shear using ultrasound and Ultraturrax. Based on the particle size generated from different crystallisation techniques further NGI experiments were performed. Theophylline is process using conventional spray drying technique is kept as reference to understand and compare the effect of aerodynamic properties of theophylline between conventional and newly

developed MASCW process. Several important processed parameters are been identified in our previous studies (see chapter 5) are considered during crystallisation of THF using MASCW process.

7.2.2 Results and discussion

7.2.2.1 Re-crystallisation process and particle size distribution

Pure anhydrous theophylline (1g) solution is prepared using water (10ml) as solvent and further this solution is processed using MASCW process at high temperature and pressure conditions till clear solution is formed. Crystallisation of the supersaturated THF solution is done using four different techniques; manual stirring, antisolvent method, ultrasound and Ultraturrax. For the method of recrystallisation (see Section 4.2.2.5.2)

Below Table no 7.11 represents the PSD results for the powdered THF samples process using different crystallisation techniques. Anhydrous THF (SD1) is processed using conventional spray drying process (method see Section 4.2.2.5.3). All the samples are analysed in triplicates.

Table 7.11 Mean particle size distribution data for raw and processed theophylline samples using different crystallisation techniques.

Batch code	Crystallisation process	PSD-d_{50}(µm),(n=3)
THF-S1	raw theophylline anhydrous	49.68 ± 0.82
THF-S2	Antisolvent crystallisation	4.60 ± 0.65
THF-S3	Ultrasound processed	5.49 ± 0.32
THF-S4	Manual stirring	5.44 ± 0.54
THF-S5	Spray dried crystallisation	4.82 ± 0.24

Based on the above results the PSD data, prominent reduction in the particle size of MASCW processed THF as compared to raw THF is observed, the PSD of processed THF using antisolvent crystallisation process and spray

drying process are below 5 µm which is the recommended particle size for inhalation study. Thus based on the above results antisolvent technique of crystallisation is finalised for further studies in this chapter.

7.2.2.2 Scanning Electron Microscopy

The morphological properties of all processed and raw samples were analysed using SEM microscopy. Below Figure 7.12 represents the microscopic images of gold coated samples under 1000X magnifications.

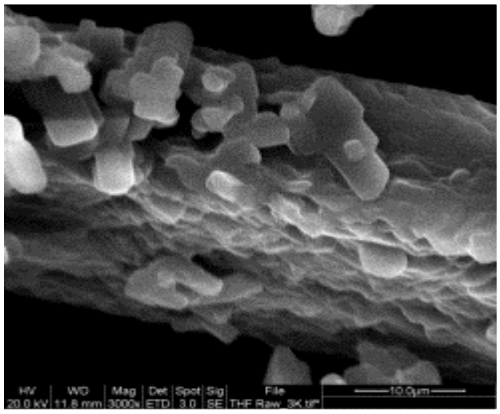

THF raw S1

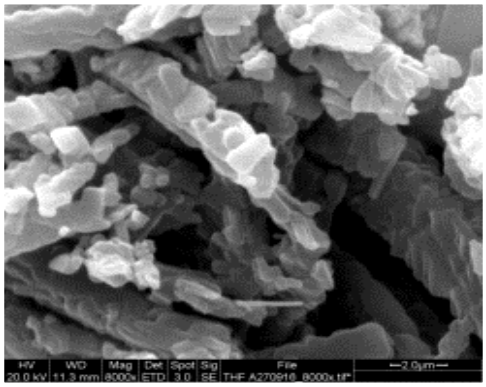

THF-S2

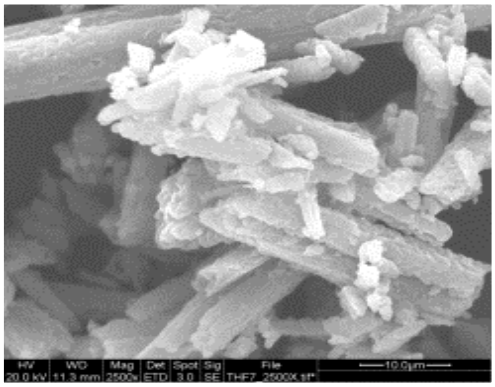

THF S3

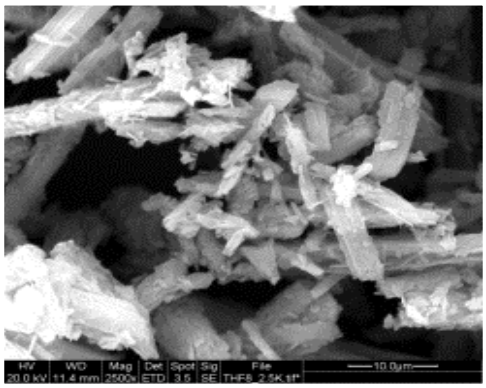

THF S4

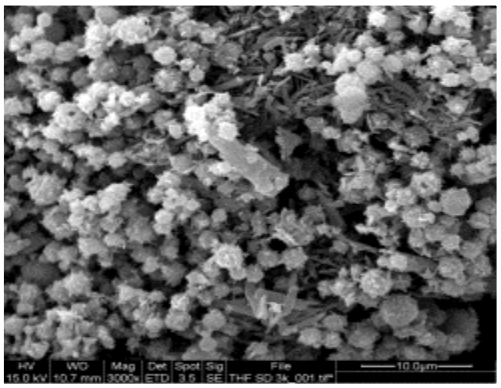

THF S5

Figure 7.12 SEM images of THF S1 raw theophylline, THF S2 antisolvent treated, THF S3 ultrasound treated, THF S4 manually treated and THF S5 spray dried THF.

All the samples processed using MASCW process have smoother surface as compared to raw theophylline samples, crystal habit of the processed powder samples are changed from large cylindrical particles to small rod shaped agglomerates. In the spray dried samples, formation of small spheres are observed.

7.2.2.3 Powder X-ray diffraction data

X-ray diffraction study is performed to analyse the crystal structure and crystal phase of all processed and raw THF powder samples. Below Figure 7.13 represents the PXRD patterns for all the samples.

Based on the literature review theophylline exists in different polymorphic forms like anhydrous and hydrate form, where the anhydrous form is further classified into form I stable, form I metastable and form II polymorphs (Phadnis and Suryanarayanan 1997). The XRD pattern of the unprocessed samples reflects characteristic peaks at 2 theta degrees 7°, 12.5° and 14.5° which matches with literature patterns of anhydrous theophylline.

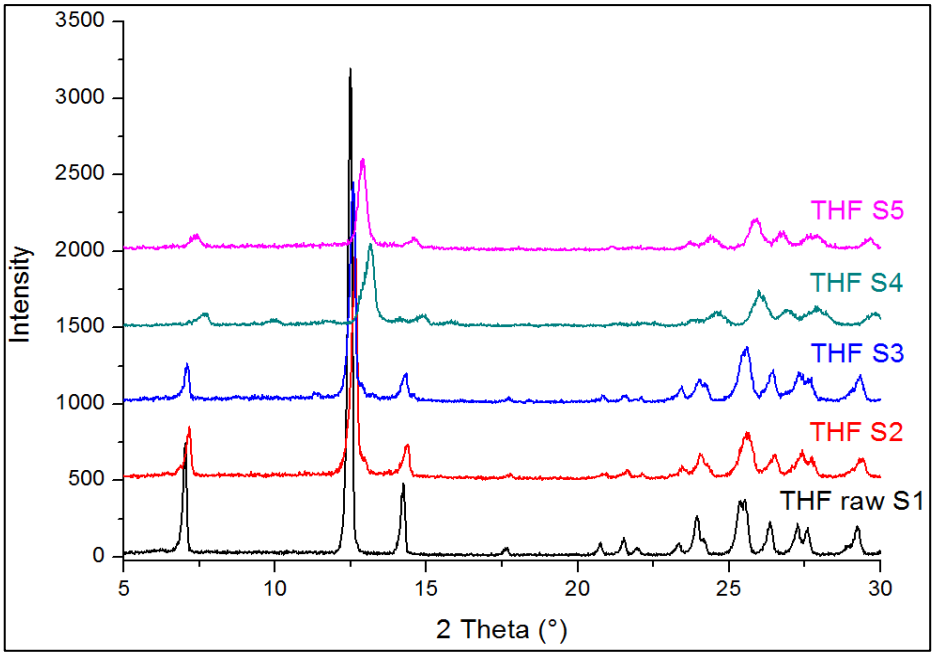

Figure 7.13 PXRD pattern for all processed and raw THF samples.

Processed THF samples also show similar XRD pattern which confirms that the samples are anhydrous THF. The intensity of the processed samples is less which depends on the variation in precipitation process, crystallinity, level of supersaturation and crystal growth.

7.2.2.4 Thermal analysis of THF

Thermal response of theophylline raw and MASCW process samples were studied using DSC and TGA at a heating rate of 10°C/min between 25°C and 300°C. Figure 7.14 represents the melting endotherms for raw THF and processed THF samples. All the powdered samples in the DSC data showed an endotherm melting point at approximately at 271°C, which is corresponding to the melting point of the raw anhydrous theophylline (Legendre and Randzio,2007) (Colacio-Rodriguez and Salas-Peregrin 1984).

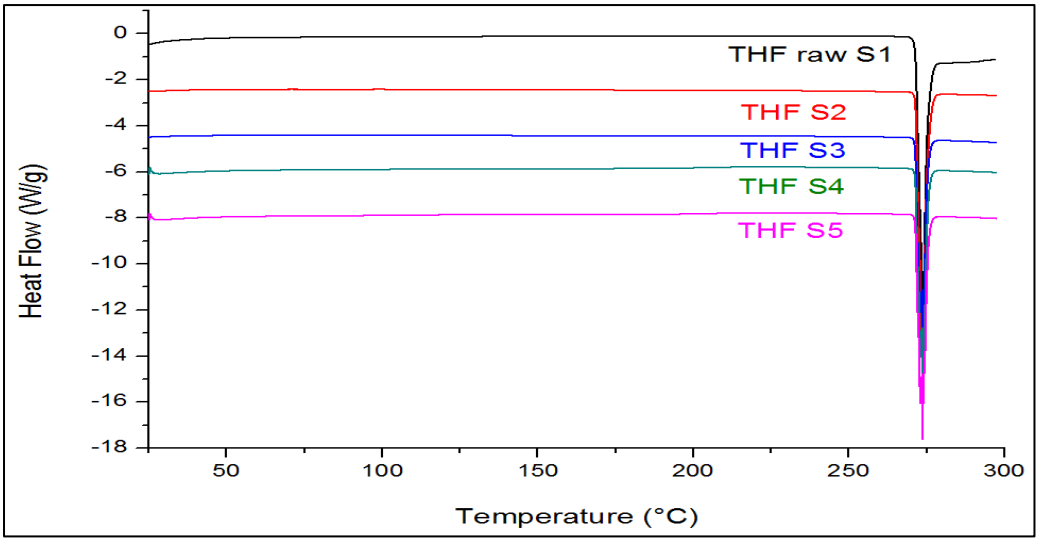

Figure 7.14 DSC thermogram of; THF raw and processed powder samples

Below Table 7.12 represents the melting point and enthalpy of all samples.

Based on the enthalpy values there is decreased in the enthalpy of the processed samples compared to unprocessed samples which reveals that there is decrease in the crystallinity of the processed samples over unprocessed.

Table 7.12 Description of melting point and enthalpy values for all THF samples.

Sample	Melting point (°C)	ΔH_f (J/g)
THF raw S1	273.83	196.9
THF S2	272.50	184.8
THF S3	271.22	156.5
THF S4	273.54	146.3
THF S5	270.78	142.9

All the samples are crystalline as there is no exothermic peak observed below 150°C. Furthermore, there is no endothermic peak observed at the temperatures between 70°C and 110°C, indicating that there is no residual

moisture present in the powdered samples thus all the samples are anhydrous theophylline. To confirm the presence of residual moisture content TGA analysis is performed, Figure 7.15 represents the TGA thermograms for all theophylline samples.

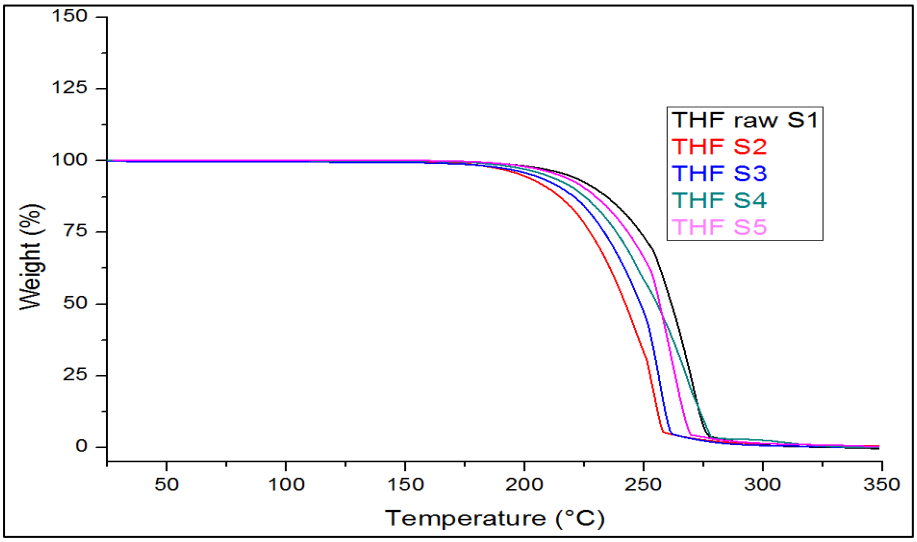

Figure 7.15 TGA thermograms of raw and processed THF samples

Table 7.13 Transition temperatures of THF samples

Sample	Transition temp (°C)
THF raw S1	270.01
THF S2	253.27
THF S3	255.87
THF S4	266.24
THF S5	260.24

The transition temperatures of the processed THF samples are less than the raw THF which is attributed to decrease in the particle size of the processed theophylline samples, due to decrease in the particle size the surface area of the particles is increase and thus they require lower temperature to decompose. The loss in weight in TGA thermogram is minimum (<0.01%w/w; data not shown) which indicates that the samples are anhydrous in nature.

Thus, based on the thermal analysis data using DSC and TGA it is confirmed that the THF samples are anhydrous in nature.

7.2.2.5 FTIR spectroscopy data

Spectroscopic analysis is performed to exploit and monitor the phase transition which is taking place in the MASCW processed samples. Below Figure 7.16 and Table 7.14 represents the IR-spectra for all the batches and correlation between the IR-peaks and structural information respectively.

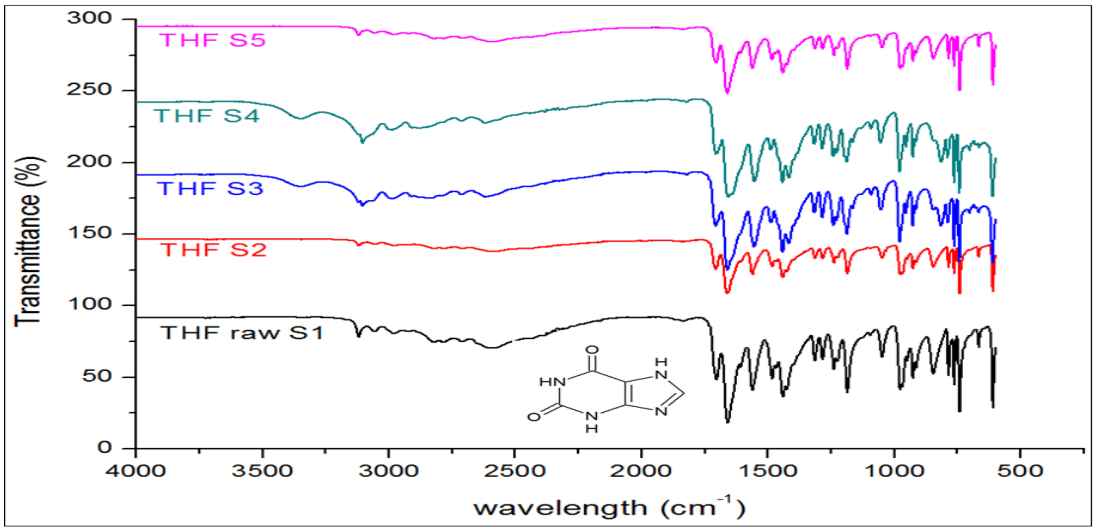

Figure 7.16 FTIR spectra for theophylline raw and processed samples.

Table 7.14 IR-band range index and structural properties of anhydrous theophylline.

Band range (cm^{-1})	**Relation with chemical structure**
3448	N-H bond stretch of amine
2998	C-H stretch
1718, 1668	C=O stretch
1610, 1566	C=C and C=N stretch
1314,1286,1240	C-N stretching
927	N-CH_3 stretching

Based on the IR spectral data the spectra of processed theophylline samples are in complete agreement with raw anhydrous theophylline thus there is no structural transition occurring during processing of theophylline using different crystallisation techniques.

Based on the data generated from PXRD, thermal analysis and FTIR spectra it is concluded that the processed samples are anhydrous theophylline. Based on the particle size antisolvent crystallisation a technique was selected to study the aerodynamic performance of MASCW treated theophylline. Quantitative analysis of the processed samples is performed using HPLC analysis (see Section 4.2.2.5.5).

7.2.2.6 Inverse gas chromatography

Gas chromatography is performed to analyse the surface properties of all the theophylline samples. This study provides us with different surface properties like total surface energy, work of cohesion between same molecules and work of adhesion between two different molecules. All the samples analysed retain similar mean particle size distribution. Figure 7.17 provides the graphical representation of THF raw, MASCW treated THF and spray dried THF.

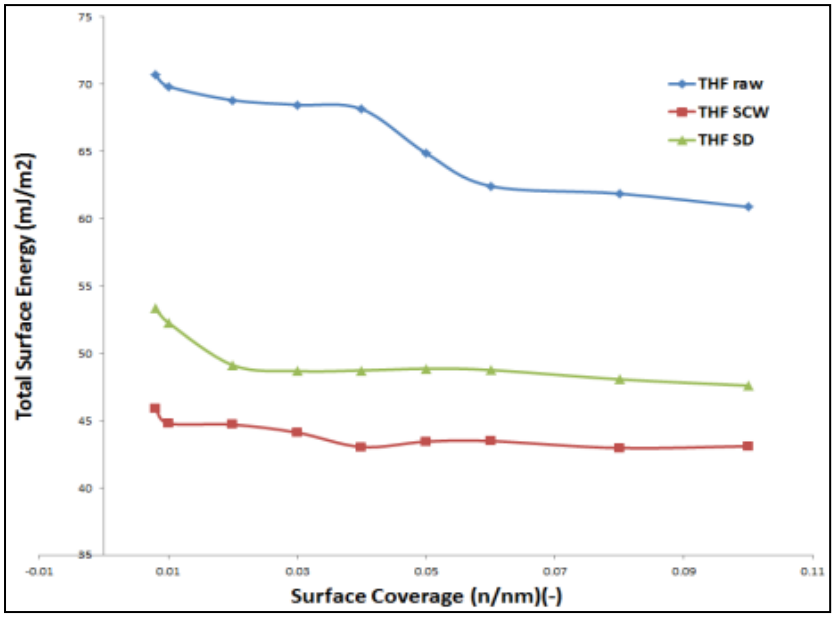

Figure 7.17 Total surface energy of THF raw, THF MASCW and THF SD

Based on the above surface energy data THF raw demonstrated maximum total surface energy followed by spray dried THF and MASCW treated THF. This variation in the surface property is attributed to amorphous nature of processed samples, and crystal surface roughness. MASCW THF sample retains minimum surface energy as compared to spray dried sample this is due to surface smoothness and more crystalline property of theophylline processed using MASCW process. Spray dried THF crystals are spherical shaped with surface roughness thus more charged groups are exposed so the total surface energy is high.

More the charged particles more is the surface energy and more the work of cohesion between the particles, Figure 7.18 represents the thermodynamic work of cohesion of all THF samples at different surface coverage's.

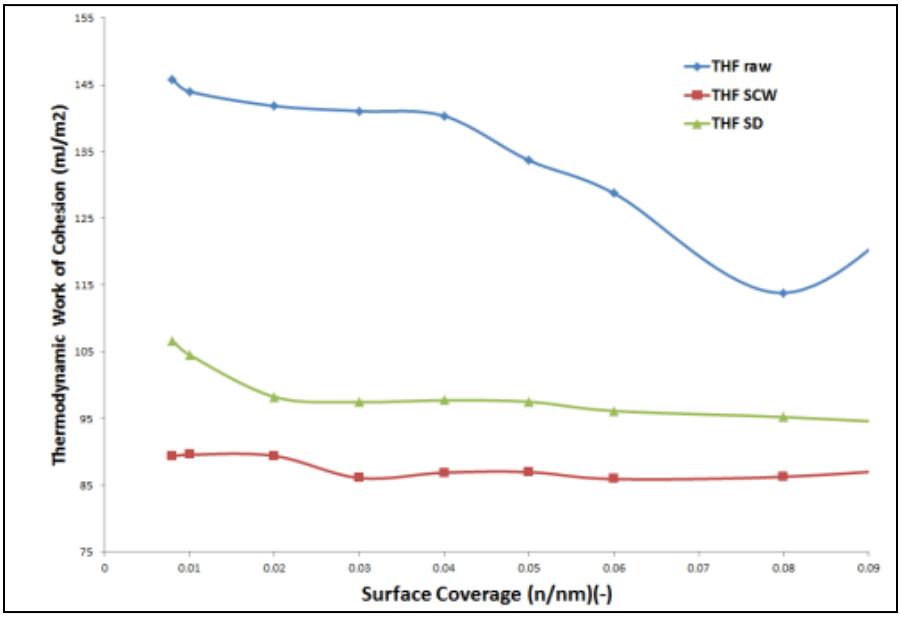

Figure 7.18 Thermodynamic work of cohesion (mJ/m^2) of THF raw, THF MASCW and THF SD processed.

Based on the literature review the particle with high total surface energy undergoes agglomeration as compared with less total surface energy particles. Thus, thermodynamic work of cohesion data rightly correlates with the total surface energy data. The aerodynamic performance of drugs is based on the work of cohesion, solid materials with high work of cohesion display less aerodynamic performance in case of dry powder inhalation as there is chances of forming agglomerates and high air flow is required to break the agglomerates. From the about data MASCW theophylline sample show minimum work of cohesion than spray dried and raw theophylline samples, thus based on this data aerodynamic performance theoretically should be more in case of MASCW processed theophylline than others.

In dry powder inhalation formulations apart from active pharmaceutical ingredient there is also pharmaceutical excipient present which will be acting as a carrier to enhance the lung deposition of drug. To analyse the

interaction between the API and excipient work of adhesion between them is analysed, in the present study determination of the thermodynamic work of adhesion between the theophylline and lactose inhalation grade blend in 1:1 w/w ration is performed. Figure 7.19 represents the work of adhesion between THF and lactose IG sample blends.

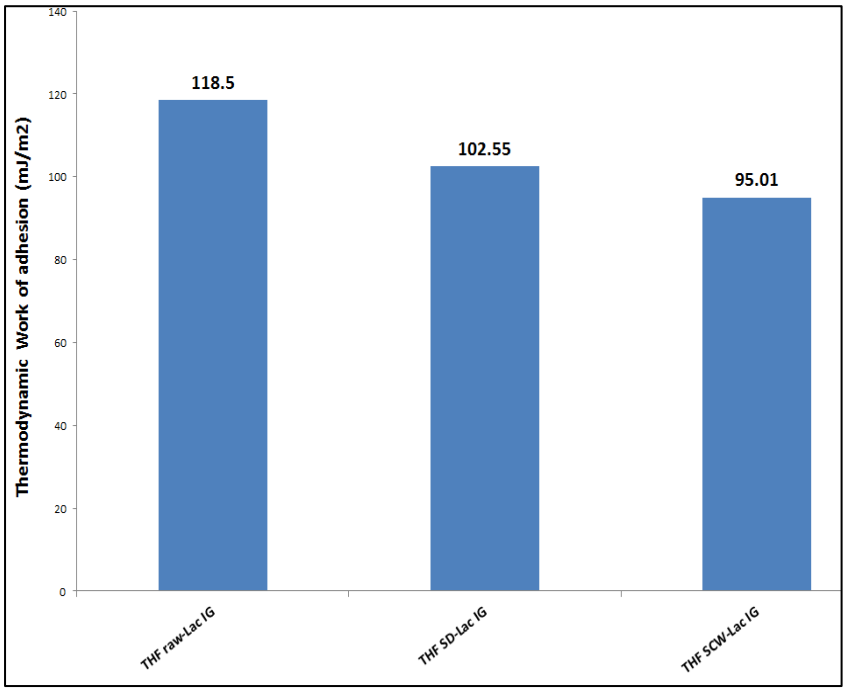

Figure 7.19 Thermodynamic work of adhesion (mJ/m^2) between THF and Lac IG blend.

The above data displayed that MASCW THF SCW-Lac IG blend retains minimum thermodynamic work of adhesion as compared to THF-SD-Lac IG and THF raw-Lac IG powder blend. Thus the blends with maximum work of adhesion there will be agglomeration taking place thus display minimum aerodynamic properties.

7.2.2.7 **In-vitro** *evaluation of the aerodynamic performance of MASCW processed theophylline using NGI*

Prepared DPI formulations were subjected to in vitro cascade impactor using Next generation impactor (NGI) in order to evaluate aerodynamic performance of theophylline powder sample and blend of theophylline and lactose monohydrate. All the blends of anhydrous theophylline and lactose are prepared using turbula mixer for 5 mins and the quantitative analysis of the samples were studies using HPLC to maintain equilibrium distribution of API and excipient in the blend. The dose of pure THF used is 25mg in soft gelatine capsules. Copley Inhaler testing data analysis software (CITDAS version 2.0) is used to calculate aerodynamic parameters of all processed and blends of theophylline formulations. The result provided gave an idea regarding aerodynamic performance of theophylline processed using MASCW technique against spray dried theophylline as reference. Samples retrieved from THF S2 and THF S5 batches were selected for the analysis.

7.2.2.7. A) Determination of total emitted dose of THF S2 and THF S5 batches

Table 7.11 represents the total emitted dose per shot, fine particle distribution; fine particle fraction (%), MMAD and GSD antisolvent MASCW processed and spray dried theophylline samples. Figure 7.20 represents the graphical pattern for the deposition of theophylline samples in different stages of impactor. Table 7.15 represents the summary of emitted dose of THF S2 and THF S4 samples.

Table 7.15 Description of emitted dose of theophylline samples

Emitted dose (20mg)						
	SCW THF S2 (n=3)			SD THF S5 (n=3)		
Stage no (mg)	**Trial 1**	**Trail 2**	**Trial 3**	**Trial 1**	**Trail 2**	**Trial 3**
Throat	5.39	5.42	5.51	3.26	2.67	1.31
Preseperator	0.91	0.56	1.21	3.92	8.91	6.8
Stage 1	3.38	3.92	3.52	0.93	0.81	0.76
Stage 2	2.55	2.58	2.41	1.51	0.81	0.83
Stage 3	1.60	1.69	1.52	0.94	0.47	0.56
Stage 4	1.01	1.15	1.10	0.49	0.26	0.3
Stage 5	0.82	1.01	0.95	0.13	0.11	0.1
Stage 6	0.24	0.65	0.62	0.04	0.03	0.03
Stage 7	0.08	0.09	0.08	0.01	0.01	0.01
Stage 8	0.05	0.06	0.045	0.00	0.00	0.00
No of doses to NGI	1	1	1	1	1	1
TED	16.03	17.13	16.97	11.23	14.08	10.7
TED per shot (mg)	16.03	17.13	16.97	11.23	14.08	10.7
FPD (mg)	5.50	6.37	5.93	2.62	1.42	1.55
FPF (%)	34.29	37.21	34.94	23.33	10.06	14.50
MMAD (µm)	4.37	4.22	4.17	4.02	4.46	4.21
GSD	2.76	3.37	3.37	1.90	2.12	2.03

Based on the data obtained for the pure theophylline samples, NGI shows that for MASCW process THF samples produced using antisolvent technique show about 30% of total dose (20mg) of THF deposition in the throat and preseperator and 50% in the NGI stages and rest in the filter, the amount of drug loss is more in the filter region due to the particle size of THF processed using MASCW process.

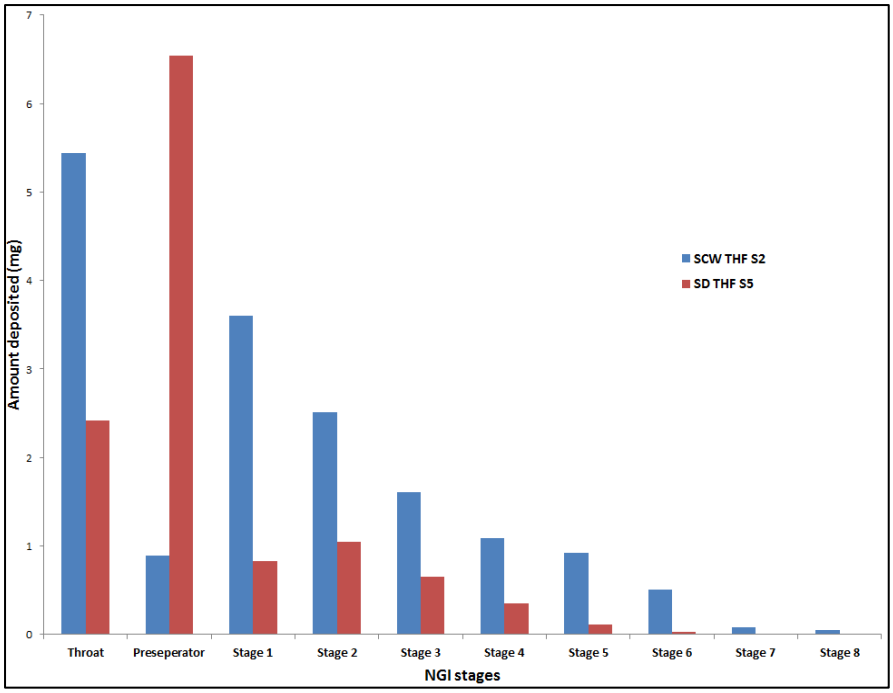

Figure 7.20 Graphical representation of amount deposition of theophylline dose in different stages of NGI

The spray dried pure THF samples displayed maximum deposition (40%) in the throat and preseperator region and minimum (20%) deposition in the NGI stages as compared to THF S2 sample. The maximum drug loss in the preseperator and throat region can be attributed to the fact that pure powdered samples without carrier may stick with each other and need higher inhalation flow rate to be de-aggregated into fine particles. Thus, based on the above data it is proved that the percent deposition of theophylline dose is more for MASCW processed samples compared to conventional spay dried theophylline. In THF S2 batch high average FPD and FPF % 5.93 and 35.48 respectively is observed and in THF S5 we can see low FPD and FPF % 1.86 and 15.96 respectively is observed. These results are in complete agreement with the SEM images and particle size analysis 4.60 for THF S2 and 4.80 for THF S5 respectively. Therefore THF S2 with smaller particle

size and smooth surface (small rod shaped) show better aerodynamic properties than spray dried theophylline THF S5 which are larger in size and spherical in shape. Thus the shape of the particle is also an important factor in DPI formulations as the particles with rod shaped structure can easy thick to the walls of the stage and do not escape with the flow rate where as in THF S5 as the particles are spherical in shape they flow along with air and show minimum decomposition in the lungs. Lactose is commonly used as a carrier as it can accomplish many of the ideal requirements; this is chemically and physically stable and inert to the drug substance. Furthermore, lactose can be easily cleared from the airway without causing any harm to the respiratory tract. Lactose is available in two form alpha and beta lactose, α-lactose monohydrate is thermodynamically stable phase and it is commonly used as carrier in DPI formulations. The physical properties of the lactose like size, shape and surface texture has shown to effect the dispersion and de-aggregation of the self-adhered drug particles. Thus, based on the aerodynamic data retrieved for pure THF samples THF S2 had showed good aerodynamic property than THF S5 sample. In MASCW process theophylline sample displayed 50% of the dose deposition in the lungs as compared to conventionally prepared THF samples.

7.2.2.7. B) Determination of total emitted dose of theophylline and lactose blends

Based on the data obtained for pure theophylline samples it was decided to analyse the effect of standard inhalable lactose monohydrate as carrier over aerodynamic properties of the drug. Standard inhalable lactose monohydrate with mean particle size of 50µm was selected as carrier mass. Blends of

theophylline 50% and lactose inhalation grade (IG) 50% were prepared using turbula mixer and the equilibrium distribution of drug in the blend is pre analysed using HPLC, 20mg of theophylline dose is selected with 20mg of lactose to analyse the aerodynamic performance of THF using NGI. Below Table 7.16 and Figure 7.21 represents the amount of API deposited in different stages of NGI and tabular format of different parameters of THF S2 50% + lactose inhalation grade 50%.

Table 7.16 Total emitted dose of THF and lactose (IG) blend

Particle size distribution of 50% THF S2 and S5 with 50 % Lactose IG (20mg)						
	SCW THF S2			**SD THF S5**		
Stage no (mg)	**Trial 1**	**Trail 2**	**Trial 3**	**Trial 1**	**Trail 2**	**Trial 3**
Throat	7.54	7.77	7.52	10.25	9.27	9.76
Preseperator	2.24	1.24	1.36	1.99	3.54	2.77
Stage 1	2.42	2.56	2.48	1.59	1.89	1.74
Stage 2	2.5	2.42	2.32	0.71	1.01	0.86
Stage 3	0.88	0.90	0.86	0.20	0.16	0.18
Stage 4	0.35	0.40	0.42	0.10	0.07	0.09
Stage 5	0.12	0.18	0.22	0.03	0.02	0.03
Stage 6	0.03	0.06	0.07	0.01	0.01	0.01
Stage 7	0	0	0.01	0	0.01	0.01
Stage 8	0	0	0	0	0	0
No of doses to NGI	1	1	1	1	1	1
TED	16.08	15.53	15.26	14.88	15.98	15.43
TED per shot (mg)	16.08	15.53	15.26	14.88	15.98	15.43
FPD (mg)	3.0	3.12	3.10	0.75	0.82	0.78
FPF (%)	18.68	20.07	20.29	5.05	5.11	5.08
MMAD (µm)	5.16	5.16	5.11	6.80	6.76	6.78
GSD	1.77	1.88	1.96	1.83	1.62	1.72

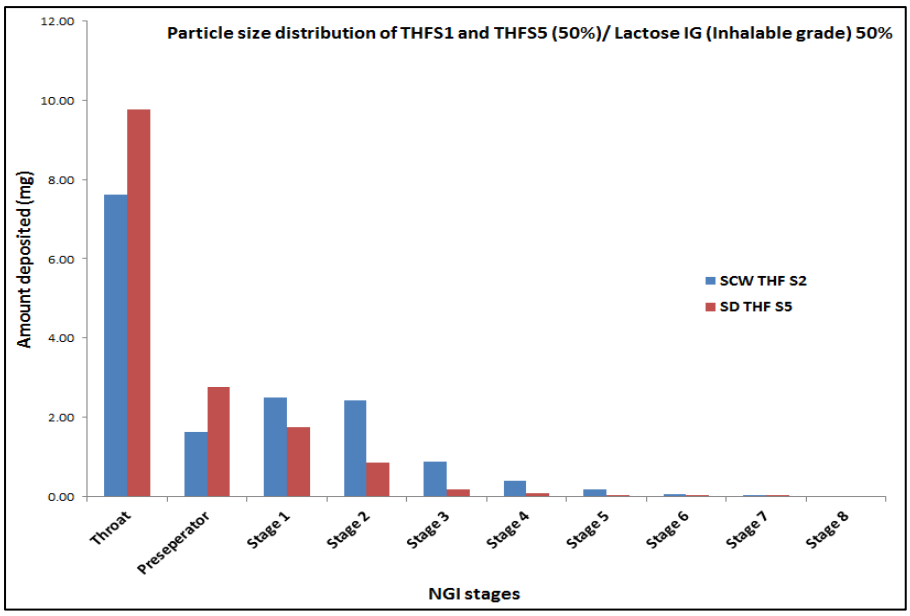

Figure 7.21 Graphical representation of: amount deposition of theophylline-lactose IG blend formulations in different stages of NGI.

The fine particle dispersion of inhaled drug is dependent on the particle size of the powder API, based on the literature particle size of the API influences the extent, distribution and site of the inhaled drug deposition within the airways. In the present study two formulations with similar particle size distribution but differ in the surface texture and crystal habit were selected. The NGI results of THF and lactose blend illustrates the aerodynamic performance and deposition profile of the inhaled particles. Based on the results SCW THF S2 with smoother surfaces and rod shaped structure, provides maximum FPD, FPF and minimum MMAD and GSD as compared to THF S5 with rough surface and spherical structure. This result proved that apart from particle size, particles shape and crystal habit also plays an important role in deposition of drug in the lungs. Based on the results it can be found that maximum deposition of drug on the throat and preseperator region this can be related to the particle surface energy and work of adhesion between the THF powder and lactose powder. The graph

illustrated that THF S2 show maximum deposition in the first 4 stages of NGI which can be correlated to lung deposition, but minimum deposition of drug in the lung region is observed when added with carrier lactose, this is attributed to the agglomeration between lactose and THF due to surface energies and thus preventing the powder to flow through NGI. Thus based on the NGI results it is observed that maximum deposition of drug is observed only when the drug is injected individually as compared with the blend of theophylline and lactose, this is attributed to the greater adhesive energy between the theophylline and lactose there is formation of agglomerated thus less drug deposition is observed in the NGI stages. The results obtained from IGC also show greater adhesive energy between the theophylline and lactose moiety so based on the results it is concluded that as there is required amount of dose deposited in the lungs, in the case observed for THF S2 pure samples there is no carrier needed to enhance the aerodynamic property of MASCW processed theophylline. Below table 7.17 represents the summary of inhalation property of pure theophylline and blend of theophylline and lactose monohydrate

Table 7.17 Summary of NGI results of all THF formulations

Formulation					
	Pure samples		50% blend		
	THF SCW	THF SD	THF S2 + LAC IG	THF S5 + LAC IG	THF S5 + LAC SCW
FPD (mg)	5.93 (0.44)	1.86 (0.66)	3.07 (0.06)	0.78 (0.04)	0.77 (0.04)
FPF (%)	35.48 (1.54)	15.96(6.75)	19.68 (0.88)	5.08 (0.03)	4.41 (0.33)
MMAD (µm)	4.25 (0.10)	4.23(0.22)	5.14 (0.03)	6.78 (0.02)	6.56 (0.38)
GSD	3.16 (0.35)	2.02(0.11)	1.87 (0.10)	1.72 (0.11)	1.70 (0.12)

7.2.3 Conclusion

In the present study description regarding the application of MASCW process for the development of micro sized particles of theophylline with enhanced aerodynamic properties as compared to standard spray dried theophylline powder sample as reference standard. THF MASCW treated THF S2 showed high FPD and FPF fraction from 5.93 mg, 35.48% respectively. THF spray dried showed low FPD and FPF fraction from 1.86 mg, 16% respectively, thus pure theophylline processed using MASCW process showed higher aerodynamic and suitable physico-chemical properties for lung delivery, as confirmed by the morphology, surface properties and *in-vitro* aerodynamic performance studies.

The FPD and FPF of THF SCW treated showed high deposition rate compared to conventional THF SD, therefore reasonable good THF dose can be achieved with the patients having difficulties in generating high level of inhalation flow such as children's and elderly patients.

Chapter 8: A Green route for the synthesis of API-loaded nano-crystalline hydroxyapatite

In this chapter, MASCW technology was implemented as the green technology for the synthesis of nanocrystalline hydroxyapatite and further explored on the prospects of combining nanoHA with a pharmaceutically active component like ibuprofen to enhance the clinical performance of the biologically active complex in the treatment of various bone-related diseases in the human body. The possibility of the attachment of ibuprofen to the surface of nanoHA via the formation of the hydrogen-bonded complex was designed and investigated.

8.1 Introduction

Hydroxyapatite (HA), with its chemical formula $Ca_{10}(PO_4)_6(OH)_2$, is a major inorganic component of bone and along with collagen fibrils, it accounts for up to 65% of the hard tissue of vertebrates. Hydroxyapatite is the inorganic biomaterials which are nano-sized, non-stoichiometric, calcium deficient carbonated ceramic material with low crystallinity which mimics the bone composition (Vallet-Regí and González-Calbet 2004). Nanocrystalline hydroxyapatite implants are used in the market for the treatment of various bone defects resulting from trauma or surgery as it possesses excellent biocompatibility and osteoconductivity properties (Ogilvie et al., 1987). This biocompatible property of HA had gained significant importance in bone tissue engineering, implant osseointegration, and drug delivery.

During the last decades, HA complexes with polymers, ceramics or hydrogels are very extensively studied, in all these studies HA is used as the drug carrier, in turn, have been particularly studied as prospective drug

delivery systems for the treatment of various bone infections. Osteoarthritis and rheumatoid arthritis, despite having different causes behind the diseases, share similar symptoms of chronic pain due to associated peripheral inflammation (Ma et al., 2008). Both are considered an important public health concern, with osteoarthritis being the most common cause of total hip or knee replacement.

One of the most common analgesic anti-inflammatory non-steroidal drugs used for relief of pain symptoms in arthritic patients is ibuprofen (Boureau et al., 2004). Ibuprofen, or 2-(4-isobutylphenyl) propanoic acid (Fig. 8.1a), exists as a cyclic hydrogen-bonded dimer in a solid state (Fig. 8.1b) and its anti-inflammatory and analgesic activity is assigned to the mono-carboxyl groups of an ibuprofen monomer (Smeyers et al., 1985). Based on this, it is beneficial to introduce ibuprofen into the body as a monomer, for instance as a sodium salt, for an improved performance due to a higher drug solubility.

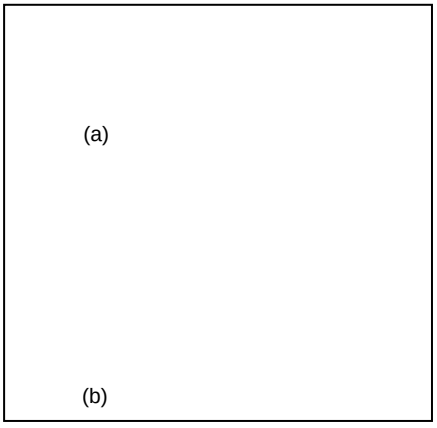

Figure 8.1 Structures of (a) ibuprofen monomer, 2-(4-isobutylphenyl) propanoic acid, and (b) dimer of ibuprofen highlighting the hydrogen bond between carboxyl groups.

Several attempts have been made to combine hydroxyapatite and ibuprofen for treating bone-associated diseases, possibly in a monomeric state to

achieve the desired drug dissolution rates (Qi et al., 2012) (Melville et al., 2008). These studies attempt to relate the prolonged retention times and drug release either with the geometry of the materials (Sambudi et al., 2016) or with the porosity of ceramics in combination with hydrogen bonding effects between hydroxyapatite and ibuprofen monomer. Whereas the majority of studies produced materials using a trial-and-error approach to find the best possible combination of an API and an excipient, they did not focus on the mechanism of the API adsorption and release, but rather on the final formulation with certain characteristics. However, to the best of our knowledge, there are currently no insights into the physical chemistry behind the ibuprofen loading onto the surface of hydroxyapatite and its release. In the present study, for the first time mechanistic studies describing the adsorption of ibuprofen on the surface of hydroxyapatite is reported and propose a possible mechanism for the interaction of ibuprofen and hydroxyapatite at the molecular level. The understanding of the surface properties of ceramics and its influence on the API dissolution rates may provide a useful conceptual platform for the rational development and design of formulations with the desired controlled and sustained drug release.

8.2 Results

8.2.1 Characterisation of synthesised hydroxyapatite

8.2.1 (a) PXRD results

Several characterisation techniques were employed to verify whether the synthesised HA using two different methods mimic the bone composition. Figure 8.2 represents the PXRD pattern comparison between HA

synthesised using conventional mixing method and MASCW process method.

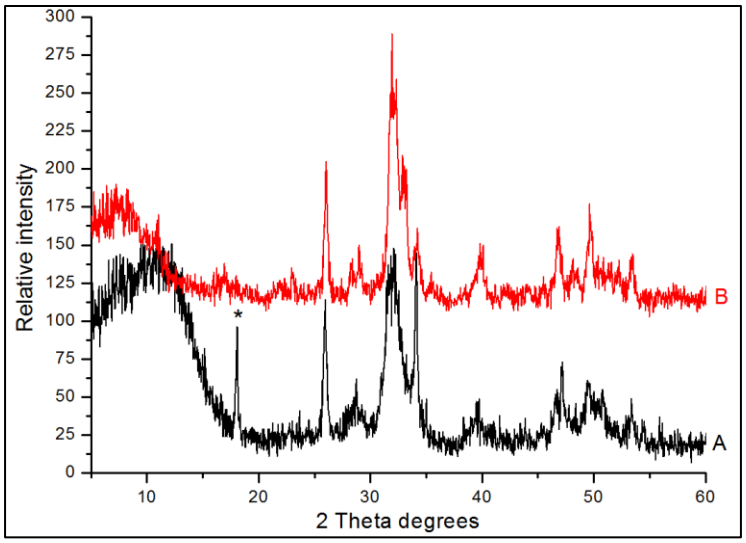

Figure 8.2 PXRD pattern of A) HA synthesised using conventional mixing method and B) HA synthesised using MASCW process

Based on the PXRD pattern in Figure 8.2, HA synthesised using conventional mixing process is not stoichiometrically similar to the bone composition. Impurities of tricalcium phosphate were produced which correlated with the peak at 18 2θ° represented as a star (*) in Figure 8.2 A. This characteristic peak is absent in the HA batch synthesised using MASCW process technology, thus MASCW process was selected over conventional method for sysnthesis of HA complex. Figure 8.3 represents the XRD patterns for HA raw or as prepared (a) and calcined HA at 1000°C overnight (b). Peak broadening of raw material is characteristic of poorly crystalline nano-dimensional hydroxyapatite, the second phase of tri-calcium phosphate is detected after calcination (major reflections not overlapping

with that of HA are marked as * symbol), thus indirectly proving non-stoichiometry of HA.

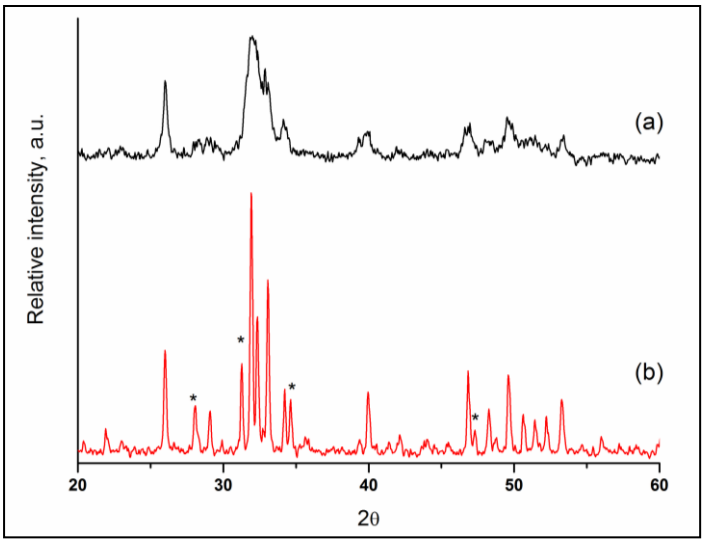

Figure 8.3 PXRD patterns of a) raw, or as-prepared, hydroxyapatite, b) hydroxyapatite calcined at 1000 °C.

Based on the results the XRD pattern of raw HA is in complete correlation with standard HA phase reported in JCPDS entry 9-432 (mineral powder diffraction file data book). There is broadening of the peak at region 20 and 50° 2θ are usually characteristic of either partially amorphous or nano-particulate material. Interestingly, Figure 8.2b reveals the thermal decomposition of non-stoichiometric HA into tricalcium phosphate (TCP) after calcination of the synthesised HA there is a decrease in the peak volume and increase in the crystallinity of the HA material. This extra phase of TCP is confirmed by comparing the XRD pattern with the standard JCPDS entry 9-169 (Liao et al., 1999). Crystallinity calculations, in turn, showed that the raw, or as-prepared HA, is made of *ca.* 35% crystalline component, whereas the crystallinity of the calcined HA expectedly reached *ca.* 96% after a prolonged heat treatment (Table 8.1).

Table 8.1 Unit cell parameters from Rietveld refinement and crystallinity evaluations of nano-hydroxyapatite as-synthesised and calcined at 1000 °C.

Material	Unit cell parameters (Å)			Unit cell, V(Å^3)	Crystallite size (nm)	Crystallinity (%)	HA phase purity (Wt %)
	a	*b*	*c*				
HA raw	9.439	9.439	6.887	531.4 ± 1.1	13	35	100
HA calcined	9.403	9.403	6.876	526.5 ± 1.1	79	96	77(*)

Contraction of the unit cell upon calcination is observed as well as increase in crystallinity. A second phase, namely tri-calcium phosphate or TCP, has also been detected after thermal treatment, showing non-stoichiometry of the as-prepared HA. (*) 23 Wt% attributed to the tri-calcium phosphate (JCPDS entry 9-169). According to the Rietveld refinement results for the lattice parameters, the calculated unit cell of the raw hydroxyapatite is 531.4 ± 1.1 Å^3 whereas for the calcined material it is 526.5 ± 1.1 Å^3, while the proportion of the second phase of tri-calcium phosphate (TCP) is 23 wt. %.

The Scherrer equation (Cullity 2001), allowed us to evaluate the crystallite size which appeared to be 13 nm for raw HA and 79 nm for calcined HA. Decomposition of HA into TCP after thermal treatment and reduction of the unit cell volume is indirect evidence of its non-stoichiometry, whereas its particle (crystallite) size lies within a nanometre range, thus proving that the HA used for this study is indeed a non-stoichiometric nano-sized material with poor crystallinity.

8.2.1 (b) FTIR spectral results

To further analyse the similarity between the synthesised HA and bone attenuated total reflectance (ATR) FTIR technique as XRD alone was implemented. ATR-FTIR being a bulk method it cannot reveal the details of

the HA composition, especially for the layers of solids close to its surface. In this technique, the IR beam is directed on the particular sample and the further reflected signals are recorded using detector (Gulley-Stahl et al., 2010). This technique is often regarded as the surface method with a penetration depth in a range of 0.5 to 3µm. However, considering that our HA is present in the form of agglomerates ranging from 20 to 200 µm and that ibuprofen is also in a similar range, the use of ATR-FTIR as a surface method can be ascribed, but with a large penetration depth. This particular aspect of the technique will be important also for the investigation of the mechanism of adsorption of ibuprofen to the HA surface. Below Figure 8.4 reveals the ATR-FTIR spectrum of raw HA, the main active band, and corresponding regions are described in table 8.2.

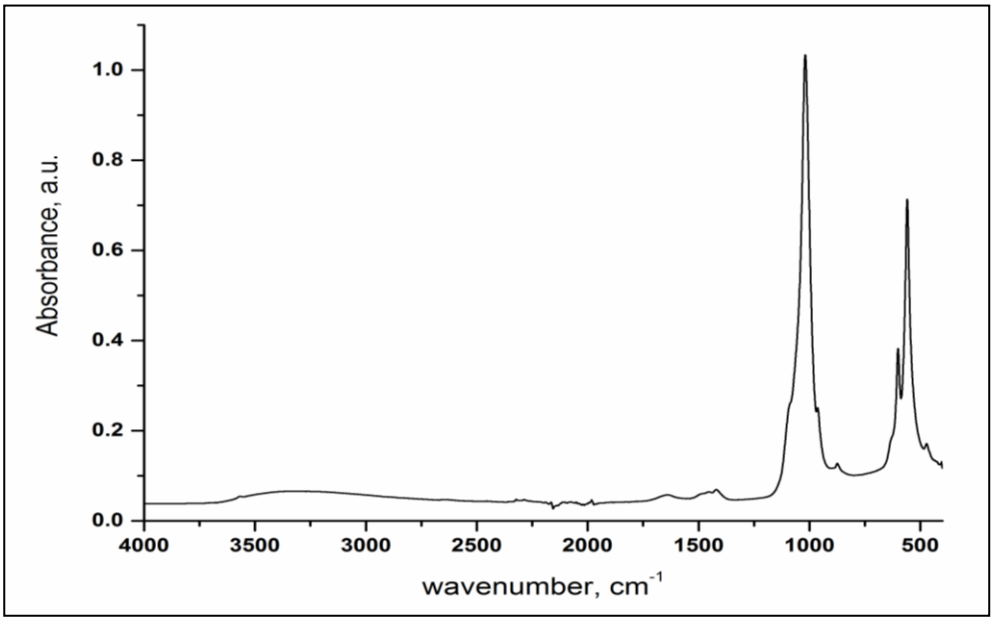

Figure 8.4 ATR-FTIR spectrum of raw hydroxyapatite.

Table 8.2 FTIR active sites and corresponding structural regions of raw HA

Active sites (cm^{-1})	Corresponding regions or functional groups
1200-900 and 600	Phosphate stretching band
3571 and 632	Hydroxyl group vibrations
870 and 1600-1300	Carbonate substituted groups with bending and stretching modes respectively.

Thus based on the FTIR results, surface carbonate formation occurred during the preparation despite the fact that carbonate anions were not deliberately introduced into the system. This is a known phenomenon where CO_2 capture from the atmosphere may occur when one of the solutions has high pH values (Viswanath and Ravishankar 2008) or a strongly basic surface in the presence of moisture. Overall, the presence of small amounts of carbonate groups on the surface of HA is characteristic for the wet precipitation preparation method. However, our results are slightly different from previously reported studies where it has been suggested that A-type carbonate substitution (CO_3^{2-} for OH^-) occurs at lower temperatures, whereas B-type substitution is a feature of the materials prepared at elevated temperature ranges (Kumar et al., 2004). Only a slightly detectable A-type substitution with the B-type dominating was observed, thus suggesting that the material mostly mimics the young bone tissue (Gibson and Bonfield 2002) as the ratio of A/B types is age-dependent and also influences the HA crystallinity and solubility (Ibrahim et al., 2011).

8.2.2 Characterisation of Ibuprofen/ HA complex formation

8.2.2.a PXRD data

In order to prepare ibuprofen-hydroxyapatite complex, SCW was used as the dissolution solvent for the IBU and subsequent stirring for 1hrs to facilitate absorption of ibuprofen molecule on the surface of HA and further vacuum filtration of the powdered complex and drying at ambient conditions. Water as the green solvent is used to minimise environmental impact in chemical reaction as compared with widely used hexane which degrades IBU (Chevalier et al., 2010), stirring of the suspension after MASCW process allows controlled loading of API molecule on HA molecule. Using PXRD it was described that the homogeneity of the attachment of ibuprofen on the surface of HA, Figure 8.5 describes the PXRD patterns of raw HA, commercial IBU, commercial IBU recrystallised from ethanol and IBU/HA complex. Based on the detection capacity of the instrument 20% w/w IBU/HA complex was selected.

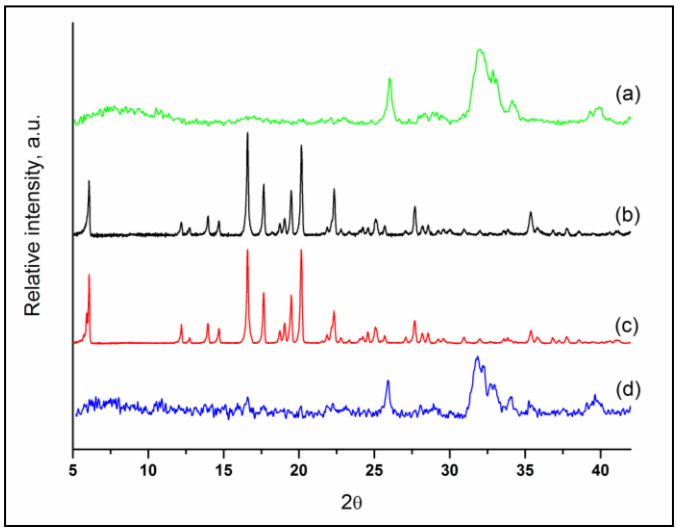

Figure 8.5 XRPD patterns of a) raw hydroxyapatite, b) commercial, or as received, ibuprofen from the supplier, c) commercial ibuprofen

recrystallised in ethanol, d) ibuprofen/hydroxyapatite (ibuprofen/HA) complex.

Based on the above PXRD pattern characteristic peak of ibuprofen in IBU/HA complex was not observed, this is due to the low crystallinity of ibuprofen, the particle size of ibuprofen less than 5µm and formation of a highly dispersed thin layer of ibuprofen on the surface of HA (Jouyban et al.,, 2004).

8.2.2.b Scanning electron microscopy images

SEM images also reveal very interesting results, Figure 8.6 describes the microscopic images of a) raw HA, b) commercial ibuprofen, c) IBU recrystallised from ethanol and d) IBU/HA complex.

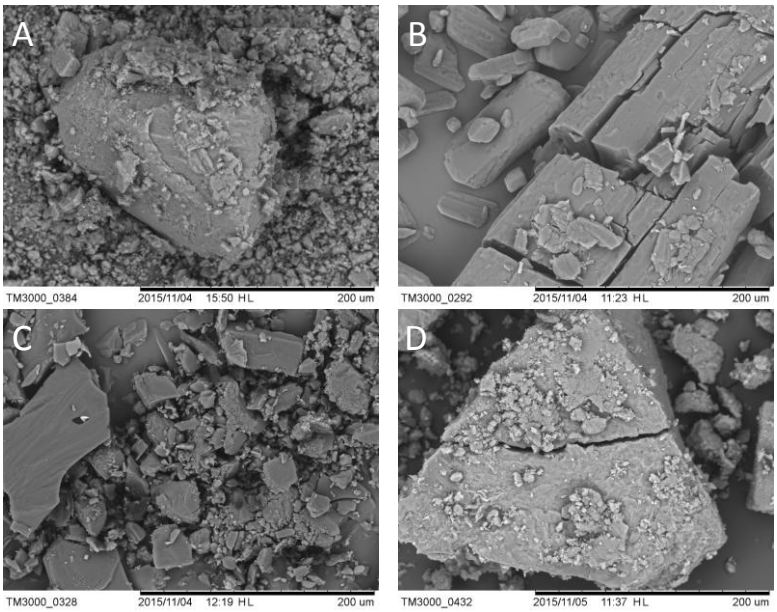

Figure 8.6 SEM micrographs of a) raw hydroxyapatite, b) commercial, or as received, ibuprofen from the supplier, c) commercial ibuprofen recrystallised in water, d) ibuprofen/hydroxyapatite (ibuprofen/HA) complex.

Similar particle shapes and sizes were observed for as-prepared HA (a) and ibuprofen/HA complex (d). It can be seen that raw HA consists of reasonably large agglomerates of ca. 200 µm and some smaller clusters of 10-20 µm. Commercial ibuprofen showed rod-shaped particles of ca. 50-200 µm, whereas water-recrystallised ibuprofen particles are randomly shaped with the average size ranging from 10 to 250 µm. It cannot be excluded that the possibility of the formation of rod-shaped particles with larger dimensions during the recrystallisation of ibuprofen, as the recrystallised sample is crushed in a mortar and pestle prior to analysis, and this may not be a complete representation of the particle shape and size. However, it is important to compare the water treated ibuprofen specimen with the ibuprofen/HA complex that has also been ground to reach a powder form, and we believe the comparison between two SEM micrographs for these materials is valid in this case.

Another interesting feature observed during SEM analysis is specimen destruction under the electron beam see Figure 8.7. Structural damage upon irradiating the sample with the beam of electrons is a well-known phenomenon and may happen not just with organic samples (Talmon 1987) but also with ceramics, though at much higher accelerated voltages and current densities. Trial were done to exploit this feature to try to visualise the presence of ibuprofen in our ibuprofen/HA complex.

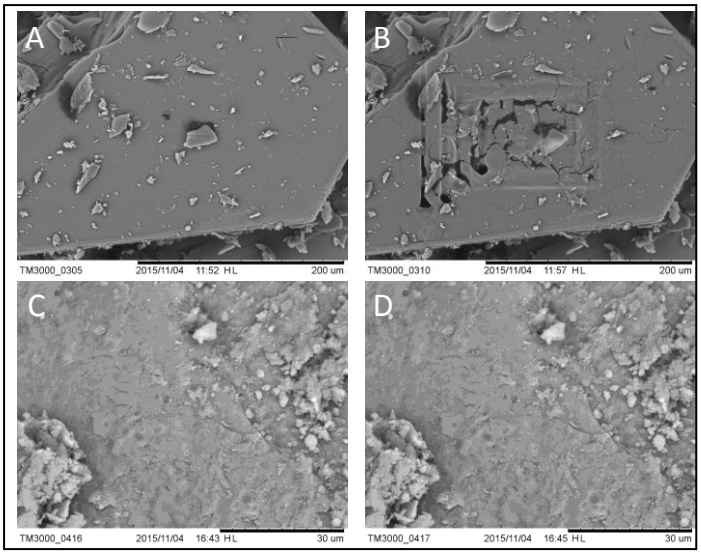

Figure 8.7 SEM micrographs of a) as received ibuprofen, b) same as a but after approx. 4 min exposure to electron beam radiation; c) ibuprofen/HA complex, d) same as c but after approx. 4 min exposure to electron beam radiation.

It is observed that when pure ibuprofen is subjected under electron beam noticeable destruction of the sample is taking place whereas no such changes are visible in the microimages of IBU/HA complex, thus suggesting the homogenous distribution of ibuprofen on the surface of HA.

8.2.2. c ATR-FTIR spectral data

Further, formation of IBU/ HA complex using ATR-FTIR spectroscopy was studied, Figure 8.8 reveals the spectra for IBU/HA complex (a) and water treated IBU (b).

Upon close inspection of the spectra, small shift in the carbonyl region of ibuprofen/HA complex to higher wavenumber (1717 cm^{-1}) compared to pure ibuprofen (1707cm^{-1}) was observed.

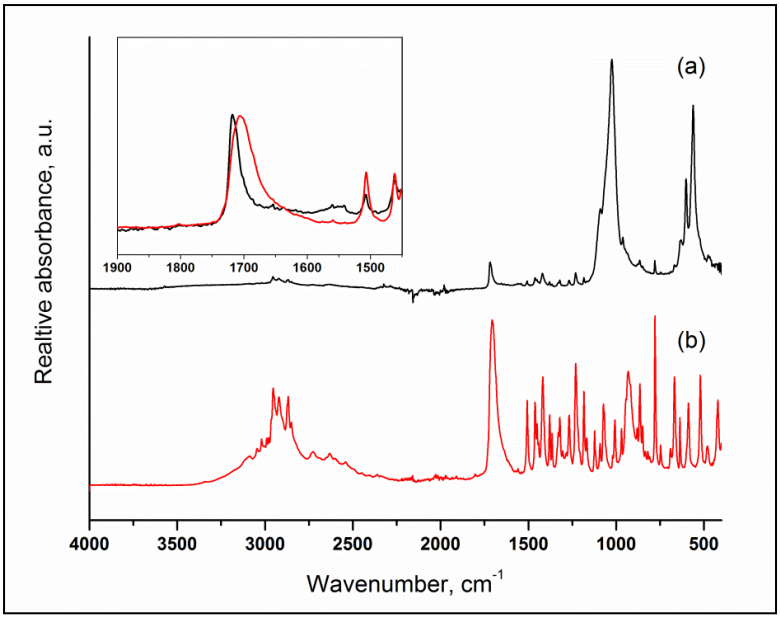

Figure 8.8 ATR-FTIR spectra of a) ibuprofen/HA complex and b) ibuprofen recrystallised in water.

Majority of the active bands are observed in the range of 1800 to 500 cm^{-1} and 3200 to 2400 cm^{-1} with the former assigned to carbonyl group, tertiary and quaternary carbon atoms and OH bending vibrations and the latter to the C-H and C-C bond stretching. Interestingly, overlapping of the two spectra (see inset on Fig. 8.8) clearly shows the shift of the ibuprofen C=O group stretching to the higher wavenumbers from the 1707 to 1717 cm-1. Similar shifts have been reported in the literature and they are usually explained, yet not proved, by the hydrogen bonding between the hydroxyl groups of HA and the carbonyl group of ibuprofen. However, the degree of this deviation is variable from study to study, ranging from 1720 cm-1(Öner et al., 2011) to 1547 cm-1 (Sambudi et al., 2016). This large variability in literature data, as well as the lack of direct evidence on the actual nature of molecular bond interactions between ibuprofen and HA prompted us to investigate this issue in more detail.

8.2.3 Analysis of ibuprofen monomer, dimer and attached species using ATR-FTIR spectroscopy

Firstly, the behavior of ibuprofen in ethanol solution based on the greater solubility of IBU in ethanol is observed. Based on the previous literature it is reported that ibuprofen exists in a hydrogen-bonded cyclic dimeric form which is stable in both solution and solid phases. Our objective is to identify the monomeric form of ibuprofen in ethanol solution as ethanol is used as the solvent system to dissolve ibuprofen. To perform this experiment known quantity of ibuprofen is dissolved in ethanol solution based on its solubility in organic ethanol and the resulting solution is subjected under ATR crystal of ATR-FTIR spectrometer and allowed it to dry at ambient conditions recording the spectra in the initial and final time points. Below Figure 8.9 represents the IR spectra of ibuprofen in ethanolic solution.

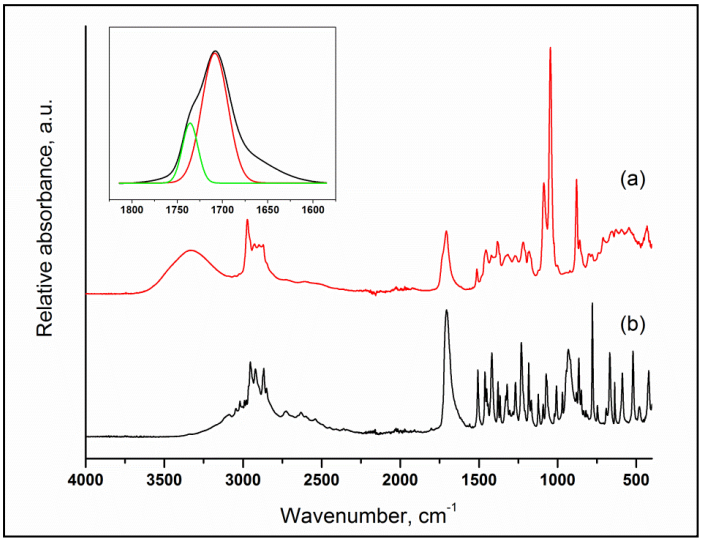

Figure 8.9 ATR-FTIR spectra of a) Ibuprofen in ethanol on the ATR crystal, b) same as a) but dried on the ATR crystal for 4 hours.

Figure 8.9 a) shows the IR spectrum at the zero time point measurement in the presence of ethanol, whereas Fig. 8.9 b) shows the spectrum of ibuprofen after 4 hours when the ethanol had completely evaporated (as

indicated by the absence of ethanol's most active bands at 880, 1046 and 1087 cm-1 and a broad band between 3600 and 3000 cm-1). What is immediately apparent is the presence of a broad shoulder in the region between 1760 and 1720 cm-1 in the spectrum corresponding to the ibuprofen dissolved in ethanol (Fig. 8.9 a). Deconvolution of this part of the spectrum (see inset in Fig. 8.9) allowed us to determine the peak position of a second species which appeared to be at ca. 1735 cm-1 and has been assigned as the C=O stretching vibration of monomer ibuprofen affected by H-bonding with ethanol (further confirmed by the computational studies). Thus it has been proved that ibuprofen may exist in both dimeric and monomeric forms when ethanol is present in the system.

Thus as the presence of monomer in the ethanol solution is proved, the next step of the analysis is to investigate the presence of monomer, dimer and attached species in IBU/HA complex generated using MASCW technology. Below Figure 8.10 shows the presence of monomer, dimer and attached species of IBU in IBU/HA complex.

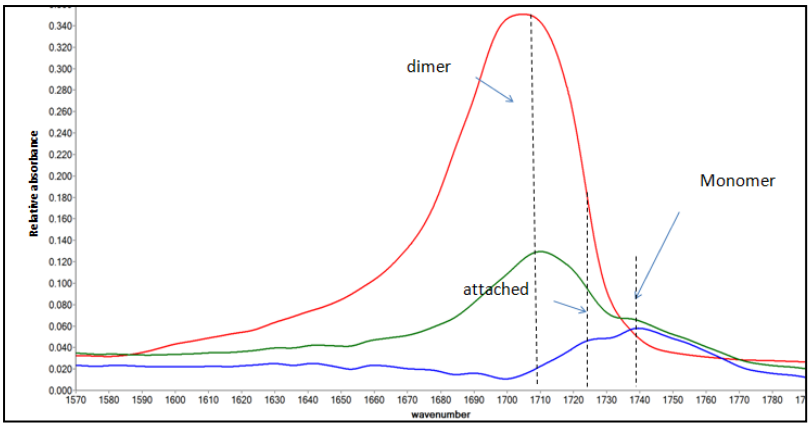

Figure 8.10: Area of the FTIR spectra characteristic of H-bonding attachment: (---) pure Ibuprofen, (---) physical mixture of Ibuprofen and HA and (---) microwave-assisted synthesis of Ibuprofen/HA complex.

Based on the above Figure it is observed that IBU in monomer, dimer and in attached state with HA molecules, at 1740 cm^{-1} wavelength region where formation of monomer species is seen and it can be seen at C=0 bond vibrations at 1735 cm^{-1} corresponding to hydrogen bonding generated due to water molecule, thus proving the formation of bonding between IBU and HA using MASCW process.

Thus the presence of ibuprofen monomer in the ethanol solution and in water suspension has been assessed, the next step of analysis is to evaluate the presence of dimer, monomer and attached species in the synthesised IBU/HA complex using time-on-line IR spectroscopy. Various *in situ* experiments were performed on synthesised IBU/HA complex which is directly transferred from the synthesis flask onto the ATR crystal of spectrometer. Measurements were recorded at different time points (6 to 180minutes) and peak at 1717 cm^{-1} was not observed (as in Figure 8.7 above), this band we believed that corresponds to absorbed monomeric ibuprofen species. To further investigate the results further *ex situ* experiments where the sample complex is directly collected from the synthesis flask every time at different time points and transferred on to the ATR crystal instead (see Figure 8.11).

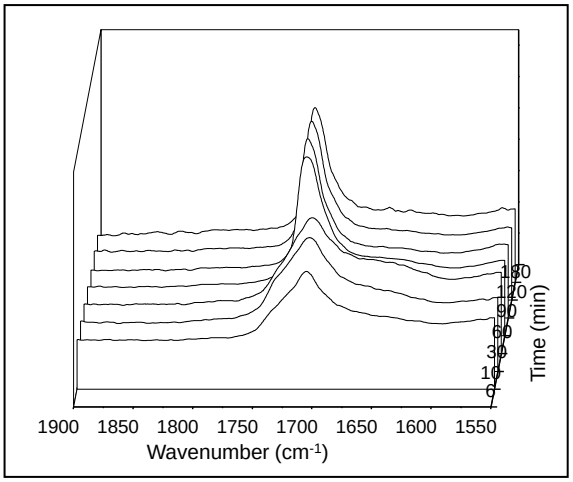

Figure 8.11 Kinetics of the ibuprofen/HA complex formation, *ex-situ* ATR-FTIR measurements of the carbonyl region of ibuprofen between 6 and 180 min, showing the evolution of the peak assigned as attached species, and the signal decay of the dimer and monomer peaks.

This is different from the previous, *in situ*, IR experiment as in the first case the specimen is always the same across the experiment, whereas in this second case the specimens are different at every measurement time point, though still originating from the same ibuprofen/HA sample (flask). Interestingly, in the case of *ex situ* kinetic studies, we were able to observe a peak at 1717 cm^{-1} instead. This suggests that keeping a specimen between the force applicator and the ATR crystal for the whole duration of the in situ experiment (180 min) prevents the formation of the adsorbed species, leading only to the re-crystallisation of the ibuprofen dimer.

8.2.4 Dissolution studies

Finally, dissolution experiments was performed to study the drug release properties of ibuprofen which is absorbed on the surface of HA nanocrystals.

Figure 8.11 shows the drug release profiles of pure ibuprofen (as a control), a physical mixture of ibuprofen and HA, and ibuprofen/HA complex which

was proved to be made up of a hydrogen-bonded API monomer weakly attached to the surface of HA. Fig. 8.11 demonstrates that the release of drug from the physical mixture and pure ibuprofen is similar whereas the drug release profile for HA loaded IBU complex is statistically slower at the initial time points (between 5 and 180 mins) but then equalizes by the 4 hours measurements. This could possibly be explained by the fact that the main cause of the retardation of ibuprofen release is due to weak intermolecular bonding between the API and the carrier, and not the geometry of the HA.

The intense drug release at the early time points of the dissolution is normally associated with the concentration gradients on the surface where diffusion pathways are short, followed by the decrease of the drug release rate due to the increase in the diffusion pathways from the bulk. Such formulations are referred to as diffusion-controlled drug delivery system, and the kinetics is based on the known cylindrical geometry of the tablets and Fick's second law of diffusion (Öner et al., 2011).

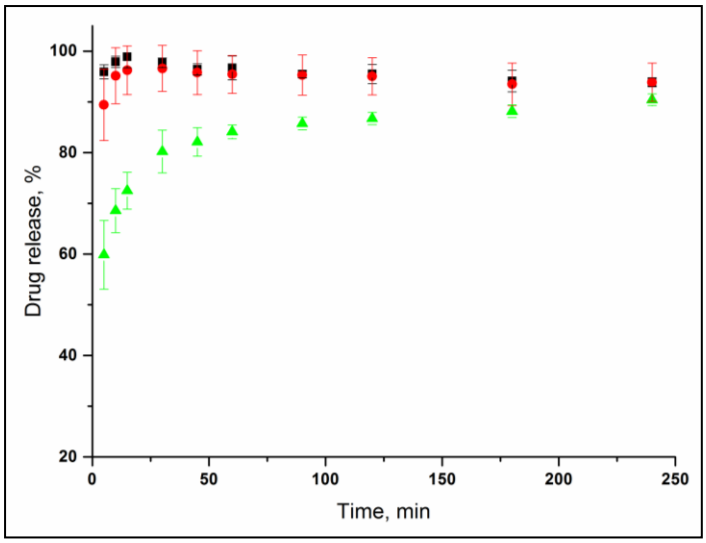

Figure 8.12 Drug release profile of: as received ibuprofen (■), physical mixture of ibuprofen and hydroxyapatite (●) and hydrogen bonded ibuprofen-hydroxyapatite complex (ibuprofen/HA) (▲).

In our case, however, no tablet was made, and therefore ibuprofen that formed a thin layer on the surface of the HA powder is readily released mostly from the surface rather than the bulk, thus suggesting that the profile observed in Fig. 8.12 is not fully diffusion controlled. The slower release rate for the ibuprofen/HA complex can be clearly noted, whereas raw ibuprofen and a physical mixture of ibuprofen and HA present similar dissolution rates. This slower, and desirable, drug release was related to the adsorption of the API compared to the bi-phasic physical mixture where the two components are not bonded to one another, thus proving that the intra-molecular bonding effect between the API and a carrier is an important factor when designing materials with controlled drug release properties. The majority of the studies on combining ceramics and anti-inflammatory concentrate their attention on prolonged drug release, whereas for the treatment of arthritic patients a “burst” drug release may be required at a point of need followed by a prolonged drug release afterward (Hite et al., 2007). Our study suggests that when ibuprofen and HA form a hydrogen-bonded complex it may be more difficult to obtain an immediate release due to an API-carrier interaction, in turn impeding design of materials with dual properties when using the method of dissolving and recrystallising drug in the presence of a ceramic carrier.

8.3 Conclusions

In this study, application of MASCW process as green route for the synthesis of nano-crystalline HA which is stoichiometrically similar to bone composition is explored and further elucidation of mechanism of the IBU adsorption onto the surface of nano-HA and its effects on the drug dissolution rate, explaining earlier findings on the shift of the FTIR signal of the carbonyl group of the API in the presence of ceramics. Herein, using an array of characterisation tools it is demonstrated that when synthesising an ibuprofen/ceramic complex, a hydrogen bonding occurs between the carbonyl group of the API and a calcium centre of hydroxyapatite. The process of surface-attachment follows the steps: (i) ibuprofen dimer partial dissolution in a solvent, (Williams W. Porter III) formation of a monomer/solvent complex from a dimer, (Williams W. Porter III) subsequent preferential attachment of the ibuprofen monomer to the hydroxyapatite. The latter is represented by a hydrogen bond between the hydroxyl group of ibuprofen and one of the hydroxyl groups of the hydroxyapatite, along with an interaction between the carbonyl group of ibuprofen and a calcium centre of HA. The formation of this complex occurs by means of a first order kinetics. Furthermore, the influence of such non-covalent bonding on the release/dissolution rate of the drug was also investigated. Through investigation of the behavior of the intramolecular bonded system ibuprofen-hydroxyapatite under physiological conditions (Ghosh et al., 2011) and comparing it with the bi-phasic mixture of the two components it is shown that the initial API release rate from the complex is influenced by the hydrogen bond induced attachment of the ibuprofen to the surface of nano-hydroxyapatite.

Chapter 9: Global Conclusions

In the present research work, for the first time a novel “Microwave Assisted Sub-Critical Water” to dissolve hydrophobic organic molecules and further explored the application of this novel technology in the fields of particle engineering and pharmaceutical processing is studied. In this process, high supersaturated solution of water and solute is prepared and further on cooling step based on the aqueous solubility of solute narrow particle size crystals induce out.

Chapter 5: In this chapter, process understanding and validation of MASCW technology is reported by generating a correlation between solute/solution concentrations (w/v) and processing temperatures of the MASCW process. Raman spectroscopy is used to track the crystallisation kinetics and polymorphic transformation of paracetamol solution from metastable phase form II to stable form I polymorph. Initially, till 90 mins of analysis no crystallisation is occured which is latter followed by generation of metastable phase of pca crystals which remained stable till 18 hrs and then conversion of metastable polymorphs to stable polymorph is observed. This proved the theory of Gibbs free energy that in solution state the polymorphic phase with higher free energy crystallises first followed by stable less free energy polymorphic phase. To understand the role of dielectric constant of water and solvent mixtures of water and organic solvents on solubility of solute at sub-critical state correlation between the change in the dielectric constant of solvent and solubility of solute is investigated. As there is decrease in the dielectric constant of solvent solubilising property of solvent enhances simultaneous resulting in producing highly supersaturated solutions of

hydrophobic APIs. Difference between conventional heating temperatures and sub-critical water heating temperatures is investigated by tracking the crystallisation time for the crystals to induce out is calculated. In this stability of supersaturated solutions of paracetamol solution is reported. In the 10% w/v aqueous solution of pca in sub-critically treated water remained stable for more than 24 hrs compared to conventional pca solution which is stable for three hours. This experimental observation indicates that on treating water at sub-critical state more water hydrogen bonds are broken compared to conventionally treated water molecules. All the solute crystals generated are analysed for its percent purity using HPLC technique.

Chapter 6: provided an evidence regarding the application of the MASCW process in cocrystallisation, based on the congruency of the cocrystal pairs used this chapter is further divided into three sections

Chapter 6.2.1: In this chapter, based on aqueous solubility of API and coformer congruent pairs (CBZ: SAC, SMT: SAC and SMZ: SAC) in 1:1 stoichiometric ratio is selected. Experimental design approach is used to understand the effect of different process and experimental parameters on end crystal phase is investigated. Generation of stable form I and metastable form II cocrystal phase of CBZ: SAC in 1:1 ratio from water is reported. SEM images have provided additional data regarding the change in crystal morphology and crystal habit of different cocrystal polymorph, the surface energy data explained the differences between the specific surface energies of CBZ: SAC form I (solution crystallised), CBZ: SAC form I and metastable form II (MASCW processed), the increase in the surface properties of the MASCW generated cocrystal has been reported which is further linked with

the study of kinetic properties (solubility) of these samples. Thermal analysis data has provided the information regarding the thermodynamic monotropic relationship between form I and form II transitions of CBZ: SAC cocrystals. PXRD and Raman spectra have elucidated the phase purity of the cocrystals formed. Minimum degradation of MASCW processed samples using HPLC analysis was observed.

Chapter 6.2.2: In this chapter, high throughput screening is done for generation of congruent cocrystal pairs of SMT: SAC, SMZ: SAC in 1:1 stoichiometric using water as solvent systems. X-ray diffraction and thermal analysis data has confirmed the formation of cocrystal based on the previous literature review.

Chapter 6.2.3: In this section, incongruent cocrystal pair of CAF: 4HBA in 1:1 stoichiometric ratios is selected for generation of anhydrous cocrystal of CAF: 4HBA in 1:1 stoichiometric ratio. The effect of decrease in dielectric properties of solvent system by using a solvent mixtures of (50% methanol + 50% water) on increase in solubility of molar concentration weight CAF: 4HBA cocrystal pairs in 1:1 ratio under subcritical environment is reported. PXRD, DSC and NMR data provides the formation of anhydrous phase of CAF: 4HBA cocrystal in 1:1 stoichiometric ratio. These results were practically generated for the first time using MASCW process.

Chapter 7: This chapter demonstrated the application of the MASCW process in the field of particle engineering. Based on the drug dosage form design for drug delivery using different routes this chapter is divided into two sections.

Chapter 7.1: This section includes the application of MASCW technology for generation of metastable polymorph of paracetamol using water as solvent system. Paracetamol commercial phase (form I) has a serious issue of compressibility during tableting. This issue can be attributed to the crystal lattice arrangements, crystal form, and crystal habit. PXRD, thermal analysis, and Raman spectroscopic data reveal the formation of metastable and stable polymorphs of pca using water as the solvent system. The SEM images reveal the change in the crystal habit and surface smoothness of MASCW processed samples compared to conventional commercial form I pca samples. Enhanced surface properties like specific surface area, dispersive surface energy are observed in the processed samples compared to raw pca, this surface energetic data attribute to increase in the compressibility and pharmacokinetic properties of MASCW processed a form I and form II polymorph of pca. Intrinsic dissolution data demonstrated that there is an increase in the solubility of MASCW processed form I polymorph of pca compared to raw which is attributed to the crystal habit and surface energies of the samples. The HPLC analysis provided the information regarding the chemical stability of MASCW processed samples as compared to conventional heating of pca in water at high temperatures.

In this chapter, the scalability of this technology with the help of external pharmaceutical processing industry was investigated and further obtained the similar results with enhancing kinetic properties and minimum chemical degradation.

Chapter 7.2: In the process of MASCW process sub-critical treated supersaturated solution is quenched in cold water which induced out crystal

with narrow particle size distribution for the generation of inhalable drug particles using dry powder inhaler. Anhydrous theophylline and lactose inhalation grade were selected as API and carrier model respectively based on their applications in nasal delivery system using DPI. The aerodynamic performance of the powdered samples is elucidated using next generation impactor (NGI). Spray dried theophylline is used as reference powder sample for analysis of aerodynamic performance. PXRD, DSC, TGA and FTIR data demonstrated the formation of stable anhydrous form I theophylline using MASCW process. Correlation between supersaturated concentration of solute and different crystallisation techniques on crystal size and morphology is investigated. iGC analysis demonstrated the surface properties, thermodynamic work of adhesion and cohesion between MASCW processed THF and spray dried THF with inhalation grade lactose.

THF MASCW treated THF S2 showed high FPD and FPF fraction from 5.93mg, 35.48% respectively. THF spray dried showed low FPD and FPF fraction from 1.86, 16% respectively, thus pure theophylline processed using MASCW process showed higher aerodynamic and suitable physicochemical properties for lung delivery, as confirmed by the morphology, surface properties, and *in-vitro* aerodynamic performance studies. The FPD and FPF of THF SCW treated showed high deposition rate compared to conventional THF SD, therefore reasonable good THF dose can be achieved with the patients having difficulties in generating a high level of inhalation flow such as children's and elderly.

Chapter 8: In this chapter, description of the application of the MASCW process for the synthesis of inorganic nano-crystalline HA and formation of

IBU/HA complex is reported for the first time. Further, in-depth understanding regarding the mechanism of hydrogen-bonded complex formation between ibuprofen and nano-crystalline hydroxyapatite is explained. Herein, using different characterisation tools the synthesis of IBU-HA complex was reported, the formation of hydrogen bonding between carbonyl moiety of API and calcium center HA. ATR-FTIR is used to track the kinetics of hydrogen bonding between IBU-HA complexes. Furthermore, the influence of such non-covalent bonding on the dissolution profile of the drug was also demonstrated.

Chapter 10: Suggestions for future work

- Development of a computational molecular dynamics model for sub-critical water to elucidate the structural and physical properties of water at different processing conditions.
- To study the influence of activation energy of microwaves over the structural vibrations of water and solute molecules.
- To study the influence of different additives (surfactants, antioxidants) in the dissociation of hydrophobic organic molecules using this technology.
- To generate computational models to differentiate different crystal phase transition regions during processing organic molecules at different processing conditions.
- To study the effect of the solvent mixture on the dielectric and dissolution properties of water which will affect the crystal form and crystallisation pathway of the molecule obtained using this technology.
- To analyse the compressibility or mechanical properties of the crystal generated from this technology and analyse its influence in post formulation performance.
- To study the effect of water dielectric constant over the solubility of the solute molecules using M-UNIFAC software.
- To develop an in-line tool to track different phases of crystallisation during processing at different temperature and pressure conditions.
- Study the application of this technology in polymer process industry, generation of stable solid dispersion of different drugs with enhanced chemical and physical stability.

Chapter 11: Bibliography

Adachi, S. (2009) Properties of Subcritical Water and Its Utilization. *Foods Food Ingredients J. Jpn* 214.

Aher, S., Dhumal, R., Mahadik, K., Paradkar, A. and York, P. (2010) Ultrasound assisted cocrystallization from solution (USSC) containing a non-congruently soluble cocrystal component pair: Caffeine/maleic acid. *Eur J Pharm Sci* 41 (5), 597-602.

Aitipamula, S., Chow, P. S. and Tan, R. B. H. (2012) Co-crystals of caffeine and piracetam with 4-hydroxybenzoic acid: Unravelling the hidden hydrates of 1 : 1 co-crystals. *CrystEngComm* 14 (7), 2381.

Alhalaweh, A., Kaialy, W., Buckton, G., Gill, H., Nokhodchi, A. and Velaga, S. (2013) Theophylline Cocrystals Prepared by Spray Drying: Physicochemical Properties and Aerosolization Performance. *AAPS PharmSciTech* 14 (1), 265-276.

Alhalaweh, A. and Velaga, S. P. (2010) Formation of Cocrystals from Stoichiometric Solutions of Incongruently Saturating Systems by Spray Drying. *Crystal Growth & Design* 10 (8), 3302-3305.

Andrew V. Trask, J. v. d. S., W. D. Samuel Motherwell, and and William Jones (2005) Achieving Polymorphic and Stoichiometric Diversity in Cocrystal Formation: Importance of Solid-State Grinding, Powder X-ray Structure Determination, and Seeding. *Crystal Growth & Design* 5 (6), 2233-2241.

Ashburn, T. T. and Thor, K. B. (2004) Drug repositioning: identifying and developing new uses for existing drugs. *Nat Rev Drug Discov* 3 (8), 673-83.

Asl, A. H. and Khajenoori, M. (2013) *Subcritical Water Extraction.* Mass Transfer - Advances in Sustainable Energy and Environment Oriented Numerical Modeling.

Babu, N. J. and Nangia, A. (2011) Solubility Advantage of Amorphous Drugs and Pharmaceutical Cocrystals. *Crystal Growth & Design* 11 (7), 2662-2679.

Bag, P. P., Patni, M. and Malla Reddy, C. (2011) A kinetically controlled crystallization process for identifying new co-crystal forms: fast

evaporation of solvent from solutions to dryness. *CrystEngComm* 13 (19), 5650-5652.

Bala Subramaniam, R. A., Rajewski and Kirk Snavely (1997) Pharmaceutical Processing with Supercritical Carbon Dioxide . *Journal of Pharmaceutical Sciences* 86 (8).

Banner, A. S. (1994) Theophylline: should we discard an old friend. *Lancet* 343 (8898), 618.

Barnes, P. J. (2005) Theophylline in chronic obstructive pulmonary disease: New horizons. *Proceedings of the American Thoracic Society* 2 (4), 334-339.

Berry David J, C. C. S., William Clegg, Ross W. Harrington, Simon J. Coles, Peter N. Horton, Micheal B. Hursthouse, Richard Storey, William Jones, Tomislav Friscic and Nicholas Blagden (2008) Applying Hot-Stage Microscopy to Co-Crystal Screening A Study of Nicotinamide with Seven Active Pharmaceutical Ingredients. *Crystal Growth & Design* 8 (5), 1697-1712.

Boureau, F., Schneid, H., Zeghari, N., Wall, R. and Bourgeois, P. (2004) The IPSO study: ibuprofen, paracetamol study in osteoarthritis. A randomised comparative clinical study comparing the efficacy and safety of ibuprofen and paracetamol analgesic treatment of osteoarthritis of the knee or hip. *Annals of the Rheumatic Diseases* 63 (9), 1028-1034.

Bruni, G., Maietta, M., Berbenni, V., Bini, M., Ferrari, S., Capsoni, D., Boiocchi, M., Milanese, C. and Marini, A. (2012) Preparation and characterization of carprofen co-crystals. *CrystEngComm* 14 (2), 435-445.

Bucar, D.-K., Filip, S., Arhangelskis, M., Lloyd, G. O. and Jones, W. (2013) Advantages of mechanochemical cocrystallisation in the solid-state chemistry of pigments: colour-tuned fluorescein cocrystals. *CrystEngComm* 15 (32), 6289-6291.

Burley, J. C., Duer, M. J., Stein, R. S. and Vrcelj, R. M. (2007) Enforcing Ostwald's rule of stages: Isolation of paracetamol forms III and II. *European Journal of Pharmaceutical Sciences* 31 (5), 271-276.

Brabander. G.Van Dan Mooter, C. V., J.P.Ramon (2002) Characterization of Ibuprofen as a Nontraditional Plasticizer of Ethyl Cellulose. *journal of Pharmaceutical Sciences* 91 (7).

Carr, A. G., Mammucari, R. and Foster, N. R. (2011) Particle formation of budesonide from alcohol-modified subcritical water solutions. *Int J Pharm* 405 (1-2), 169-80.

Champion, J. A., Katare, Y. K. and Mitragotri, S. (2007) Particle shape: A new design parameter for micro- and nanoscale drug delivery carriers. *Journal of Controlled Release* 121 (1–2), 3-9.

Charoenchaitrakool, M., Dehghani, F., Foster, N. R. and Chan, H. K. (2000) Micronization by Rapid Expansion of Supercritical Solutions to Enhance the Dissolution Rates of Poorly Water-Soluble Pharmaceuticals. *Industrial & Engineering Chemistry Research* 39 (12), 4794-4802.

Chevalier, E., Viana, M., Cazalbou, S., Makein, L., Dubois, J. and Chulia, D. (2010) Ibuprofen-loaded calcium phosphate granules: Combination of innovative characterization methods to relate mechanical strength to drug location. *Acta Biomaterialia* 6 (1), 266-274.

Childs, S. L., Kandi, P. and Lingireddy, S. R. (2013) Formulation of a Danazol Cocrystal with Controlled Supersaturation Plays an Essential Role in Improving Bioavailability. *Molecular Pharmaceutics* 10 (8), 3112-3127.

Childs, S. L., Rodriguez-Hornedo, N., Reddy, L. S., Jayasankar, A., Maheshwari, C., McCausland, L., Shipplett, R. and Stahly, B. C. (2008) Screening strategies based on solubility and solution composition generate pharmaceutically acceptable cocrystals of carbamazepine. *CrystEngComm* 10 (7), 856-864.

Chiou, W. L. R., S (1969) Preparation and dissolution characteristics of several fast-release solid dispersions of griseofulvin. 58 (12).

Chow, S., Chen, M., Shi, L., Chow, A. L. and Sun, C. (2012) Simultaneously Improving the Mechanical Properties, Dissolution Performance, and Hygroscopicity of Ibuprofen and Flurbiprofen by Cocrystallization with Nicotinamide. *Pharmaceutical Research* 29 (7), 1854-1865.

Choy, K. L. (2003) Chemical vapour deposition of coating. *Progress in Material Science* 48, 57-170.

Chadwick K, R. D. a. W. C. (2007) How does grinding produce co-crystals Insights from the case of benzophenone and diphenylamine. *CrystEngComm* 9, 732-734.

Clark, D. (2011) *The Electromagnetic Spectrum*. Available at: http://weeklysciencequiz.blogspot.co.uk/2011/09/electromagnetic-spectrum.html.

Clarke, H.D., Arora, K.K., Wojtas, L. and Zaworotko, M.J. (2011) Polymorphism in Multi Component Crystals: Form III and IV of Gallic Acid Monohydrate. Crystal Growth & Design 11(4),964-966.

Colacio-Rodriguez, E. and Salas-Peregrin, J. M. (1984) Thermal studies on purine complexes. V. Thermal behaviour of tetrachloropalladates of theophylline and theobromine and theophylline complexes of Cd(II) and Hg(II). *Thermochimica Acta* 74 (1), 45-54.

Cullity, B. D. S. S. R. (2001) *Elements of X-ray Diffraction.* Prentice-Hall Inc, Upper Saddle River:

Datta, S. and Grant, D. J. W. (2004) Crystal structures of drugs: advances in determination, prediction and engineering. *Nat Rev Drug Discov* 3 (1), 42-57.

Dejan-Kresimir Bucar, J. A. E., Mark D.Eddleston, Jeremy K. Cockcroft and William Jones (2017) Sonocrystallization Yields Monoclinic Paracetamol with Significantly Improved Comapction Behavior. *Angewandte Chemie International Edition* 54 (1), 249-253.

Dejan-Kresimir Bucar, R. F. H., Xiaochun Lou, Richard W. Duerst,Leonard R. MacGillivray and Geoff G. Z. Zhang (2008) Cocrystals of Caffeine and Hydroxybenzoic acids composed of Multi Supramolecular Heterosynthons : Screening via Solution-Mediated Phase Transformation and Structural Characterisation. *Crystal Growth & Design* 9 (4), 1932-1943.

Dhumal, R. S., Kelly, A. L., York, P., Coates, P. D. and Paradkar, A. (2010) Cocrystalization and simultaneous agglomeration using hot melt extrusion. *Pharm Res* 27 (12), 2725-33.

Dritan Hasan, William Jones (2017). Screening for new pharmaceutical solid forms using mechanochemistry: A practical guide. *J. Adv. Drug.Delivery reviews* 117-147-161.

Duarte, A. R. C., Gordillo, M. D., Cardoso, M. M., Simplício, A. L. and Duarte, C. M. M. (2006) Preparation of ethyl cellulose/methyl cellulose blends by supercritical antisolvent precipitation. *International Journal of Pharmaceutics* 311 (1–2), 50-54.

Dwayne T. Friesen, Ravi Shanker,Marshall Crew, Daniel T. Smithey,W. J. Curatolo, and J. A. S. Nightingale (2008) Hydroxypropyl Methylcellulose Acetate Succinate-Based Spray-Dried Dispersions: An Overview. *Molecular Pharmaceutics* 5 (6), 1003–1019.

Eddleston, M. D., Patel, B., Day, G. M. and Jones, W. (2013) Cocrystallization by Freeze-Drying: Preparation of Novel Multicomponent Crystal Forms. *Crystal Growth & Design* 13 (10), 4599-4606.

El-Zhry El-Yafi, A. K. and El-Zein, H. (2015) Technical crystallization for application in pharmaceutical material engineering: Review article. *Asian Journal of Pharmaceutical Sciences* 10 (4), 283-291.

Elebring, T., Gill, A. and Plowright, A. T. (2012) What is the most important approach in current drug discovery: doing the right things or doing things right? *Drug Discov Today* 17 (21-22), 1166-9.

Etienne Joiris, P. D. M., Christophe Berneron, Anne-Marie Guyot-Hermann and Jean-Claude Guyot (1997) Compression Behaviour of Orthorhombic Paracetamol. *Pharmaceutical Research* 15 (7).

Frampton, G. N. C. S. (1998) Physicochemical Characterization of the Orthorhombic Polymorph of Paracetamol Crystallized from solution. *journal of pharmaceutical sciences* 87 (6).

Francois Dietlin, L. P. D. F., Gif-sur-Yvette, both of France (1998) Stable liquid Racetamol composition, and method for preparing same.

Fu, X., Li, J., Wang, L., Wu, B., Xu, X., Deng, Z. and Zhang, H. (2016) Pharmaceutical crystalline complexes of sulfamethazine with saccharin: same interaction site but different ionization states. *RSC Advances* 6 (31), 26474-26478.

Gabriel, C., Gabriel, S., H. Grant, E., S.J. Halstead, B.& Michael P. Mingos, D.1998. Dielectric parameters relevant to microwave dielectric heating. *Chemical Society Reviews*, 27, 213-224.

Gbashi, S., Adebo, O. A., Piater, L., Madala, N. E. and Njobeh, P. B. (2016) Subcritical Water Extraction of Biological Materials. *Separation & Purification Reviews* 46 (1), 21-34.

Gedye, R., Smith, F., Westaway, K., Ali, H., Baldisera, L., Laberge, L. & Rousell,J.1986. The use of microwave ovens for rapid organic synthesis. Tetrahedran Letters, 27, 279-282.

Ghosh, I., Snyder, J., Vippagunta, R., Alvine, M., Vakil, R., Tong, W. Q. and Vippagunta, S. (2011) Comparison of HPMC based polymers performance as carriers for manufacture of solid dispersions using the melt extruder. *Int J Pharm* 419 (1-2), 12-9.

Gibson, I. R. and Bonfield, W. (2002) Novel synthesis and characterization of an AB-type carbonate-substituted hydroxyapatite. *Journal of Biomedical Materials Research* 59 (4), 697-708.

Gulley-Stahl, H., Hogan, P. A., Schmidt, W. L., Wall, S. J., Buhrlage, A. and Bullen, H. A. (2010) Surface Complexation of Catechol to Metal Oxides: An ATR-FTIR, Adsorption, and Dissolution Study. *Environmental Science & Technology* 44 (11), 4116-4121.

Habgood, M. and Price, S. L. (2010) Isomers, Conformers, and Cocrystal Stoichiometry: Insights from the Crystal Energy Landscapes of Caffeine with the Hydroxybenzoic Acids. *Crystal Growth & Design* 10 (7), 3263-3272.

Heng, J. Y., Bismarck, A., Lee, A. F., Wilson, K. and Williams, D. R. (2006) Anisotropic surface energetics and wettability of macroscopic form I paracetamol crystals. *Langmuir* 22 (6), 2760-9.

Hickey, M. B., Peterson, M. L., Scoppettuolo, L. A., Morrisette, S. L., Vetter, A., Guzmán, H., Remenar, J. F., Zhang, Z., Tawa, M. D., Haley, S., Zaworotko, M. J. and Almarsson, Ö. (2007) Performance comparison of a co-crystal of carbamazepine with marketed product. *European Journal of Pharmaceutics and Biopharmaceutics* 67 (1), 112-119.

Hilfiker, R. (2006) *Polymorphism: In the Pharmaceutical Industry.* Wiley.

Hite, M., Federici, C., Brunelle, A. and Turner, S. (2007) *Modified release ibuprofen dosage form*. Google Patents.

Hulme, A. T., Price, S. L. and Tocher, D. A. (2005) A New Polymorph of 5-Fluorouracil Found Following Computational Crystal Structure Predictions. *Journal of the American Chemical Society* 127 (4), 1116-1117.

Ibanez, E., Kubatova, A., Senorans, F. J., Cavero, S., Reglero, G. and Hawthorne, S. B. (2003) Subcritical Water Extraction of Antioxidant Compounds from Rosemary Plants. *Journal of Agricultural and Food Chemistry* 51 (2), 375-382.

Ibrahim, D. M., Mostafa, A. A. and Koroish, S. I. (2011) Chemical characterization of some substituted hydroxyapatites. *Chemistry Central Journal* 5 (1), 74.

Ibanez, E., Oca, A., de Murga, G., Lopez-Sebastian, S., Tabera, J. and Reglero, G. (1999) Supercritical Fluid Extraction and Fractionation of Different Preprocessed Rosemary Plants. *Journal of Agricultural and Food Chemistry* 47 (4), 1400-1404.

Irani, A. N. P. S. A. (1966) Solubility Profile for the Xanthines in Aquous Solution of a Glycol Ether II. *Pharm. Science* 55.

Ismael Rafols, M. M. a. J.-H. P. (2010) Hybrid Nanomaterials Research: Is It Really Interdisciplinary?, in The Supramolecular Chemistry of Organic-Inorganic Hybrid Materials. *John Wilet and sons*.

Jampilek, J. and Dohnal, J. (2012) Investigation of Carbohydrates and Their Derivatives as Crystallization Modifiers.

Jayasankar, A., Good, D. J. and Rodríguez-Hornedo, N. (2007) Mechanisms by Which Moisture Generates Cocrystals. *Molecular Pharmaceutics* 4 (3), 360-372.

Jones, W. and Eddleston, M. D. (2014) Introductory lecture: Mechanochemistry, a versatile synthesis strategy for new materials. *Faraday Discuss* 170, 9-34.

Jouyban, A., Soltanpour, S. and Chan, H.-K. (2004) A simple relationship between dielectric constant of mixed solvents with solvent

composition and temperature. *International Journal of Pharmaceutics* 269 (2), 353-360.

Kappe, C. O. (2004) Controlled microwave heating in modern organic synthesis. *Angew Chem Int Ed Engl* 43 (46), 6250-84.

Karki, S., Fris• , T., Fajbiajn, L. s., Laity, P. R., Day, G. M. and Jones, W. (2009) Improving Mechanical Properties of Crystalline Solids by Cocrystal Formation: New Compressible Forms of Paracetamol. *Advanced Materials* 21 (38a€ 39), 3905-3909.

Karásek, P., Planeta, J. and Roth, M. (2006) Solubility of Solid Polycyclic Aromatic Hydrocarbons in Pressurized Hot Water: Correlation with Pure Component Properties. *Industrial & Engineering Chemistry Research* 45 (12), 4454-4460.

Kauffman, J. F., Batykefer, L. M. and Tuschel, D. D. (2008) Raman detected differential scanning calorimetry of polymorphic transformations in acetaminophen. *J Pharm Biomed Anal* 48 (5), 1310-5.

Kelly, A. L., Gough, T., Dhumal, R. S., Halsey, S. A. and Paradkar, A. (2012) Monitoring ibuprofen-nicotinamide cocrystal formation during solvent free continuous cocrystallization (SFCC) using near infrared spectroscopy as a PAT tool. *Int J Pharm* 426 (1-2), 15-20.

Korang-Yeboah, M., Rahman, Z., Shah, D., Mohammad, A., Wu, S., Siddiqui, A. and Khan, M. A. (2016) Impact of formulation and process variables on solid-state stability of theophylline in controlled release formulations. *Int J Pharm* 499 (1-2), 20-8.

Kumar, R., Prakash, K. H., Cheang, P. and Khor, K. A. (2004) Temperature Driven Morphological Changes of Chemically Precipitated Hydroxyapatite Nanoparticles. *Langmuir* 20 (13), 5196-5200.

Kumar, S. S. (2014) Polymorphism and solubility of Selected Active Pharmaceutical Ingredients., 352.

Lee, E. H. (2014) A practical guide to pharmaceutical polymorph screening & selection. *Asian Journal of Pharmaceutical Sciences* 9 (4), 163-175.

Legendre, B. and Randzio, S. L. (2007) Transitiometric analysis of solid II/solid I transition in anhydrous theophylline. *International Journal of Pharmaceutics* 343 (1–2), 41-47.

Lehmann, C. W. and Stoisser, F. (2007) The crystal structure of anhydrous beta-caffeine as determined from X-ray powder-diffraction data. *Chemistry* 13 (10), 2908-11.

Lidstrom, P.,Tierney, J., Wathey, B & Westman J.(2001)Microwave assisted organic synthesis. Tetrahedron,57,9225-9283.

Liao, C.-J., Lin, F.-H., Chen, K.-S. and Sun, J.-S. (1999) Thermal decomposition and reconstitution of hydroxyapatite in air atmosphere. *Biomaterials* 20 (19), 1807-1813.

Liming Yang, L. E. Y., Madumita B. Ray (2008) Degradation of paracetamol in water important article. *Water Research* 42, 3480-3488.

Ma, M.-Y., Zhu, Y.-J., Li, L. and Cao, S.-W. (2008) Nanostructured porous hollow ellipsoidal capsules of hydroxyapatite and calcium silicate: preparation and application in drug delivery. *Journal of Materials Chemistry* 18 (23), 2722.

Maeno, Y., Fukami, T., Kawahata, M., Yamaguchi, K., Tagami, T., Ozeki, T., Suzuki, T. and Tomono, K. (2014) Novel pharmaceutical cocrystal consisting of paracetamol and trimethylglycine, a new promising cocrystal former. *Int J Pharm* 473 (1-2), 179-86.

Maghsoodi, M., Taghizadeh, O., Martin, G. P. and Nokhodchi, A. (2008) Particle design of naproxen-disintegrant agglomerates for direct compression by a crystallo-co-agglomeration technique. *International Journal of Pharmaceutics* 351 (1–2), 45-54.

Mahajan, R. K. and Sharma, R. (2011) Analysis of interfacial and micellar behavior of sodium dioctyl sulphosuccinate salt (AOT) with zwitterionic surfactants in aqueous media. *Journal of Colloid and Interface Science* 363 (1), 275-283.

Maniruzzaman, M., Rana, M. M., Boateng, J. S., Mitchell, J. C. and Douroumis, D. (2013) Dissolution enhancement of poorly water-soluble APIs processed by hot-melt extrusion using hydrophilic polymers. *Drug Dev Ind Pharm* 39 (2), 218-27.

Matthew L. Peterson, David McIlroy, Paul Shaw, J. Peter Mustonen,Mark Oliveira, and Orn Almarsson(2003) Crystallization and Transformation of Acetaminophen Trihydrate. *Crystal Growth & Design* 0 (0), 1-5.

Marc.Antoine Perrin, Marcus A. Neumann, Hagit Elmaleh and Lionel Zaske (2011) Crystal structure determination of the elusive paracetamol Form III. ChemComm (3181-3183).

Mehta, B. (2013) *Spray drying as a green technique for the development of co-crystals of incongruently soluble pair*. M Phil transfer report. University of Bradford.

Melville, A. J., Rodríguez-Lorenzo, L. M. and Forsythe, J. S. (2008) Effects of calcination temperature on the drug delivery behaviour of Ibuprofen from hydroxyapatite powders. *Journal of Materials Science: Materials in Medicine* 19 (3), 1187-1195.

Morissette, S. L., Almarsson, O., Peterson, M. L., Remenar, J. F., Read, M. J., Lemmo, A. V., Ellis, S., Cima, M. J. and Gardner, C. R. (2004) High-throughput crystallization: polymorphs, salts, co-crystals and solvates of pharmaceutical solids. *Adv Drug Deliv Rev* 56 (3), 275-300.

Newman, N. S. a. A. (2009) Pharmaceutical Cocrystals and Their Physicochemical Properties. *Crystal Growth & Design* 9 (6), 2950-2967.

Nehm Sarah J, B. R.-S. a. N. R.-H. (2005) Phase Solubility Diagrams of Cocrystals Are Explained by Solubility Product and Solution Complexation. *Crystal Growth & Design* 6, 592-600.

Nehm Sarah J, B. R.-S. . N. R.-H. (2006) Phase Solubility Diagrams of Cocrystals Are Explained by Solubility Product and Solution Complexation.pdf. *Crystal Growth & Design* 6 (2), 592-600.

Novoa, Juan.J, Dario. B. Addadi, Lia. (2008) Engineering of Crystalline Material Properties.

Ogilvie, A., Frank, R. M., Benqué, E. P., Gineste, M., Heughebaert, M. and Hemmerle, J. (1987) The biocompatibility of hydroxyapatite implanted in the human periodontium. *Journal of Periodontal Research* 22 (4), 270-283.

Oner, M., Yetiz, E., Ay, E. and Uysal, U. (2011) Ibuprofen release from porous hydroxyapatite tablets. *Ceramics International* 37 (7), 2117-2125.

P. Alessi, A. C., and I. Kikic (1996) Particle Production of Steroid Drugs Using Supercritical Fluid. *Ind.Eng.Chem.Res* 35, 4718-4726.

P. Postorino, R. H. T., M. A Ricci, ,A. K Soper, G. W.Neilson, (1993) The interatomic structure of water at supercritical temperatures. *Nature* 366 (6456), 668-670.

Padrela, L., Rodrigues, M. A., Tiago, J., Velaga, S. P., Matos, H. A. and de Azevedo, E. G. (2015) Insight into the Mechanisms of Cocrystallization of Pharmaceuticals in Supercritical Solvents. *Crystal Growth & Design* 15 (7), 3175-3181.

Padrela, L., Rodrigues, M. A., Velaga, S. P., Fernandes, A. C., Matos, H. A. and de Azevedo, E. G. (2010) Screening for pharmaceutical cocrystals using the supercritical fluid enhanced atomization process. *The Journal of Supercritical Fluids* 53 (1–3), 156-164.

Perrin, M. A., Neumann, M. A., Elmaleh, H. and Zaske, L. (2009) Crystal structure determination of the elusive paracetamol Form III. *Chem Commun (Camb)* (22), 3181-3.

Phadnis, N. V. and Suryanarayanan, R. (1997) Polymorphism in anhydrous theophylline—implications on the dissolution rate of theophylline tablets. *Journal of Pharmaceutical Sciences* 86 (11), 1256-1263.

Piera Di Martino, G. F. P., and Sante Martelli (2000) Molecular Mobility of the Paracetamol Amorphous Form. *Chem Pharm Bull (Tokyo)* 48 (8), 1105-1108.

Pitzer, K. S. (1983) Dielectric constant of water at very high temperature and pressure. *Applied Physical Sciences* 80, 4575-4576.

Porter, W. W., 3rd, Elie, S. C. and Matzger, A. J. (2008) Polymorphism in Carbamazepine Cocrystals. *Cryst Growth Des* 8 (1), 14-16.

Properties, P. C. a. T. P. (2009) Nate Schultheiss and Ann Newman. Pharmaceutical Cocrystals and Their Physicochemical Properties. *Crystal Growth & Design* 9 (6), 2950-2967.

Pu, Y., Li, Y., Wang, D., Foster, N. R., Wang, J.-X. and Chen, J.-F. (2017) A green route to beclomethasone dipropionate nanoparticles via solvent anti-solvent precipitation by using subcritical water as the solvent. *Powder Technology* 308, 200-205.

Qi, C., Zhu, Y.-J., Lu, B.-Q., Zhao, X.-Y., Zhao, J. and Chen, F. (2012) Hydroxyapatite nanosheet-assembled porous hollow microspheres: DNA-templated hydrothermal synthesis, drug delivery and protein adsorption. *Journal of Materials Chemistry* 22 (42), 22642.

Qiao, N., Li, M., Schlindwein, W., Malek, N., Davies, A. and Trappitt, G. (2011) Pharmaceutical cocrystals: An overview. *International Journal of Pharmaceutics* 419 (1–2), 1-11.

R. S. Dhumal, A. L. K., T. Gough, S. K. Pagire, A. R. Paradkar (2012) Cocrystallisation and stoichiometric control of incongruently soluble pair by solvent free continuous cocrytsallisation (SFCC)In *UK PharmSci.* Nottingham, UK.

Rabinow, B. E. (2004) Nanosuspensions in drug delivery. *Nat Rev Drug Discov* 3 (9), 785-796.

Radacsi Norbert, Joop H. ter Horst and Georgios D. Stefanidis (2013) Microwave- Assited Evaporative crystallisation of Niflumic Acid for Particle Size Reduction. *Crystal Growth & Design* (13),4186-4189

Rager, T. and Hilfiker, R. (2010) Cocrystal Formation from Solvent Mixtures. *Crystal Growth & Design* 10 (7), 3237-3241.

Rahul Banerjee, P. M. B., Nittala V.Ravindra and Gautam R. Desiraju (2005) Saccharin salt of Active Pharmaceutical Ingredient, Their crystal structure and increased water solubility. *Crystal Growth & Design* 5 (6), 2299-2309.

Rajesh Goud, N., Khan, R. A. and Nangia, A. (2014) Modulating the solubility of sulfacetamide by means of cocrystals. *CrystEngComm* 16 (26), 5859.

Ravindra Acharya, K., Kuchela, K. N. and Kartha, G. (1982) Crystal structure of sulfamerazine. *Journal of Crystallographic and Spectroscopic Research* 12 (4), 369-376.

Revelli, A.-L., Laugier, S., Erriguible, A. and Subra-Paternault, P. (2014) High-pressure solubility of naproxen, nicotinamide and their mixture in acetone with supercritical CO2 as an anti-solvent. *Fluid Phase Equilibria* 373, 29-33.

Reverchon, E. and Della Porta, G. (1999) Production of antibiotic micro- and nano-particles by supercritical antisolvent precipitation. *Powder Technology* 106 (1–2), 23-29.

Robin K. Harris, P. Y. G., Horst Puschmann, David C. Apperley,Ulrich J. Griesser, Robert B. Hammond, and Caiyun Ma, K. J. R., Greg J. Pearce,| Jonathan R. Yates,| and Chris J. Pickard (2005) Structural Studies of the Polymorphs of Carbamazepine, Its Dihydrate, and Two Solvates. *Organic Process Research & Development* 9 (6), 902-910.

Rodríguez-Hornedo, N., Nehm, S. J. and Jayasankar,(2008). A. Cocrystals: Design, Properties and Formation Mechanisms. *Encyclopedia of Pharmaceutical Technology, Third Edition.* 615-635.

Rodríguez-Spong, C. P. P., Adivaraha Jayasankar , Adam J .Matzger, Naír Rodríguez-Hornedo, (2004) General principles of pharmaceutical solid polymorphism: A supramolecular perspective. *Advanced Drug Delivery Reviews* 56 (3), 241-274.

Sarah L.Price (2014), Predicting crystal structures of organic compounds. *Chem.Soc.Rev,43,2098-20111*

Sahle, C. J., Sternemann, C., Schmidt, C., Lehtola, S., Jahn, S., Simonelli, L., Huotari, S., Hakala, M., Pylkkänen, T., Nyrow, A., Mende, K., Tolan, M., Hämäläinen, K. and Wilke, M. (2013) Microscopic structure of water at elevated pressures and temperatures. *Proceedings of the National Academy of Sciences* 110 (16), 6301-6306.

Sambudi, N. S., Cho, S. and Cho, K. (2016) Porous hollow hydroxyapatite microspheres synthesized by spray pyrolysis using a microalga template: preparation, drug delivery, and bioactivity. *RSC Advances* 6 (49), 43041-43048.

Sander, J. R. G., Bučar, D.-K., Henry, R. F., Zhang, G. G. Z. and MacGillivray, L. R. (2010) Pharmaceutical Nano-Cocrystals: Sonochemical Synthesis by Solvent Selection and Use of a Surfactant. *Angewandte Chemie International Edition* 49 (40), 7284-7288.

Sanphui, P., Goud, N. R., Khandavilli, U. B. R., Bhanoth, S. and Nangia, A. (2011) New polymorphs of curcumin. *Chemical Communications* 47 (17), 5013-5015.

Sachin K., Pagire Sudhir, He Pan, Colin Seaton, Adrian Kelly, Yinghong Chen, Qi Wang, Phil Coates and Anant Paradkar (2018). Continuous Manufacturing of cocrystals using solid state shear milling technology. *Crystal Growth and Design*

Sekhon BS. (2009) Pharmaceutical co-crystal - a review. *ARS Pharmaceutica* 50 (0004-2927), 99-117.

Shan, N., Bond, A. D. and Jones, W. (2002) Crystal engineering using 4,4′-bipyridyl with di- and tricarboxylic acids. *Crystal Engineering* 5 (1), 9-24.

Shariare, M. H., Blagden, N., de Matas, M., Leusen, F. J. and York, P. (2012) Influence of solvent on the morphology and subsequent comminution of ibuprofen crystals by air jet milling. *J Pharm Sci* 101 (3), 1108-19.

Shi, B., Wang, Y. and Jia, L. (2011) Comparison of Dorris-Gray and Schultz methods for the calculation of surface dispersive free energy by inverse gas chromatography. *J Chromatogr A* 1218 (6), 860-2.

Singhal, D. and Curatolo, W. (2004) Drug polymorphism and dosage form design: a practical perspective. *Advanced Drug Delivery Reviews* 56 (3), 335-347.

Sládková, V., Cibulková, J., Eigner, V., Šturc, A., Kratochvíl, B. and Rohlíček, J. (2014) Application and Comparison of Cocrystallization Techniques on Trospium Chloride Cocrystals. *Crystal Growth & Design* 14 (6), 2931-2936.

Smeyers, Y. G., Cuéllare-Rodriguez, S., Galvez-Ruano, E. and Arias-Pérez, M. S. (1985) Conformational Analysis of Some α-Phenylpropionic Acids with Anti-inflammatory Activity. *Journal of Pharmaceutical Sciences* 74 (1), 47-49.

Smith, R. (2006) Superheated water: the ultimate green solvent for separation science. *Analytical and Bioanalytical Chemistry* 385 (3), 419-421.

Somnath S. Kadam, Samir A. Kulkarni, roger Coloma Ribera, Andrzej I. Stankiewicz, Joop H.ter Horst, Herman J.M.Kramer (2012) A new review on the metastable zone width during cooling crystallisation. *Chemical Engineering Science* 72(10-19).

Stass, D.V., Woodward, J.R. Timmel C.R Hore.P.J & Mclauchlan, K.A (2000). Radiofrequency magnetic field effects on chemical yeilds. Chemical Physics Letters,329,15-22..

Suresh, K., Goud, N. R. and Nangia, A. (2013) Andrographolide: Solving Chemical Instability and Poor Solubility by Means of Cocrystals. *Chemistry – An Asian Journal* 8 (12), 3032-3041.

Talmon, Y. (1987) Electron Beam Radiation Damage to Organic and Biological Cryospecimens. In Steinbrecht, R. A. and Zierold, K. (editors) *Cryotechniques in Biological Electron Microscopy.* Berlin, Heidelberg: Springer Berlin Heidelberg. 64-84.

Telko, M. J. and Hickey, A. J. (2005) Dry powder inhaler formulation. *Respiratory care* 50 (9), 1209-1227.

Thakuria, R., Delori, A., Jones, W., Lipert, M. P., Roy, L. and Rodriguez-Hornedo, N. (2013a) Pharmaceutical cocrystals and poorly soluble drugs. *Int J Pharm* 453 (1), 101-25.

Thakuria, R., Delori, A., Jones, W., Lipert, M. P., Roy, L. and Rodríguez-Hornedo, N. (2013b) Pharmaceutical cocrystals and poorly soluble drugs. *International Journal of Pharmaceutics* 453 (1), 101-125.

Toor, S. S., Rosendahl, L. and Rudolf, A. (2011) Hydrothermal liquefaction of biomass: A review of subcritical water technologies. *Energy* 36 (5), 2328-2342.

Tralau-Stewart, C. J., Wyatt, C. A., Kleyn, D. E. and Ayad, A. (2009) Drug discovery: new models for industry-academic partnerships. *Drug Discov Today* 14 (1-2), 95-101.

Trask, A. V. (2007) An overview of Pharmaceutical cocrytsal as Intellectual Property. *Molecular Pharmaceutics* 4 (3), 301-309.

Trask, A. V., Motherwell, W. D. S. and Jones, W. (2006) Physical stability enhancement of theophylline via cocrystallization. *International Journal of Pharmaceutics* 320 (1–2), 114-123.

Tsapatsaris, N., Kolesov, B. A., Fischer, J., Boldyreva, E. V., Daemen, L., Eckert, J. and Bordallo, H. N. (2014) Polymorphism of paracetamol: a new understanding of molecular flexibility through local methyl dynamics. *Mol Pharm* 11 (3), 1032-41.

Vallet-Regí, M. and González-Calbet, J. M. (2004) Calcium phosphates as substitution of bone tissues. *Progress in Solid State Chemistry* 32 (1–2), 1-31.

Vangala, V. R., Chow, P. S. and Tan, R. B. H. (2012) Co-Crystals and Co-Crystal Hydrates of the Antibiotic Nitrofurantoin: Structural Studies and Physicochemical Properties. *Crystal Growth & Design* 12 (12), 5925-5938.

Variankaval, N., Cote, A. S. and Doherty, M. F. (2008) From form to function: Crystallization of active pharmaceutical ingredients. *AIChE Journal* 54 (7), 1682-1688.

Vasconcelos, T., Sarmento, B. and Costa, P. (2007) Solid dispersions as strategy to improve oral bioavailability of poor water soluble drugs. *Drug Discov Today* 12 (23-24), 1068-75.

Vemavarapu, C., Mollan, M. J. and Needham, T. E. (2002) Crystal doping aided by rapid expansion of supercritical solutions. *AAPS PharmSciTech* 3 (4), 17-31.

Venugopalan, P, R. Purohit. (2009) Polymorphism: An overview.

Viswanath, B. and Ravishankar, N. (2008) Controlled synthesis of plate-shaped hydroxyapatite and implications for the morphology of the apatite phase in bone. *Biomaterials* 29 (36), 4855-4863.

Wang, I.-C., Lee, M.-J., Sim, S.-J., Kim, W.-S., Chun, N.-H. and Choi, G. J. (2013) Anti-solvent co-crystallization of carbamazepine and saccharin. *International Journal of Pharmaceutics* 450 (1–2), 311-322.

Wernet, P., Nordlund, D., Bergmann, U., Cavalleri, M., Odelius, M., Ogasawara, H., Näslund, L. Å., Hirsch, T. K., Ojamäe, L., Glatzel, P., Pettersson, L. G. M. and Nilsson, A. (2004) The Structure of the First Coordination Shell in Liquid Water. *Science* 304 (5673), 995-999.

Woodward, J.R., Jackson, R.J., Timmel, C.R., Hore, P.J. & McLauchlan, K.A.1997. Resonant radiofrequency magnetic field effects on a chemical reaction. Chemical Physics Letters, 272,376-382.

William Jones, W. D. S. M., and Andrew V.Trask (2006) Pharmaceutical Cocrystals: An Emerging Approach to Physical Property Enhamcement. *Biomedical, crystal growth, crystalline* 31.

Williams W. Porter III, S. C., Elie, and Adam J.Matzger (2008) *Polymorphism in Carbamazepine Cocrystal.* Vol. 8.

Williams*, J. Y. Y. H. a. D. R. (2006) Wettability of Paracetamol Polymorphic Forms I and II. *Langmuir* 22, 6905-6909.

Xi Xu, Q. W., Xiangan Kong, Xiaodong Zhang and Jingui Huang (1996) Pan Mill type Equipment Designed for Polymer Stress Reactions Theoretical Analysis of Structure and Milling Process of Equipment. 25, 152-158.

Yang, D., Kulkarni, R., Behme, R. J. and Kotiyan, P. N. (2007) Effect of the melt granulation technique on the dissolution characteristics of griseofulvin. *Int J Pharm* 329 (1-2), 72-80.

Yu, L., Reutzel-Edens, S. M. and Mitchell, C. A. (2000) Crystallization and Polymorphism of Conformationally Flexible Molecules: Problems, Patterns, and Strategies. *Organic Process Research & Development* 4 (5), 396-402.

Yu, Z. Q., Chew, J. W., Chow, P. S. and Tan, R. B. H. (2007) Recent Advances in Crystallization control. *Chemical Engineering Research and Design* 85 (7), 893-905.

Zhu, B., Haghi, M., Nguyen, A., Goud, M., Yeung, S., Young, P. M. and Traini, D. (2015) Delivery of theophylline as dry powder for inhalation. *Asian Journal of Pharmaceutical Sciences* 10 (6), 520-527.

Appendix 1

The research work is performed at Centre for Pharmaceutical Engineering Science and Interdisciplinary Research Centre at the University of Bradford, UK since April 2014 to April 2017 under the supervision of Prof Anant Paradkar and Dr Venu Vengala.

Presentation of research work in conference

- "Effect of plasticisers on the degradation kinetics of cellulose ester derivative polymers" APS Particle Engineering - Joint Meeting with SSPC'' at Trinity College, Dublin between the periods of 11-14th April 2015.
- "Mechanistic understandings of sphere formation during melt granulation of Lactose monohydrate and PEG-6000"; 2016, Glasgow, UK.
- "Effect of processing technology on Surface properties and drug release performance of polymeric films"; European Inverse Gas Chromatography (iGC) Symposium, 2016, Imperial college London, UK.
- "Thermodynamic investigation of carbamazepine-saccharin co-crystal polymorphs"; Formulation Science & Technology Group, Royal Society of Chemistry, 2016, UK.
- "A green route to the manufacturing of API-loaded nanoscale hydroxyapatite"; MEIbioeng15, 2016, Leeds, UK

Open Publications

- Yulia Ryabenkova, Niten Jadav, Marco Conte, Michael F.A. Hippler, Nik Reeves-McLaren, Phil D. Coates, Peter Twigg, Anant Paradkar,

(2017). “The mechanism of hydrogen-bonded complex formation between ibuprofen and nanocrystalline hydroxyapatite”. Langmuir, 2017, 33 (12), pp 2965–2976, DOI: 10.1021/acs.langmuir.6b04510.

- Sudhir K. Pagire, Niten Jadav, Venu R. Vangala, Benjamin Whiteside, Anant Paradkar. “Thermodynamic Investigation of Carbamazepine-Saccharin Co-crystal Polymorphs”. Journal of Pharmaceutical Sciences, 2017.
- E.Khan, A. Shukla, Niten Jadav, R. Telford, A.P. Ayala, P. Tandon and V.R. Vangala. “Study of molecular structure, chemical reactivity and H-bonding interactions in the cocrystal of nitrofurantoin with urea”. New journal of chemistry.

Manuscripts under preparation

- Mechanism for formation and internal structure of Lactose-PEG 6000 granules obtained by Hot Melt Granulation
- Nano-indentation in crystal engineering: Mechanical properties of nitrofurantoin cocrystals.
- Microwave assisted sub-critical water synthesis of metastable form II of paracetamol with enhanced compaction property